



DTU Civil Engineering
Department of Civil Engineering



s121590 Luca Gennari

s121584 Thibault Péan

Conditioning of a Plus-energy House using Solar Systems for both Production of Heating and Nighttime Radiative Cooling

Master Thesis Report – Spring 2014



Supervisors

Bjarne W. Olesen

Ongun B. Kazanci

Peter Weitzmann

Jørn Toftum

Table of contents

Table of contents	3
Abstract	6
Acknowledgements	7
Symbols	8
Introduction	10
I. Solar Decathlon Europe 2014	13
1. The Solar Decathlon competition	13
2. Rules applying to Comfort conditions	15
3. Other rules related to HVAC	17
4. Discussion and conclusion	18
II. EMBRACE	19
1. Overall description of the house	19
1.1. Architectural and urban concept	19
1.2. Dwelling division	20
1.3. Thermal Envelope	21
1.4. Technical features	22
2. Thermal properties of the envelope.....	24
2.1. Thermal insulation	24
2.2. Thermal inertia	25
3. HVAC design process	28
3.1. Design strategies.....	28
3.2. Heating and cooling production	28
3.3. Description of the specific system adopted.....	31
3.4. Hydraulic scheme.....	37
4. Discussion	39
III. Detailed design of the radiant floor	40
1. Radiant floor limitations	40
1.1. Heat flux.....	40
1.2. Heat transfer coefficient	40
1.3. Dew point limitations.....	41
2. Load calculations (IDA-ICE)	43
2.1. Boundary conditions	43
2.2. HVAC system definition	43
2.3. Building geometry and operation	44
2.4. Obtained power demands	45
3. Radiant floor sizing	46
3.1. Method	46
3.2. Results.....	50
4. Verification of the performance (HEAT2)	53
4.1. Input to the model.....	53
4.2. Discussion on the pipe model	55
4.3. Results.....	57
5. Conclusion and discussion	61
IV. Heating and cooling production	62
1. Study of heat pump and its integration in the system layout	62
1.1. First option.....	64

1.2.	Second option	65
1.3.	Third option	65
2.	Performance of the selected heat pump.....	66
2.1.	Heating, Daikin simulation	67
2.2.	Cooling, Daikin simulation	69
2.3.	Considerations	70
3.	Domestic hot water	71
3.1.	Domestic hot water from solar collectors	71
4.	Storage tank.....	72
5.	Discussion	73
V.	Control.....	74
1.	Central control.....	74
2.	Switch between heating and cooling mode	75
3.	Control of the solar collectors	77
4.	Control of the radiant floor and heat pump.....	78
5.	Choice of the temperature set point in the storage tank.....	79
5.1.	Heating.....	79
5.2.	Cooling	82
6.	Conclusion and discussion	84
VI.	Testing and performance of the house.....	85
1.	Simulation results / Energy consumption.....	85
1.1.	Systems energy	85
1.2.	Hot water consumption-production	86
1.3.	System efficiency	87
1.4.	Electrical energy.....	88
2.	Performances in Versailles, during the competition	90
2.1.	Indoor climate in the prototype	90
2.2.	Electricity production and HVAC consumption.....	93
2.3.	Nighttime radiative cooling in Paris	96
3.	Conclusion and discussion on the house performance	103
VII.	Nighttime radiative cooling.....	104
1.	Introduction.....	104
2.	Theoretical analysis	106
2.1.	Cooling power	106
2.2.	Bottom and edges' heat losses	106
2.3.	Top heat losses	107
2.4.	Radiative cooling.....	108
2.5.	Convective cooling	112
2.6.	Discussion	116
3.	Economical potential of nighttime radiative cooling.....	117
3.1.	Method	117
3.1.	Results.....	117
3.2.	Conclusion.....	118
3.3.	Further considerations.....	118
4.	Experiment	119
4.1.	Description and objectives.....	119
4.2.	Methods.....	120
4.3.	Results.....	131

4.4.	Discussion and conclusion on the experiment	139
5.	Modeling: evaluation of nighttime radiative cooling potential (TRNSYS)	141
5.1.	Description of TRNSYS	141
5.2.	Model of unglazed solar collectors	141
5.3.	Simulations	144
5.4.	Study on the flow rate	145
5.5.	Study on the inlet temperature	147
5.6.	Final choice of flow rate, size of tank and cooling hours	149
6.	Comparison between the experimental and simulated results	151
7.	Discussion and conclusion on nighttime radiative cooling	152
	Discussion.....	153
	Future research	154
	Conclusion	155
	References.....	157
	Standards.....	157
	Articles and Books	158
	Other references	159
	Lists of figures.....	161
	List of tables	164
	Appendix	165
	Annex 1: House envelope, materials properties	165
	Annex 2: Tanks size and losses.....	168
	Annex 3: Solar collectors' data	171
	Annex 4: Dynamic simulation schedules	173
	Annex 5: Hydraulic scheme, domestic hot water and space heating/cooling losses	174
	Annex 6: Pumps data and consumption	177
	Annex 7: House appliances data and energy consumption	181
	Annex 8: EN 1264 part 2 and 5 calculations	186
	Annex 9: Nilan Compact P functions	193
	Annex 10: Electrical energy price	195
	Annex 11: Mechanical and instrumentation drawings from PD#6, Team DTU	196
	Annex 12: Control drawings from PD#6, Team DTU	197
	Annex 13: Power graphs from the experiment (August 12th-25th)	198
	Annex 14: Final estimation of cooling power based on TRNSYS simulation	199
	Annex 15: Operation period and outdoor temperature for Daikin heat pump simulations.....	201

Abstract

The plus-energy house EMBRACE was designed and built by Team DTU for the Solar Decathlon Europe 2014 competition in France. The authors have tried to conceive and optimize the layout and integration of the HVAC systems, in order to reach the highest performance possible. Annual simulations have shown a total electricity consumption of 38 kWh/m²·year in Copenhagen (less than half the estimated production). During the competition in Versailles, the house consumed less than it produced, keeping the operative temperature in the range required to get maximum available points more than 70% of the time. Out of 20 teams, the house ranked #8 in the Comfort Conditions category, #9 in the Energy Efficiency, and #8 for the overall competition.

In order to study deeper the radiative cooling technology implemented in EMBRACE, the authors have developed simulation and experimental work in order to estimate the potential of this unexploited technology. Photovoltaic/thermal panels and unglazed solar collectors have been chosen as case studies for this research. The results from software simulation, theoretical calculations and experimental tests showed relatively good consistency. The output cooling power is estimated to range from 20 to 75 W/m² for both types of panels, depending on the sky clearness, without noticeable difference between the PVT and the unglazed collectors. The panels can produce between 0,2 and 0,9 kWh/m² of cooling energy per night. The overall COP (defined as the ratio between the gained energy and the energy consumed by the two panels) reached very high values, ranging from 19 to 58, which highlights the potentials of this technology for energy savings in cooling.

Keywords: Solar Decathlon, plus-energy house, energy efficiency, sustainable housing, PVT, unglazed solar collectors, nighttime radiative cooling.

Acknowledgements

The Solar Decathlon project has been such an adventure, and the authors would like to thank warmly all the people that enabled to make EMBRACE come to life. Every team member has brought his/her own skills to participate in this great achievement, gathering a team of international, dynamic and creative students.

All along the work covered by this M.Sc. thesis, the guidance of the supervisors Professor Bjarne W. Olesen and Ph.D. Ongun B. Kazanci has been continuous and helpful. Their fruitful comments and directions have helped to conduct the work in a proper way, achieving the results visible in the present report. Associate Professors Peter Weitzmann and Jørn Toftum should also be thanked for always responding with good will when help on specific topics was needed.

The sponsoring companies have brought precious help from various experienced and professional point of views. Lasse Bach from Daikin should be thanked for the precious time he spent and the efforts he made to integrate the heat pump in our system, and for sponsoring it for the team. Henrik Kjeldgaard, Lars Sund Mortensen and Nikolai Rud from Grundfos should be thanked for helping us in the choice of the pumps and supplying them to Team DTU. Jesper Hansen from Uponor should be thanked for the wise advice he gave during the design phase, and the radiant floor products Uponor provided through him. Niels Nilausen from Bravida is thanked for his support during the design phase; Henri and Flemming for their practical help and extra time spent in the mounting of the systems. Nilan should also be thanked for sponsoring the Compact P unit that EMBRACE is equipped with.

The technicians from DTU building 412, Nico Henrik Ziersen and Peter Slotved Simonsen have brought a precious help in the setup of the radiative cooling experiment. Their knowledge on sensors has been profitable, and they enabled to build the small experimental facility on the roof of building 412.

Finally, the authors would like to thank Bengt Perers for sharing his knowledge on PVT testing and sky temperature measurements, and Angela Simone for her precious help in the design of the handcrafted sensors aimed at obtaining sky temperature.

Symbols

Symbol	Physical parameter	Unit
$\alpha(\lambda)$	Absorptivity	-
c_a	Air heat capacity	J/kg·K
P_v	Air vapour pressure	Pa
β	Angle	deg
A	Area	m ²
p_o	Atmospheric pressure at zero elevation, sea level, typically 10 ⁵ Pa	Pa
p_{atm}	Atmospheric pressure of ambient air	Pa
C	average measurable area of all projects	m ²
L_c	Characteristic length	m
N	Cloud cover factor	-
COP	Coefficient of performance: power gained / power used	-
F'	Collector efficiency factor	-
E_F	Consumption of appliances, lighting and home automation systems	kWh
E_V	Consumption of heating, cooling, ventilation and hot water systems	kWh
\dot{Q}_{conv}	Convective component of the heat flux	W
x_c	Critical distance	m
f	Damping ratio	-
ρ	Density	kg/m ³
T_{dp}	Dew point temperature	°C
$\Delta\vartheta$	Difference between average water temperature in the radiant floor and room temperature	K
D	Dimension	mm
L_{\downarrow}	Downward long wave radiation	W/m ²
$L_{\downarrow}(0)$	Downward long wave radiation for orthogonal incident surfaces	W/m ²
T_a	Dry bulb air temperature	K or °C (specified in the text)
$\varepsilon(\lambda)$ or ε	Emissivity	-
ε_0	Emissivity of clear sky	-
ε_r	Emissivity of the radiator (considered panel)	-
ε_{sky}	Emissivity of the sky	-
EER	Energy Efficiency Ratio: power gained / power used (in cooling operation)	-
B	Expansion coefficient	1/K
T_f	Film temperature	°C
n	Fractional cloud amount of the sky covered by opaque clouds	-
G_r	Grashof number	-
g	Gravitational acceleration	m ² /s
c	Heat capacity	J/kg·K
\dot{Q}	Heat flux	W
q	Heat flux per unit of area	W/m ²
h	Heat transfer coefficient	W/m ² ·K
G	Heat transmittance: solar heat gain / incident solar radiation. For windows	%
ε_c	Hemispherical cloud emissivity	-

ν_a	Kinematic viscosity of air	m^2/s
LT	Light transmittance: visible light transmitted / incident visible light (for windows)	%
E	Load consumption per surface area	kWh/m^2
\dot{m}	Mass flow rate	kg/s
t_m	Number of hours from midnight of the considered instant, in solar time	-
Nu	Nusselt number	-
Pr	Prandtl number	-
\dot{Q}_{rad}	Radiative component of the heat flux	W
Ra	Rayleigh number	-
$\rho(\lambda)$	Reflectivity	-
RH	Relative humidity	-
Re	Reynolds number	-
$P_{v,sat}$	Saturation air vapour pressure in Pa	Pa
T_{sky}	Sky temperature	K
δx	Standard deviation	-
σ	Stefan-Boltzmann constant or Temperature drop between supply and return in radiant floor	$5,67 \times 10^{-8} \text{ W}/\text{m}^2 \cdot \text{K}^4$ or K
T_r	Surface temperature of the radiator (considered panel)	K
T	Temperature	K
ΔT	Temperature difference	K
T_{tank}	Temperature in the tank	K
T_{ret}	Temperature of the return	K
T_{sup}	Temperature of the supply	K
Z_c	Cloud base height	km
λ	Thermal conductivity	$\text{W}/\text{m} \cdot \text{K}$
k_a	Thermal conductivity of air	$\text{W}/\text{m} \cdot \text{K}$
R	Thermal resistance	$\text{m}^2 \cdot \text{K}/\text{W}$
U	Thermal transmittance	$\text{W}/\text{m}^2 \cdot \text{K}$
L	Thickness	m
α	Tilt angle or thermal diffusivity	deg or m^2/s
Δt	Time difference	h or s (specified in the text)
$\tau(\lambda)$	Transmissivity	-
\dot{q}	Volume flow rate	m^3/s
c_w	Water heat capacity	$\text{J}/\text{kg} \cdot \text{K}$
U_w	Wind speed	m/s

Introduction

Now that global warming has become a widespread concern, with the energy crisis and increase of waste and pollution, scientists all over the world concentrate their efforts to slow it down. Numerous governments and organizations have understood the emergency, and try to implement policies to incite builders and consumers to manage their energy in a more sustainable way. The 20-20-20 European plan reflects this awareness by setting the EU's targets for 2020: the aim is to reduce the greenhouse gas emissions by 20 % from the level of 1990, increase the energy efficiency by 20 %, and increase the level of the renewable energies to 20 % of the total energy mix. Improving energy efficiency in buildings represents a major opportunity to achieve these goals. Indeed, 41 % of all the energy used in the EU is consumed by buildings, and among that quantity, 2/3 are spent on heating and cooling (Jianhua F., 2013). The importance of the building sector places it at the forefront of the combat against climate change. Denmark tries to lead the way in Europe by setting even more ambitious goals, with the 2015 and 2020 strict energy thresholds fixed for residential and public buildings (See Table 1).

Table 1¹ – Danish energy classes for residential buildings taking into account energy supply for heating, ventilation, cooling and domestic hot water

BR2015	BR2020
(30+1000/A)kWh/m ² per year, in which A is the heated floor area.	20 kWh/m ² per year

Sustainability is a complex and multidimensional concept that is difficult to identify with only one definition. One of the most complete descriptions of sustainability is the one of the Brundtland Commission (1987): *"the development that meets the needs of the present without compromising the ability of future generations to meet their own needs."*

Meeting the needs of the future depends on how the current society will manage the social, economic, and environmental objectives/ needs, balancing and combining them in the most appropriate way. Some of these needs are itemized around Figure 1.



Figure 1 – Main concepts concerning sustainability

Several energy-efficient and sustainable strategies for designing buildings are already known, such as the Trias Energetica developed in 1979 at TU Delft. This approach consists first in reducing the demand to a minimum, then in providing the remaining needs with renewable energies, and finally in completing the residual demand by using fossil fuels but in the most efficient way possible. In order to incite builders to use this sort of strategies, governmental authorities have developed labels to rate energy efficient buildings. LEED in the USA, DGNB in Germany, BREEAM in the UK or HQE in France are some of these labels which recognize and highlight the efforts made towards sustainability and green buildings. In the area of heating and cooling, which is the focus of this report, savings can be undertaken by improving the insulation and air

Several energy-efficient and sustainable strategies for designing buildings are already known, such as the Trias Energetica developed in 1979 at TU Delft. This approach consists first in reducing the demand to a minimum, then in providing the remaining needs with renewable energies, and finally in completing the residual demand by using fossil fuels but in the most efficient way possible. In order to incite builders to use this sort of strategies, governmental authorities have developed labels to rate energy efficient buildings. LEED in the USA, DGNB in Germany, BREEAM in the UK or HQE in France are some of these labels which recognize and highlight the efforts made towards sustainability and green buildings. In the area of heating and cooling, which is the focus of this report, savings can be undertaken by improving the insulation and air

¹ http://bygningsreglementet.dk/br10_04_id106/0/42

tightness of the thermal envelopes, choosing low-temperature heating and high-temperature cooling, or increasing the efficiency of the generation and distribution systems.

Most of those simple steps should have become rule of thumbs by now. But despite the global awareness previously described, a fringe of the building designers profession still seem to carry misconceived ideas about energy efficiency. The German architect Thomas Herzog quotes the Swiss architect Fritz Haller: *“I will never be interested in reducing energy consumption because there is enough energy”* (Bjerregaard Jensen L., 2008). This sentence is a glaring example of the above statement. Even though Thomas Herzog is acknowledged as a leading architect in the field of sustainability, this ambiguous sentence with which he agrees can plant seeds of doubt in the minds of young designers. What he probably means, but this is only subject to interpretation and that is why it is problematic, is that there is a *potential* for enough renewable energy, if we consider the resources in solar radiation, wind or ocean currents. But the world industries stay very far from making the most of this resource, and as long as they continue to use massively fossil fueled energies, the only way to tackle climate change is to reduce the consumption. The fact that Thomas Herzog was chosen as a member of the jury of the Solar Decathlon competition demonstrates that even among the specialists, some improvements can still be carried out in order to raise the global awareness on energy-efficiency in buildings. Fighting inaccurate and hasty judgments, and alerting the general public and the building professionals represents the main reason for being of the Solar Decathlon competition¹. Energy-efficient buildings are too often seen by the general public as prototypes, museum objects or lab products, not as homes where inhabitants would actually like to live in. The competition tries to advertise on the liveability of sustainable houses, in order to spread their use.

DTU also makes its own contribution by teaching the “integrated design” method through several courses aimed at Architectural Engineers. In this concept of designing buildings, the engineers are involved in a project from the beginning, enabling them to integrate energy-efficient strategies from the early stages, when changes are still possible. In the traditional approach, engineers join a project later in the process, and they often experience difficulties in trying to implement such strategies when the architectural design is already over. The participation of DTU in the Solar Decathlon represents a concretization of this concept, since the house presented by the team was conceived and built only by engineers. All these initiatives show good will in completing the potential lacks of understanding which undermine the sector.

At the smaller scale of the present master thesis, the students have tried to implement this concept during the design of the heating and cooling systems² for the house EMBRACE, Team DTU entry to the Solar Decathlon Europe 2014 competition. The HVAC and other technical systems have been developed in parallel with the rest of the house, resulting in an adapted integration of those systems. The students have first designed and sized the production, emission and control systems producing heating and cooling for the house. This work was based on computer simulation results and calculations relying on the existing standards. They participated in the mounting of the actual chosen products in the built house on DTU campus. The whole real-scale installation was tested in situation during the competition in France, and the results are reported in this thesis.

A focus has been drawn on innovative cooling, based on two main statements: firstly, the rising levels of indoor comfort often imply a need for cooling, even under temperate climates such as Denmark. This is

¹ See chapter I.1. for a description of the competition.

² The detailed ventilation design is left apart as another student has been working on this topic for his own thesis. However, the main concepts and choices have obviously been proceeded in close cooperation, in order to match the desired performances of the overall Heating, Ventilation and Air Conditioning (HVAC).

especially true in office buildings with high internal gains, or for highly-insulated buildings. Secondly, the ambitious standards for new buildings incite builders to integrate solar panels on the roofs to provide energy to the buildings and hence improve their energy balance. Thermal solar panels (standard collectors or photovoltaic/thermal (PVT)) could be used also at night to exploit the radiation towards the cold sky and therefore produce cooling at both a low financial and energy costs. Nighttime radiative cooling applications are not widespread; therefore the students have decided to investigate this field through simulation and experimental work, in order to estimate the potential of this new technology.

I. Solar Decathlon Europe 2014

This chapter describes the Solar Decathlon competition, and the main rules that apply to the design of the HVAC systems.

1. The Solar Decathlon competition

“Solar Decathlon is an award-winning program that challenges collegiate teams to design, build, and operate solar-powered houses that are cost-effective, energy-efficient, and attractive. The winner of the competition is the team that best blends affordability, consumer appeal, and design excellence with optimal energy production and maximum efficiency.” (U.S. DOE, 2014)

The first Solar Decathlon competition was inaugurated in 2002, in Washington D.C., under the initiative of Richard King from the U.S. Department of Energy (DOE). He noticed that the solar technology was too restricted to high-tech applications such as spaceships, and that architects or engineers did not really know how to integrate solar panels in houses in both an aesthetical and functional way. From this observation, he decided to gather universities from the whole country: each one of them had to build a solar powered house, assemble it in few days on the site of the competition where it was evaluated under 10 main criteria, hence the name of the Solar *Decathlon*. The 10 contests¹ are as follows:

1. Architecture (120 points, juried)
2. Engineering and Construction (80 points, juried)
3. Electrical Energy Balance (120 points, measured)
4. Energy Efficiency (80 points, juried)
5. Comfort Conditions (120 points, measured)
6. House Functioning (120 points, measured)
7. Communication and Social Awareness (80 points, juried)
8. Urban Design, Transportation and Affordability (UDTA) (120 points, juried)
9. Innovation (80 points, juried)
10. Sustainability (80 points, juried)

The Solar Decathlon has not ceased to grow since its first edition in the USA: the European edition (Solar Decathlon Europe, SDE) has been held twice in Madrid, Spain (2010, 2012) and once in Versailles, France (2014). DTU participated in 2012 with the house FOLD and in 2014 with the house EMBRACE, which is described in this report. An edition was organized in China in 2013 and a memorandum of understanding has recently been signed with the authorities of Colombia to start the Solar Decathlon Caribbean and Latin America. The competition has become an international event, with universities coming from more than 16 different countries to the Solar Decathlon Europe 2014 in France. Several millions of people have visited the houses or heard of the competition through the important media coverage, participating in raising the global awareness about energy, solar power and sustainable housing.

The core concept of the competition is to balance the 10 contests, since they are often competing against each other: by minimizing the HVAC consumption, one can earn points in the energy efficiency or electrical energy balance, but the comfort conditions will become very poor; or very innovative materials can be used, which will be sustainable, but not affordable. It is all a matter of finding efficient compromises between all aspects of the construction and use of a house. That is what makes the competition challenging and brings it closer to the real issues faced by our societies. In order to go deeper in this direction, the

¹ The list presented here corresponds to the 2014 edition in Europe. The 10 contests and the amount of points they cover are subject to changes for every edition.

French organization decided to focus the competition of 2014 on the local context and the affordability: the teams really had to anchor their projects in the local urban context of their own countries. For example, the Dutch team Prêt-à-Loger developed a refurbishment plan for the typical row houses that are numerous in the Netherlands, or the Chilean team created emergency housing in response to the frequent earthquakes of their country. As described later in the report, Team DTU focused on the densification of large cities like Copenhagen by building on the rooftops of existing constructions.

The Solar Decathlon Europe 2014 represented one and a half year of work through different steps. Team DTU was selected in December 2012, based on its project proposal. From then until the competition in June 2014, the students have worked in clearing out the main outlines of the project, proposing a design and refining it step by step, taking into account all the constraints included in the Solar Decathlon rules. The house EMBRACE was born through this long and iterative process, and its construction started in May 2014 at DTU campus. The modular house was disassembled and sent by trucks to Versailles where the assembly started on June 15th, for 10 days. After validating the inspections of the building, the competition took place, starting from June 30th: EMBRACE was then open to the public, along with 19 other houses.

After the official opening, the prototypes were evaluated during two weeks. The awarding of points is different for each sub contest and stated in the rules. For some of them (see list of contests above), a jury visits the house and listens to the presentation given by the team. The jury members can then discuss the different points related to the sub contest and award points accordingly. For others, the project is evaluated by monitored parameters such as indoor temperature or humidity, or by executing in-house tasks such as hot water draw-offs or cooking. A total of 1000 points is available throughout the competition, and the ranking is therefore evolving every day of the competition, as the sub contests are gradually evaluated.

The SDE2014 was won by the project RhOME for DenCity, developed by the Università di Roma Tre. Team DTU and the house EMBRACE ranked #8, with a total of 780,01 points, distributed as follows for the 10 competitions:

Table 2 – Points distribution and rankings for Team DTU

Sub contest	Points earned by Team DTU	Ranking of Team DTU
Architecture	78 / 120	#12
Engineering and Construction	69,6 / 80	#8
Electrical Energy Balance	79,22 / 120	#7
Energy Efficiency	71,84 / 80	#9
Comfort Conditions	99,23 / 120	#8
House Functioning	90,66 / 120	#11
Communication and Social Awareness	64 / 80	#8
Urban Design, Transportation, Affordability	101,64 / 120	#4
Innovation	59,81 / 80	#9
Sustainability	68 / 80	#6
Penalties	-2	-
TOTAL	780,01 / 1000	#8

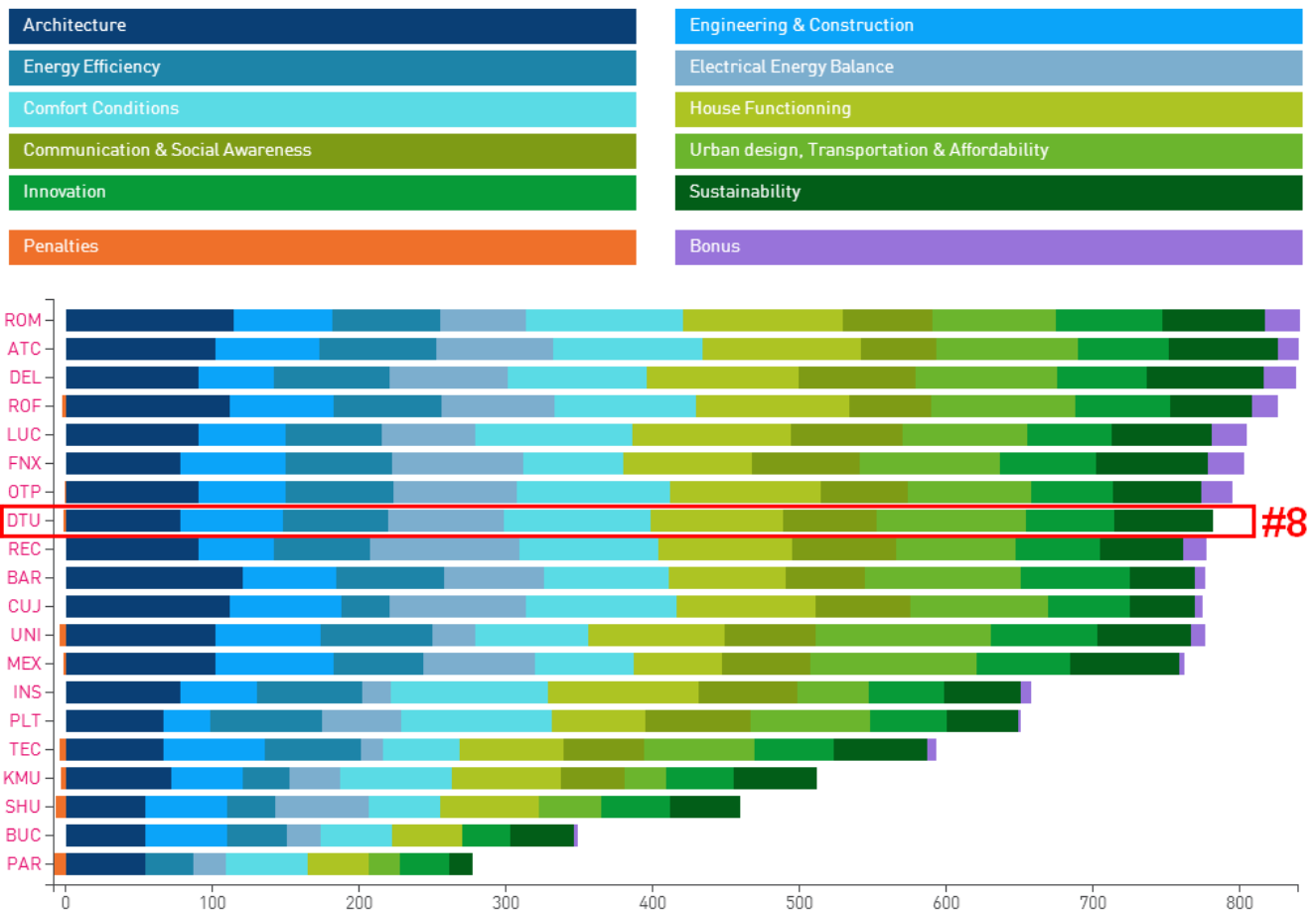


Figure 2 – Final ranking of SDE2014

2. Rules applying to Comfort conditions

As previously mentioned, the Solar Decathlon organization provides every team with all the specifications that the houses must fulfill (Solar Decathlon Europe, 2014. “Règlement / Rules / V5.0”). The competing teams also had to hand in every few months an updated deliverable of their project, including drawings and a manual describing all aspects of the house. These deliverables enabled the organization to check that the houses were meeting the requirements.

As the present report focuses on the HVAC systems, the rules related to the Comfort Conditions influenced considerably the design choices. Table 3 sums up the indoor climate criteria that give the maximum amount of points during the competition.

Table 3 – Desired comfort conditions, based on Solar Decathlon 2014 regulation

Criteria	Range to get the maximum amount of points	Comments
Indoor Operative Temperature day	$T_{av}-1 < T_{indoor} < T_{av}+1$	The temperature set point T_{av} is fixed every day by the competition organization, calculated in function of the weather data of the previous 7 days.
Indoor Operative Temperature night (from 0:00 to 8:00)	$18 < T_{indoor} < T_{av}+1$	T_{min} for the night hours has been fixed to 18° C for 100% points, providing the opportunity to start to earn points from 16° C.
Relative Humidity	$40 \% < RH < 55 \%$	
CO ₂	$CO_2 < 800 \text{ ppm}$	
Formaldehyde concentration	Formaldehyde conc. $< 30 \mu\text{g}/\text{m}^3$	

These requirements are strict: a range of indoor temperature of 2°C is relatively narrow, and it can result difficult to maintain the temperature within this range, given the fluctuating outdoor conditions and internal gains, especially because of the public tours taking place in the house¹. It should be noted that the initial rules did not differentiate between day and night for the indoor temperature set point, which was therefore valid for the 24 hours of the day. This could have caused problems, because the weather in Paris in July is not necessarily warm: the outdoor temperature can frequently drop down to less than 15°C, especially at night. The following graph shows the weather data of a typical year in Paris, taken from the French regulation RT2012.

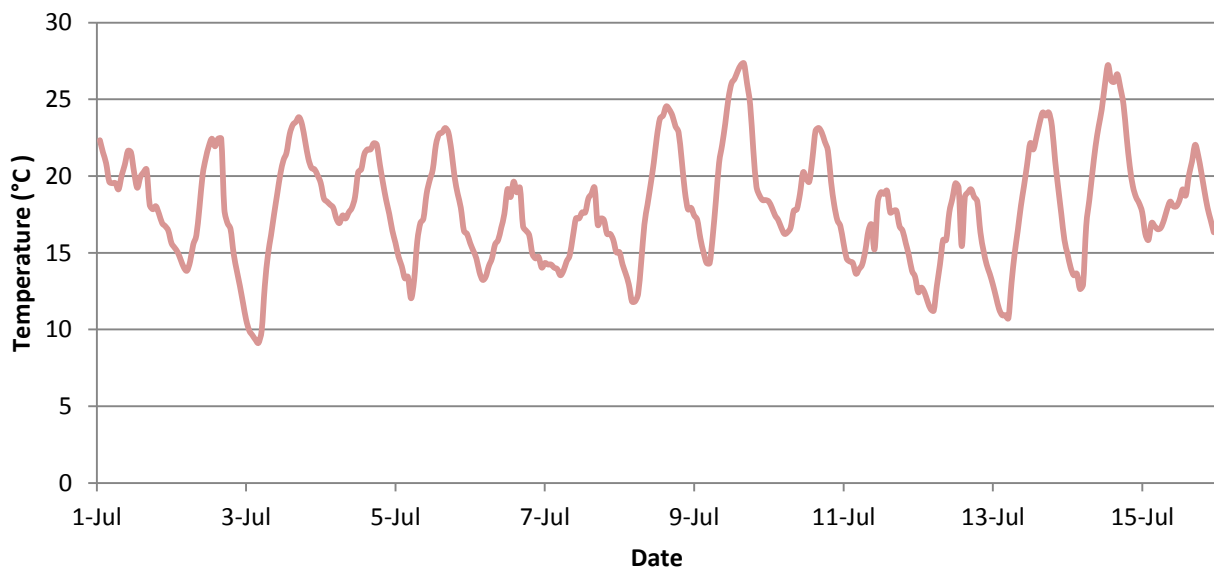


Figure 3 – Outside weather data of Paris in July – Typical year from RT2012

With this weather data, the calculated set point is around 23 or 24°C, so it could be necessary to heat the house at night to keep this temperature, even with the high level of insulation of the envelope. From an energy-efficiency point of view, this strategy would be disastrous: to heat the building at night and to cool it during the day is completely paradoxical for a house that aims to be passive. Furthermore, it is irrelevant in

¹ The monitoring stops during the public tours, but it can still affect the indoor climate of the monitored periods, if for instance the doors have stayed open or a lot of people came inside the house at the same time.

terms of comfort and habits: the occupants usually prefer a cooler temperature to sleep at night, and the heating systems are normally shut down in France from a period that ranges from May to September.

Based on these observations, Team DTU formulated a request to the organization, in order to obtain a modification of the rules for the temperature set point at night. The answer was negative, but other teams probably reported the same observations. The organizers finally figured out that the rules were more suited to the climates of Madrid or California (where the competition was held before), but that they needed some adjustments for Paris. Therefore, they decided to establish a setback function for the night. This means the minimum set point is lowered to 18°C from 0:00 to 8:00, regardless of the outside conditions. The actual weather in Paris during the competition was exceptionally cold for this period of the year, so this decision proved to be adapted to the circumstances.

3. Other rules related to HVAC

As stated previously, the ten contests of the competition are closely related, and even though the Comfort Conditions is the more relevant when designing the HVAC systems, the other contests must also be kept in mind. The “Architecture” and “Engineering and Construction” contests relate to the HVAC design mainly with the space and envelope organization, which determinates the heat gains/losses, volumes distribution and the space available where to integrate the technical installations. Some room needs to be saved in order to integrate all the pipes, ducts and mechanical equipment in the walls and in the technical room, without interfering with the bearing structure of the house.

After the Comfort Conditions, the most relevant contests would be Energy Efficiency and Electrical Energy Balance. A complete part of the evaluation criteria within the Energy Efficiency contest is about the efficiency of the HVAC systems. The concept, dimensioning and resolution of the HVAC systems facilities, the passive and/or active strategies of the house are evaluated, as well as their efficiency to fulfill the house’s needs. The choices made for the design must therefore be duly argued and supported by tangible evidence of their performance since they are evaluated during this juried contest.

In the Electrical Energy Balance contest, the load consumption per surface area E is measured, according to the following formula:

$$E = \frac{E_V}{A} + \frac{E_F}{C} \quad (kWh/m^2)$$

Where:

E_V is the consumption of heating, cooling, ventilation and hot water systems (kWh)

E_F is the consumption of appliances, lighting and home automation systems (kWh)

A and C are respectively the measurable area of the house, and the average measurable area of all projects (m^2)

In order to get maximum points in this sub-contest, the consumption of the HVAC and hot water systems E_V must be lowered down as much as possible (as well as E_F but it is less relevant to the present work). The positive electrical balance of the house can also benefit from it, since the HVAC consumption represents an important part of the total energy consumption.

The House Functioning contest consists in executing several in-house tasks such as cooking or washing clothes with the house’s appliances. In order to get the maximum amount of points, some tasks require

using hot water at a certain temperature: 40°C for the clothes washing, 49°C for the dishwashing, 43°C for the hot water draws. The HVAC designers must keep in mind that the hydraulic systems need to reach these temperatures for these amounts of water every day of the competition.

The other contests affect the HVAC design on a more theoretical level: for the UDTA contest, the students must integrate the house in an urban context, and a strategy for heating and cooling must therefore be implemented in the local scenario in Copenhagen. The systems used must be chosen among the state-of-the-art technologies, taking into account value for money, or combine existing systems in an original way in order to gain points in the Innovation contest. Finally, the bioclimatic strategies for passive heating and cooling, the active systems and equipment, the solar and water systems are part of the subjects evaluated in the Sustainability contest.

Keeping these numerous rules in mind, the students have tried to design an optimal system performing well in most of the contests.

4. Discussion and conclusion

The Solar Decathlon is a competition, and as such, it defines specific criteria to evaluate the different contestants. Those rules and the manner in which they are applied by the organization can be subject to critics. In the specific contest of the Comfort Conditions, the set-point calculation could be re-evaluated for more temperate climates such as Paris: the running mean temperature results to be too high, with the risk of having to use heating in the houses during the competition in summer. This case happened in France during the 2014 competition, and it is obviously an undesired situation. It serves badly the cause promoted by the Solar Decathlon when extra energy is needed to condition houses that are supposed to be passive, in a period where heating is habitually off even for traditional buildings, regardless of the outside weather conditions.

The limits of the competition are also visible when the participating teams come from all around the world. The rules specifically mention that the prototypes must be adapted to the competition location climate, but on the other hand, the design and narratives must anchor the projects in a local urban context. How then can be compared houses designed for the tropical climate of Costa Rica, the monsoon seasons of Thailand, the coastal and mountainous weather of Chile, or the rigorous windy winters of Denmark? Adaptations have been made in each case to fit with the French climate, but when these modifications go against the way of building locally, the competition has reached a dead end.

The method used to assign the points to the Energy balance competition may also be subject to criticism. In fact, regardless of the size of the dwelling and the number of people for which it is designed, all the teams had to tap the same amount of hot water per day, which has a greater impact when the measurable area is smaller.

However, even though it is difficult to compare such different prototypes, the competition must state clear rules. All the contestants that enter the competition are aware of the regulation, they must therefore abide by the rules. The competition might be somehow biased by the broad diversity of the projects and countries represented, but a participation in such an event still remains a great opportunity to showcase the innovations and design strategies developed by the universities. The ranking finally has a small importance as long as the competition reaches its goal of broadening the knowledge on sustainable housing and raising the global awareness on the topic.

II. EMBRACE

“Team DTU named its entry for the Solar Decathlon Europe 2014 EMBRACE. It is a dwelling designed for a two people family, brought to life by combining passive architectural solutions and active technological solutions in one building. The concept behind the name relies on the splitting of the building envelope in two different parts: the thermal envelope, and what we refer to as the weather shield. EMBRACE was conceived as an addition to be installed on the roof of an existing building, in order to densify the cities.” (Team DTU, 2014)



Figure 4 – EMBRACE in Versailles (@SDEurope)

1. Overall description of the house

1.1. Architectural and urban concept

There is a worldwide tendency of people moving from the countryside to larger cities. Megacities are a phenomenon, which is getting more common because of this urbanization. It results in an increased demand for dwellings in the cities, and therefore requires finding alternative housing solutions. A lot of rooftops in the cities are not utilized to their full potential: the idea proposed by Team DTU is to use them as a base for the new EMBRACE add-on unit. This unit *embraces* the local environment, the users of the existing building and the new inhabitants. The building is optimized in an efficient and smart manner, which gives the possibility of sharing the extra energy production.

The main focus area has been to try to move people from the suburbs to the city centres, in order to minimize the impact of transportation. EMBRACE takes the suburbs of Copenhagen and puts them on top of the existing city where the suburban atmosphere is mixed with the vibrant inner city.



Figure 5 – Urban concept: integration of EMBRACE on the rooftop of existing buildings

1.2. Dwelling division

The envelope of EMBRACE is divided into two parts: a Thermal Envelope and a Weather Shield. The Thermal Envelope refers to the conditioned dwelling unit and the Weather Shield is a shelter protecting from water, wind, and snow. The shield extends from the dwelling and creates a covered outdoor area - the Sheltered Garden. Separating the envelope and having a Sheltered Garden on the rooftop gives the possibility to extend the comfortable outdoor season during the year. The Weather Shield allows building with simpler and different materials than usual such as using indoor materials outdoor.

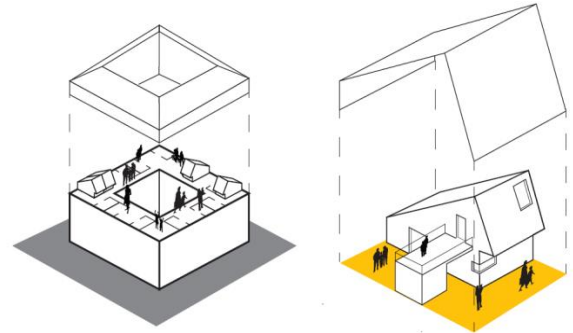


Figure 6 – Weather Shield concept

The acoustic environment is optimized in the Sheltered Garden by using acoustic panels as outdoor cladding and integrating a vertical garden, to reduce the reverberation time and possibility of echo. The Hobby Room provides possibilities for the inhabitants to use it as laundry room, storage for garden tools or space for fixing bikes. In a large-scale EMBRACE community, each Hobby Room could have its own function and then be shared with the entire community. To give the possibility for the residents to get an intimate space, a private terrace is located on top of the Hobby Room with access directly from the bedroom.

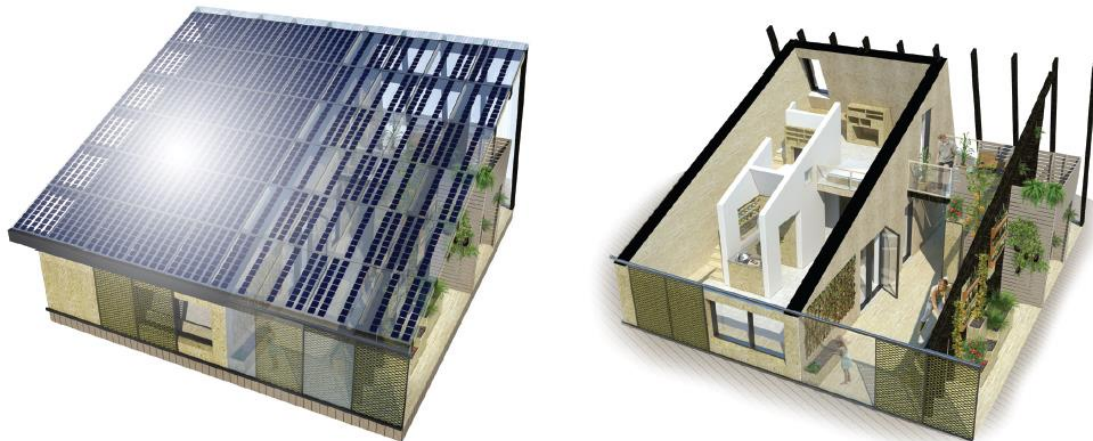


Figure 7 – Renderings of the Weather Shield and Sheltered Garden (Team DTU, 2014)

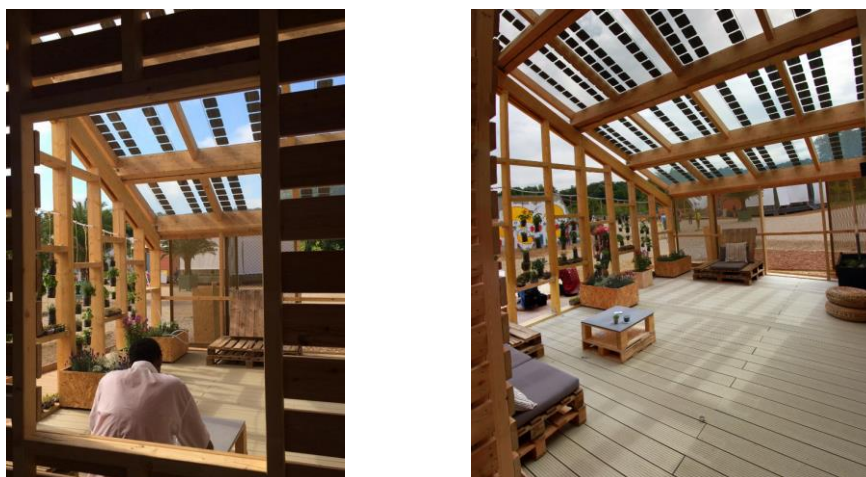


Figure 8 – Photographs of the constructed Sheltered Garden

1.3. Thermal Envelope

The Thermal Envelope consists of four prefabricated modules. One of them is the technical module, concentrating the main equipment: the plumbing pipes, the hydronic systems and their control, the home automation, the electric panels, the ventilation ducts are all installed in this unit, minimizing the connection problems across modules. The rest of the house consists of one large living zone, where the living room, dining area and kitchen are integrated. This division gives the user the opportunity to adjust the interior according to their needs. In extension to the living zone there is a flexible room, which can be used as a room for children, an extra bed for guests or an office. The spatial design is based on the main idea to invert the trend in Denmark of living in larger and larger houses. In this way the conditioned space is limited, reducing the heated and cooled area to the minimum needed and consequently the demands of the dwelling. To convince and attract people to live in smaller areas, two main strategies are implemented: create high indoor quality comfort spaces and provide an outdoor space which is an extension of the living area that does not need to be conditioned, the Sheltered Garden.

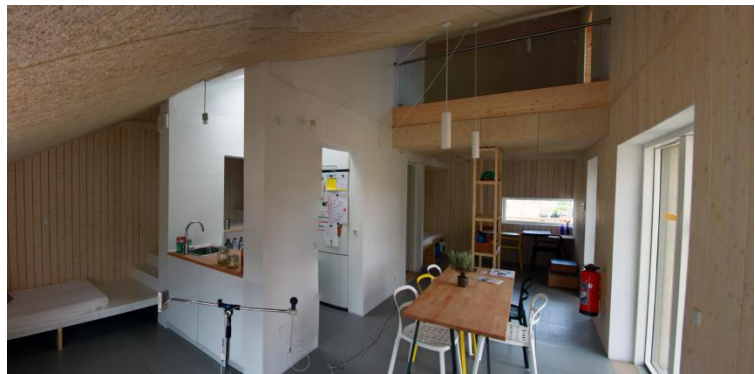


Figure 9 – Rendering and photo of the ground floor (living room, kitchen and flex room) (Team DTU, 2014)

The EMBRACE prototype built by Team DTU for the purpose of the Solar Decathlon competition was assembled as shown in Figure 10. The fact that the house needed to be assembled/disassembled several times in a short period, and transported all the way to France added some additional constraints to the design. Figure 11 shows the craning of the last element of the thermal envelope.

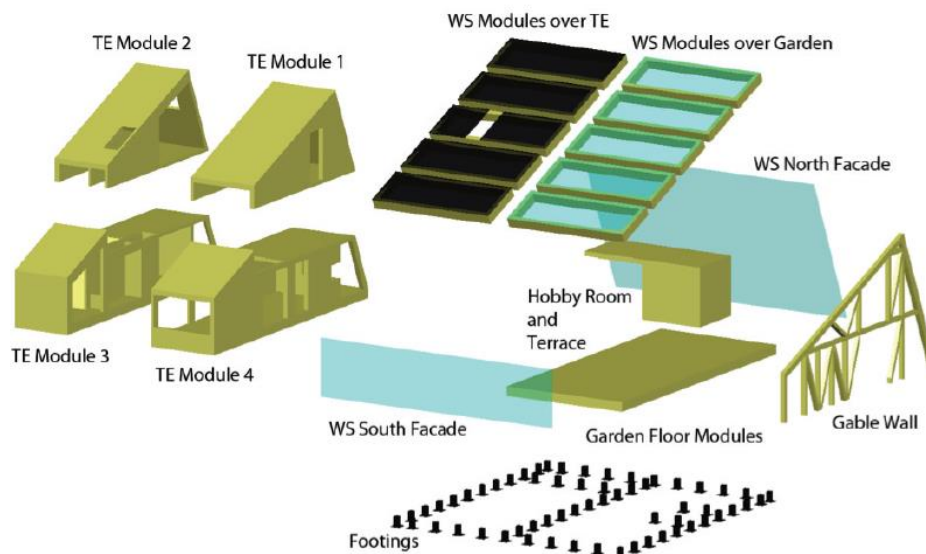


Figure 10 – EMBRACE main construction elements (Team DTU, 2014)



Figure 11 – Two perspectives from the modules assembly

Table 4 sums up the floor areas of EMBRACE. As mentioned in the description of the concept of the house, it is a small and compact dwelling, keeping only the necessary area in order to densify the cities in an efficient way.

Table 4 – Main floors' areas of EMBRACE

Description	Area (m ²)
Gross Floor Area	80,5
Gross Floor Area, Ground Floor	55,5
Gross Floor Area, 1st Floor	25
Net Floor Area	59
Net Floor Area, Ground Floor [Technical Room]	4
Net Floor Area, Ground Floor [Bathroom]	3
Net Floor Area, Ground Floor [Living+Kitchen+Flexible room]	31
Net Floor Area, 1st Floor [Bedroom+Stairs]	21
Measurable Area	46
Measurable Area, Ground Floor	30
Measurable Area, 1st Floor [+ stairs]	16
Glazing areas (including frames)	14,6
Windows to the outside	5,7
Windows and glazed doors to the sheltered garden	8,9

1.4. Technical features

EMBRACE is equipped with photovoltaic (PV) panels that supply the house with electricity. Opaque black panels with monocrystalline cells are installed on the roof above the thermal envelope, where they produce 2/3 of the electricity. On top of the Sheltered Garden, the remaining 1/3 of PV panels consist of tiles integrated in the glazing panes. They are arranged in a lightened pattern, in order to find a balance between the daylight and the shading provided to the garden. The two kinds of panel sum up to 5 kWp installed, as it is the maximum allowed by the competition. They can be seen in Figure 12.



Figure 12 – The two different sorts of PV panels in EMBRACE

Another important feature of EMBRACE is the home automation app developed by the team of students from the IT department. Several studies (e.g. Brohus H. et al., 2010) have shown that even if the most efficient technologies are implemented in a building, the behaviour of the final user remains the major influence on the energy consumption. Based on this statement, the students have designed an intuitive and easy-to-use application for tablet, which gives feedback to the user in order to help him/her manage his/her energy consumption in a better way. Some parameters can be controlled automatically by the app, such as the opening of the motorized windows of the south and north façades, or the ventilation rates. On Figure 13 can be seen an example of feedback given by the app to the user about his/her daily energy consumption.

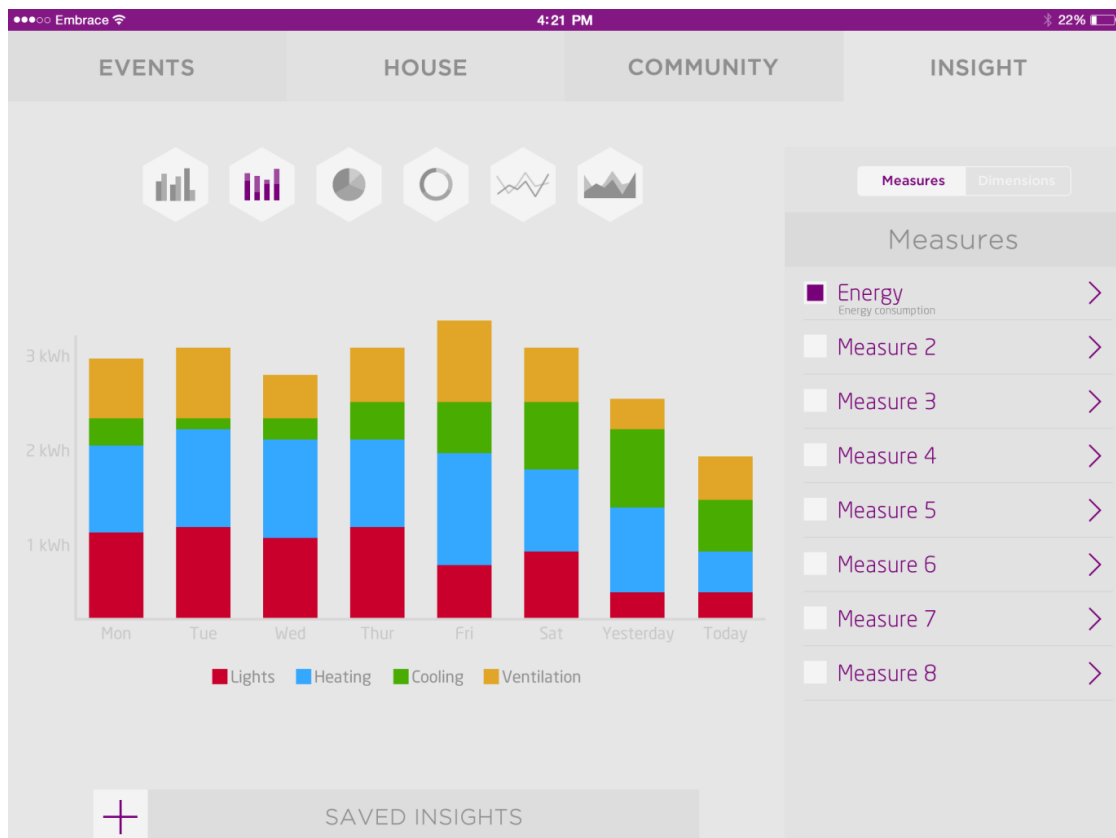


Figure 13 – Example of feedback from the app to the user about his/her energy consumption

2. Thermal properties of the envelope

The location of EMBRACE on the roof top of an existing building required designing a light weight structure, entirely made of wood, and the thermal mass of the house was therefore reduced. A thick layer of insulation was installed in the envelope, as it is the basics of the construction of any passive house. It enables to minimize the heat losses and therefore the energy consumption of the building.

2.1. Thermal insulation

Due to the severe Danish weather conditions and the desired optimal energy performances, the envelope has been designed with high levels of thermal insulation, consisting of glass wool. Glass wool has been selected taking into account and balancing different factors like thermal conductivity, eco-friendliness, constructability, fire safety, acoustics, cost and possible sponsorships. The U-values of the different constructions are presented in Table 5, the total transmissions of the envelope in Figure 14. The detailed construction layers of the external walls and the roof can be found in Table 6 and Table 7, and the reader can refer to “Annex 1: House envelope, materials properties” for details about the composition of the other construction layers.

Table 5 – Envelope thermal transmittances

Construction	U-value (W/m ² K)
External wall	0,08
Roof	0,085
External floor	0,1
Internal walls	0,38
Internal floor	0,25
Glazing 1 st type	U-window 0,83
Glazing 2 nd type	U-window 0,79

EMBRACE transmissions Total 41,7 W/K

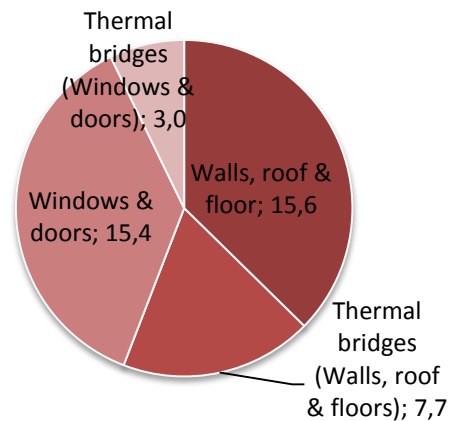


Figure 14 – Specific thermal transmittance, obtained applying the envelope surfaces (W/K)

Table 6 – Characteristics of the south external wall

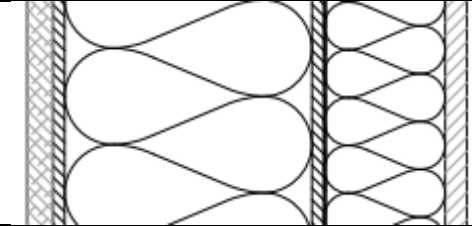
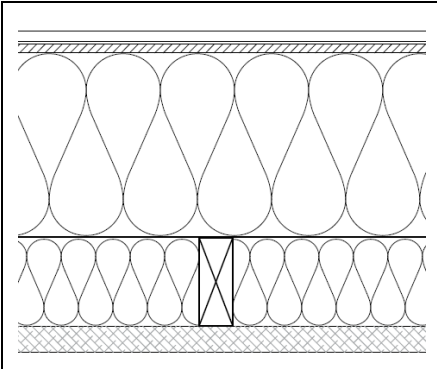
	Exterior wall (from outside to inside)	Plywood – wind protector	Glass Wool	Glass Wool	Vapour barrier	Glass Wool	Gypsum
Thermal conductivity (λ)	W/(mK)	0,14	0,03	0,03	0,2	0,03	0.42
Density (ρ)	kg/m ³	530	30	30	620	30	1200
Specific heat (c)	J/(kgK)	1800	670	670	1500	670	837
Thickness (d)	m	0,015	0,195	0,12	0,0002	0,045	0,013

Table 7 – Characteristics of the roof

		Glass PV Panels	Wood Beams	OSB	Glass Wool	Vapour barrier	Glass Wool	Acoustic cladding
Thermal conductivity (λ)	W/(m·K)	1,06	0,14	0,13	0,03	0,2	0,03	0,072
Density (ρ)	kg/m ³	2500	450	650	30	620	30	480
Specific heat (c)	J/(kg·K)	840	2500	2100	670	1500	670	900
Thickness (d)	m	0,004	0,2	0,012	0,245	0,0002	0,095	0,025

2.2. Thermal inertia

Thermal inertia is an important design parameter to consider when designing a house for the Solar Decathlon, because of the narrow temperature range that must be maintained indoors, independently from the outside conditions that may vary significantly. Thermal inertia is usually used to describe the capacity of a material or a building element to store thermal energy, delaying the heat transfer. An object has a high thermal inertia when its temperature varies slowly in time, while the surrounding environment is subject to rapid temperature variations. The thermal inertia depends by the heat capacity (J/kg·K), the superficial mass (kg/m²) and heat conductivity of the material (W/m·K).

The effects of a high thermal inertia are particularly evident in summer period because of the elevated temperature fluctuations and intense solar radiation. In particular, the effect due to thermal inertia of a building component is measurable considering two properties which can be described analysing the heat wave and which can be assessed according to EN ISO 13786:

- The thermal phase shift (Δt) is the period of time (hours) the heat wave takes to flow from outside to inside through a building material.
- The damping f , quantifies the reduction of amplitude of the heat wave passing through the considered element. It is a dimensionless number, smaller than 1, given by the ratio between the peak flow through the considered material and through the same material without thermal mass.

As a rule of thumb, it is possible to say the thermal phase shift is mainly influenced by the mass and the damping by the level of thermal insulation (Casini M., 2009).

In order to determine those two parameters in the case of EMBRACE, the building has been simulated dynamically in the program IDA-ICE with time steps of 3 minutes. The simulated day, corresponds to the cooling design day in Paris. This is the warmest day based on ASHRAE IWEC¹ database (16-July-2014), used later on to size the cooling installation.

The south façade wall is here presented as an indicator of performance of the entire envelope.

The phase shift has been here analysed as the difference in time, between the moment of maximum outside surface temperature and the time at which the maximum surface temperature inside is recorded. This simulation has been performed without cooling sources in the indoor space.

The damping is here expressed as the ratio between the maximum variation of the temperature of the external surface and that of the internal one ΔT_e , and ΔT_i respectively, where the average temperature of the inner surface is used as reference base value.

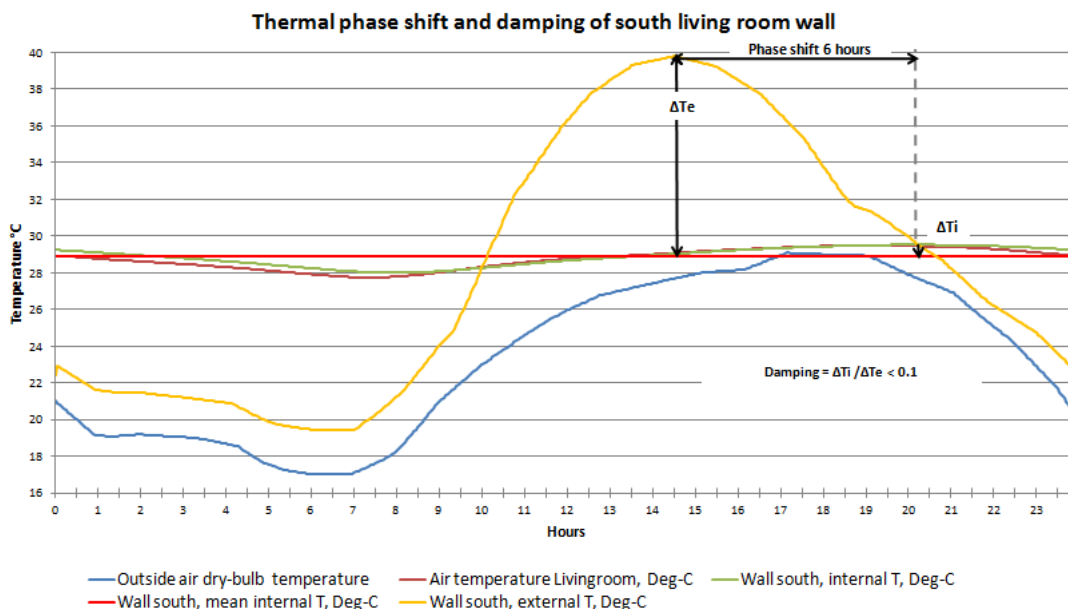


Figure 15 – Heat flux shift obtained with data from IDA-ICE 4.6 program

¹ ASHRAE is the American Society of Heating, Refrigerating and Air Conditioning Engineers. The IWEC is the International Weather for Energy Calculations, developed by ASHRAE; the data can be found online at: http://www.equaonline.com/iceuser/ASHRAE_IWEC.html

The maximum outdoor temperature is reached during the 14th hour (2:30 pm) while the indoor one during the 20th hour, resulting in a thermal shift of around 6 hours. This value can be accepted in case of light structures, but the optimal range suggested is 8-12 hours (see Table 8).

On the other hand the fluctuation of indoor temperature results smooth. 0,6°C is the maximum daily change of temperature of the wall surface, compared to its average temperature. This results in a relatively small damping ratio (< 0,1 for the analysed day) which means low thermal excursion and consequently high indoor thermal comfort.

The values are double checked with simple hand calculations, in order not to rely only on a simulation program. For homogeneous solid elements, the phase shift Δt , expressed in seconds, and the damping ratio f can be obtained with the following equations:

$$\Delta t = \frac{L}{2} \sqrt{\frac{24 \cdot 3600}{\pi \cdot \alpha}} \quad (\text{s}) \quad \text{and} \quad f = e^{(-L \sqrt{\frac{\pi}{\alpha \cdot 24 \cdot 3600}})} \quad (-)$$

Where:

L is the thickness of the element (m),

$\alpha = \frac{\lambda}{\rho \cdot c}$ is the thermal diffusivity of the element (m²/s),

λ is the thermal conductivity (W/m·K),

ρ is the density (kg/m³),

c is the specific heat (J/kg·K)

Applying those equations to a simple system of 36 cm of glass wool insulation, $\Delta t = 6,8$ h and $f = 0,17$ are obtained. The values obtained through simulation and hand calculations are similar and can therefore be further analysed. According to Table 5, EMBRACE has a poor quality in terms of thermal phase shift, but a good quality in terms of damping ratio, close to optimal. A heat wave hitting the house would be attenuated but would enter the building relatively fast. Such results were expected because of the lightweight structure chosen for EMBRACE.

Table 8 – Thermal inertia and quality of the building envelope (Italian Ministerial Decree, June 26, 2009) (Casini M., 2009)

Thermal phase shift (h)	Damping ratio f	Quality
$\Delta t > 12$	$f < 0,15$	Optimal
$10 < \Delta t \leq 12$	$0,15 \leq f < 0,3$	Good
$8 < \Delta t \leq 10$	$0,3 \leq f < 0,4$	Sufficient
$6 < \Delta t \leq 8$	$0,4 \leq f < 0,6$	Poor
$\Delta t \leq 6$	$f \geq 0,6$	Bad

3. HVAC design process

In this section are described the design process of the HVAC systems, the heating and cooling production sources, as well as the chosen products implemented in EMBRACE, and how they interact with each other.

3.1. Design strategies

The strategies here presented are related to the real Versailles prototype design. Other strategies have been adopted for the Copenhagen ideal scenario, such as sharing the HVAC systems among five dwellings and exploit the heat from the exhausted air of the underneath existing building. The present report focuses on the real dwelling, constructed for the Versailles competition, so the installations described are the ones designed for this prototype. EMBRACE is a plus-energy house, therefore keeping the energy balance positive represents one of the main design parameter to keep in mind during the conception.

The first approach in the design of a plus-energy house is obviously to reduce the demand, implementing passive strategies such as shading and cross-natural ventilation. The high level of insulation, the air tightness and the shape of the envelope are the most important parts of the passive design, because they minimize the heat losses to the outside. The amount of windows and their orientation have been studied in order to keep a balance between the daylight, the heat losses (especially for the skylights), and the cross-natural ventilation. The south window and the north window situated in the bedroom can be opened through the home automation app, favoring the air movement across the house. To reduce the heat gains in summer, shadings have been implemented in the form of external sliding panels in front of the south window, and fixed wooden lamellas above the kitchen skylight. In addition, the Weather Shield acts as a thermal buffer zone and reduces the wind speed and hence the infiltration.

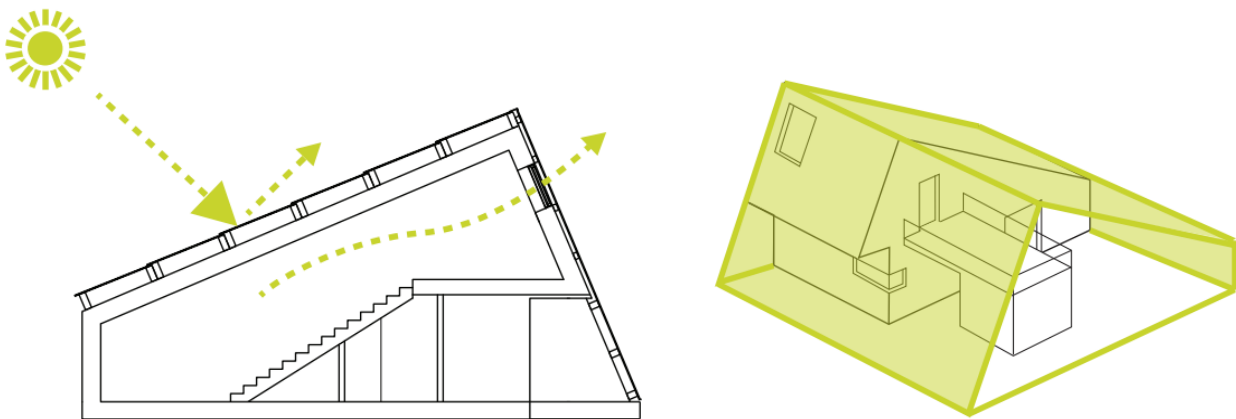


Figure 16 – Passive strategies: main concepts regarding shading, natural ventilation and Weather Shield/buffer zone

Once the demand has been reduced to a minimum, the second step consists in implementing the systems able to generate the remaining needs in heating and cooling in an efficient way. The amount of electricity to be produced by the photovoltaic (PV) panels can then be defined in order to proceed in the next steps of the design.

3.2. Heating and cooling production

Because of the constraints of the competition and the irregularity of renewable energy production, several sources have been implemented to produce heating and cooling for EMBRACE. The complexity of the whole HVAC system comes from the diversity of these sources and their interaction. The different sources and their usage are represented in Figure 17.

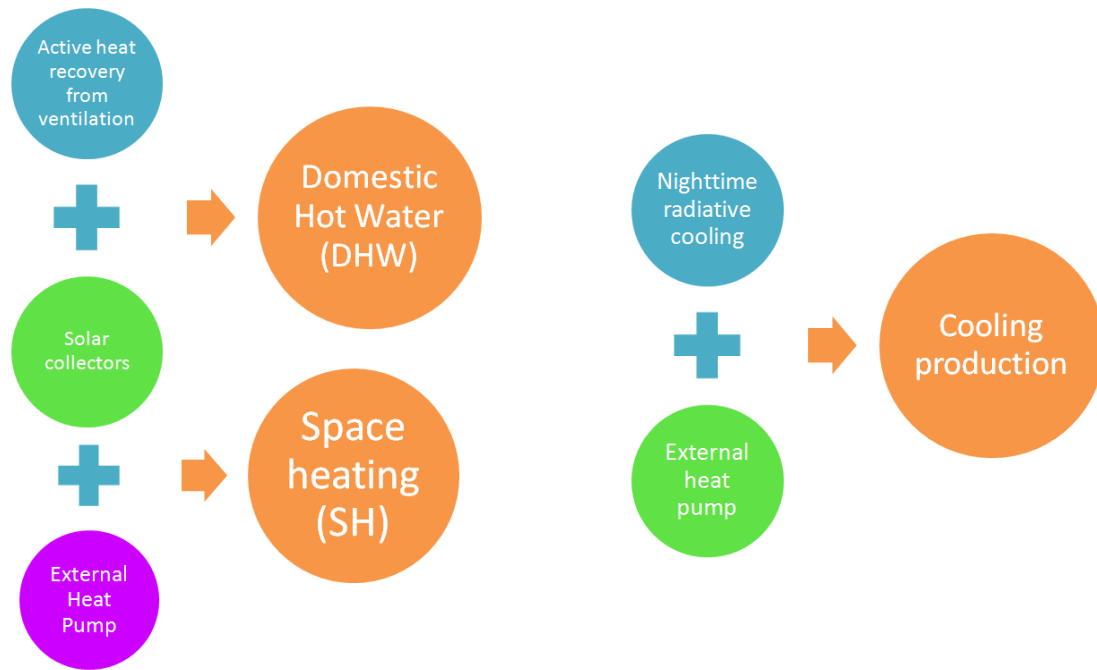


Figure 17 – Heating and cooling production schemes

For heating production, thermal solar collectors are mounted on the weather shield: they produce hot water that is mainly used for domestic hot water (DHW), but also for space heating (SH) in spring and autumn. The solar resource being irregular and unpredictable, other systems must be implemented: the ventilation system includes a compressor, which acts as active heat recovery and transfers heat from the air exhausted by the mechanical ventilation to the DHW tank, thanks to a thermodynamic cycle. This system is integrated in the Compact P unit from Nilan (see paragraph 3.3.2). The DHW tank is equipped with a backup electric heater and two spiral heat exchangers (one connected to the solar collectors, the other one being the condenser of the ventilation heat recovery, see Figure 18). The DHW is also used to supply the appliances of the house: washing machine, dishwasher and dryer are indeed connected with the domestic hot water circuit.

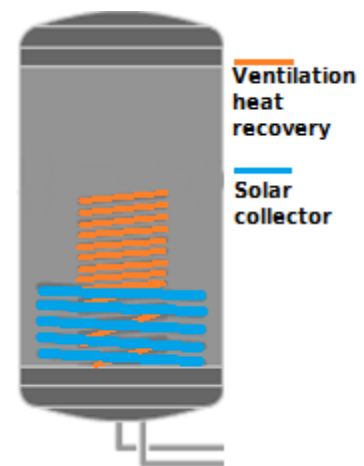


Figure 18 – Coil heat exchangers, of the DHW tank, integrated in Nilan Compact P

The solar collectors are not sufficient to cover the space heating demand in winter; therefore another system has been implemented: an air-to-water external heat pump is placed outside the house for this purpose, and connected to a storage tank in the technical room.

For cooling, the main concept is to exploit nighttime radiative cooling with unglazed solar collectors. Cold water is circulated in the floor and stored in a tank, during the day. In this way the water subtracts heat and cools the rooms; as a result the water stored in the tank is warmed up. At night, the warmed water is circulated in the unglazed collectors, where it is cooled down by radiation towards the sky. The cold water

is then stored again in the tank for usage during the next day. In case this free cooling is insufficient, the external air-to-water heat pump is reversible and can be used to produce cold water as well. Both the space heating and cooling water are first stored in a buffer tank and then circulated in a dry radiant floor system. During the transition period if the radiant floor is used for heating and cooling is needed, it is not possible to provide it through the hydraulic system, for more detail see Chapter V.2. The HVAC is still able to cool thanks to the mechanical ventilation. Indeed, as above mentioned, the Air Handling Unit (AHU) is provided with an independent thermodynamic cycle which allows to condition the supply air. Vice versa if the radiant floor is in cooling mode.

It is possible to distinguish two heating/cooling carriers: on the side of the solar collectors, water with glycol is used to avoid freezing of the fluid while water is stored and circulated in the radiant floor and DHW circuit. The heat provided by the collectors, or cooling in case of nighttime radiative cooling, is transferred through spiral heat exchangers so that the two mediums do not enter in contact.

Graphical representations of the heating and cooling production concepts are presented on Figure 19.

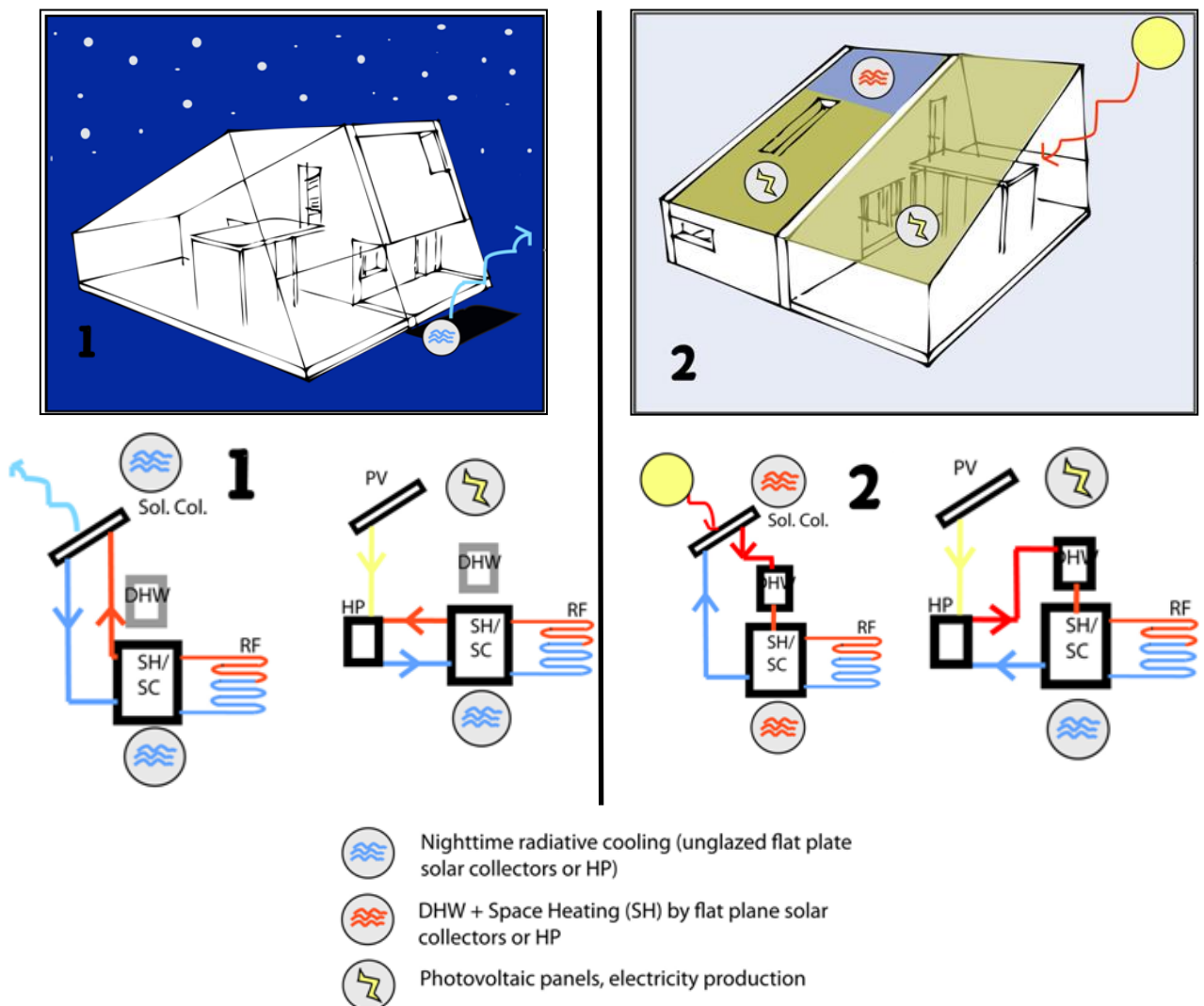


Figure 19 – Scheme of the heating/cooling/electricity strategies

3.3. Description of the specific system adopted

3.3.1. Solar thermal collectors

The solar thermal collectors are mounted on the upper part of the weather shield, with connection pipes going down to the technical room. The company BATEC Solvarme A/S provided two copper collectors of 2,2 m², summing up to 4,4 m² absorber area. They were integrated in the weather shield, below the glazing panels and above an insulation layer of 10 cm of glass wool. The system includes an expansion vessel of 20 liters and does not allow drain back. The technical data of the collectors can be found in Annex 3: Solar collectors' data.



Figure 20 – Photograph of the solar thermal collector module before its mounting on the Weather Shield

3.3.2. Compact P

The Compact P unit is a product developed by Nilan. Below are described all its features: it includes a ventilation system with passive and active heat recovery, and a DHW tank of 180 L.



Figure 21 – Features of the Nilan Compact P unit (picture based on Nilan Compact P brochure¹)

When the heat pump cycle is active (active heat recovery), between the exhaust air and the condenser in the DHW tank, it is possible to define the COP and heating power Q_w (W) for sanitary hot water as a function of the exhausted amount of air q_v (m³/h).

The following chart is derived from the Compact P datasheet, for a tank temperature of 41°C, room temperature of 20°C and outdoor temperature of 20°C in accordance with EN 255-3.

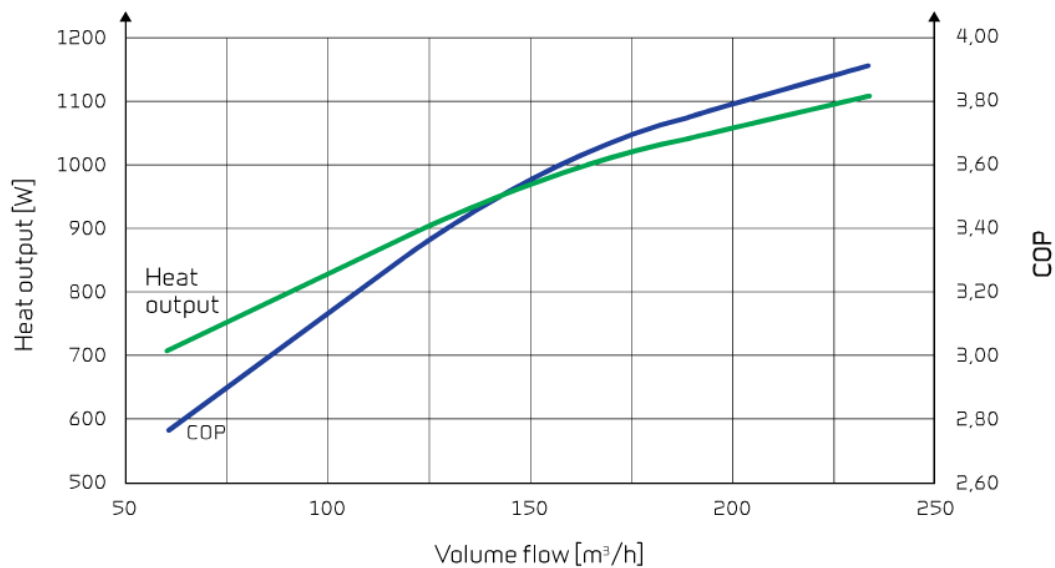


Figure 22 – COP and heat output for sanitary hot water as a function of the volume flow
Data from the Nilan Compact P datasheet

Three steps have been designed for the mechanical ventilation flow rate, in function of the different activities inside the house. When the occupants of the house are at home (2 people), the ventilation system runs in the normal mode. If they are receiving guests or if they are doing activities producing a lot of moisture, such as cooking, the forced mode is activated, providing a higher flow rate. When the occupants leave the house to go to work or on holiday, the “away mode” is activated in order to minimize the energy consumption, still providing a minimum air change.

Table 9 – Three steps of flow rate, defined for the demand controlled mechanical ventilation

	Normal mode	Forced mode	Away mode
Overall air flows	Exhaust	Exhaust	Exhaust
l/s	30,3	42,3	4,5
m ³ /h	109	152	16
air change h ⁻¹	0,83	1,16	0,12
Derived from	Category I from DS/EN 15251	4 x 10 l/s/person	

The “away mode” should not be considered concerning the production of sanitary water. With the condition of the above graph and table the heating power ranges from 850 W to 980 W, and the COP ranges from 3,2 to 3,5 for the normal mode and forced mode respectively.

The heating and cooling performance on the supplied air side will not be described further here, since the Compact P is an available product on the market and more information can be retrieved from the manufacturer. A short extract from the data sheet, describing the available operation modes, can be found in Annex 9: Nilan Compact P functions.

3.3.3. Air-to-water heat pump

The heat pump integrated in the system is a reversible air-to-water heat pump. The chosen product is Altherma from Daikin. It includes an external and an internal unit. The external unit is the heat pump in itself and the indoor unit consists mainly of the heat exchanger, the circulation pump and the controlling

equipment (other elements are present such as a water filter, control panel, release valve in case of over pressure and so forth).

The external module is placed next to the West façade, close to the technical room, 40 cm away from the wall, with connections to the storage tank. Because of issues related to noise, the minimum length of the pipes between the two units is three meters.

More detailed characteristic of the heat pump will be described afterwards (see chapter “IV.2. Performance of the selected heat pump”).

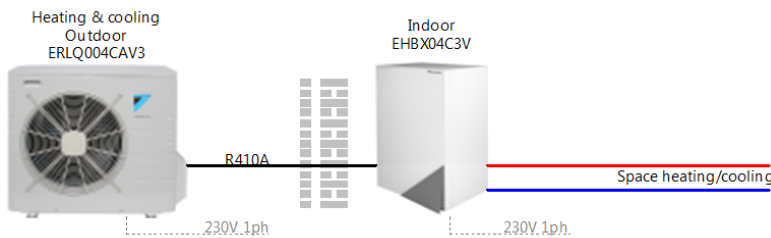


Figure 23 – Principle of the Daikin heat pump



Figure 24 – Photograph of the Daikin heat pump installed on the wall of the technical room of EMBRACE

3.3.4. Unglazed solar collectors

The unglazed solar collectors have been installed on the north terrace, to exploit nighttime radiative cooling. Four bands of 0,6 x 6 m of panels were expected to be installed on the northern side of the house outdoor deck, summing up to 14,4 m². But for installation practical issues the amount has been reduced to two bands of the same size, for a total of 7,2 m². The technical data can be found in Annex 3: Solar collectors' data. Simulation and calculation supported by relevant literature (see chapter VII) have shown that in Paris and Copenhagen the cooling power can be estimated to range from 0,2 and 0,9 kWh/m² per night, depending by different factors such as the flow rate, sky clearness and so forth. Considering the area of panels installed, this leads to a cooling energy between 1,5 kWh and 6,5 kWh per night, which represents 11% and 47% of the maximum daily cooling need estimated in Paris. In fact 13,9 kWh of cooling have been estimated for the design day. If 14,4 m² of panels were installed as expected, the estimated power provided, would have covered between 22% and more than 90% of the total cooling need. The more detailed investigation about the cooling potential of this technology can be found in the following paragraphs where both the result from TRNSYS simulation tool (see chapter VII.5.) and experimental outputs (see chapter VII.0.) are analysed.

The implemented cooling system is based on one of the cheapest solar collectors on the market making this solution very affordable. Indeed the unglazed solar collectors are simply polypropylene hoses normally used to produce hot water at low temperature because of the high heat losses. Conventionally they are used to supply outdoor swimming pools during summer. In the case of EMBRACE, the high heat losses are exploited as a benefit, allowing a more efficient production of cold water.



Figure 25 – Views of the unglazed solar collectors installed for EMBRACE

3.3.5. Terminal unit: radiant floor¹

Radiant floor is installed both in the ground floor and in the first floor, for heating and cooling purpose. A water-based heating and cooling system has been chosen as it is commonly known as the most efficient kind of system, given the high heat capacity of water, and because it is able to provide homogenous comfort conditions (Babiak J. et al., 2007). As explained in the architectural description, the main concept of EMBRACE is to reduce to the minimum the living area, in order to densify the cities. The remaining indoor space must then provide a high quality environment to compensate for the reduction of space. To achieve this goal, an underfloor heating/cooling system was preferred to standard radiators, for multiple reasons:

- It guarantees a free use of the space. The concept of EMBRACE focuses on reducing the dwelling size, and opening it to shared spaces that become part of the living space. Therefore, the house (the thermal envelope) is relatively small. Placing radiators in several places on the walls would hinder the use of the limited space available.
- Once it is installed, the underfloor system requires less maintenance or cleaning than radiators.
- The large surface offered by the floor for heating enables to decrease the temperature of the water supply. Thus the underfloor system enables to use both low-temperature heating and high-temperature cooling. This is critical in a highly sustainable building like EMBRACE, because the heat pump efficiency increases when the ΔT it has to overcome is smaller.
- The underfloor system provides more comfortable environment thanks to its large surface: a good uniformity of operative temperature in the space is achieved. Radiators produce thermal plumes that can create draught or temperature asymmetry in the room.

Both ceiling and floor panels can offer the advantages described above. Because of the buoyancy effect, floor is more efficient in heating and ceiling in cooling, as described also in Figure 26, which represents the heat transfer coefficients of different combinations.

¹ Content partially based on “Subject 3 – Building Services and Energy – Solar Decathlon Team 2014” (Gennari L. and Péan T., 2014).

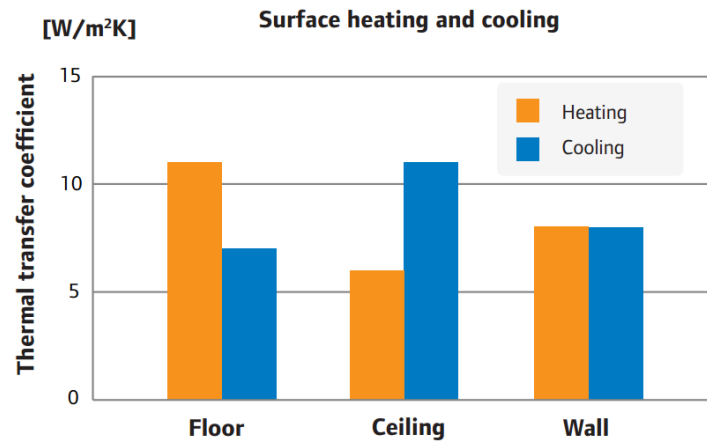


Figure 26 – Heat transfer coefficients of surface heating and cooling (Uponor (2013)- Free cooling guide)

The floor solution was chosen because more efficient for heating, which is the highest demand for the Danish climate. An additional system could have been integrated in the ceiling, in order to provide cooling with better performances, but the affordability of the house had to be taken into consideration.

Therefore, an underfloor system has been integrated in the whole house, to provide both heating and cooling. A dry lightweight system was chosen over a wet system, which would have requested to embed the pipes into a screed. A wet system would increase the weight of the house, which is problematic because of the transport of the house by trucks to Paris, and because it is aimed at being constructed on the rooftop of existing buildings that were not conceived for it and must withstand this additional weight. A wet system also has a bigger environmental impact because of the concrete screed, and it complicates the assembly because of the connection between modules. The dry system has less thermal mass to dampen the indoor temperature, but its response time is faster, making the control more reactive. Indeed a low inertia system suits better the narrow temperature range in the competition rules. Furthermore in case of leakages or maintenance, a dry system is easier to be fixed.

The solution chosen for EMBRACE is a dry radiant floor produced by Uponor and designed for timber suspended floors. It consists of aluminum heat emission plates where the PEX pipes can be inserted. The floor lies on timber beams, and in between a layer of thermal insulation is positioned. The radiant floor is divided into 6 different loops intended to control better the power output in the different rooms. These loops are controlled with thermostats and relative humidity (RH) sensors. The different loops and their control are described in Table 10 and Figure 29.

The mixing station is another important element of the radiant floor systems. It consists basically of the circulation pump (on/off three steps of speed – Grundfos ALPHA2) and a three-way valve that connects the return water with the supply, allowing recirculation. The control system, based on the data received from the room thermostats, define the amount of water to be recirculated to reach the desired supply temperature. The utilized control is Uponor Radio 24V DEM. It controls also dynamically the opening of the radiant floor manifold actuators. In this way the water flow supplied to each loop is balanced automatically, in order to provide the needed power to maintain the desired room set point temperature, see Figure 28.



Figure 27 – Chosen system from Uponor

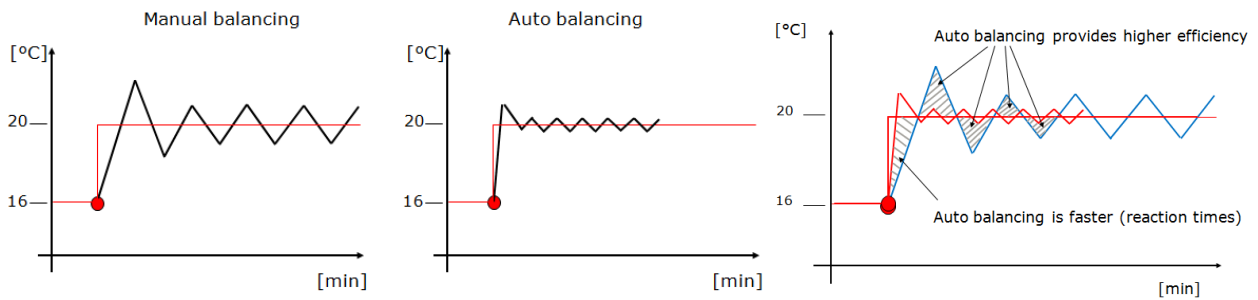
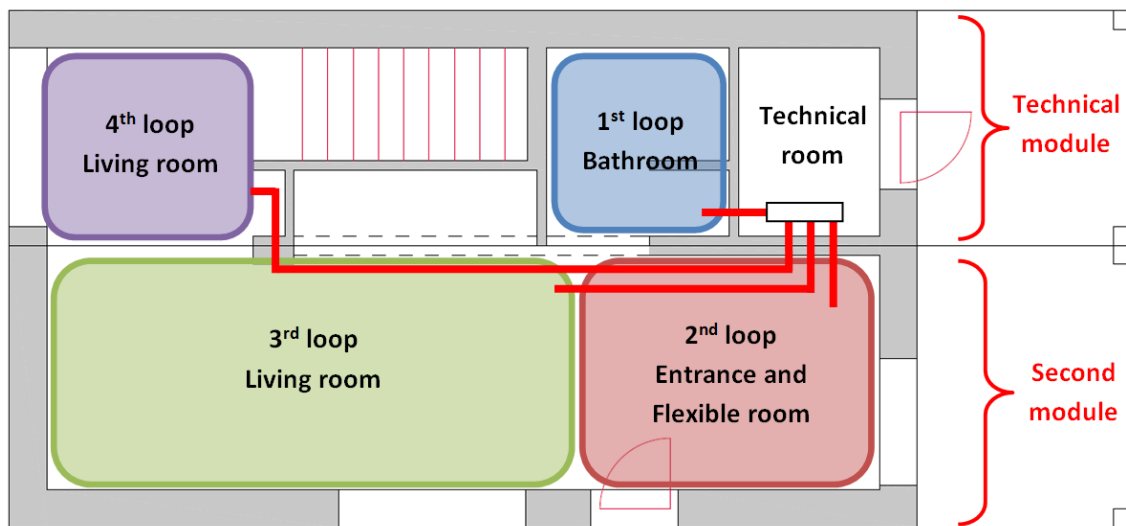


Figure 28 – Comparison of the accuracy obtained by opening radiant floor loops’ actuators manually or automatically (Uponor 2014. “Radio 24V DEM”, Training Material)

Table 10 – Radiant floor loops and control

Loop number	Location	Temperature control	RH control
1	Bathroom	1 thermostat	1 RH sensor
2	Entrance and flexible room	1 thermostat	1 common RH sensor
3	Living room	1 common thermostat	
4	Living room – Below the stairs		
5	Bedroom	1 common thermostat	1 common RH sensor
6	Bedroom – Above the stairs		

See “Annex 11: Mechanical and instrumentation drawings from PD#6, Team DTU” for more detailed plan views of the radiant floor.



BOTTOM MODULE PLAN

Scale: 1:100

Figure 29 – Module division and radiant floor loops, ground floor

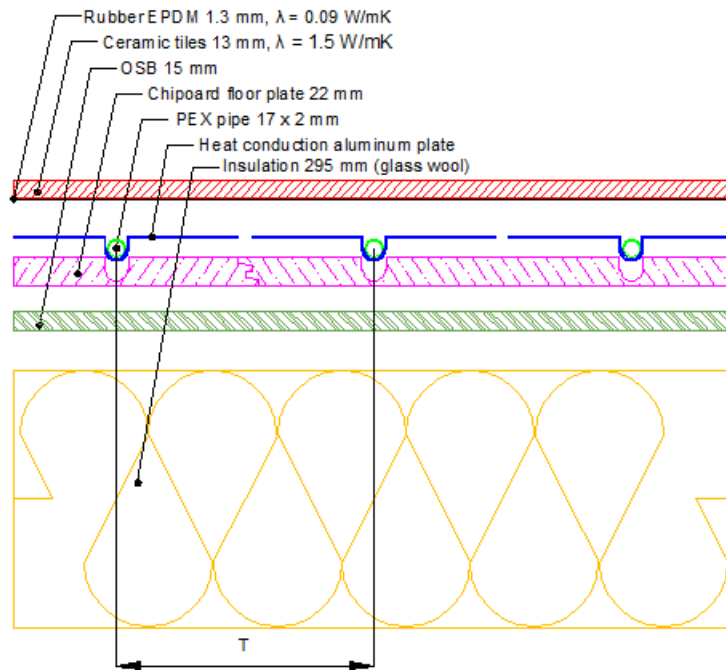


Figure 30 – Construction layers of the designed radiant floor

3.4. Hydraulic scheme¹

The chosen heating and cooling production and distribution systems are described in the previous section. They need to interact and to be connected in the complete hydraulic scheme of the house, which is presented in the drawing ME-201, available in the Annex 11: Mechanical and instrumentation drawings from PD#6, Team DTU. The present explanations are intended as a complement to the drawings ME-211/212/213 and ME-221/222 that describe the operation modes of the systems. The reader is invited to simultaneously look at the drawings and read the following explanations to understand better the functioning. The overall system described in ME-201 has been split in different loops in order to explain the operation loop by loop, and this division in loops (collectors loop and radiant floor loops) has been kept here. The following description corresponds to the hydraulic scheme as it was intended by the students for EMBRACE. Some adaptations have been made for the prototype built in Versailles, because of financial, time-related or complication level issues. Those differences are mentioned in the footnotes (if no difference is mentioned, the system was working in the same way in both cases).

3.4.1. Heating modes

The heating system has three possible sources: the solar resource collected by the solar collectors, the heat of the outside air “captured” by the external heat pump, and the heat recovered from the ventilation air (supply or exhaust). It is important to note that the circuits connecting the solar collectors, the heat pump and the two heat exchangers do not contain water, but an antifreeze mixture (brine or water and glycol) to avoid freezing issues in winter².

Collectors loop (ME-211)

The first operation mode of this loop uses the first heat source: it represents the case of sunny days, when the solar irradiation is strong enough to supply the house for both DHW and space heating. The water

¹ Content based on “Technical Note on Heating and Cooling Modes for Deliverable#6” (T.Péan, 2014).

² In Versailles, pure water was used in all systems as there was no risk of freezing in July, and because the heat capacity of pure water is higher than the one of a mix of glycol and water.

heated by the solar collectors can reach high temperatures (up to 70-90 °C), thus it is first circulated in the heat exchanger of the DHW, where the expected temperature is higher (~55 °C). Then, the same water is circulated through the heat exchanger of the storage tank¹, where the temperature demand is lower (~35°C for space heating through a radiant floor). The large storage tank is here used to store a maximum of heat during the day, in order to possibly use it at night if needed.

The second operation mode corresponds to the case of low solar irradiation. In that case, the hot water produced by the solar collectors does not reach levels acceptable for the use of DHW, so the heat exchanger of the DHW tank is bypassed and the solar collectors supply directly the storage tank. This mode can also be activated when the DHW tank is full.²

Radiant floor loop (ME-212)

In this loop, the external heat pump is activated when needed. In the first operation mode, the water in the tank is warm enough to supply directly the radiant floor, therefore the heat pump is not activated. If the temperature in the tank drops down, the heat pump is activated. In this case, part of the hot water thus produced is directly supplied to the radiant floor, the rest is stored in the storage tank. When the hot water tank is warm enough, the system goes back to the first operation mode³.

DHW production (ME-213)

As seen before, the solar collectors are used to supply DHW. If the production is not sufficient, the Compact P unit from Nilan is able to supply the DHW tank by recovering heat actively from the ventilation air. In the summer case, the heat is extracted from the supply air, in the winter case, the heat is extracted from the exhaust air (the compressor is reversible). An additional backup electrical coil is implemented in the DHW tank for safety reason, to ensure always the possibility to provide DHW at the temperature required by the competition (43 °C).

3.4.2. Cooling modes

As for the heating, there are different cooling sources in the system: radiative nighttime cooling and the reversible heat pump. As the radiative cooling occurs during the night, the operation mode needs to be described during a 24 hours cycle.

Collectors loop (ME-221)

During the day, the solar collectors are used to supply the DHW tank. At night, the unglazed collectors are used to cool down the warm water that was stored in the storage tank during the day through nighttime radiative cooling (see chapter VII for further information).

Radiant floor loop (ME-222)

The functioning of this loop for cooling is similar to the heating mode. The tank is primarily used to supply directly the radiant floor. The heat pump is activated when the storage tank is not cold enough, and it supplies both the radiant floor and the storage tank⁴. The only notable difference is that the cold water is

¹ In Versailles, there was no need for heating, so the solar collectors were only connected to the DHW tank; they could not supply the storage tank.

² Inexistent mode in Versailles for the same reason.

³ In Versailles, the heat pump was only connected to the storage tank, not to the radiant floor.

⁴ In Versailles, the heat pump was connected only to the storage tank, not to the radiant floor.

inserted at the bottom of the tank, and the warm water is taken from the top of the tank (this difference between heating and cooling mode is made possible due to the 4-way alternative valve).

4. Discussion

EMBRACE reached a satisfactory level of 8 out of 20 teams in the overall ranking of Solar Decathlon 2014 in Paris. Some design decisions had to be arbitrated, which sometimes did not prove to be adapted. The double-skin concept of EMBRACE possesses certain qualities, but it has probably not been studied thoroughly and optimized sufficiently. The Sheltered Garden offers a pleasant space to live in, but it might get overheated in summer, despite the shading provided by the integrated PV tiles. The covered terrace also has its advantages, but Danish citizens might prefer to enjoy fresh air and direct sunlight when they are forced to stay indoors most of the winter period. The design of the openings in the north façade has also not been studied in details by lack of time and finance; therefore the natural ventilation fluxes have not been optimized.

In winter, the climate under the Weather Shield is milder than the outside conditions, but the effects are mainly limited to protection from the wind and the rain, since the temperature would only reach few degrees above the outside temperature. The danger of such a closed space is that the inhabitants would try to heat it up in an inefficient way (with infrared heaters for example), while the building has been designed in the exact opposite way. Maintaining the sheltered garden not completely air tight is a strategy to dissuade the inhabitants from this misbehaviour. If they try to heat the sheltered garden, it would be almost impossible to reach acceptable thermal comfort levels and it would also affect the energy consumption in a drastic way, with the effects directly visible through the app.

Other reservations can be expressed on the choices of products and materials. The sponsors are obviously gratefully thanked for supplying the team with their products, but it can be unfortunate if it influences the design. The choice of the insulation material shows an appropriate example: glass wool was selected mainly for sponsoring reasons, while the environmental impact of such material can be discussed. Regarding the HVAC system, EMBRACE is over-equipped for a house of its size. This has again been possible thanks to the numerous sponsors, but it resulted in a highly complex setup. Numerous efforts have been drawn by the students all along the projects to try and integrate all products into one overall functional HVAC system, but it would be unrealistic to apply such a strategy in a real professional case. In this matter, EMBRACE remains a prototype which would require a large amount of adaptations in order to be built in a real urban scenario.

III. Detailed design of the radiant floor

Once the radiant floor option is chosen as the terminal unit for the emission of heating and cooling in the house, the system needs to be sized in order to be adapted to the special case of EMBRACE. First, some physical and normative limitations set a frame for the design of the radiant floor. Computer simulation tools have been used to define the loads of the house, which were then used to size the system using the methods available in the European standards. The results were verified and corroborated with a 2D heat transfer computer simulation.

1. Radiant floor limitations¹

Before starting the specific design of a radiant floor, it is necessary to point out which parameters need to be investigated and studied more in detail. This is the reason why the performances and limitations of radiant systems are exposed here.

1.1. Heat flux

The heat flux expresses the ability of a surface to transfer heating or cooling to a room. Based on EN 1264/EN 15377, the following equations can be used to express the heat flux.

$$\text{Floor heating, ceiling cooling: } q = 8,92 \cdot |T_{s,m} - T_i|^{1,1} \quad (W/m^2)$$

$$\text{Wall heating, wall cooling: } q = 8 \cdot |T_{s,m} - T_i| \quad (W/m^2)$$

$$\text{Ceiling heating: } q = 6 \cdot |T_{s,m} - T_i| \quad (W/m^2)$$

$$\text{Floor cooling: } q = 7 \cdot |T_{s,m} - T_i| \quad (W/m^2)$$

Where:

q is the heat flux in W/m^2

$T_{s,m}$ is the average surface temperature. This value is limited by dew point and thermal comfort.

T_i is the room design operative temperature

The variation of q is directly depending on the heat transfer coefficient, in function of the considered mode (heating or cooling) and the used surface.

1.2. Heat transfer coefficient

The heat transfer coefficient is an expression of how much power a surface is able to transfer to a room per m^2 , per degree of temperature difference between the surface and the room. Different surfaces orientations correspond to diverse heat transfer coefficients as shown in Figure 31, for heating and cooling respectively.

¹ Text and pictures partially derived from Uponor Corporation (2013). "Free cooling guide-cooling integration in low energy houses"

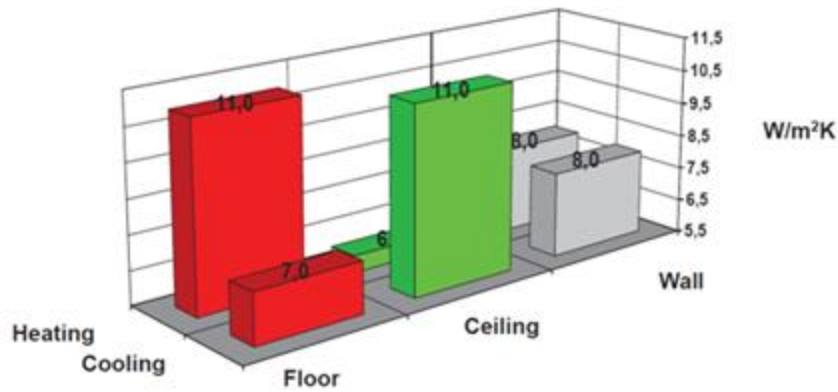


Figure 31 – Heat transfer coefficients of surface heating and cooling (Bjarne W. Olesen, 2012)

Due to differences in air density that produce natural convective motions, the floor provides the best heat transfer coefficient for heating while the ceiling provides the best heat transfer coefficient for cooling. For comfort conditions, the floor surface temperature should stay in the range between 19 and 29°C (EN 1264). The heat transfer coefficient of a radiant floor is 11 and 7 W/m²K for heating and cooling respectively. This limits the maximum power that it is possible to provide with a floor to around 45 and 95 W/m² for cooling and heating respectively, depending on the desired indoor temperature.

1.3. Dew point limitations

The supply water temperature needs to be controlled so that the surface temperature of the emitter is always above dew point, in order to avoid condensation on the surface. The diagram in Figure 32 shows different dew point temperatures in function of the relative humidity (RH) level and room air temperature:

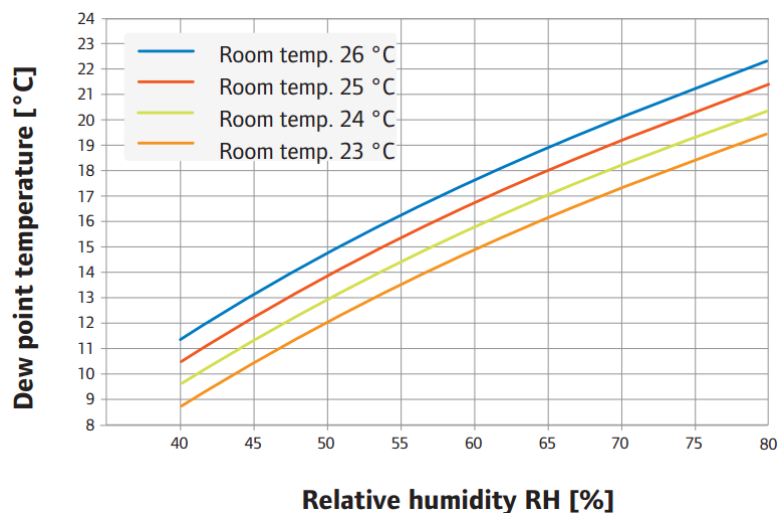


Figure 32 – Dew point temperature at different air temperatures and relative humidity levels (Uponor, 2013)

The dew point temperature can be derived in function of the relative humidity and air temperature with the following equations:

$$T_{dp} = 100 \cdot \left[\left(\frac{P_v}{288,68} \right)^{1/8,02} - 1,098 \right]$$

$$P_v = P_{v,sat} \cdot RH$$

$$P_{v,sat} = 288,68 \cdot \left(1,098 + \frac{T_a}{100}\right)^{8,02}$$

Where

T_a is the air temperature in °C

$P_{v,sat}$ is the saturation air vapour pressure in Pa

P_v is the air vapour pressure in Pa

RH is the relative humidity in %

T_{dp} is the dew point temperature in °C

2. Load calculations (IDA-ICE)

The heating and cooling loads are the basic inputs needed to size a radiant floor. They are necessary in order to proceed with the sizing method described in the standard EN 1264. For this project, the building simulation tool IDA-ICE has been used to define these loads. The model created in IDA-ICE has also been exploited to estimate the yearly energy consumption of EMBRACE and extract weather data.

The weather files used are Test Reference Year (TRY) for Copenhagen (Værløse) and ASHRAE IWEC 1.1 for Paris (Orly). The TRY weather data are composed from measured data of representative months to form a whole representative year. The ASHRAE IWEC 1.1 database contains "typical" weather files for 227 locations outside the USA and Canada. The International Weather for Energy Calculation (IWEC) files are derived from up to 18 years of DATSAV3 hourly weather data originally archived at the National Climatic Data Center (EQUA, 2013). Heating season is defined from October to April and cooling season for the remaining months.

Load calculations are instrumental to size the power demanded to cool or heat the different zones of the dwelling and reach the desired indoor environment. To perform load calculations, different parameters such as the boundary conditions, the building geometry and systems need to be defined; they are presented in the following sections.

2.1. Boundary conditions

The dwelling is expected to perform in both Copenhagen and Paris weathers. The most unfavorable conditions of both cases have therefore been used to size the systems. Consequently the heating power is defined in function of design values for Copenhagen, and cooling in function of Paris.

Table 11 – Boundary conditions for load calculations

	Heating	Cooling
Design case	Copenhagen	Paris
Type of simulation	Steady-state	Dynamic
Outside weather	Constant outside air temperature of -12°C	Design day of the weather file from Paris (highest outside air temperature of 30°C)
Solar radiation	0 %	From the weather file, with shading through external blinds to all windows, except for the north oriented ones
Internal gains	0 %	100 %
Set-point for indoor operative temperature	21°C	25°C
Natural ventilation	None	
Infiltration	0,2 ¹ ACH	

2.2. HVAC system definition

A 3D model has been constructed with the standard level of the software IDA-ICE 4.6, reproducing the last geometry and materials of the building. The heating and cooling sources are kept as simple as possible to avoid complications which could distort the results when performing load calculations. Therefore ideal heaters and coolers have been used in every zone, with a capacity of 1000 W each. Ideal heaters and coolers are simplified units used in IDA-ICE for simple estimations such as the load calculations, when the

¹ This value has been obtained by previous dynamic simulations performed by other team members, taking into account also the Weather Shield presence, with the program IESVE. This value is here considered reasonable also because close to the infiltration level for new constructions.

use of a detailed system is not motivated. They provide the necessary amount of heating/cooling, in the limit of the capacity given as input. They have no given physical location on any room surface and are not connected to the plant of the building. Physically, it is possible to think of it as a standalone unit with fixed performance parameters (IDA-ICE version 4.6 Manual, 2013).

A ventilation rate of 0,5 ACH is always provided through conditioned mechanical ventilation in order to fulfil the minimum requirement of air changes for residential building as defined in the Danish Building Regulation (BR10).

The obtained powers demanded have been afterwards used to design the radiant floor capacity and define if this technology is sufficient or requires to be supported with additional systems. This investigation is based on Standard EN 1264 and finite differences simulation program HEAT2.

2.3. Building geometry and operation

Geometry and envelope of the building, internal and external gains, schedule of the building devices and occupants are defined and presented in Table 12 and Table 13. The internal gains are not taken into account for sizing the heating demand. Conversely, they are fully taken into account to design the cooling system.

Table 12 – Internal gains as assigned in the IDA-ICE simulation model

Room	Artificial light (W/m ²)	Equipment (W)	Number of occupants	Activity level of occupants (met)	Area (m ²) in the IDA-ICE model
Flex Room	2,5	0	0,5 ¹	1 ²	11
Bedroom	2,5	0	0,5	1	23,4
Bathroom	2,5	0	0,5	1	3,3
Living room - kitchen	2,5	350 ³	0,5	1	24,8

Table 13 – Main thermal properties of the envelope as defined in the IDA-ICE model

Construction	U-value (W/m ² ·K)	Simplified layers
External wall	0,08	Gypsum (0,03 m), Glass wool (0,36 m, λ=0,03 W/mK), Plywood (0,03 m)
Roof	0,085	Plywood (0,03 m), Glass wool (0,34 m, λ=0,03 W/mK), Render (0,03 m)
External floor	0,1	Plywood (0,03 m), Light insulation (0,24 m, λ=0,026), Plywood (0,03 m)
Internal walls	0,38	Gypsum (0,013m), Glass wool (0,095 m, λ=0,037), Plywood (0,013 m)
Internal floor	0,25	-
Glazing 1 st type	U-window 0,83	3 Panes: G=0,63, LT=0,74
Glazing 2 nd type	U-window 0,79	3 Panes: G=0,4, LT=0,74

¹ ASHRAE Fundamentals Handbook (SI), 2001, suggests two persons for the first bedroom, plus one person for each additional bedroom. In this way two people are estimated and divided equally in the four zones of the house.

² The activity levels and the amount of clothing, defines how much heat (sensible and latent) and carbon dioxide a person emits. 1 met corresponds to 58,2 W/m² body surface, which is the amount for one sitting person, inactive person is assumed to emit. In IDA-ICE, body surface has been selected to be 1,8 m², corresponding to an average adult (Source: ANSI/ASHRAE Standard 55, 2004). Therefore each person in the model emits 108 W (sensible plus latent). 67 W is estimated to be the sensible component (Source: ASHRAE Fundamentals Handbook (SI), 2001).

³ ASHRAE Fundamentals Handbook (SI), 2001, suggests a total of 470 W for a single-family house, that should be divided between the kitchen and/or the laundry and the adjacent room or rooms. So it has been decided to assign 75% of this value to the kitchen. The remaining 25% is not taken into account because assigned to the bathroom appliances (washing machine and dryer) which are located outside the Thermal Envelope.

2.4. Obtained power demands

The settings previously described have been used to define the heating or cooling power needed by every room. The maximum powers presented below have then been used to dimension the possible water temperature to supply in the radiant floor, based on EN 1264-2.

Table 14 – Maximum cooling and heating loads W/m^2 , obtained per surface area of radiant floor in each room

Loop	Room floor area	Area of radiant floor	Maximum heating Copenhagen	Maximum cooling Paris
Unit	(m^2)	(m^2)	(W/m^2)	(W/m^2)
Flex room	11	8,3	33	23
Bedroom bed side	23,4	10,6	32	20
Bedroom stairs side		8	32	20
Bathroom	3,3	2	30	20
Living room - kitchen	24,8	12,5	36	41
Living room - stairs		6	36	41

As can be seen from Table 14, the dimensioning room both for heating and cooling is the living room. The total demands for the design conditions are **1600** and **1500 W** for heating and cooling respectively, in Copenhagen and Paris (see Table 15).

Table 15 – Cooling and Heating maximum demands, for both Copenhagen and Paris

	Copenhagen (-12/26°C) ¹	Paris (-7,2/30°C) ²
Heating design load (indoor 21°C)	1600 W	1400 W
Cooling design load (indoor 25°C)	1300 W	1500 W

¹ Design temperatures for heating/cooling season from Danish building regulation and weather database.

² Design temperatures for heating/cooling season from weather database.

3. Radiant floor sizing

With the obtained heating and cooling loads from IDA-ICE, the radiant floor has been sized using the standard EN 1264, which consists mainly in determining the characteristic curves of the system and the supply temperature of the water supplied to the radiant floor. The range of products available at Uponor has been used when specific geometry or materials were needed for the calculations.

3.1. Method

The difference between average water temperature in the radiant floor and room temperature, $\Delta\vartheta_H$ for heating and $\Delta\vartheta_C$ for cooling season, has been calculated in function of the heating and cooling demand q of each room, previously obtained with IDA-ICE load simulations.

The method utilized is the single power equation as defined in EN 1264-2:

$$q = B \cdot \Pi_i(a_i^{m_i}) \cdot \Delta\vartheta_H, \quad B \cdot \Pi_i(a_i^{m_i}) = K_H$$

- B is a system dependent coefficient, which can be taken equal to $6,5 \text{ W/m}^2 \cdot \text{K}$ if the thickness of the pipes is 0.002 m and their conductivity is $0,35 \text{ W/m} \cdot \text{K}$.
- $\Pi_i(a_i^{m_i})$ is a power product, which links the parameters of the structure, such as surface covering, pipe spacing, pipe diameter and pipe covering.
- K_H is the slope of the characteristic curve of the system.

The parameter $\Pi_i(a_i^{m_i})$ has been calculated for System B: “system with pipes installed below the screed or timber floor”. K_H has been adapted for cooling purpose following section 4 of EN 1264-5.

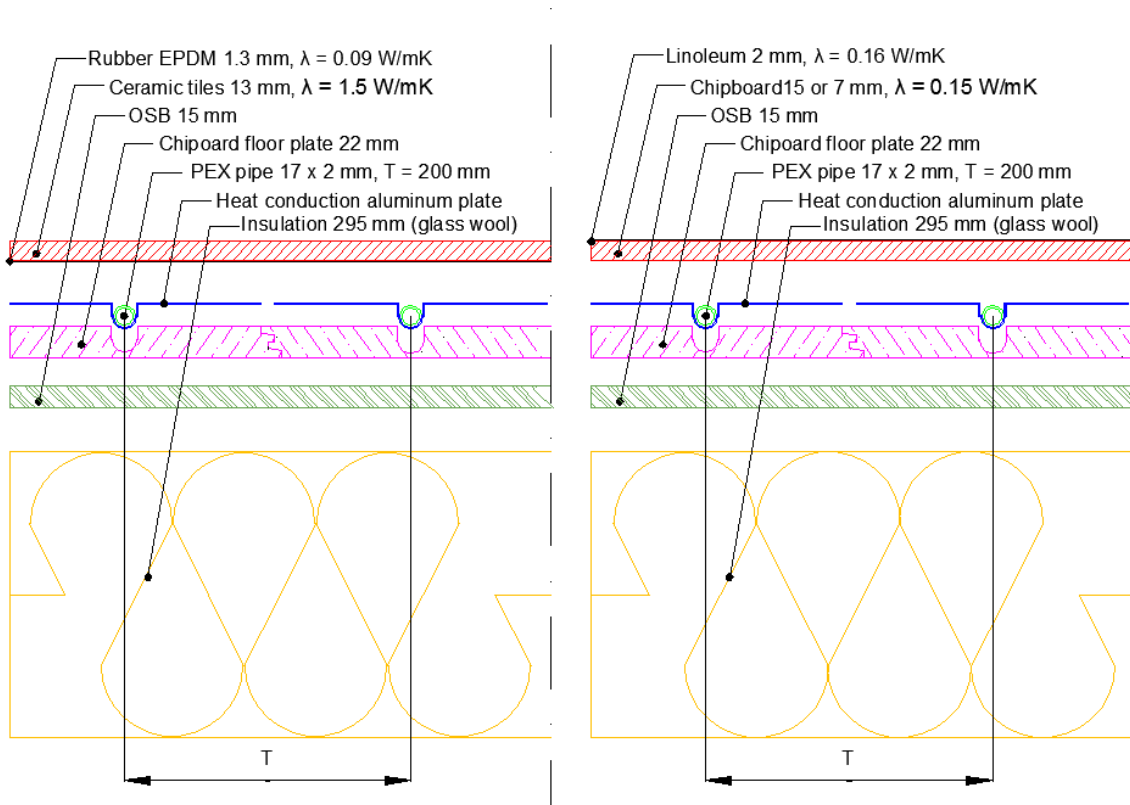


Figure 33 – Designed floor sections: two options of floor covering

As an output of the architectural/construction design choices, two floor coverings are investigated (see Figure 33). The first is linoleum; in this case a chipboard plate in between the heat distribution plate and the floor covering is needed. The second solution consists in a floating ceramic floor; large tiles are provided with 1,3 mm of EPDM rubber. The rubber guarantees a high friction factor to the bottom and the size which provides stability, combined with the high density of sandstone ceramic material. In this way, the tiles can be placed “dry” directly on the aluminum plate, without the need of any kind of glue.

For the option with linoleum, the thermal output has been investigated with two different chipboard thicknesses (15 and 7 mm). 15 mm have been selected because it is a standard size on the market, while 7 mm has been suggested by a professional from Uponor as minimum allowed thickness.

In the case where linoleum is used, the properties (thickness S_u and conductivity λ_E) of the chipboard plate are given to the "weight bearing layer" as defined by the Standard EN 1264-2 and the resistance of the linoleum is given to $R_{\lambda,B}$, “floor covering”.

The floor with ceramic tiles has required some assumptions to fit with type B, since the load bearing layer is absent and the tiles are lying directly on the aluminum diffusion sheet. Three different models have been calculated:

- In the 1st model, the weight bearing layer is defined with a thickness S_u equal to zero and the thermal resistance of tiles is combined with the one of the rubber and assigned as a single property to the floor covering.
- In the 2nd method, the properties of the rubber layer are given to the weight bearing layer and just those of the ceramic tiles (sandstone material) to the floor covering ($R_{\lambda,B}$).
- In the 3rd method, both the properties of the rubber layer and tiles are used to define the weight bearing layer and the floor covering resistance $R_{\lambda,B}$ is set to zero.

The surface heat transfer coefficients used to calculate $\Delta\vartheta_H$ and $\Delta\vartheta_C$ are $10,8$ and $7 \text{ W/m}^2 \cdot \text{K}$, for heating and cooling respectively (Olesen B.W., 2001).

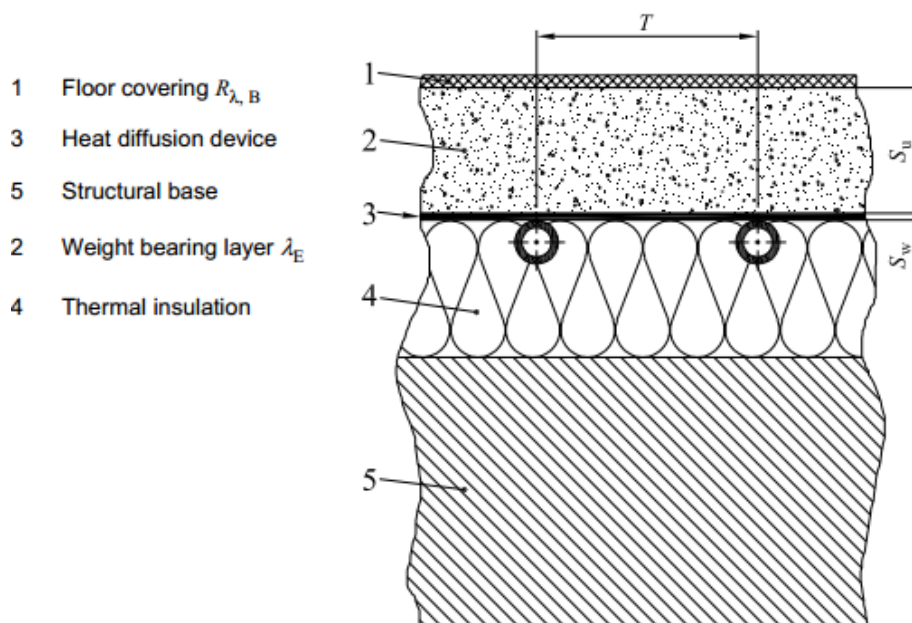


Figure 34 – Type B system as described in EN 1264-2

3.1.1. Heating

Once $\Delta\vartheta_H$ in the dimensioning room has been defined the following equations have been derived from eq. (8) and (9) of EN 1264-3, and used to calculate the water supply temperature, in function of the desired temperature drop σ between supply and return water in the dimensioning room:

$$\text{If } T_{av.w} \geq \frac{\sigma}{0,5} + T_{room}; \quad T_{supply} = T_{av.w} + \frac{\sigma}{2}$$

$$\text{If } T_{av.w} \leq \frac{\sigma}{0,5} + T_{room}; \quad T_{supply} = T_{av.w} + \frac{\sigma}{2} + \frac{\sigma^2}{12 \cdot (T_{av.w} - T_{room})}$$

$$(T_{av.w} = \Delta\vartheta_H + T_{room})$$

In the specific design the σ for heating is 5 K.

For all the other (*i*)-rooms operated at the same supply temperature T_{supply} as the dimensioning room, the temperature drop σ_i can be derived from eq. (10) and (11) of EN 1264-3 in function of the average water temperature of the (*i*)-room, $T_{av.w,i} = \Delta\vartheta_{H,i} + T_{room,i}$.

$$\text{If } T_{av.w,i} \geq \frac{\sigma}{0,5} + T_{room}; \quad \sigma_i = 2 \cdot (T_{supply} - T_{av.w,i})$$

$$\text{If } T_{av.w,i} \leq \frac{\sigma}{0,5} + T_{room}; \quad \sigma_i = 3 \cdot (T_{av.w,i} - T_{room}) \cdot \sqrt{1 + \frac{4 \cdot (T_{supply} - T_{av.w,i})}{3 \cdot (T_{av.w,i} - T_{room})}} - 1$$

From σ_i , the required flow rate at each room can be calculated, taking into account both the heating demand and downward losses to the ground, which can be obtained with eq. (28) of EN 1264-2. The equation used to define the flow rate is (13) of EN 1264-3:

$$m_H = \frac{A_F \cdot q}{\sigma \cdot c_W} \cdot \left(1 + \frac{R_o}{R_u} + \frac{\vartheta_i - \vartheta_u}{q \cdot R_u} \right) \quad (kg/s)$$

Where:

m_H is the flow rate (kg/s)

$A_F \cdot q$ is the power demand of the room (W/m²) multiplied by the radiant floor surface area (m²)

c_W is the specific heat of the water, equal 4200 J/kg·K

R_u is the downward partial heat transmission resistance of the floor structure (m²·K/W)

R_o is the upwards partial heat transmission resistance of the floor structure (m²·K/W)

$\vartheta_i - \vartheta_u$ is the difference of the indoor temperature and the temperature of the environment under the floor heated room (K)

3.1.2. Cooling

Once $\Delta\vartheta_C$ in the dimensioning room has been defined the following equations have been derived from eq. (18) and (20) of EN 1264-3, and used to calculate the water supply temperature, in function of the desired temperature drop σ_c between supply and return water in the dimensioning room:

$$\text{If } \sigma_c \leq 2; \quad T_{supply} = T_{av.w} - \frac{\sigma_c}{2}$$

If $\sigma_c > 2$;

$$T_{supply} = \frac{1}{2} \cdot T_{av.w} - \frac{1}{2} \cdot \sigma_c + \frac{1}{2} \cdot T_{room} - \frac{1}{6} \cdot \sqrt{9 \cdot T_{av.w}^2 - 18 \cdot T_{av.w} \cdot T_{room} + 3 \cdot \sigma_c^2 + 9 \cdot T_{room}^2}$$

$$(T_{av.w} = T_{room} - \Delta\vartheta_C)$$

In the specific design the σ_c for cooling is 2 K.

For all the other (*i*)-rooms operated at the same supply temperature as the dimensioning room T_{supply} , the temperature drop $\sigma_{c,i}$ has been derived in function of the average water temperature of the (*i*)-room, $T_{av.w,i} = T_{room,i} - \Delta\vartheta_{c,i}$.

$$\sigma_{c,i} = 2 \cdot (T_{av.w,i} - T_{supply}) \quad (K)$$

From $\sigma_{c,i}$, the flow rate needed at each room can be calculated as shown previously in the equation for the heating scenario.

3.2. Results

The following results refer to the dimensioning room (living room) radiant floor loop.

It is possible to see the calculation based on EN 1264 in “Annex 8: EN 1264 part 2 and 5 calculations”.

Table 16 – Supply water temperature of the dimensioning room, for the different floor covering and methods considered

Supply temperature T_{supply} (°C)	HEATING			COOLING		
	Chipboard 15 mm	Chipboard 7 mm	Tiles	Chipboard 15 mm	Chipboard 7 mm	Tiles
1 st Method	32,3	29,8	28,4	11,2	14	15,7
2 nd Method			28,5			16,4
3 rd Method			28,5			15,6

Table 17 – Radiant floor parameters for the design conditions

		Heating			Cooling		
$T_{outdoor}$	°C	-12			26		
T_{room}	°C	20			26		
Average $T_{floor\ surface}$	°C	24			20		
Flow rate dimensioning room loop	kg/s	0,023			0,041		
Total flow rate in all loops	kg/s	0,076			0,072		
Pressure drop in the pipes ¹	Pa	3900			11200		
Water velocity	m/s	0,18			0,31		
Dimensioning room demand	W/m ²	36			41		
Downward heat losses	W/m ²	Tiles	Wood 15 mm	Wood 7 mm	Tiles	Wood 15 mm	Wood 7 mm
		3,6	3,9	3,7	0,7	1	0,8

¹ The pressure drop has been calculated considering the length and bends of the design room loop pipes. Other components which introduce local pressure drops, like valves and manifold, have not been taken into account here.

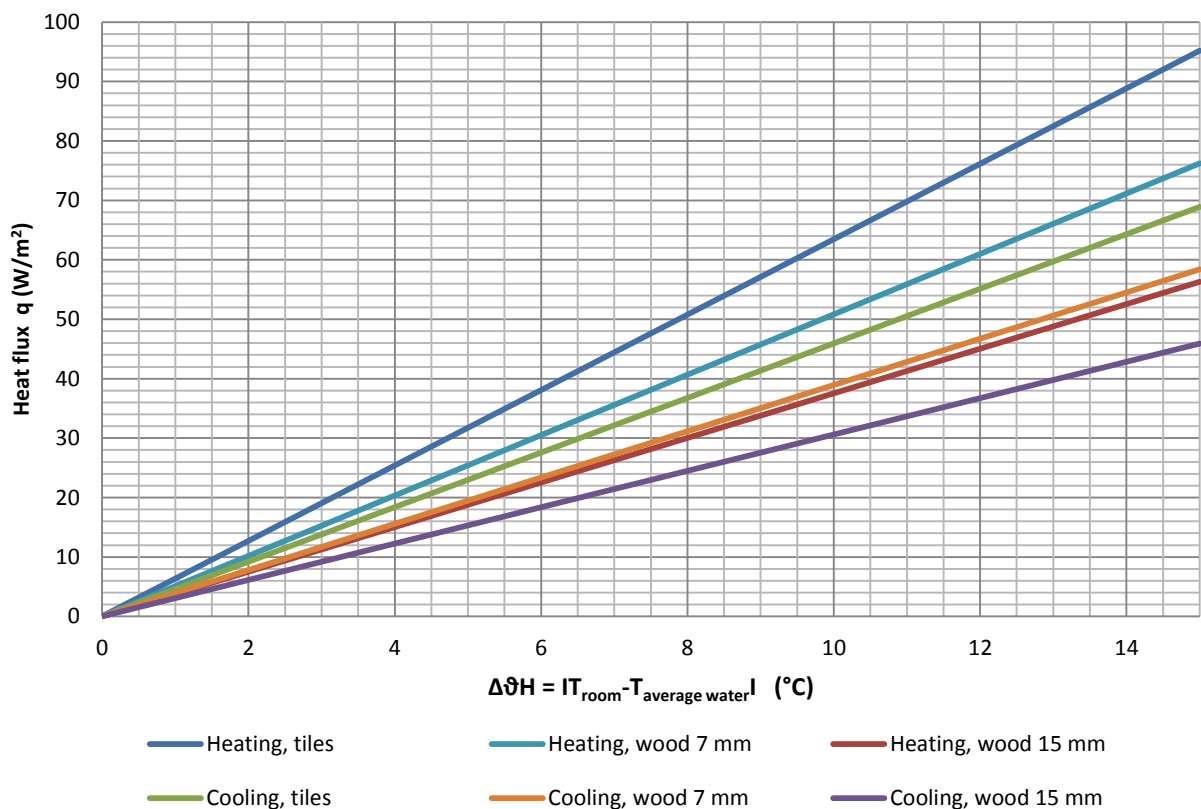


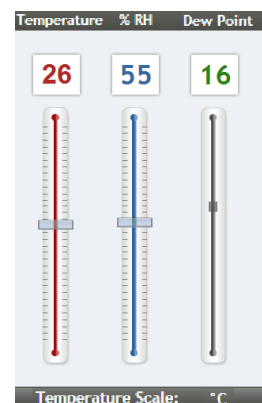
Figure 35 – Characteristic curves of the designed radiant floor as defined in EN 1264-2. For the tiles covering, method 3 is here represented.

3.2.1. Conclusion

Regarding the tiles floor covering, the 3rd method results to be the most pessimistic, the supply water temperature is higher for heating and lower for cooling than those of the other two methods. To stay on the safe side, the results from this method will be used further on.

The supply water temperature rises in heating and decreases in cooling, when increasing the resistance of the floor covering. The tiles solution allows supplying the highest water temperature in cooling and lowest in heating. Figure 36 and Figure 37 show how much the water temperature can be influenced by the three floor coverings. The demand (W/m²) to cover is the one of Table 17.

Dew point seems not to be an issue if tiles are used, both on the pipes surface and on the floor covering surface. Indeed in this case the supply water and the floor covering should not reach temperatures lower than 15,6 and 20 °C, respectively. Based on SDE regulation, the indoor operative temperature range to be provided is not fixed but depends by the outdoor running mean temperature of the previous 7 days, as stated in equation (3) and Annex A.2 of Standard EN 15251. The relative humidity has to be in the range between 40 and 55 %. Dew point temperature of 16°C is calculated, if considering the indoor temperature at a high tolerable value for thermal comfort, of 26°C (EN 15251), and upper relative humidity design limit of 55% (worse design conditions are applied for safety reasons).



The surface temperature of the floor is for both heating and cooling, inside the comfort range between 19 and 29°C as stated in EN 1264.

Water velocity in the pipes does not exceed the recommended value of 0,5 m/s (11127 Sustainable heating and cooling of buildings, DTU, 2013).

The radiant floor with tiles seems to be a sufficient solution to cover the demands of the house both in heating and cooling seasons, still respecting comfort and design parameters.

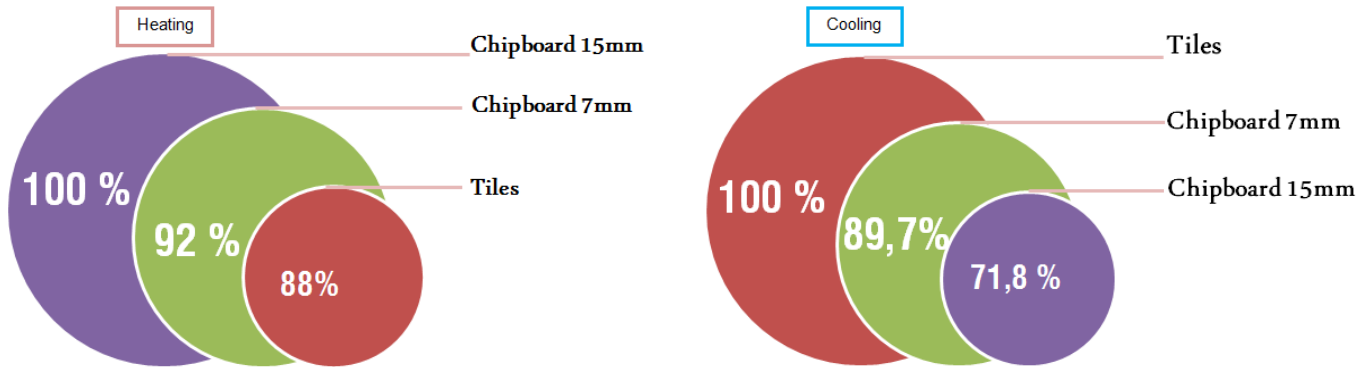


Figure 36 – Supply water temperature in heating design load Figure 37 – Supply water temperature in cooling design load

3.2.2. Comparison between Standard EN 1264 and software HEAT2

A simulation has been carried out with the software HEAT2 to verify the performance of the radiant floor (see next chapter, III.4.). In HEAT2 the average water temperature in the radiant floor pipes has been set as an input and the heat flow through the floor was the output. In the previous calculations the approach was reverse, the water temperature was calculated based on the dimensioning room power demand.

In this paragraph the characteristic curves obtained based on EN1264-2, are used to calculate the heat flows with the same $\Delta\vartheta$ used in HEAT2, to compare both results.

Average water temperature: 27,9°C / 17,4°C

Inside temperature: 20°C / 26°C

So $\Delta\vartheta$ heating /cooling: 7,9°C / 8,6°C

Table 18 – Power provided with a fixed temperature difference between average water and room temperature, both in heating and cooling

q (W/m²) to the room		$\Delta\vartheta$ heating = 7,9°C		$\Delta\vartheta$ cooling = 8,6°C	
		Tiles heating	Chipboard 15 mm heating	Tiles cooling	Chipboard 15 mm cooling
EN 1264-2	Method 1	51,3	29,6	40,2	26,3
	Method 2	50,6		43,7	
	Method 3	50,1		39,5	
HEAT2 (case C)		46	27,5	39,9	25,9

Method number 3 appears to be the closest to the HEAT2 model. This confirms the precedent choice of referring to the results obtained with the 3rd method, further on.

4. Verification of the performance (HEAT2)

A HEAT2 model was developed to check the heating and cooling outputs of the radiant floor, and the floor surface temperature profile. HEAT2 is a PC-program for two-dimensional transient and steady-state heat transfer. It corresponds well to the study of a radiant floor section, which can be approximated by a 2D heat transfer problem, taking into account the conduction in the different layers and the convection on the borders (Blomberg, 2000).

The two same cases of floor covering are investigated:

1. Ceramic tiles with an underneath layer of rubber
2. Linoleum laying on a wood chipboard plate

4.1. Input to the model

The different layers of the floor structure are modelled as presented in the tables below, with the corresponding physical parameters. Those values are used as input to the HEAT2 model. A graphical representation of the model is also shown in Figure 38, for the ceramic tiles case.

Table 19 – Material layers for case 1

MATERIAL LAYERS	Thickness	Thermal conductivity ¹	Volumetric heat capacity
	[m]	[W/m·K]	[MJ/m ³ ·K]
Floor tiles (ceramic)	0,013	1,5	1,95
Rubber	0,0013	0,09	2,4
Aluminum	0,001	226	2,48
Particle board	0,022	7,7	0,64
OSB	0,015	0,13	1,37
Glass wool	0,295	0,03	0,020
Bottom OSB	0,03	0,13	1,37

Table 20 – Material layers for case 2

MATERIAL LAYERS	Thickness	Thermal conductivity	Volumetric heat capacity
	[m]	[W/m·K]	[MJ/m ³ ·K]
Linoleum	0,002	0,17	1,68
Chipboard	0,015	0,13	1
Aluminum	0,001	226	2,48
Particle board	0,022	7,7	0,64
OSB	0,015	0,13	1,37
Glass wool	0,295	0,03	0,020
Bottom OSB	0,03	0,13	1,37

¹ It is possible in HEAT2 to set a different thermal conductivity for the two main directions x and y. In this application, the thermal conductivity was considered to be isotropic (i.e. $\lambda_x = \lambda_y$), hence the unique value given in the table.

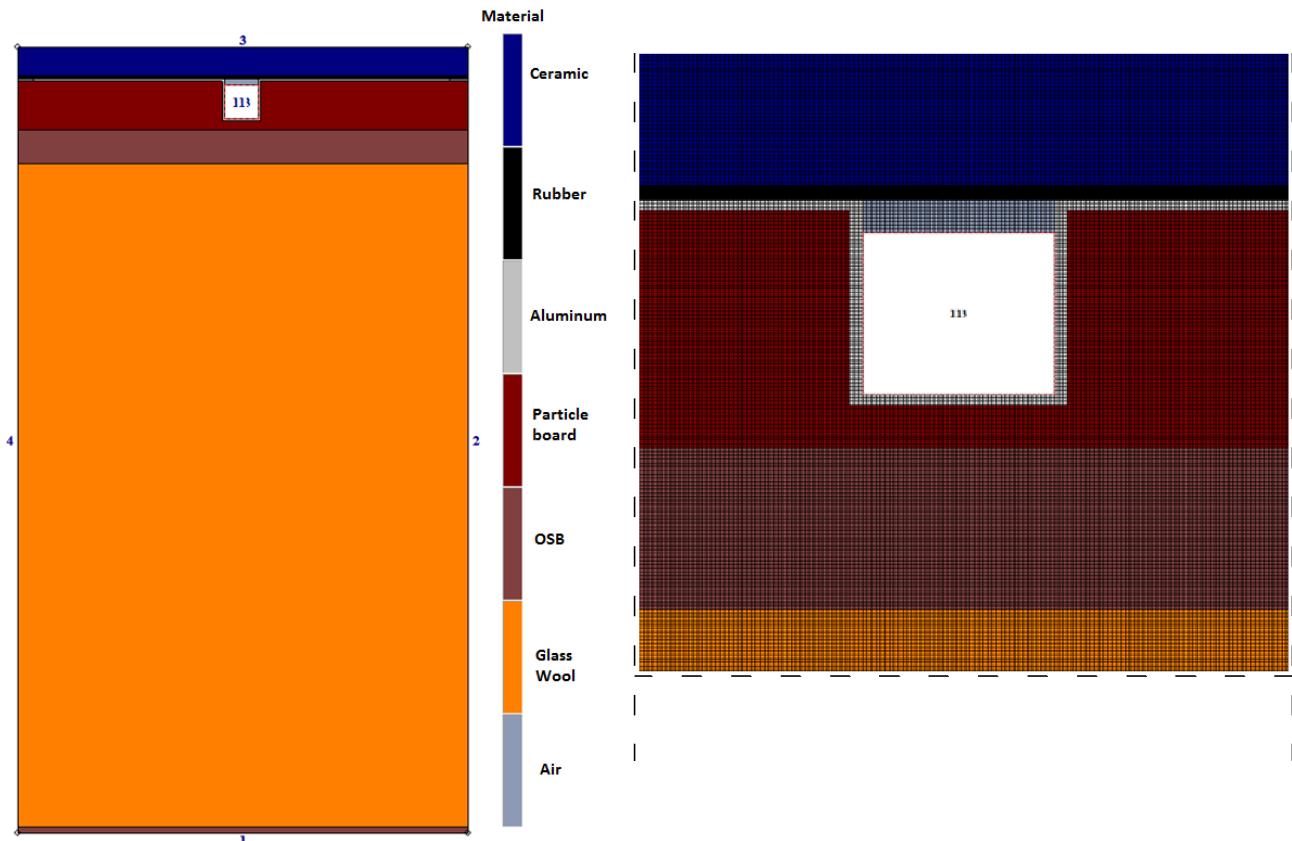


Figure 38 – HEAT2 model with the materials of the tiles solution, and detail of the mesh

The mesh used for the simulations has 572 cells in the x-direction, and 1001 cells in the y-direction, which makes a total of 572·572 cells.

The convergence criterion is defined in the program as $\frac{\sum \dot{Q}_b}{\sum |\dot{Q}_b|} = F$. Which means that the ratio between the sum of all the heat fluxes entering the boundary surfaces and the absolute value of the sum these heat fluxes must be lower than an assigned value F (Blomberg, 2000). This value was given as 10^{-2} .

The boundary conditions are presented in Table 21, and they correspond to the design cases for heating and cooling. The heat transfer coefficients are obtained from the Standard DS 418. The temperatures of the water supplied into the pipes for the heating and cooling case were calculated in Chapter III.3 Radiant floor sizing.

Table 21 – Boundary conditions for the HEAT2 model

Heat flux, temperatures and resistances		HEATING	COOLING
Boundary heat flux on the sides	W/m ²	0	0
Boundary temperature inside	°C	20	26
Boundary surface resistance inside	m ² K/W	0,0925	0,143
Boundary temperature outside	°C	-12	26
Boundary surface resistance outside	m ² K/W	0,04	0,04
Constant temperature inside the pipe	°C	27,9	17,4

4.2. Discussion on the pipe model

HEAT2 uses a square mesh to solve the 2D problem. This feature of the software complicates the modelling of round pipes, since only squares can be drawn. One solution provided in the program manual (Blomberg, 2000) is to approximate the pipe by a square of equivalent area (length of one side $D = \sqrt{\pi} \cdot r$, where r is the pipe radius). This solution will be referred to as “case C” in the following text.

To take into account the resistance of the pipe wall, it must be assigned on the four sides of the square representing the pipe. This is done by drawing resistance lines all around. The resistance of those lines is calculated as follows:

$$R_c = \frac{2 \cdot D \cdot \ln\left(\frac{r}{r - d_i}\right)}{\pi \cdot \lambda_i} = 0,0074 \text{ m}^2\text{K/W}$$

Where (in the case of the chosen Uponor dry radiant floor) $D = \sqrt{\pi} \cdot r = \sqrt{\pi} \cdot 17 \approx 15 \text{ mm}$ is the length of the square sides, $r = 8,5 \text{ mm}$ is the pipe radius, $d_i = 2 \text{ mm}$ is the pipe wall thickness, and $\lambda_i = 0,35 \text{ W/mK}$ is the heat conductivity of the pipe material (PEX).

Another solution consists in using the feature of the program called modification pipe, the model of pipe selected is MOD:J, which has a constant temperature inside. With this option, the user shall draw a square, and the program will draw a circle fitted into this square (Case A in Table 22). The given temperature will be uniformly distributed in all the cells which have the centre inside the circle, as shown on the right side of Figure 39.

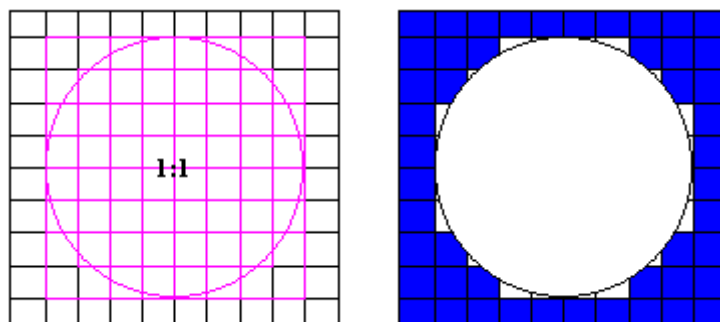


Figure 39 – Example of modification pipe (Blomberg, 2000)

There is still a need to model the resistance of the pipe wall by resistance lines, with in the case of this approach with modification pipes, $D = 17 \text{ mm}$, and R_c becomes $0,0083 \text{ m}^2\text{K/W}$.

Both the steps described above lead to an accurately approximated model of the radiant floor pipe. However the material surrounding the pipe is a remaining issue. It can be seen in Figure 40 that the aluminum plate (in grey) is theoretically touching the pipe on its entire bottom half.

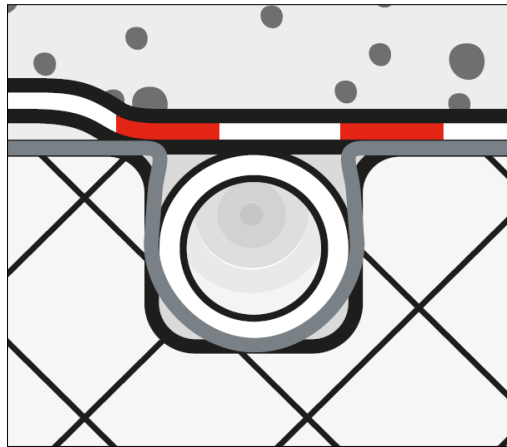


Figure 40 – Section of the radiant floor (from Uponor documentation)

There should be full contact between the aluminum plate and the pipe all along a half circle, in order to favour the heat transfer. Yet the model in HEAT2 introduces air gaps that misrepresent this reality, as can be seen in the Case A in Table 22. Another model has been introduced (Case B in Table 22), where the bottom half, where the modification pipe is drawn, is entirely made of aluminum. In this way, as it appears in the post-processor of HEAT2, there is full contact between the pipe and the aluminum.

Table 22 – Comparison of the 3 model cases

	Case A: Air gaps between the pipe and the aluminum plate	Case B: Full contact between the pipe and the aluminum plate	Case C: Square of the same area than the pipe
Image of the preprocessor (the red square is the modification pipe)			
Image of the postprocessor			
	Heating output $q = 30,3 \text{ W/m}^2$	Heating output $q = 43,9 \text{ W/m}^2$	Heating output $q = 46,0 \text{ W/m}^2$

The heat output in the heating and cooling mode has been calculated for the three cases (see more detailed results in the next section III.4.3.). It appears to vary significantly. For instance, in the case of the heating mode with tiles as floor covering, it ranges from 30,3 W/m² with air gaps in Case A, until 46 W/m² in Case C, where three quarter of the pipe are in contact with the aluminum. Hence the importance to discuss and select the proper representation of the pipe in the layout.

Case A with the air gaps has been first disregarded, because it underestimates the heat flux. The air gaps introduce a high resistance that hinders the heat transfer. The heat flux is reduced of around 40% than the value obtained with Standard EN1264, in heating mode with tiles covering.

Case B and C are relatively close (they differ only by 2 W/m²), and they give a more accurate idea of the reality by simulating better the full contact between the aluminum plate and the pipe. They also provide values closer to the ones calculated with the standard. As can be seen in Figure 41, the aluminum plates are actually slightly curved to the inside, in order to stick to the pipe surface more than just half of the perimeter. Therefore case C is a good approximation, since with the square model, three edges of the square are in direct contact with the aluminum.

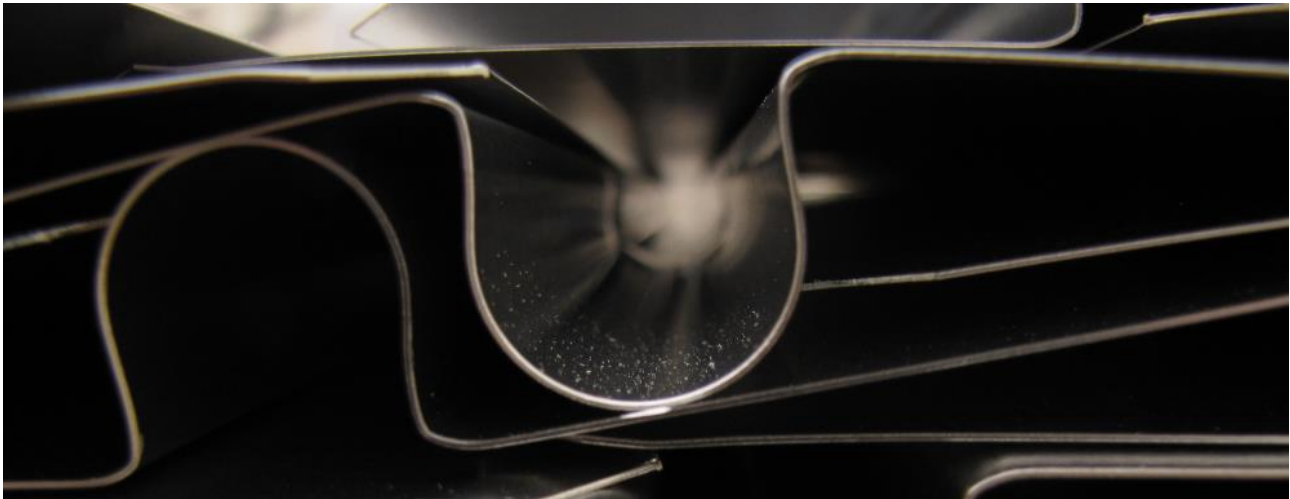


Figure 41 – Photo of the profile of the Uponor aluminum plates used for EMBRACE

4.3. Results

The results of the simulations are summed up in Table 23. Each case has been investigated with regards to heating and cooling, according to the input described previously. The main interesting output is the heat flux to the room, which is presented here in relation to the room area. The losses downwards are also presented here, in order to check that they do not represent a too important part of the output.

For comparison, the heat flux was calculated with Standard EN1264 to be 51 W/m² for the tiles case, and 30 W/m² for the chipboard case. The full comparison table can be found in section III.3.2.2., Table 18.

Table 23 – Heat flux results of the different cases

		Heat flux to the room		Heat flux downwards	
		[W/m ²]		[W/m ²]	
		Heating	Cooling	Heating	Cooling
1. Ceramic tiles + rubber	Case A	-30,3	28,8	-3,5	0,5
	Case B	-43,9	37,9	-3,6	0,7
	Case C	-46,0	39,9	-3,7	0,7
2. Chipboard + linoleum	Case B	-26,7	25,3	-3,8	0,7
	Case C	-27,5	25,9	-3,8	0,7

It is clear from the results of the simulations that the chipboard and linoleum solution provides a significantly lower output. These layers introduce a resistance to the heat transfer, so the output is reduced by around 20 W/m² for heating and 15 W/m² for cooling. The solution with ceramic tiles is therefore preferred.

Apart from the technical advantages related to their high conductivity, the ceramic tiles are also a more practical option than chipboard and linoleum. The chosen product, manufactured by Newfloor in Italy, can be installed easily: thanks to the rubber layer below and on the edges, there is no need for any kind of glue, joint or cement. The tiles stay in place thanks to their own weight and the friction caused by the rubber. They are therefore easily installed and removed with simple tools. In the case of EMBRACE, this characteristic is an important design parameter, since the ground floor is composed of one space that goes across two different modules. Once the modules are assembled, the tiles can be put on the floor in order to create a continuous covering that hides the connection between modules. Because of the transportation and modularity constraints, the tiles are therefore also a more functional option.

Among the three cases investigated with the ceramic tiles, case C is chosen. As previously introduced, it is the solution that models the system in the most accurate way, and gives values comparable to the ones obtained through the standards. From this point, the results are shown for the ceramic tiles, and the pipe modelled as a square (Case C). Figure 42 shows the temperature distribution in the structure of the floor, for the heating and the cooling cases.

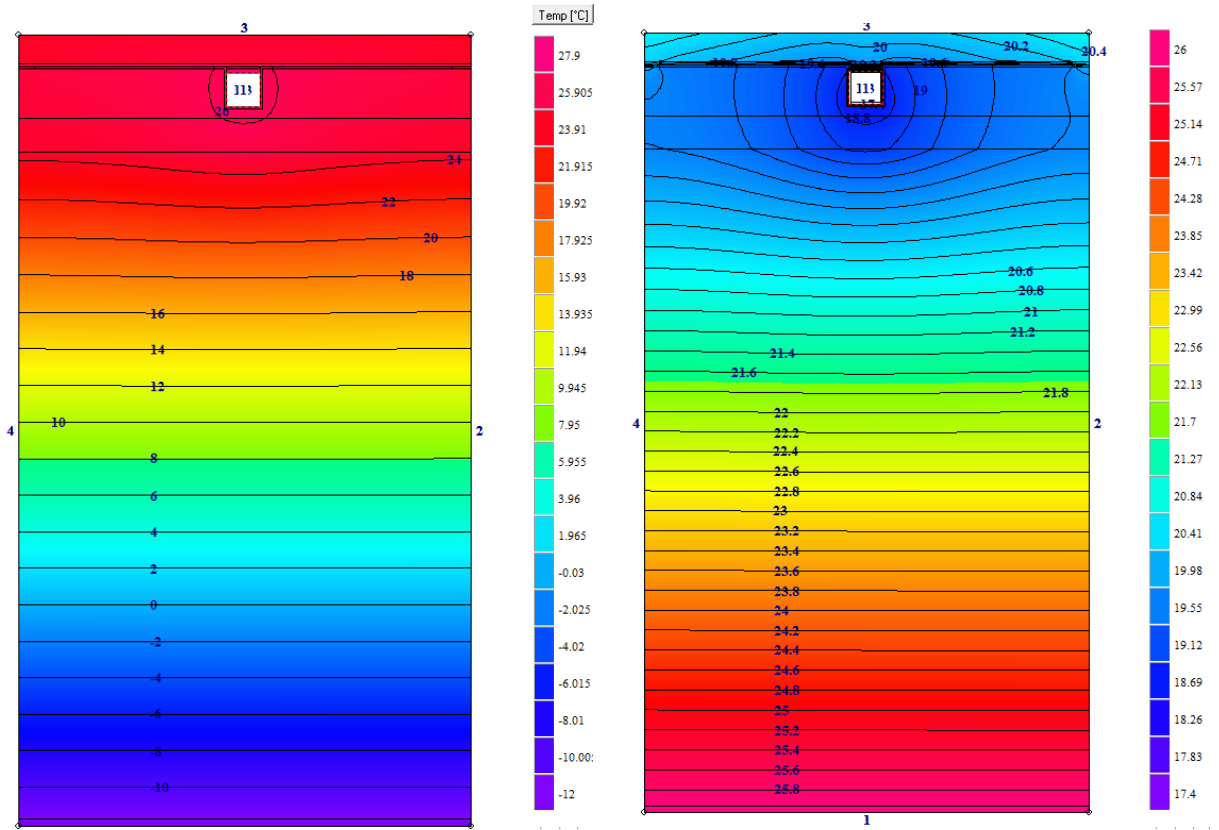


Figure 42 – Temperature distribution and isotherms in the floor structure, for heating (left) and cooling (right)

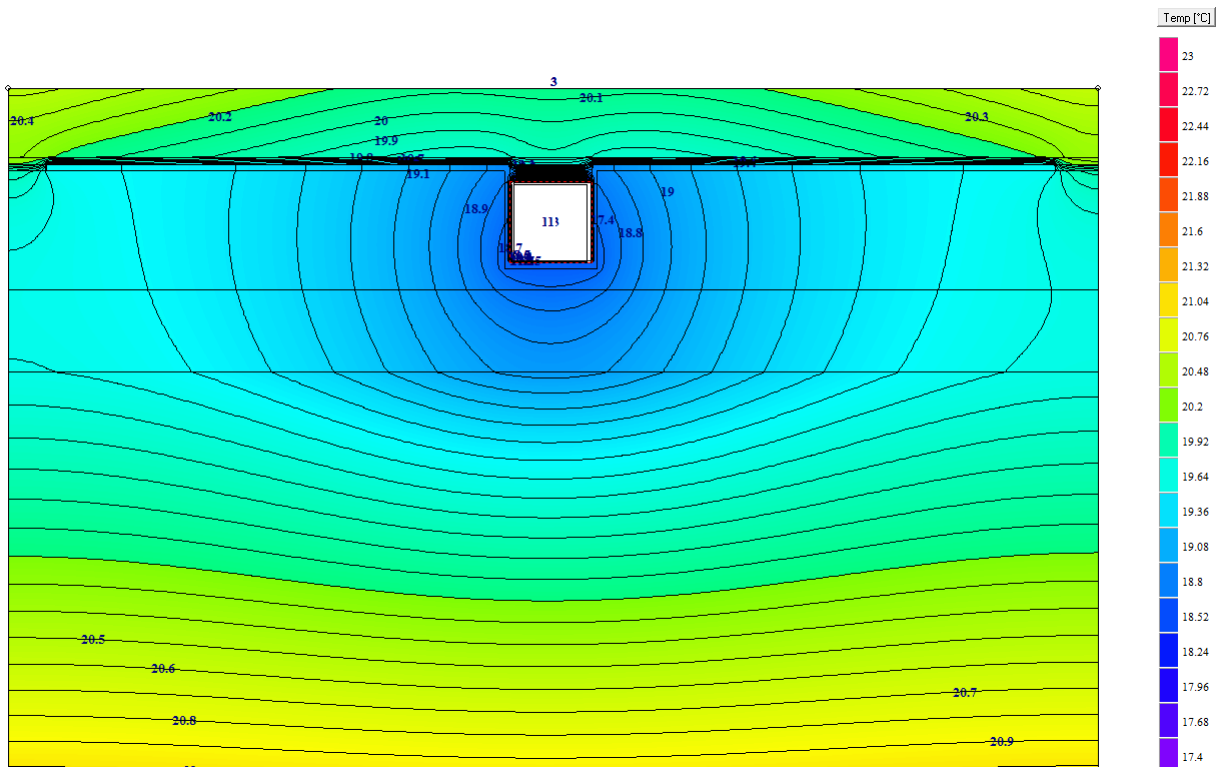


Figure 43 – Detail of the temperature distribution around the pipe for the cooling case

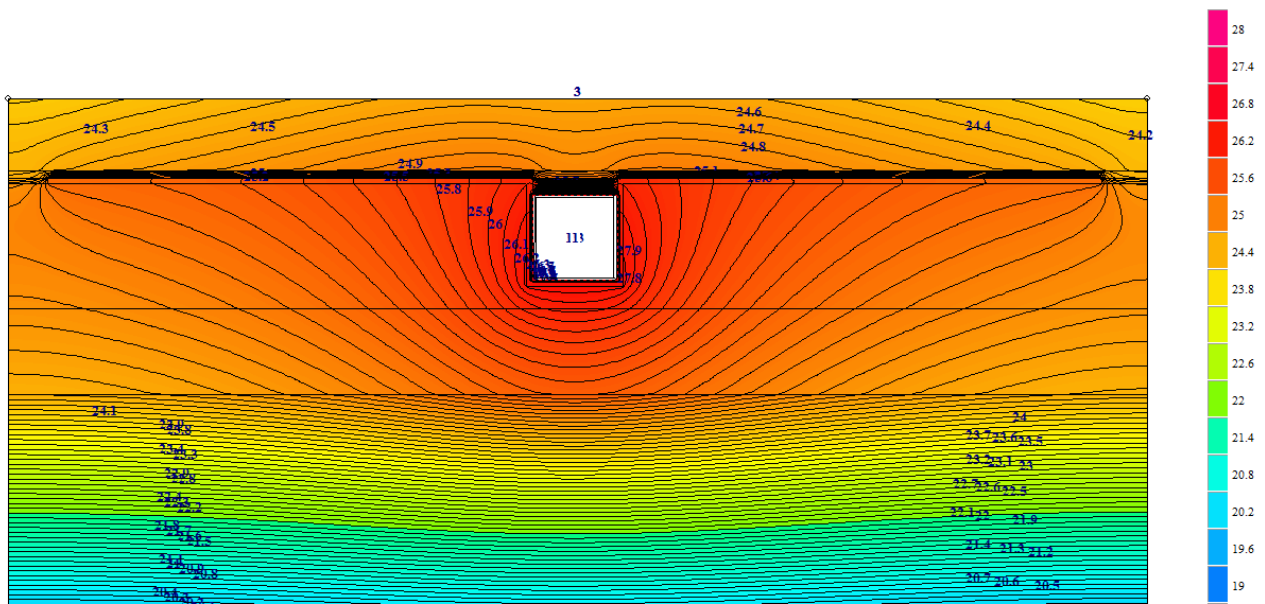


Figure 44 – Detail of the temperature distribution around the pipe for the heating case

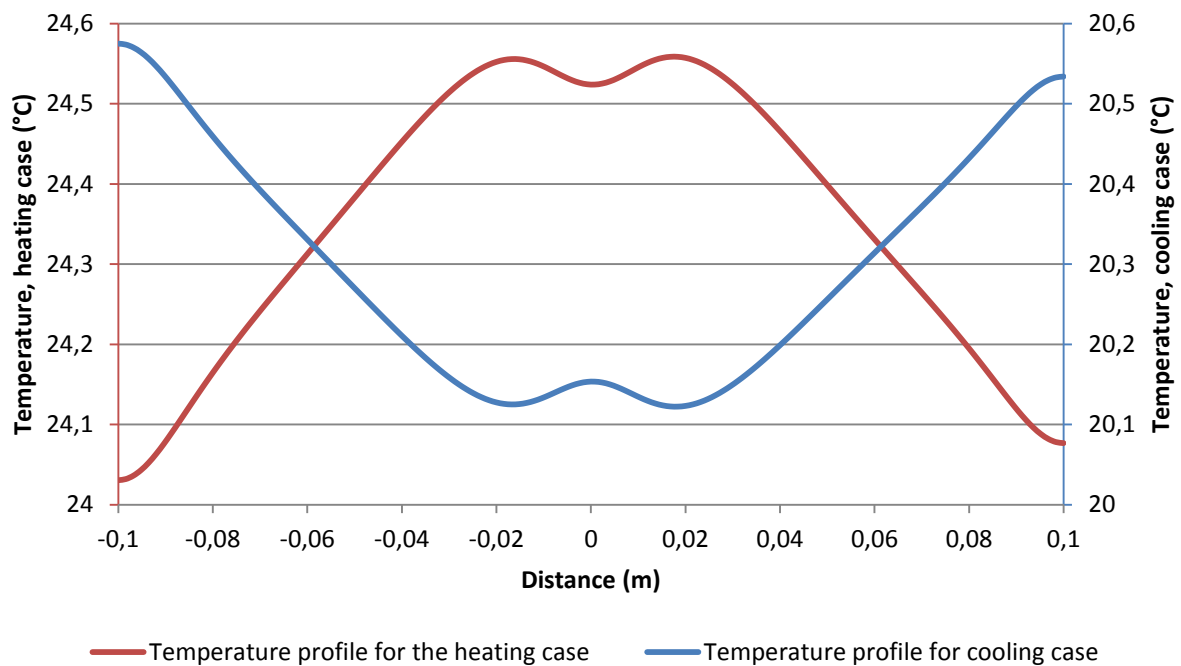


Figure 45 – Temperature profiles on the floor surface (0 is the center of the pipe)

The floor surface temperature always stays in the comfort range specified by the standard EN 1264: the surface temperature must not exceed 29°C in winter, and must not go below 19°C in summer. These conditions are largely met for EMBRACE: as the building is small and well insulated, the supply temperature to the radiant floor is not extreme, therefore the surface temperature stays within the comfort range specified by the standard (the surface temperature stays below 25°C in winter and above 20°C in summer). Inside this range of surface temperatures, condensation is also not a problem since dew point is never reached, as already shown in section III.3.2.1.

5. Conclusion and discussion

From the previous studies, it can be concluded that the ceramic tiles used as a floor covering offer improved performance compared to the linoleum and chipboard option. The only drawback is the sensation of cold feet that they can cause when the radiant floor is not activated and the occupants walk bare feet. For instance, the heat loss in ten minutes through a marble floor has been estimated to be 511 kJ/m², while it is 176 kJ/m² for a linoleum on wooden floor (Olesen B.W., 1977)¹, requiring a higher surface temperature to provide satisfactory thermal comfort. The optimal floor temperatures for marble² and linoleum are 29°C and 26°C when standing for ten minutes.

The tiles are therefore chosen as a floor covering, installed on the dry radiant floor which has a pipe spacing of 20 cm. The outputs from the calculations based on the Standard EN 1264 and the HEAT2 simulation showed good consistency, with a heating power of approximately 50 W/m² and a cooling power of approximately 40 W/m² for the dimensioning cases. The water should be supplied respectively at 28,5°C and 15,6°C. The downward losses are negligible in both cases.

However, all methods presented in this chapter present some level of inaccuracy. The first one is the load calculations that depend largely by several parameters such as the diversity factors or the schedules applied in the building simulation tools (Abushakra et al., 2004). A perfect level of accuracy should not be expected from the software used, since it is influenced by several unknowns. The standard EN 1264 needs to be carefully adapted to the case of ceramic tiles directly laid on the radiant floor, since the weight-bearing layer is then not properly defined. Finally, the 2D simulation with the HEAT2 software shows some limitations in the modelling of pipes, which again need to be considered with great attention. It is believed that those inaccuracies are however not damageable for the design of the radiant floor.

Another aspect of the radiant floor design that can be discussed is the complexity of the selected approach for its sizing. The methods described in the present report include the load calculations, the sizing based on the standards, and the verification by software simulation. These numerous and time-consuming steps can appear futile, considering the fact that there is a limited freedom in the actual design. Limited are in fact the systems available on the market. For conventional designs, the choices are often taken based on the characteristic curves, which are normally provided by the producer and the practical experience of the designer. For example, Uponor only proposes two different dry-systems of radiant floor, therefore the method used for sizing the radiant floor of EMBRACE could appear like a loss of time. It could have been simpler to select the characteristics of the system applying design graphs/tables provided in the product datasheets. The methods and calculations have been in fact mainly useful to check if the desired heating or cooling output was actually achieved, and to support the choice of the floor covering during the discussions with the architectural team.

¹ The method applied in this paper is based on German standard DIN 52614, with a floor temperature at 18°C and foot at 33°C.

² Marble heat conductivity is comparable with that of the ceramic tiles.

IV. Heating and cooling production

In this chapter, the design of the heating and cooling production systems of EMBRACE is detailed. The unglazed solar collectors are not mentioned here as a complete chapter is dedicated to nighttime radiative cooling (see chapter VII). The choice of the heat pump and its integration in the hydraulic systems is detailed in the following sections, as well as the choice of the storage tank.

1. Study of heat pump and its integration in the system layout

The following section analyzes the power demand of the building in relationship with the heat pump capacity, in order to select the proper heat pump, integrate it in the HVAC and design the possible cooling and heating storage strategies.

In the beginning, the different heat pump technologies have been investigated, especially the difference between a heat pump without or with an inverter (variable speed compressor). In brief, the inverter heat pumps are able to modulate the power of the compressor and present a higher efficiency in partial load operation. The non-inverter heat pumps operate the compressor either at full speed or off. To meet a partial load they have to switch on and off constantly.

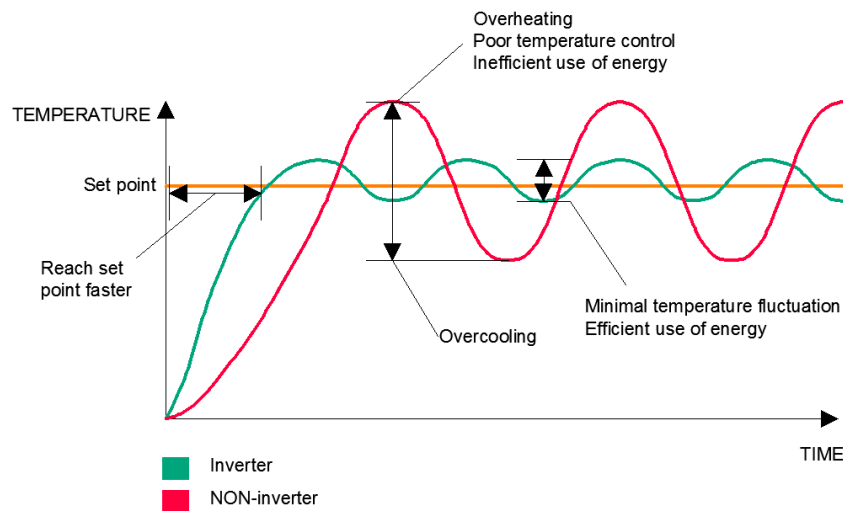


Figure 46 – Control and adaption of an inverter heat pump compared to a non-inverter heat pump

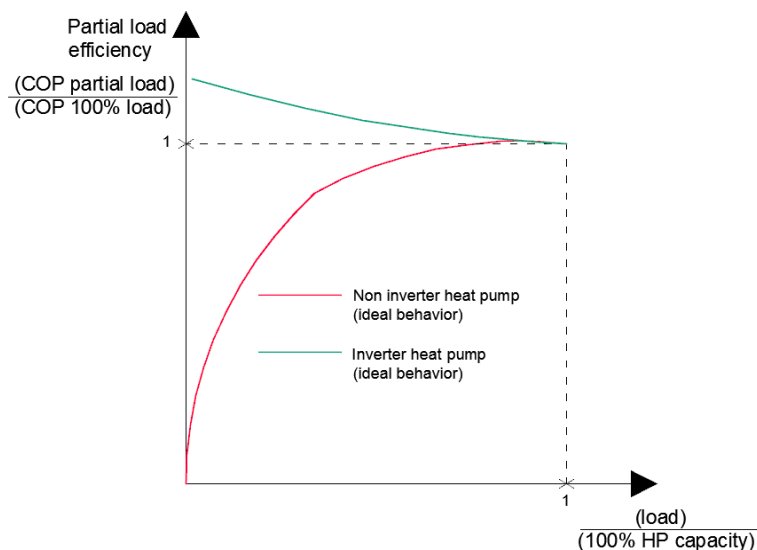


Figure 47 – Efficiency of a heat pump related to the load of heating or cooling provided.
(Figure partially derived from Huang Y.J. and Parker D., 1999)

In general when sizing the capacity of a heat pump in function of the demand of the building, three scenarios can be defined:

1. The demand of the building can be higher than the heat pump capacity and therefore an additional source is needed to support the heat pump,
2. It can be in the heat pump range of operation,
3. Or it can be lower than the minimum capacity that the heat pump can provide.

In case a non-inverter heat pump is considered, the second scenario should not be taken into account, because the capacity of the compressor is not adaptable. For the three cases, the heat pump will function according to the descriptions of Table 24.

Table 24 – Example of the possible operation modes for an inverter heat pump during heating season¹

1	<p>Heat load > max heating capacity: <u>full load</u></p> <p>Compressor will operate at 100% frequency, with additional electrical assistance if required.</p> <p>The equilibrium point or equilibrium temperature is the outside ambient temperature at which the heat pump capacity matches the heating demand. It is therefore the lowest outside temperature at which no additional heat source is needed. The heat pump can cover the entire heating demand down to this outside temperature. For outside temperatures below this equilibrium temperature, additional heat from the backup heater is required to fulfill the heating demand. During transient conditions at system heat-up, the equilibrium point can shift to a higher temperature than the one it would be at during normal operations.</p>
2	<p>Min heating capacity < heat load < Max heating capacity: <u>partial load</u></p> <p>Compressor will reduce its frequency delivering the capacities required by the house, with high operating efficiencies</p>
3	<p>Heat load < Min heating capacity: <u>partial load with on/off operation</u></p> <p>Compressor will work at its minimum frequency with high operating efficiencies, but switching on/off to deliver the capacities required</p>

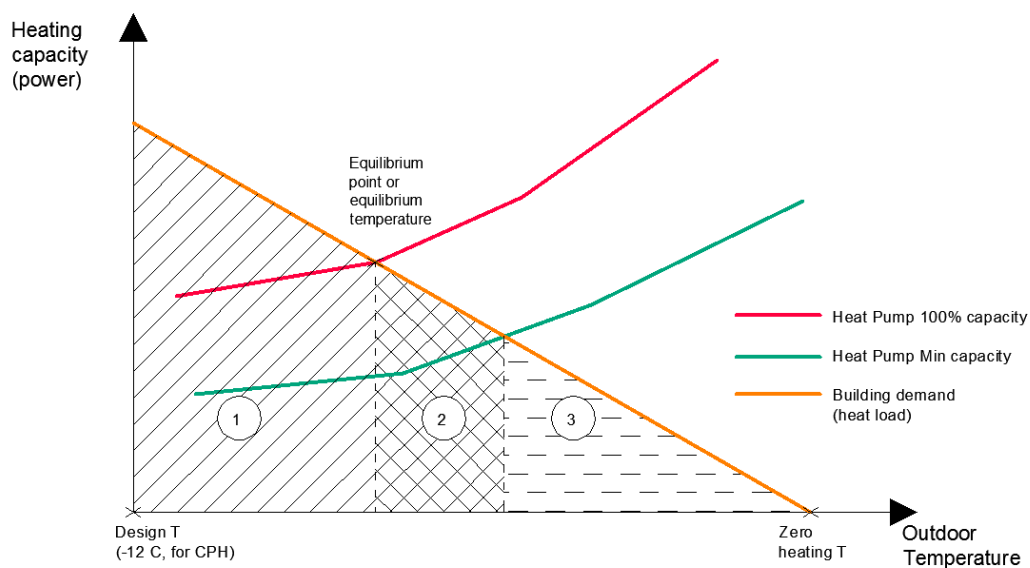


Figure 48 – Possible operations of a heat pump in relation to the building demand (Based on Daikin Altherma datasheet)

¹ Table partially derived from “New Daikin Altherma Low Temperature” presentation (not published).

Both inverter and non-inverter heat pumps do not perform optimally when the building demand is lower than the minimum capacity of the installation and this is due to the fact that the compressor has to turn on and off repeatedly.

For the specific design of EMBRACE, it is planned to cover the highest percentage of the house cooling load by nighttime radiative cooling. During the night, water is circulated in unglazed solar collectors which cool down the water by emitting the excess heat through convection and radiation towards the night sky. The water cooled during the night needs to be stored for utilization in the radiant floor during the next day. This requires the implementation of a large storage tank.

As shown previously in the load calculations, the heating and cooling demands are relatively small, proportionally to the size of the house. Compared to the capacity of small heat pumps available on the market, the demand of the building always results lower¹. For instance, Daikin has recently introduced a small air-to-water unit to supply a low demand to the increasing number of low-energy houses (Daikin Corporation, 2014). This unit, the Altherma heat pump, has been selected for this project. Despite the low capacity of this product, it still has a minimum capacity both in heating and cooling higher than the design demand of the house.

Based on the previous considerations, three different heat pump configurations in the HVAC system have been analyzed; they are presented in the following three sections. The third option has been identified as the most efficient but due to the impossibility to control the heat pump operation in the desired way and time issues, the first option has been realized for the prototype house in Versailles.

1.1. First option

Non inverter heat pumps have the ideal COP, at equal boundary conditions, when operated at maximum load. In principle, they are cheaper than variable speed heat pump, so they can find a worthwhile field of application for instance if operated connected to a storage tank. Indeed in this way the heat pump can operate at full load for a shorter period to bring the water in the buffer at the desired set point, for instance when there is a peak of electricity production from the PV panels. The water can be stored and subsequently circulated when needed. In this design, the storage tank, sized for nighttime radiative cooling purpose, could be too large. The risk is that the heat pump would cool more water than the amount needed for the radiant floor, resulting in higher energy consumption (Chinello E., 2013).

Inverter heat pumps can also find an application in this configuration when they are in operation mode 3 as explained in Table 24 and Figure 48. In fact in that case they can operate at partial load.

¹ Market survey carried out among the heat pump products of the companies Daikin, Sonnenkraft, Nilan, Immergas and Baxi.

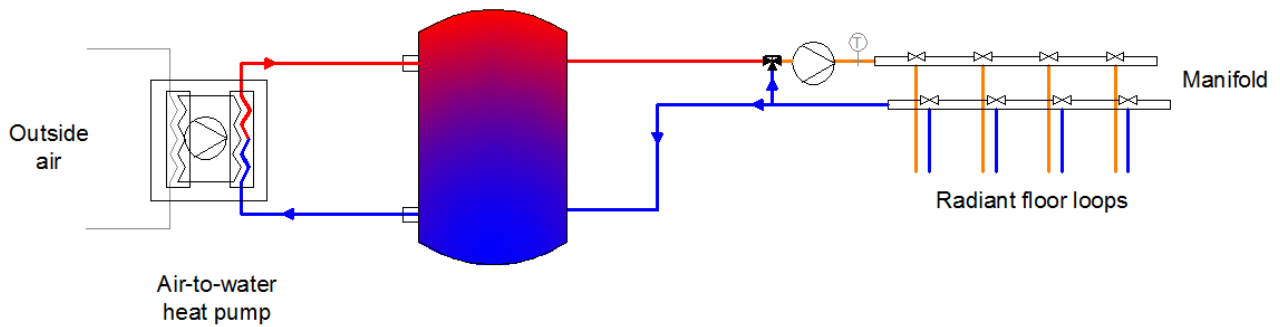


Figure 49 – Option 1 simplified representation. The heat pump is located before the storage tank and the radiant floor mixing station controls the supply temperature with recirculation.

1.2. Second option

Variable speed heat pumps find a good application for instance when exchanging heating or cooling directly with the medium to be supplied in a conditioned zone. In this case the load of the zone changes dynamically and the compressor modulates to adapt to those changes, working at partial load. For this option, the heat pump operation needs to be controlled by room thermostats signals. An additional control with manifold actuators or mixing station for the radiant floor loops is therefore not needed.

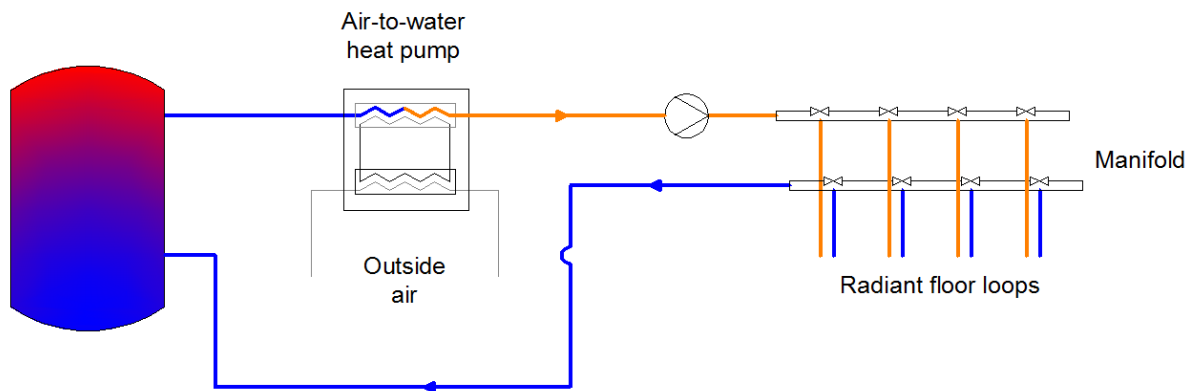


Figure 50 – Option 2 simplified representation. The heat pump controls the supply temperature so recirculation is not needed.

1.3. Third option

The second option allows exploiting the higher efficiency of an inverter heat pump when operated at partial load (as in the second scenario of Figure 50). But as previously explained, the demand of the designed dwelling is lower than the minimum capacity of the heat pump selected, both in heating and cooling. Therefore a new solution has been elaborated. The inverter heat pump has been located between the radiant floor and the buffer tank. When the heat pump is on, it can provide water both to the radiant floor and the tank. In this way, the compressor can work at a capacity higher than its minimum and the water in excess can be stored in the buffer tank. The speed of the compressor could be controlled by room demand and in function of the electrical production peak from the PVs. A temperature set point of the water in the tank could be an alternative way of controlling the heat pump, but this could result in overproduction as in the first option, since the heat pump could be activated also when there is no demand of circulation in the floor. When the temperature set point is reached in the storage tank, the heat pump is switched off, excluded from the loop thanks to motorized valves and the radiant floor can withdraw water directly from the tank. The water supply temperature is controlled with recirculation by a mixing station,

before the manifold of the radiant floor. A control was designed and elaborated for this option thanks to the RTD - LT/CA interface for the monitoring and controlling of Daikin products (see Annex 12: Control drawings from PD#6, Team DTU), but this specific interface was not yet released for sale at the moment of the installations' assembly. The particularity of the controller RTD-LT is that it would have enabled to establish set-points by a 0...10 V dry contact signal compatible with the PLC (Proportional Linear Control) designed by the team members of EMBRACE.

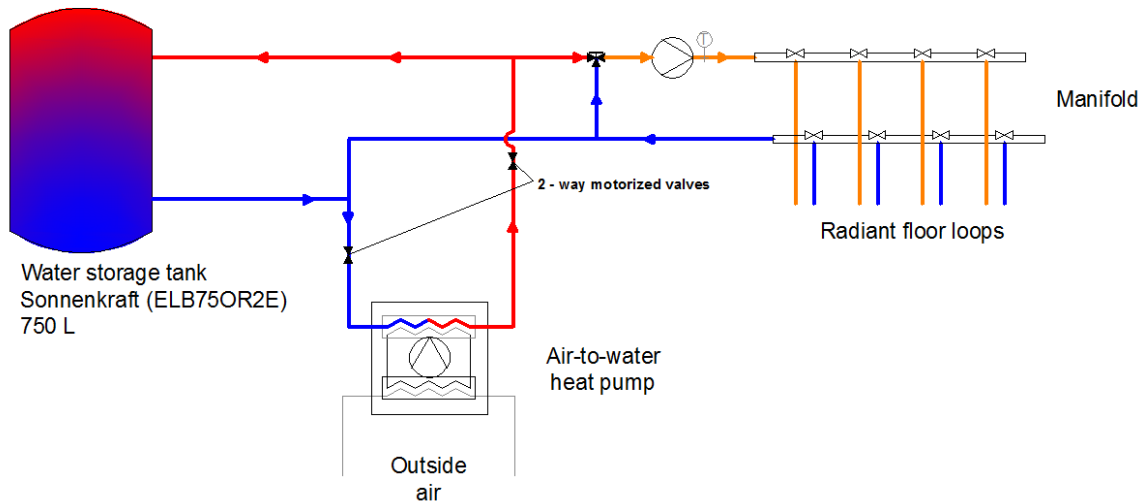


Figure 51 – Option 3 simplified representation. The heat pump can provide water both to the storage tank and radiant floor

2. Performance of the selected heat pump

The heat pump selected is air-to-water, model Altherma ERLQ004CAV3 from Daikin. It is a high efficiency model, provided with inverter technology. As can be seen on Figure 52, the heat is first extracted from the air by the outdoor unit. It is then transferred to the water circuit in the indoor box, by means of the thermodynamic cycle. On the side of the indoor box, the heat is transferred to the water circuit through the plate heat exchanger. It then goes to the final heat exchanger, where it can be utilized as intended by the user. The performance of this heat pump is assessed and reported in this section.

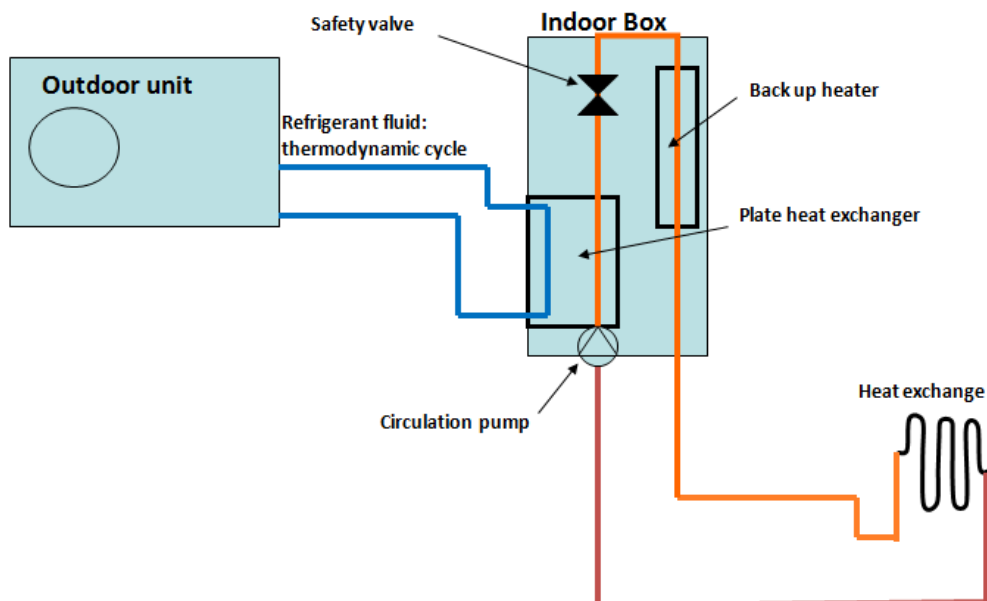


Figure 52 – Schematic representation of the main components of the heat pump

The heating and cooling demand obtained with the load calculations in IDA-ICE, have been used to calculate the seasonal COP and EER in both Paris and Copenhagen with a simulation tool provided by Daikin company.

In Table 25 and “Annex 15: Operation period and outdoor temperature for Daikin heat pump simulations”, it is possible to see the data input in the Daikin simulation tool. Table 26 reports the main features of the heat pump selected based on datasheet, while Table 27 shows an overview of the main results obtained with the simulation tool. The results are further explained in sections IV.2.1 and 2.2.

Table 25 – Design input in the Daikin simulation tool

Design conditions	
Leaving water temperature range heating	25,0°C/35,0 °C
Leaving water temperature range cooling	15,5°C/20,0 °C
Bottom plate heater	No

Table 26 – Information concerning the heat pump selected

Heat Pump overview ¹	
Nominal heating capacity	4,31 ² /3,50 ³ kW
COP	4,72 ² /3,81 ³
Operation range heating	-25,0 / 25,0°C (ambient condition, wet bulb)
Nominal cooling capacity	7,04 ⁴ /4,98 ⁵ kW
EER	3,21 ⁴ /2,58 ⁵
Operation range cooling	10,0 / 43,0°C (ambient condition, dry bulb)
Refrigerant	R410A
Power supply	230V 1ph

Table 27 – Performances of the heat pump selected, as an output of the Daikin simulation tool, both in Paris and Copenhagen

Paris

Performance	
System model	Daikin ERLQ004CAV3
Required heating capacity	1,4 kW
% covered by heat pump	100,0%
Seasonal COP	4,5
Required cooling capacity	1,5 kW
% covered by heat pump	100,0%
Annualized EER	4,4

Copenhagen

Performance	
System model	Daikin ERLQ004CAV3
Required heating capacity	1,6 kW
% covered by heat pump	100,0%
Seasonal COP	3,8
Required cooling capacity	1,3 kW
% covered by heat pump	100,0%
Annualized EER	4,5

More input and graphical output from the Daikin simulation tool can be found in Annex 15: Operation period and outdoor temperature for Daikin heat pump simulation.

2.1. Heating, Daikin simulation

Based on dynamic simulation (IDA-ICE), heating is no more needed to keep a minimum indoor $T_{op} = 21^{\circ}\text{C}$, when the outdoor temperatures reaches 12°C , if the air supplied by mechanical ventilation and

¹ The heating/cooling capacity and performance of the heat pump have been derived from Daikin datasheet (Daikin Europe N.V.)

² Entering water 30°C ; Leaving water 35°C ; ambient conditions: 7°C dry bulb/ 6°C wet bulb

³ Entering water 30°C ; Leaving water 35°C ; ambient conditions: 2°C dry bulb/ 1°C wet bulb

⁴ Entering water 23°C ; Leaving water 18°C ; ambient conditions: 35°C dry bulb

⁵ Entering water 12°C ; Leaving water 7°C ; ambient conditions: 35°C dry bulb

solar/internal gains are taken into account¹. If the free gains and the contribution of mechanical ventilation are not considered, heating is needed until a temperature of 16 °C is reached outdoor (see Figure 53).

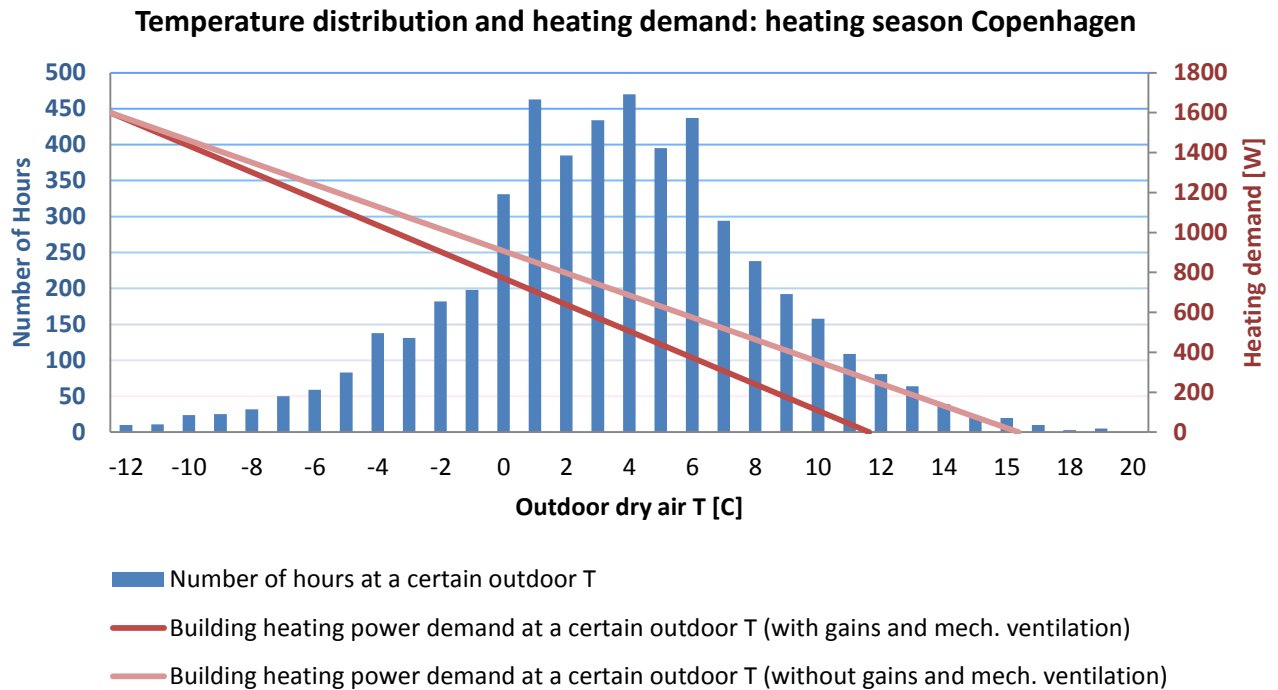


Figure 53 – Building demand compared to number of hours of outdoor temperature in heating season for Copenhagen

For Copenhagen the demand of space heating has been set to 1,6 kW at -12°C outdoor (indicated by (1) in Figure 54) and null at +12°C. The heat pump capacity depends on the outside temperature and the leaving water temperature. As starting point, the simulation tool from Daikin, assign the designed maximum leaving water temperature, 35 °C, to the minimum temperature in the winter profile.

The calculated seasonal COP in heating is 3,8.

With an outdoor temperature lower than 7°C, the minimum heating capacity of the heat pump is steady at 1,8 kW.

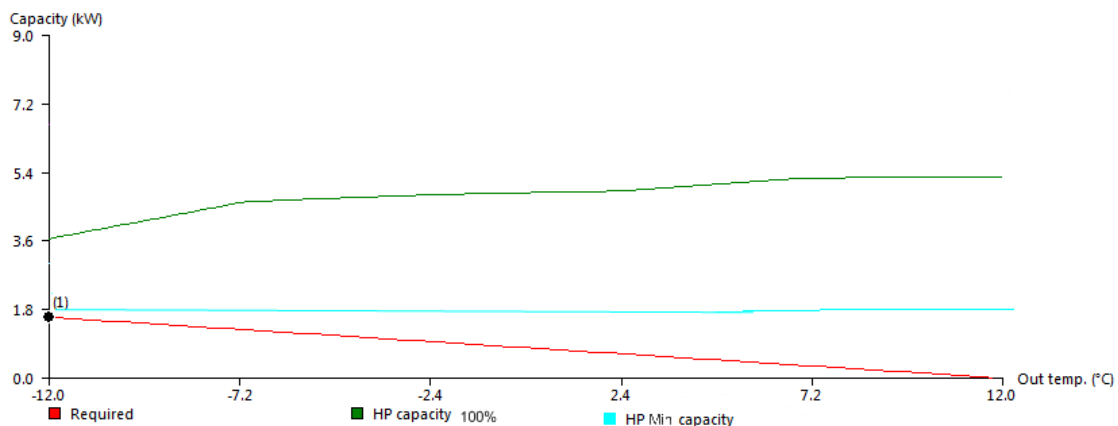


Figure 54 – Heating capacity of the heat pump and dwelling demand in Copenhagen

For Paris the calculated seasonal COP in heating is 4,5. The demand of space heating has been set to 1,4 kW at -7,2°C outdoor.

¹ Mechanical ventilation is set to a minimum of 0,5 h⁻¹ with a temperature supply equal to 16°C (IDA-ICE 4.6 model).

In both Copenhagen and Paris scenarios, backup heater capacity is not needed since the capacity of the heat pump is always higher than the building need. Indeed the equilibrium point or equilibrium temperature are never reached.

2.2. Cooling, Daikin simulation

In cooling mode, most of the heating source derives from solar and internal gains and the outdoor temperature contribution is less relevant. This is the reason why cooling is still needed until the outdoor temperature drops to 22°C (see Figure 55), to keep a maximum indoor $T_{op} = 25^{\circ}\text{C}$. In cooling mode, both the mechanical ventilation and gains have been considered.

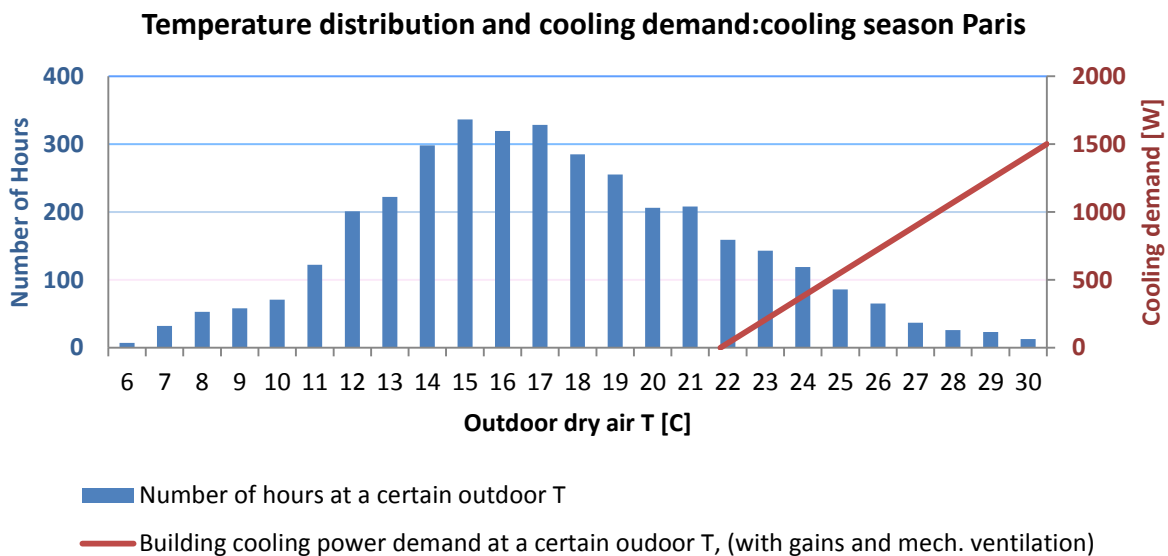


Figure 55 – Building demand compared to number of hours of outdoor temperature in cooling season for Paris

For Paris the demand of space cooling has been set to 1,5 kW at 30°C outdoor (indicated by (1) in Figure 56) and null at 22 °C. As starting point for cooling, the designed minimum leaving water temperature, 15,5°C, is assigned to the maximum day temperature in the summer. The calculated annualized EER in cooling is 4,4. With an outdoor temperature lower than 35°C, the minimum cooling capacity of the heat pump is steady at 2,5 kW.

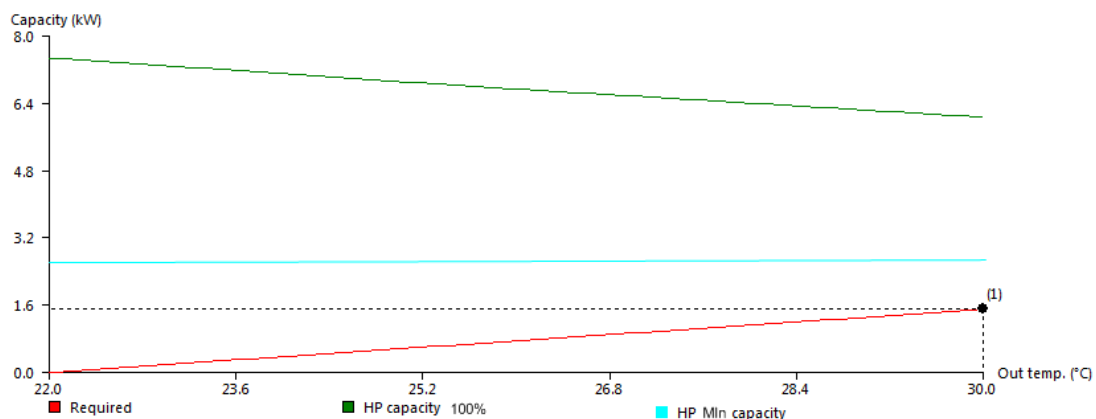


Figure 56 – Cooling capacity of the heat pump and dwelling demand in Paris

For Copenhagen the calculated annualized EER in cooling is 4,5. The demand of space cooling has been set to 1,3 kW at 26,3°C outdoor.

2.3. Considerations

In conclusion regarding the heat pump selection, even though a model with low capacity has been selected, the building demand is lower than the minimum capacity of the heat pump both in heating and in cooling. This supports the strategy of implementing a storage tank in the HVAC system. In this way the higher efficiency of the inverter compressor can be still exploited, operating the heat pump in the range between minimum and maximum capacity. Furthermore the heat pump is provided with an option called “Silent mode”. This option is generally used to diminish the noise of the external unit, but also induces a reduction of the maximum capacity of and power used by the compressor. This mode has been therefore selected to limit partially the capacity of the heat pump which has been proved to be excessive for EMBRACE.

3. Domestic hot water

As previously defined (see Figure 22), the Compact P provides 850 W of heating power, in normal ventilation mode. This value has been used to size the DHW tank based on tapping program n°2, as defined in EN 15316-1. To determinate the size, one uses the maximum energy content of the tank E1 at the end of each draw-off of the tapping program. With this approach, a tank of 50 liters would be sufficient. However, in Sub-contest 6.7 of SDE2014 regulation: “Hot water draws”, the Organization requires the possibility to tap 50 liters at 43 °C three times in a row (i.e. 150 liters). Thus, it has been decided to use the 180 liters tank of the Compact P just for DHW. The calculated losses for this tank are 1,61 W/K. For details about the tapping program and the calculations concerning the losses see Annex 2: Tanks size and losses.

Recirculation is not implemented in the distribution because the short distribution length guarantees a waiting time smaller than 9 seconds in the worst scenario. All the water terminations are designed in parallel as it is possible to see in drawing PL-101 of Annex 11: Mechanical and instrumentation drawings from PD#6, Team DTU.

Avoiding recirculation, this results in a reduction of the heat losses per day which correspond to 0.33 kWh, calculated based on the following equation, from EN 15316-3-2 (eq. 4):

$$Q = \frac{\rho_w \cdot c_w}{1000} \cdot V_w \cdot (\theta_{avg,w} - \theta_{amb}) \cdot n_{tap} \quad (MJ)$$

Where:

ρ_w is the specific mass of water (density) (kg/m³)

c_w is the specific heat capacity of water (kJ/kg·K)

V_w is the volume of water contained in the pipes (m³)

$\theta_{avg,w} - \theta_{amb}$ is the difference between the average water temperature of the water and the ambient (°C)

n_{tap} is the number of times that water is tapped

Based on the previous calculations, the losses through the tank and the distribution pipes have been determinate to be around 400 kWh/year, of which around 70% are from the DHW tank.

3.1. Domestic hot water from solar collectors

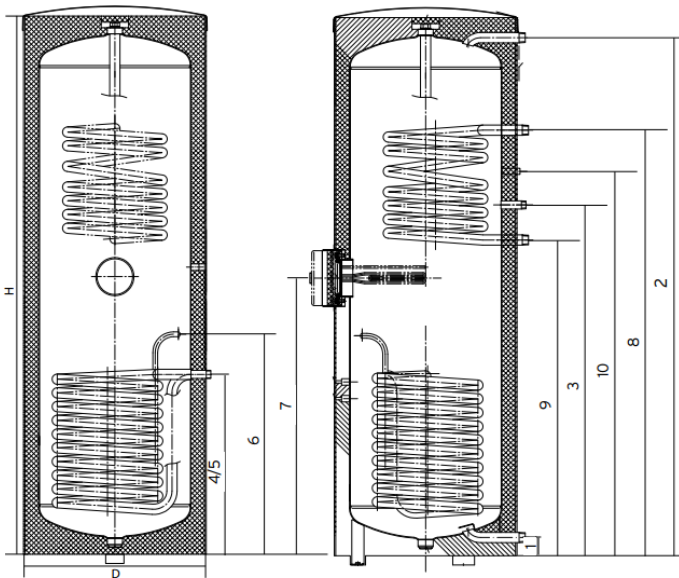
The detailed design of the solar collectors for hot water production is left apart as other students have been working on this topic. The main concepts and choices have obviously been proceeded in close cooperation in order to reach the desired performance of the hot water production. The appliances connected to DHW consume 272 kWh/year as calculated in Annex 7: House appliances data and energy consumption. The calculated tank and pipes' losses amount to 402 kWh/year, adding those values, the DHW yearly consumption becomes 1855 kWh/year. Inserting those data as an input in the program Polysun, 4 m² of flat plate solar collectors cover 65% and 55% of DHW needs, based on Versailles and Copenhagen solar radiation respectively. See Annex 3: Solar collectors' data, for further information.

Table 28 – Hot water production with solar collectors per year and efficiency, estimated for Paris

Coverage needs DHW [%]	65%
Global efficiency [%]	77%

4. Storage tank

The volume of the storage tank has been decided mainly in function of the amount of water cooled during the night, which can be stored and the amount circulated during the day in the radiant floor. In this way, by coupling with natural ventilation, it is expected to cut down the use of the heat pump for cooling.



D = diameter with insulation = 970 mm

H = height with insulation = 1816 mm

Insulation thickness = 85 mm

Capacity 750 liters

1. Radiant floor return/supply in heating/cooling mode (H = 140 mm)
2. Radiant floor supply/return in heating/cooling mode (H = 1598 mm)
3. Not used in Versailles
4. Daikin supply (heat exchanger)(H = 823 mm)
5. Daikin return (heat exchanger)(H = 823 mm)
6. Temperature sensor T_{bottom} (H = 467 mm)
7. Electrical coil (not installed)
8. Return unglazed solar collectors (heat exchanger) (H = 1405 mm)
9. Supply unglazed solar collectors (heat exchanger) (H = 1000 mm)
10. Temperature sensor T_{top} (H = 1542 mm)

Figure 57 – Layout of the Sonnenkraft storage tank DWH750 R2, extract from Sonnenkraft datasheet. The connections explained on the right side are those as assembled for the showcase in Versailles

Table 29 – Estimation of the expected storage tank cooling with unglazed solar collectors

Unglazed solar collector surface (m ²)	7,2
Average cooling power, based on TRNSYS	56 W/m ² = 0,4 kW
Hours of operation, based on TRNSYS	9 (from 21:30 to 6:30)
Flow rate (l/min·m ²), based on TRNSYS	0,7 l/min·m ² = 5 l/min
Tank size (Litres)	750
Time needed to circulate once the water in the tank	150min=2,5 hours
N° of time all the water in the tank is circulated	3,6
Temperature drop in the tank over the night (°C), based on TRNSYS. (Initial temperature 22 °C)	4,5

From the results obtained sizing the radiant floor, during the design day around 1555 litres are circulated in the floor (flow rate 0,072 kg/s and operated time around 6 hours). The volume of water circulated during the cooling season in the floor will always be lower than this value. Smaller size of storage tank can be accepted, since it means that the water from the same reservoir will be circulated more than once during the night, increasing the overall temperature drop. Thus a tank of 750 litres has been selected, based on the products available on the market and also in order to fit the architectural design.

Based on TRNSYS simulations it is expected a drop in the tank of 4,5 °C with a flow rate of 0,7 l/min·m² and 7,2 m² of unglazed solar collectors. For details about the calculations concerning the losses of the buffer tank, both in heating and cooling season, see Annex 2: Tanks size and losses.

5. Discussion

During this project, it has been experienced that the theoretical concept and dimensioning of the HVAC system can differ from its actual realization. In fact, the team members learnt that all the choices weighed carefully during the design stage can rapidly change when passing from the theoretical to the tangible level. Time, finance, inexperience, poor flexibility of products, human mistakes during the design or assembly phase, lack of cooperation or wrong communication between students, companies and installers are all factors difficult to anticipate. The “integrated design” approach of the team, which incites the designers to take into account energy-efficient strategies from the early stages of the design, has limited the effects caused by those issues. Nevertheless, some last-minute changes had to be made in order to enable the realization of the project. Among those, the location of the heat pump in the hydraulic scheme had to be changed. Analysis had shown that a better integration and control would have resulted in lower energy consumption, but it has not been possible to realize because of the issues previously described.

The systems combine the heating and cooling produced by different sources: solar thermal collectors, unglazed collectors, and an air-to-water heat pump. The choice of the heat pump capacity and temperature set-points has been based on the distribution of the building demand during the year. Other technologies such as geothermal water-to-water heat pumps or district heating/cooling are recognized to be efficient as well, but would not have met the requirements of the competition. For highly insulated building provided with low temperature heating and high temperature cooling, air-to-water heat pumps are still quite effective because of the smaller ΔT they have to overcome. Furthermore, the selected model presents high performances; it is featured with inverter technology and one of the smallest compressors on the market for residential applications.

A possible issue inherent to the HVAC design is the use of a single tank to store the cooled and heated water for the radiant floor in the different seasons. Frequent switches between cooling or heating modes are thus not allowed. This could be a problem especially during the transition periods, if the weather turns out to be unusually cold or warm (this issue is also discussed in part V.2). From the indoor climate point of view, splitting the storage in two separate tanks could have been a better option. But taking into account economical and architectural aspects, this option has been discarded. In fact, for a highly insulated dwelling of this size, exceptional short-term changes of temperature affect less the indoor environment (see damping ratio f in section II.2.2.). Furthermore, passive houses are supposed to limit the use of active technologies, achieving a good indoor climate mainly with passive strategies. Limiting the use of the active radiant floor by having only one tank incites the user to exploit more the passive means. This was experienced during the competition with the exploitation of free gains (like the ones generated by the appliances) to rise the temperature when slight heating was needed. If this is not sufficient, the supply air of the mechanical ventilation can be conditioned as well.

V. Control

The control system is a crucial part of the design of any HVAC system. A house can be equipped with the most advanced and efficient individual devices, if they are not controlled in a proper way, the overall HVAC will not perform as efficiently as promoted by the manufacturers. In fact, this is especially true for low-energy buildings such as the Solar Decathlon houses, that must reach the highest levels of performance. Centralizing the control in one unique system is a challenge, since the manufacturers develop products which sometimes have their own control embedded or use different protocols that cannot communicate with others.

As previously stated in paragraph IV.1., for the showcase of Versailles the layout and control of the HVAC system has been simplified in order to fit the tight timetable and overcome unexpected difficulties in finding or assembling components. The main difficulty has been encountered in combining products from different companies which have already their own controls built-in, and are not able to receive or send information to other systems. A more advanced control was designed and it is exposed in “Annex 12: Control drawings from PD#6, Team DTU”. One of the main differences between the designed system and the realized one is that the design case enables at the same time to deliver the chilled/warmed water to the radiant floor and store it in a tank. Once the desired temperature set-point is reached in the tank, the heat pump is switched off and the water is drawn just from the storage tank. In the realized system the chilled/warmed water is produced by the heat pump, stored in a tank and from there supplied to the radiant floor (see differences between 1st and 3rd option in paragraph IV.1.).

The control strategy here exposed is the one implemented for the competition prototype.

1. Central control

The home automation of EMBRACE is based on a central control cloud-based. This House Management System allows residents to monitor their energy production and consumption, enabling them to access the installations from a tablet and adapt their behavior in order to reduce their own energy consumption.

It is possible to access the PLC (Proportional Linear Control) and the IHC (Intelligent Home Control) through an app¹ which gives the tenants a user-friendly graphical interface of the house automation. The management system controls different terminals such as heating, ventilation, cooling and lighting devices. The degree of freedom of the occupants is limited and is mainly based on their needs and not how to achieve them. This has been done with purpose since an inexperienced management of the technical systems can produce wrong decisions. The user can choose the cooling and heating set-point for each of the conditioned zones, switch between cooling and heating operation mode and increase the ventilation rate in the kitchen hood and bathroom. The PLC control of the solar collectors’ pumps cannot be modified but just switched on and off. The radiant floor set-points can be set either manually on the rooms thermostats or in the app which integrates U@home application from Uponor (Figure 58).



Figure 58 – Uponor Digital Display Thermostat T-75 and U@home application

¹ The app has been developed in collaboration with Schneider Electric Denmark, Lauritz Knudsen.

The three mechanical ventilation steps, as defined in Table 9, are mainly automatically controlled in function of the instant RH_i and the 24 hours averaged relative humidity level \overline{RH}_{24} (see Table 30). The relative humidity thresholds have been obtained based on air quality simulations and on similar approaches already adopted in the control strategies of Nilan.

Table 30 – Main equations controlling the mechanical ventilation demanded flow rate

Normal mode is on if:	Forced mode is on if:	Away mode is on if:
$0 < RH_i \leq 30$ and $RH_i < 1,1 \cdot \overline{RH}_{24}$ Or $30 < RH_i \leq 80$ and $RH_i < 1,05 \cdot \overline{RH}_{24}$	$0 < RH_i \leq 30$ and $RH_i \geq 1,1 \cdot \overline{RH}_{24}$ Or $30 < RH_i \leq 80$ and $RH_i \geq 1,05 \cdot \overline{RH}_{24}$ Or $80 < RH_i$	Switched manually by the users or activated together with the home alarm

2. Switch between heating and cooling mode

The storage tank implemented in EMBRACE is used in the cooling season to store cold water, and in the heating season to store warm water, both aimed at being circulated in the radiant floor. Using the same tank for both heating and cooling purpose makes the hydraulic system more complex, because it is desired to maintain stratification in the tank. It means that in the heating mode, the water for the radiant floor is taken from the top of the storage tank where it is warmer. Once it is cooled down by circulation in the floor, the water is given back to the bottom. Conversely in cooling mode, the order is inverted: the water is supplied from the bottom and returned to the top. In this way the temperature stratification of the water in the tank is favoured; by limiting mixing, the energy need is reduced.

In order to make this operation possible, a motorized 4-ways rotary valve is used to switch between heating and cooling mode as shown in Figure 59. The actuator of the 4-ways valve is controlled by PLC, setting either heating or cooling mode in the app from where the user can control the home automation of the dwelling.

It has been decided to keep the switch between heating/cooling season decided by the user. The switch could have been commanded automatically when the outside temperature would reach certain levels previously defined. But the inhabitants usually like to keep a minimum of decision power about the systems implemented in their house, therefore it is appropriate to let the user decide when he/she feels too cold/warm in the house and wants to start heating/cooling.

However, this switch must happen only once per year. Indeed the tank contains 750 liters of water, and it requires a lot of energy to cool it down or warm it up. Therefore it would be highly inefficient to try and switch too often between heating and cooling, because it would require changing the temperature of the whole tank. It is not possible to provide heating through the radiant floor during the cooling season, even if the outside weather becomes unusually cold for a short period. The user interface must block this kind of too frequent switching. It is also common and traditional practice to start the heating/cooling systems of a house only once annually, at approximately the same period each year.

However the Nilan Air Handling Unit (AHU) is provided with an independent thermodynamic cycle which allows to condition the supply air.

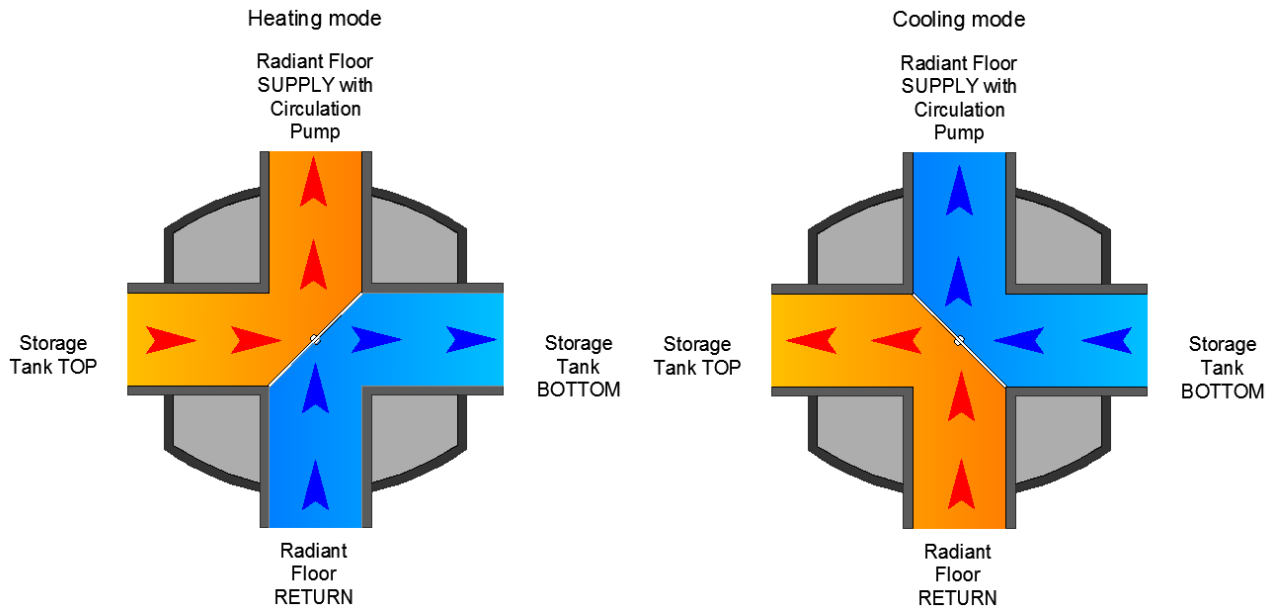
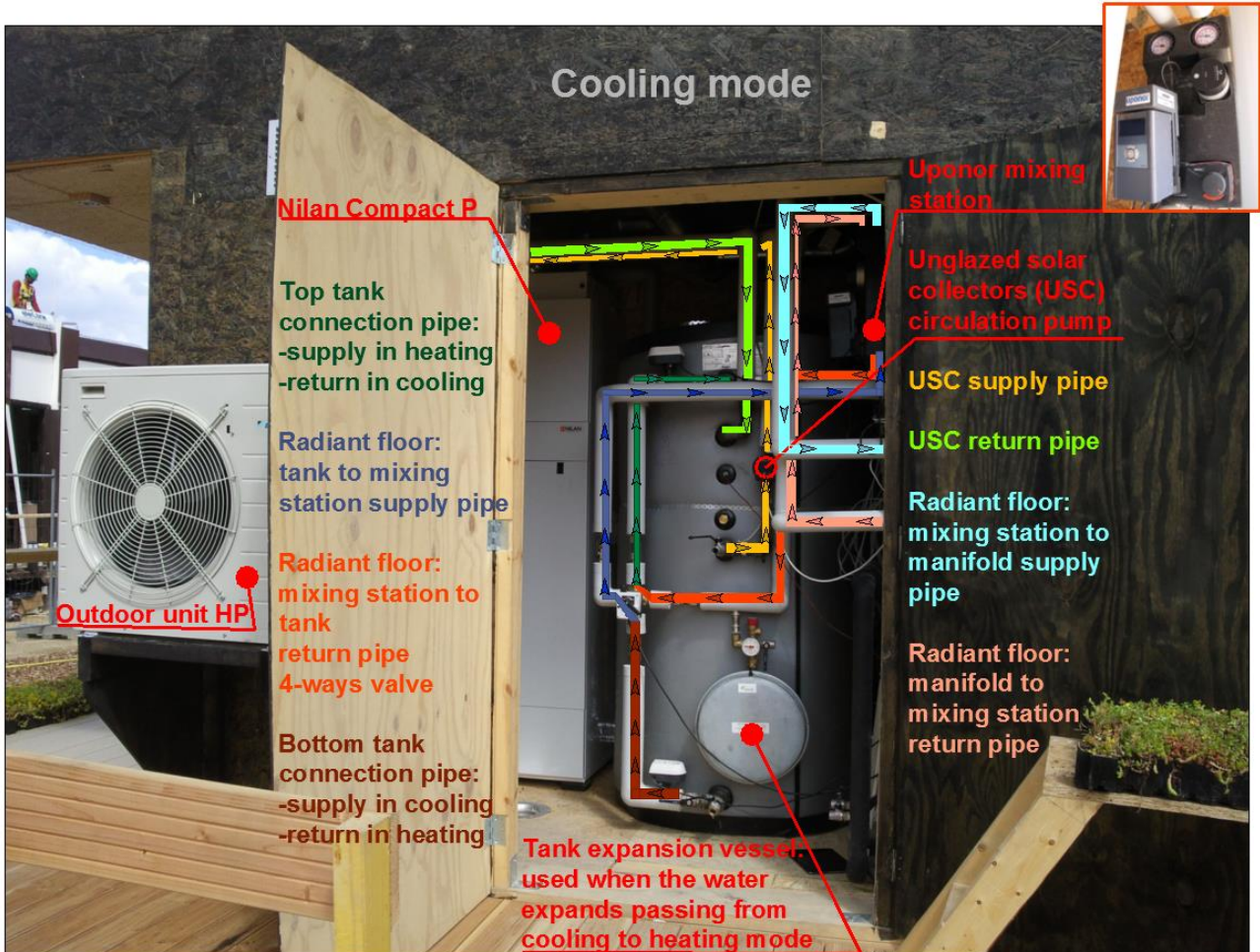


Figure 59 – Schematic representation and operation of the 4-ways rotary valve HRB 4 from Danfoss



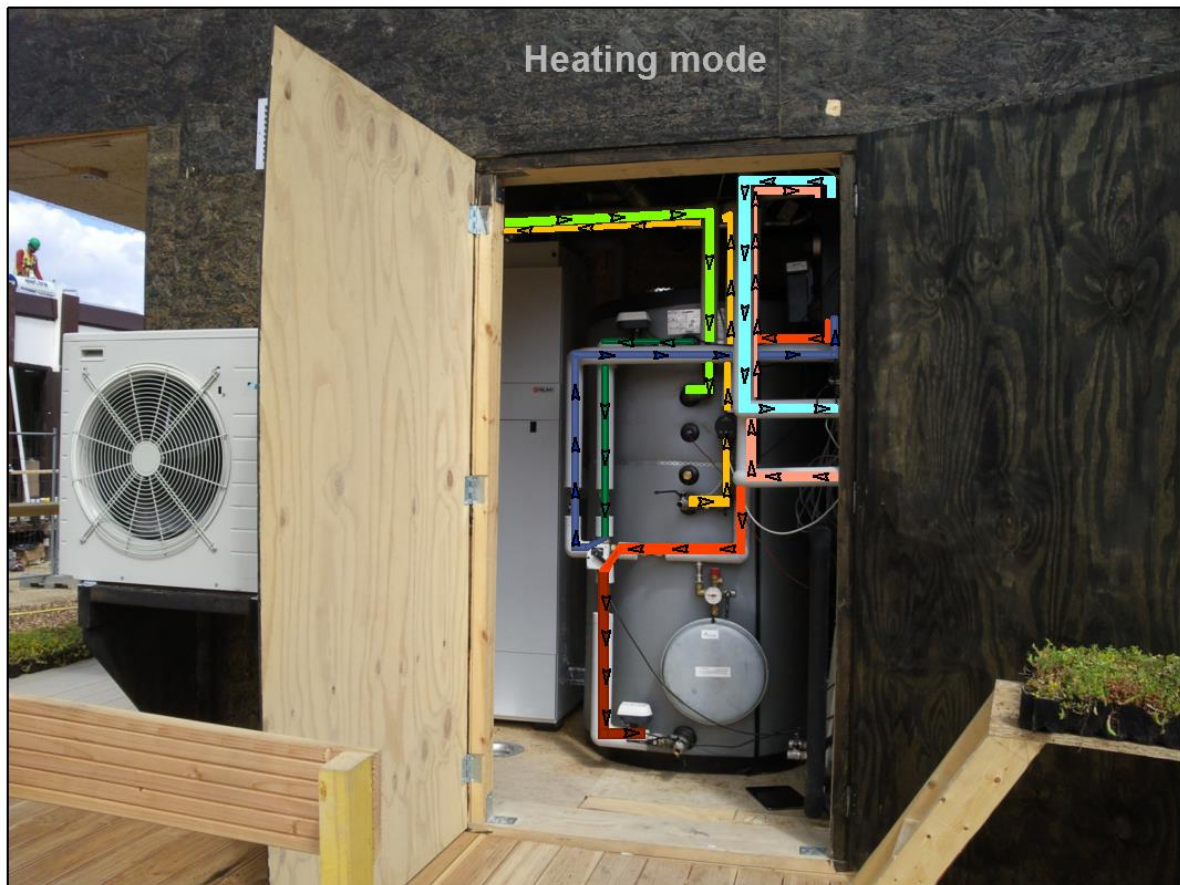


Figure 60 – Technical room visualization with components and flow directions, for both cooling and heating mode

3. Control of the solar collectors

The output of a solar collector is controllable through the circulation pump that runs the heat carrier in it. Grundfos for instance has developed special types of pumps with a flow rate adaptable to the needs. The use of such pumps can enable to produce more hot water in the mornings or evenings, when the sun and the solar irradiance are low, by reducing the flow rate. Opinions differ on this topic: professionals from Batec suggested that the benefits of such type of pump were not worth it the investment in time to integrate this complex system in the overall control. Therefore a simple on/off circulation pump (Grundfos ALPHA2) was chosen, in which it is possible to set manually three different levels of flow rate. The pump is switched on or off by the PLC, in function of the temperature recorded by a sensor in the DHW tank and in the solar collectors return pipe. The same circulation pump is used for the unglazed solar collectors loop. A dynamic control algorithm could have been implemented to start the pump when beneficial, but based on TRNSYS simulations (chapter VII.5.), the cooling period is relatively stable every night.

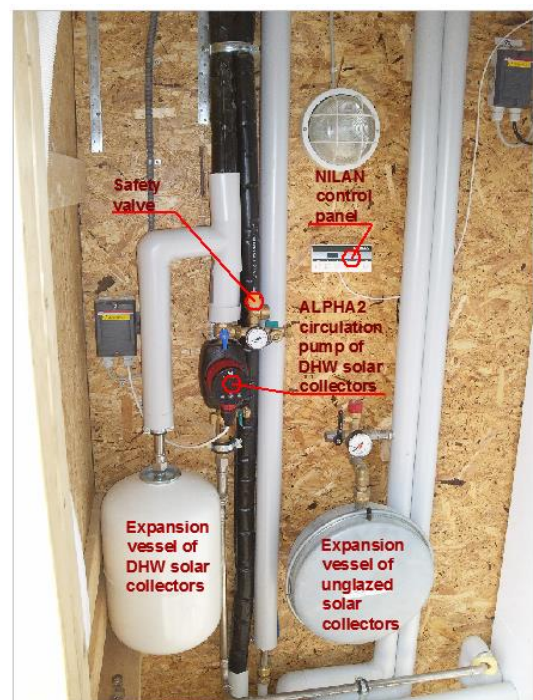


Figure 61 – Solar collectors' main components in the technical room

Thus it has been decided, based on the same simulations, to fix the operation time from 22:00 to 6:00 every night.

4. Control of the radiant floor and heat pump

The conditioning of the space occurs in EMBRACE mainly through the radiant floor. The latter is connected to the storage tank, which is supplied by the heat pump, therefore the control needs to consider all those components. Because of the time and complexity issues already mentioned, the control is simplified: the Uponor system controls the radiant floor independently, and the heat pump controls the temperature in the tank. The actual systems built in EMBRACE are shown in Figure 62.

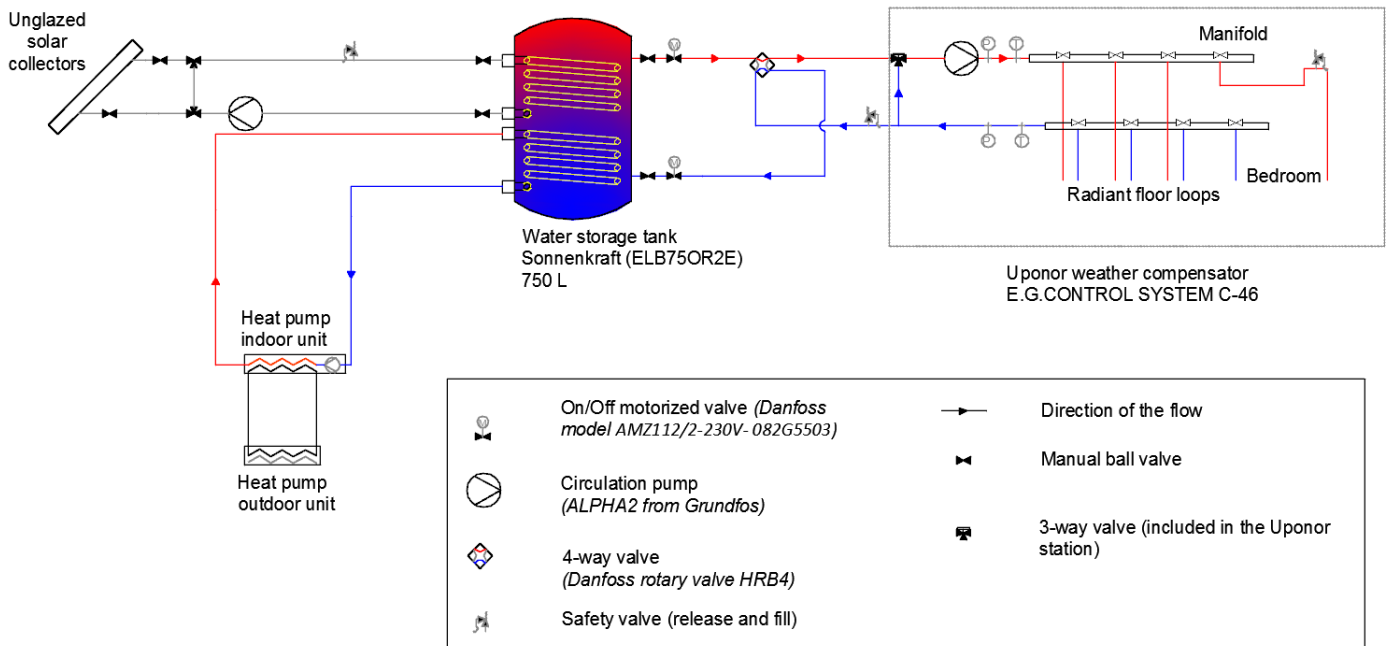


Figure 62 – Implemented system in EMBRACE (storage tank, heat pump, radiant floor and unglazed collectors)
Example given for heating

The radiant floor manifold actuators for each loop and the recirculation valve (mixing station) are controlled by the C-46 component from Uponor, which has its own internal algorithm. It is based on the input received by the relative humidity and air temperature sensors placed indoor and the set-points desired by the user. The number and kind of sensors linked to each loop and the operation of the manifold can be seen in Table 10 and Figure 28 respectively. At the top right of Figure 60 is shown the Uponor mixing station and in Figure 63 the manifold actuators and the C-46 control.

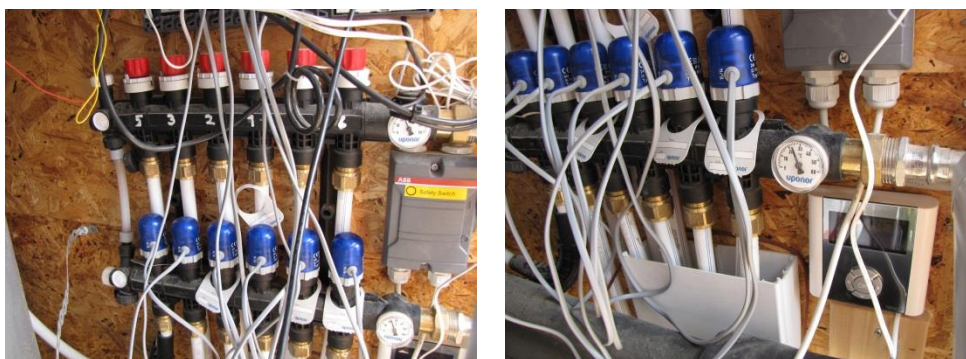


Figure 63 – On the right it is possible to see the radiant floor manifold, where the blue covers are the radio controlled actuators on the supply loops. On the right the console for the C-46 control

The Uponor radiant floor takes the water at the temperature available in the tank, but it cannot command the production of heating or cooling. This is done by the heat pump controller. On the console of the internal unit of the heat pump, the leaving water temperature set-point has to be set manually. If the difference between water supply and return is less than 3°C, both the compressor and the circulation pump are switched off. The circulation pump is then activated by “Sample” operation mode: every 5 minutes it starts and runs for 3 minutes. If during those 3 minutes the ΔT between supply and return water temperature is higher than 5°C the thermodynamic cycle of the heat pump is switched on again. In paragraph V.5, the value to assign to the leaving water temperature is analysed.

A better control to switch on/off the heat pump and define the leaving water temperature would have been room demand based, linking its control with the one of the radiant floor. But it resulted to be particularly complicated to modify and combine the controls of products from different companies. Furthermore, this control would have likely reduced the energy consumption, linking the production directly to the demand but could have also introduced higher thermal discomfort because of the response time needed to heat or cool part of the tank.

5. Choice of the temperature set point in the storage tank

For the configuration of the HVAC selected, described in the chapter IV.1. and 4., it is needed to define the temperature set point of the water in the storage tank, to switch on/off the heat pump. The water in the storage tank is used for space heating/cooling through the radiant floor. This is why the temperature in the tank has been studied in relationship with Standard EN 1264-2 to define the most likely supply temperature. This value is needed as a reference starting point, once the system is assembled and tested, the set point can then be adjusted to meet the best comfort conditions and energy savings. For more data about the storage tank and other assumptions related, see Annex 2: Tanks size and losses.

5.1. Heating

The outdoor temperature has been analysed in comparison to the corresponding power demand of the building. In particular the percentage of time at which a certain temperature is present, has been considered. From Figure 64 it is possible to see that for instance for 70% of the heating season the outdoor temperature is higher than 2°C and that the heating demand is 1 kW at this temperature.

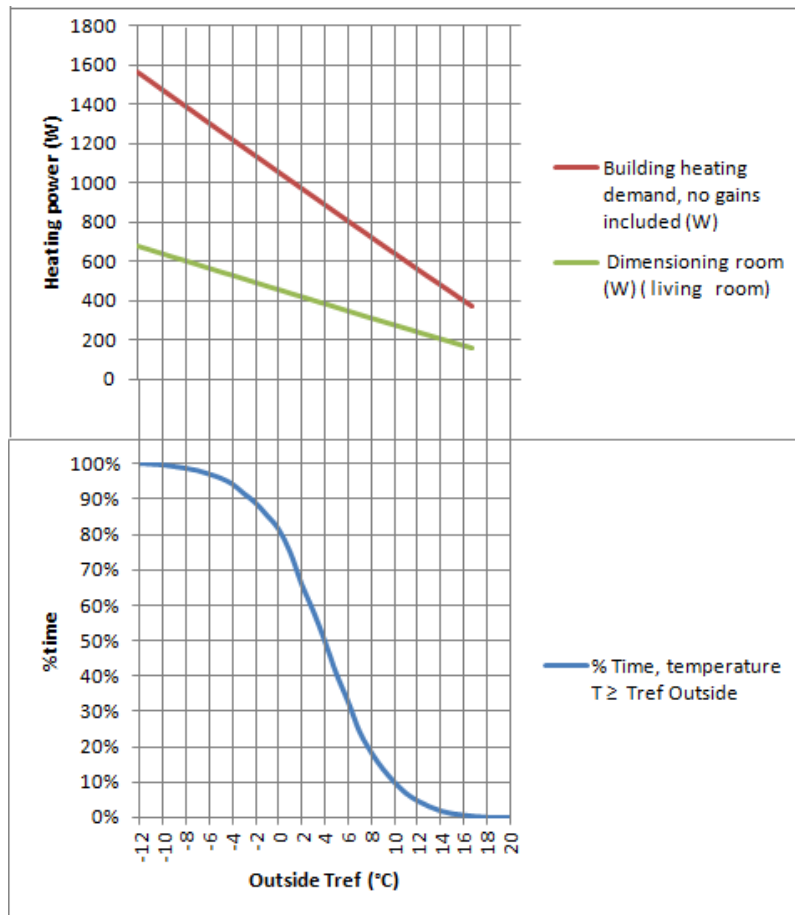


Figure 64 – Temperature distribution from October to April and corresponding heating power demand for the dimensioning room and the entire dwelling

The following table reports some of the values used to construct Figure 64. It has been decided to set the water temperature in the tank so that to cover 92% of the heating season. Based on weather data, 92% of the winter, the outdoor temperature in Copenhagen is equal or higher than -3 °C and based on EN 1264-2, a supply water temperature equal to 27,4 °C is needed for the design room, with this outdoor temperature.

Table 31 – Heating demand in function of the outdoor temperature per percentage of time in the heating season

Tref Outside (°C)	Building heating demand, no gains (W)	Dimensioning room (W) (living room)	Dimensioning room water supply T (°C) (EN 1264-2)	Dimensioning room (W/m ²)	N° of hours at a certain T _{outside}	% Time, temperature T ≥ T _{ref} Outside
-12	1565	676	28,5	37	10	100%
-11	1522	658	-	36	11	100%
-10	1478	639	-	35	24	100%
-9	1435	620	-	34	25	99%
-8	1391	602	-	33	32	99%
-7	1348	583	27,9	32	50	98%
-6	1304	564	-	30	59	97%
-5	1261	545	-	29	83	96%
-4	1218	527	-	28	138	94%
-3	1175	509	27,4	28	131	92%
-2	1132	490	-	26	182	89%
-1	1089	471	-	25	198	85%
0	1046	453	-	24	331	81%
1	1003	434	-	23	463	75%
2	960	416	-	22	385	66%
3	917	397	26,4	21	434	58%
4	874	379	-	20	470	50%
5	831	360	-	19	395	41%
6	788	342	-	18	437	33%
7	746	323	-	17	294	24%
8	703	305	25,8	16	238	18%
9	661	287	-	16	192	14%
10	619	269	-	15	158	10%
11	577	251	-	14	109	7%
12	534	233	-	13	81	5%
13	493	215	-	12	64	3%
14	452	197	-	11	39	2%
15	410	179	-	10	20	1%
16	369	162	25,4	9	20	1%
17	-	-	-	-	10	0%
18	-	-	-	-	3	0%
19	-	-	-	-	5	0%
20	-	-	-	-	0	0%

To take into account also the losses through the tank, some assumptions have been done to simplify the model, keeping it on the safe side. The entire storage tank has been considered at an initial temperature of 30 °C. It is assumed that the maximum period of inactivity for the heat pump is 7 hours and during this time the tank is considered as a closed system (no water is inlet or outlet from outside). The surrounding temperature is at 20 °C.

Based on the previous assumption the following graph (Figure 65) has been obtained, calculating the heat losses through the tank in time steps of 5 minutes.

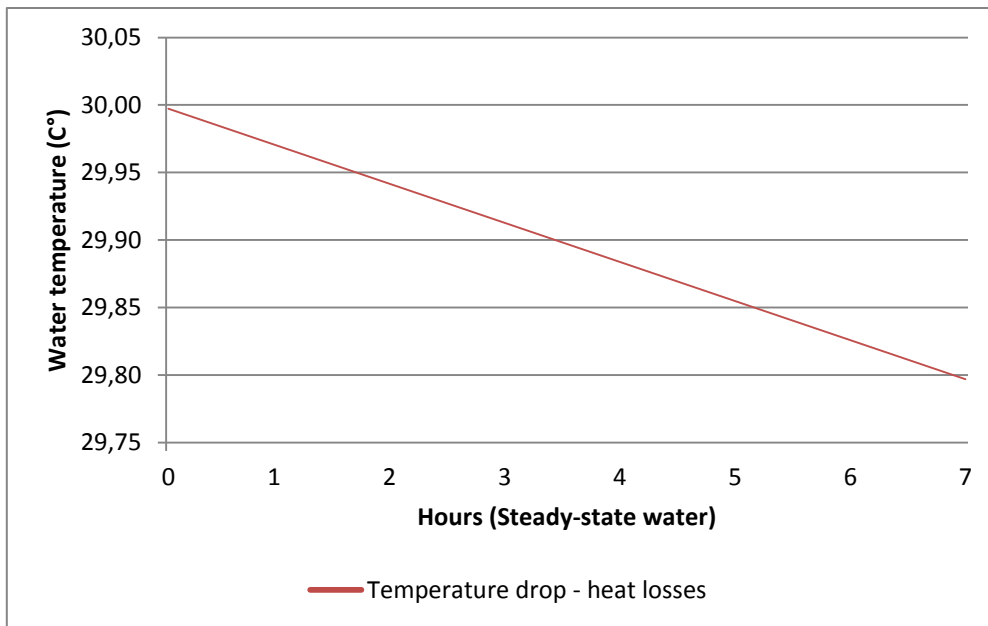


Figure 65 – Temperature drop due to heat losses in the water storage tank, when heat is not provided by heat pump

After 7 hours, the temperature drop is around 0,2 °C, which added to the previous 27,4 °C, defines an initial water temperature needed at 27,6 °C.

5.2. Cooling

For cooling the approach has to be different, since the cooling load depends mainly on the internal and solar gains and not on the outdoor temperature. In this case, it is irrelevant to analyse the entire cooling season in comparison with the outdoor temperature. In fact the indoor set point can be both higher and lower than the outdoor temperature. The demand of cooling is intermittent, with peaks when solar gains are predominant or cooking is performed in the dwelling (afternoon), (see Figure 67).

Conversely the demand of heating is more homogenous and continuous during the day and night because the outdoor temperature is almost always lower than indoor set point (see Figure 66).

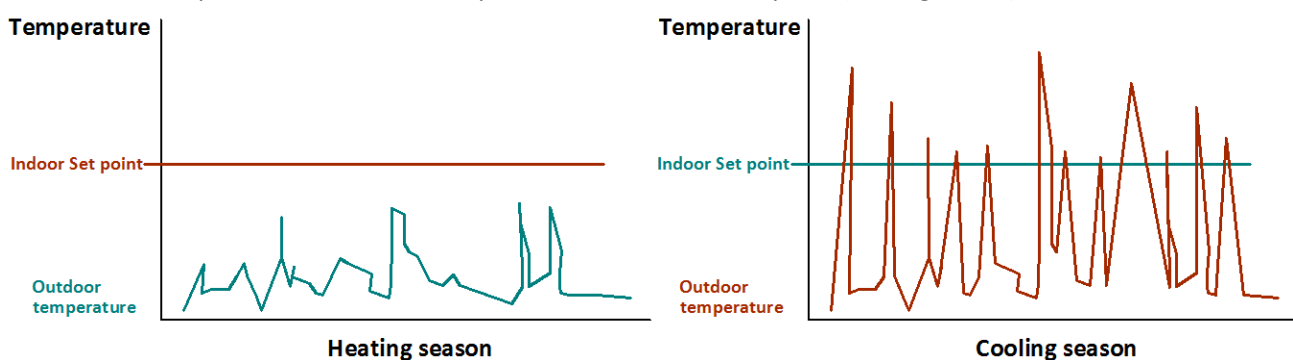


Figure 66 – Representation of the outdoor temperature trend in comparison with the indoor set point, in summer and winter

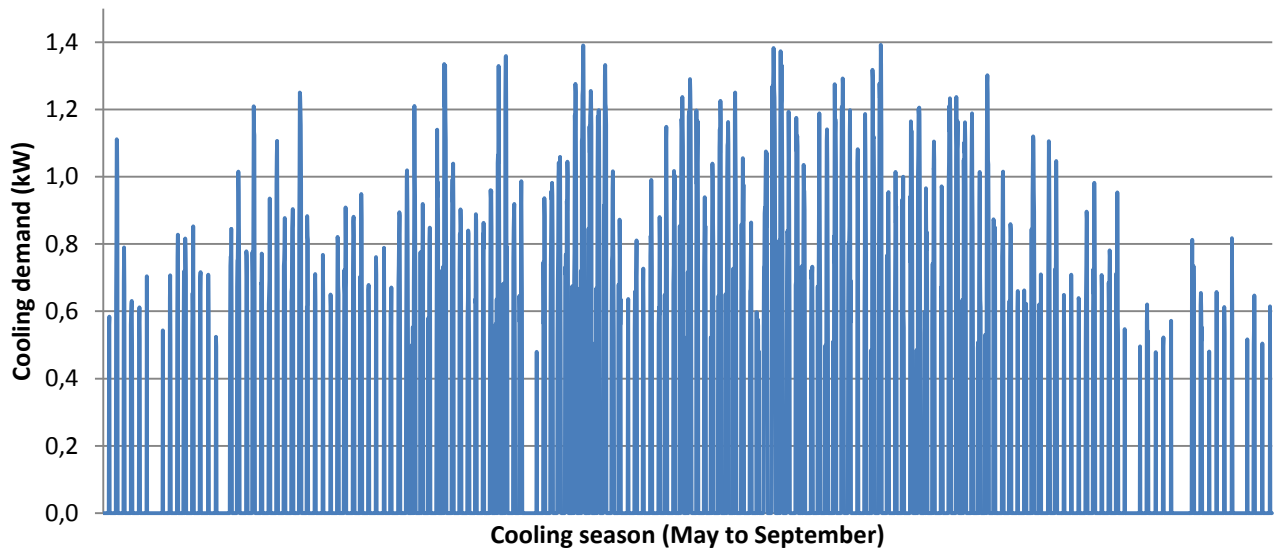


Figure 67 – Cooling demand peaks over the cooling season, in Paris

It has been decided to consider a daily cooling demand curve and see how it changes in function of the internal and external loads. A dynamic simulation has been performed for the design day in Paris, used also to size the cooling demand (16th of July in ASHRAE IWEC weather data). The difference between the load calculation, is that in this case a schedule is given to occupants and appliances so that to simulate more realistic gains (see Annex 4: Dynamic simulation schedules).

The following graph is so obtained:

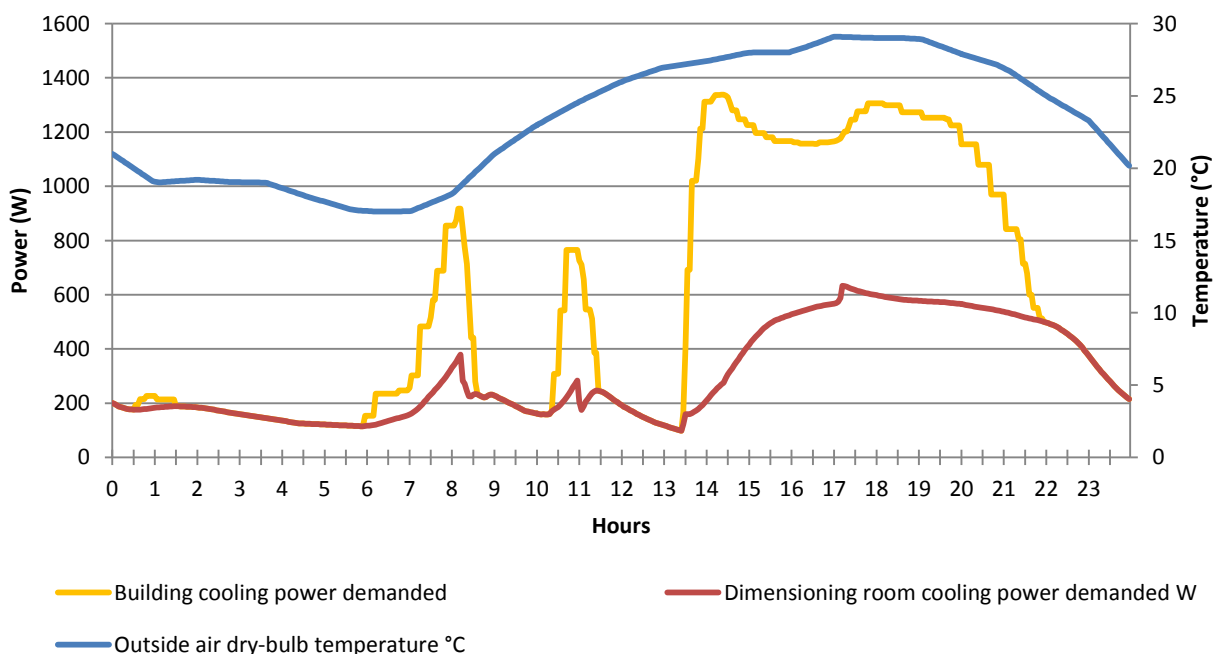


Figure 68 – Temperature and cooling load for the design day

In this way the cooling peak is reduced to a maximum of 1340 W, of which 633 W are from the dimensioning room, corresponding to 34 W/m² (instead of the 41 W/m² obtained in the load calculations).

Based on section 4 of EN 1264-5 and EN 1264-3, for the designed radiant floor, this corresponds to a supply water temperature of 17 °C.

With the same procedure applied before, after 7 hours the temperature increases in the tank of less than 0,1°C, leading to a set point temperature for the heat pump of 16,9°C (initial room temperature assumed at 26°C).

6. Conclusion and discussion

The control of a HVAC system plays a crucial role, at least as important as the choice of its components. As the project was developed at the academic level, where the latest research is developed, it is understandable why the team dared experimental and innovative approaches in this domain. The team firstly raised high ambitions in the home automation of EMBRACE, with the will to merge the controls of products from different companies in a unique app. The initial misconception of the team has been to under evaluate the difficulty of such an approach, which appeared to be a real challenge. The initial ambition to design a unique central control able to operate automatically all the systems of the dwelling has been partially abandoned.

In the end, a home automation system has been developed where all the controls have been gathered in the same graphic interface, but it was not fully functional. This achievement has been possible thanks to the support of professionals from Schneider Electric Denmark. The different sections of the HVAC, like mechanical and natural ventilation, radiant floor, heat pump and circulation pumps have been controlled by independent inputs. The simplifications have been made for the systems where a more complex design would have introduced only slight differences in terms of energy production or consumption. This simplification approach found application for instance in the control of the solar collectors pumps or in the switch between cooling and heating mode.

Regarding the definition of the set-points to control the leaving water of the heat pump, a different approach has been adopted in heating or cooling. The main factor considered for heating is the outdoor temperature, and the solar and internal gains for cooling. The design leaving water temperature to be set in the heat pump control has been calculated to be 27,6°C and 16,9°C for the chosen heating and cooling dimensioning cases. In the heat pump console, the temperature inputs can be set without decimals digits, those values have been rounded to 28 °C and 16 °C respectively, to stay on the safe side.

VI. Testing and performance of the house

In this chapter, the performance of EMBRACE is reported. The annual performance is first presented, based on computer simulations. The performance in Paris is then described, with the details of the competition results.

1. Simulation results / Energy consumption

The previously described IDA-ICE model (chapter III.2. Load calculations (IDA-ICE)) has been implemented in the definition of the systems and used to run dynamic simulations regarding the energy consumption. Radiant floor is inserted as terminal unit in each zone of the model. The energy consumption so obtained is useful to have a general idea about the total energy need and its division among systems.

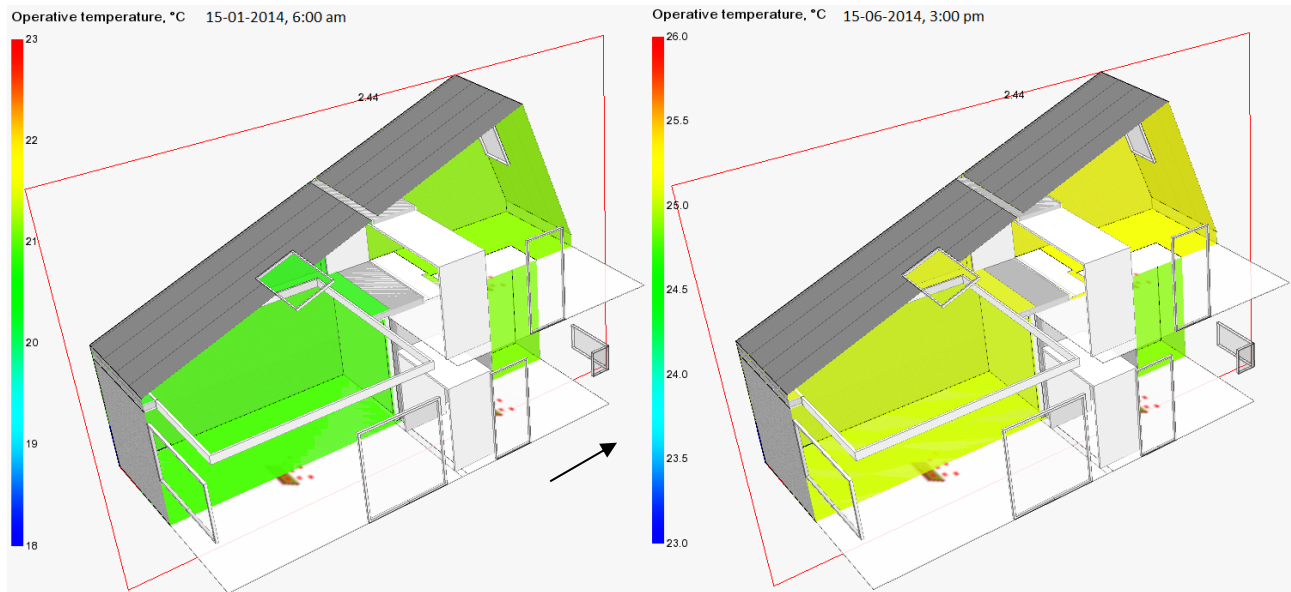


Figure 69 – Example of operative temperature visual distribution, obtainable with IDA-ICE model. Pictures from Copenhagen scenario in January and June

1.1. Systems energy

What is called “Systems energy” in IDA-ICE is the energy provided to the room without applying any efficiency and primary energy factors. In Paris the amount of heating provided is half the one in Copenhagen, for both water and air-based systems. In Copenhagen the cooling demand is halved and almost entirely provided through the radiant floor, as can be seen in Figure 70.

In general the heating provided through mechanical ventilation is 1/5 of the amount provided with the radiant floor in both cities. While the cooling is 1/2 and 1/3 in Paris and Copenhagen, respectively.

Paris:

Copenhagen:

kWh (sensible and latent)

Month	Zone heating	Zone cooling	AHU heating	AHU cooling
1	222.6	0.0	43.1	0.0
2	153.3	0.0	36.6	0.0
3	46.4	0.0	16.5	0.1
4	6.9	16.7	4.6	4.4
5	0.0	97.3	0.0	32.0
6	0.0	162.6	0.0	68.5
7	0.0	254.2	0.0	129.7
8	0.0	243.0	0.0	139.1
9	0.0	76.0	0.0	46.6
10	4.0	6.6	2.5	7.8
11	116.4	0.0	21.5	0.0
12	217.6	0.0	38.3	0.0
Total	767.2	856.5	163.1	428.2

kWh (sensible and latent)

Month	Zone heating	Zone cooling	AHU heating	AHU cooling
1	395.0	0.0	84.2	0.0
2	309.5	0.0	79.9	0.0
3	184.3	0.0	52.0	0.0
4	28.4	3.8	15.4	0.7
5	0.0	24.6	0.4	3.0
6	0.0	126.3	0.0	32.8
7	0.0	131.7	0.0	57.0
8	0.0	114.8	0.0	55.4
9	0.0	18.8	0.0	10.4
10	48.0	0.8	7.2	0.9
11	173.3	0.0	30.9	0.0
12	314.4	0.0	63.6	0.0
Total	1452.9	420.7	333.4	160.3

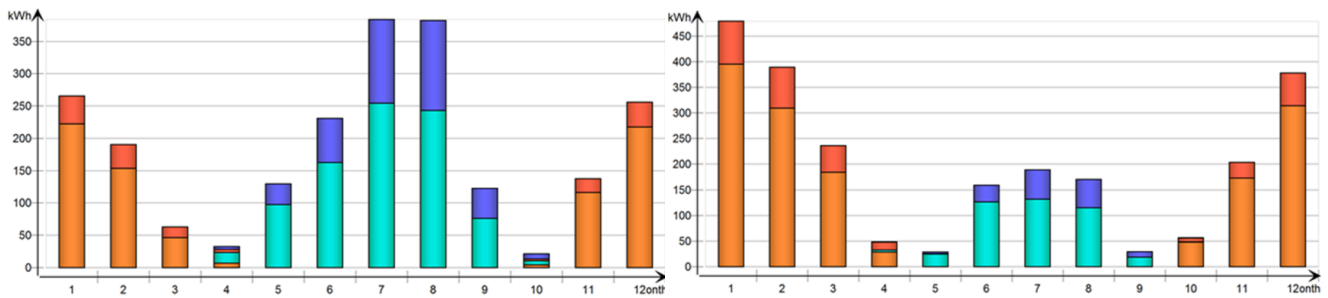


Figure 70 – Monthly system energy provided, divided between mechanical ventilation (AHU) and radiant floor (Zone) for both Paris and Copenhagen

1.2. Hot water consumption-production

According to Danish energy consumption calculation through the SBi-direction 213¹, one person uses 15 m³ DHW at 55°C per year. Since 1,5 people on average are considered for the house, 22,5 m³ is considered per year. This gives a yearly heated water consumption of 1181 kWh/year, assuming the initial cold water temperature at 10°C, $(1181[kWh] = 22500[kg] \cdot 4,2[kJ/kg \cdot K] \cdot 45[K]/3600)$. The value obtained fits also with the tapping programs according to EN 15316 3-1. In fact the amount of water calculated with SBi-direction for 1,5 people results to be in the middle between the consumption for one person and an average family according to EN 15316 3-1, see Table 32.

Table 32 – Domestic hot water consumption profiles, based on Danish SBi-direction 213 and EN 15316 3-1

Reference	N° of people	DHW litres/day		DHW litres/year		DHW kWh/day		DHW kWh/year	
		55°C	60°C	55°C	60°C	55°C	60°C	55°C	60°C
SBi-direction 213	1,5	61,64	61,64	22500	22500	3,235	3,6	1181	1312
EN 15316 3-1 Tapping No. 1	1	-	36	-	13140	-	2,1	-	766,5
EN 15316 3-1 Tapping No. 2	Family (3-4)	-	100,2	-	36573	-	5,845	-	2133,4

As previously stated, the appliances connected to DHW consume 272 kWh/year (calculation in Annex 7: House appliances data and energy consumption). The tank and pipes' losses amount to 402 kWh/year. Adding those values, the DHW yearly consumption becomes 1855 kWh/year. The solar collectors cover 65% and 55% of DHW needs, based on Versailles and Copenhagen solar radiation respectively.

In this way it is derived that the amount of systems energy to be delivered by the Nilan heat pump to the DHW, is 650 and 835 kWh/year, in Versailles and Copenhagen respectively.

¹ This direction describes the methods for calculation of the energy requirements for buildings referring to the energy provisions in Danish Building Regulation 2010, based on program Be10 (Aggerholm S. et al., 2011).

1.3. System efficiency

When considering the heating and cooling demand of a building, the amount delivered to the rooms is always lower than the total power produced. This is due to losses during the storage, distribution, emission, as well as to the generator efficiency as stated in EN 15316-1, see Figure 71.

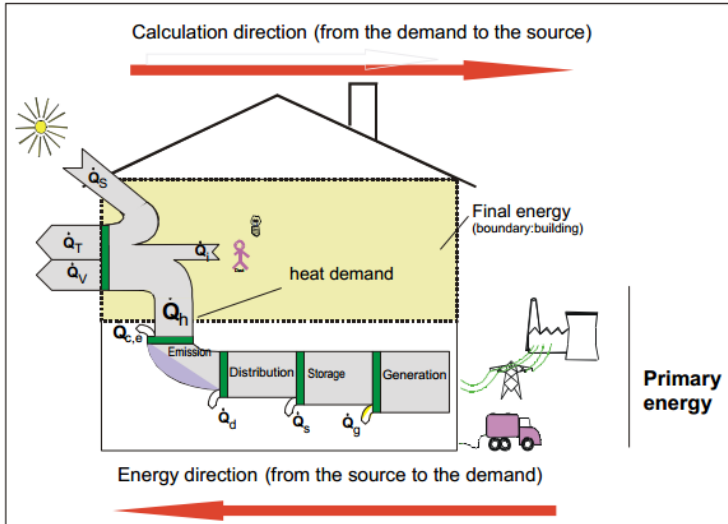


Figure 71 – Calculation concept and building-system boundaries for heating (EN15316-1)

This additional energy that needs to be produced depends by the specific systems implemented and their integration in the building. A good design should aim to reduce the energy demand of the building and also optimize the systems efficiency, minimizing the losses. According to EN 15316-2-1 the systems selected and their insulation level and control have been combined to define the total emission and distribution efficiency, as shown in Table 33. The calculated distribution heat losses and the other parameters used for the calculation of the emission efficiency can be found in Annex 5: Hydraulic scheme, domestic hot water and space heating/cooling losses.

The emission efficiency of the radiant floor when used as a cooling terminal is lower than in heating, this is mainly due to the different superficial heat transfer coefficient, as previously explained in Chapter III.1.

Table 33 – Efficiency of the considered radiant floor system, based on EN 15316-2.1 (emission), EN 15316-2.3 (distribution)

	Heating mode	Cooling mode
Distribution efficiency [%]	99,2 %	99,2 %
Distribution type	Insulated pipes	Insulated pipes
Emission efficiency ¹ [%]	94 %	86,2 %
Emission type	Dry, water based, radiant floor	Dry, water based, radiant floor
Efficiency emission+distribution	93,1%	85,5 %

¹ It includes the efficiency of a PI (proportional integral) control.

1.4. Electrical energy

Here the cooling produced by nighttime radiative cooling is not taken into account. The electrical energy reported in the following table does not include the application of the primary energy factors. Indeed the intent is to compare the electricity consumed with the amount produced thanks to the PV panels.

Table 34 – Estimated energy consumption per year, in Paris

Paris	Installation (kWh)							
	Zone heat	Zone cool	AHU heat	AHU cool	DHW not from SC	Pumps	Light	Electrical appliances
Annualized EER, Daikin	4,4	856				110	179	752
Seasonal COP	4,5	767						
COP Nilan DHW ¹	3,2				650			
COP Nilan AHU ²	3		163	428				
Emission Efficiency (%)	93,9	86,2						
Distribution Efficiency (%)	99,1	98,3	-	-	-			
Total efficiency (%)	93,0	84,7	85,5	85,5				
Electricity (kWh)	185	232	64	167	203			
Total electricity (kWh) year	1891							
Total electricity (kWh/m ² net area)	32							

Table 35 – Estimated energy consumption per year, in Copenhagen

Copenhagen	Installation kWh							
	Zone heat	Zone cool	AHU heat	AHU cool	DHW not from SC	Pumps	Light	Electrical appliances
Annualized EER, Daikin	4,5	421				110	394	752
Seasonal COP	3,8	1453						
COP Nilan DHW	3,2				835			
COP Nilan AHU	3		333	161				
Emission Efficiency (%)	93,9	86,2						
Distribution Efficiency (%)	99,1	98,3	-	-	-			
Total efficiency (%)	93,0	84,7	85,5	85,5 ³				
Electricity (kWh)	415	111	130	63	261			
Total electricity kWh year	2236							
Total electricity (kWh/m ² net area)	38							

¹ COP for "Normal mode" ventilation flow rate

² Lowest COP from Nilan datasheet

³ From AHU (Nilan) data sheet

The DHW losses through the tank and the distribution system have been already included. The artificial light consumption is taken from the Delivery 6 Project Manual. The data concerning the pump and their energy are included in Annex 6: Pumps data and consumption.

Electricity production

The electricity production has been simulated with the program PVSYST V5.06, considering also the losses as shown in Figure 72.

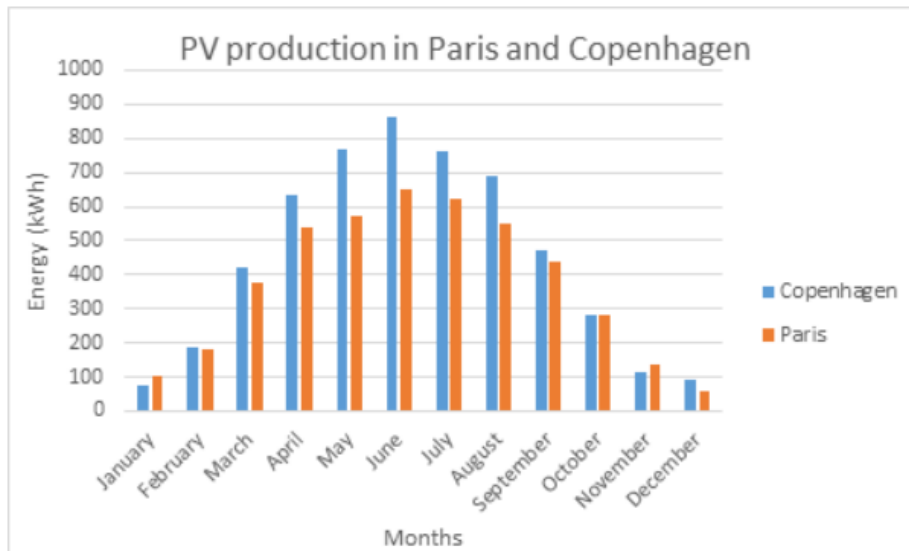


Figure 73 – Monthly PV production for Paris and Copenhagen

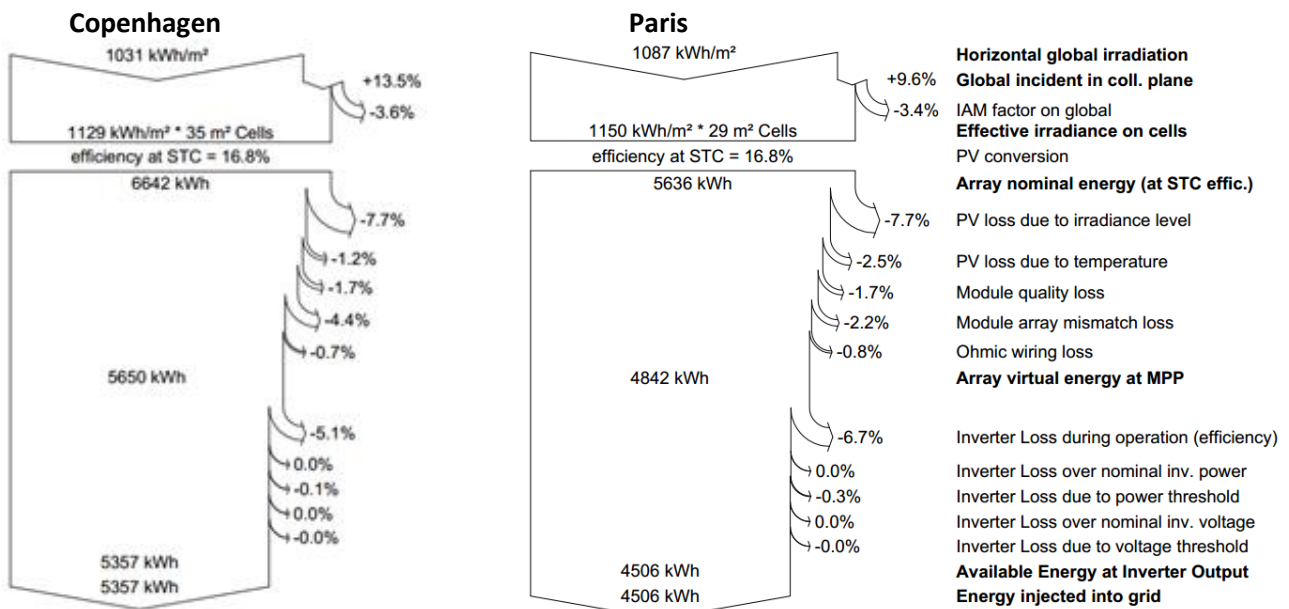


Figure 72 – Loss diagram over the whole year for Copenhagen and Paris

Table 36 – Comparison of the electricity consumed and produced with PVs consumed

Energy (kWh/year)	Paris	Copenhagen
Electricity consumed	1891 kWh, (32 kWh/m ²)	2236 kWh, (38 kWh/m ²)
Electricity consumed per person	1260 kWh/person	1490 kWh/person
Electricity consumed no light, no appliances	960 kWh, (16 kWh/m ²)	1090 kWh, (18 kWh/m ²)
Electricity produced	4506 kWh	5357 kWh

The electricity consumed is lower than the one produced both in Copenhagen and in Paris. The amount produced is 2,4 times larger compared to the consumption, both in Paris and Copenhagen. Consuming less energy than the amount produced, the house reaches the requirements for a “Plus-Energy House”.

Furthermore the production results to be higher in Copenhagen, because of the low tilt angle of the photovoltaic panels of 22°, combined to the higher latitude of Copenhagen.

Based on Danish Building Regulation 2010, artificial light and appliances should not be included when considering the energy frame of a residential building. This is why, for comparison reasons, the electricity demand is exposed without taking into account those consumptions in Table 36, even if the results are not obtained through the Be10 tool.

2. Performances in Versailles, during the competition

2.1. Indoor climate in the prototype

Points regarding the indoor climate were distributed among continuous measurements of temperature, CO₂ and humidity and single test measurements of acoustical, daylight indoor climate and VOCs in the air. The conclusions regarding acoustical and daylight indoor climate are not presented here because not strictly related to the HVAC design. Three tripods were located in the living room (1), bedroom (2) and flexible room (3). The 1st and 2nd were including a PT100 sensor equipped with a black globe (Ø40 mm) suitable to measure operative temperature, at a height of 1,1 m. All the tripods were provided with a thin-film capacitive and a non-dispersive infrared sensors for humidity and CO₂ respectively. The sensor used was the SCR110-H from Schneider Electric. For the horizontal plan views with the sensors location, see Annex 11: Mechanical and instrumentation drawings from PD#6, Team DTU.

2.1.1. Operative temperature

The team has allocated more effort in meeting the set point for operative temperatures since 65 out of 120 points were allocated to this sub-contest. EMBRACE and Team DTU managed to gain 62,03 points out of these 65. The challenge was expected to be on keeping the house cool enough in the Parisian summer through passive means of solar shading and natural ventilation and when necessary using the radiant floor system to cool.

The equation used to determine the official set points also reflects the expectation of a cooling scenario, since it was taken from EN 15251, Annex A.2 “Acceptable indoor temperatures for design of buildings without mechanical cooling systems”.

$$T^{\circ}_{ea} = (T^{\circ}_{ed-1} + 0,8 \cdot T^{\circ}_{ed-2} + 0,6 \cdot T^{\circ}_{ed-3} + 0,5 \cdot T^{\circ}_{ed-4} + 0,4 \cdot T^{\circ}_{ed-5} + 0,3 \cdot T^{\circ}_{ed-6} + 0,2 T^{\circ}_{ed-7}) / 3,8$$

Where T°_{ea} is the average exterior temperature of the day and T°_{ed-x} are the daily average exterior temperatures of precedent days.

Based on the Competition rules, to get all the available points, during the day (from 8:00 to 23:59) the range of temperatures is:

$$T^{\circ}_{i\ min} = 0,33 \cdot T^{\circ}_{ea} + 18,8 - 1 \quad \text{and} \quad T^{\circ}_{i\ max} = 0,33 \cdot T^{\circ}_{ea} + 18,8 + 1$$

During the night (from 0:00 to 7:59):

$$T^{\circ}_{i\ min} = 18^{\circ}C \quad \text{and} \quad T^{\circ}_{i\ max} = 0,33 \cdot T^{\circ}_{ea} + 18,8 + 1$$

To fulfil Category I as defined in EN 15251, the range of temperature is:

$$T^{\circ}_{i\ min} = 0,33 \cdot T^{\circ}_{ea} + 18,8 - 2 \quad \text{and} \quad T^{\circ}_{i\ max} = 0,33 \cdot T^{\circ}_{ea} + 18,8 + 2$$

Heating and cooling systems are implemented in EMBRACE, but it had been chosen to make EMBRACE function with the radiant floor only in the cooling mode (which cannot run simultaneously with the heating mode, see section V.2. about the control of the modes). If the organization had not introduced the setback, it would have become a problem to heat the building at night only with mechanical ventilation.

Table 37 – Competition range of indoor temperature for getting 100% points

Date	Min. T	Max. T	Date	Min. T	Max. T
30/06/2014	23,3	25,3	06/07/2014	24,1	26,1
01/07/2014	23,1	25,1	07/07/2014	24,2	26,2
02/07/2014	23,2	25,2	08/07/2014	23,9	25,9
03/07/2014	23,3	25,3	09/07/2014	23,7	25,7
04/07/2014	23,6	25,6	10/07/2014	23,3	25,3
05/07/2014	24	26	11/07/2014	23	25

Table 38 represents the percentage of time that the operative temperature of the three rooms, was outside different ranges. The first range is the one used by the SDE2014 Organization in order to gain all the available points. The second range is the one stated in EN 15251, Annex A.2 to stay within Category I of thermal indoor comfort. The third range considers that the method suggested by EN 15251 defines mainly the upper maximum tolerable temperature value in cooling season and it is not supposed to be used to define heating set points. Thus, in this case the lower threshold has not been taken into account.

Table 38 – Percentage of time during the competition outside the considered comfort ranges

Percentage of time outside the range	T1	T2	T3
Organization range	27 %	20 %	38 %
EN 15251, Category I range	11 %	4 %	17 %
$T_{room} < 0,33 T^{\circ}_{ea} + 18,8 + 1$	2 %	3 %	0 %

In general it is possible to state that the range defined by the competition was quite strict and that the main problem for the team has been to fulfil the lower limit of the range. In fact, if just cooling set points are considered, the percentage of time of discomfort would be lower than 5 % of the time in all rooms. The strategy of the team has also to be taken into account: concerned about the electricity consumption, the

students preferred to avoid activating the heat pump of the mechanical ventilation to warm the air, trying to heat the space by the internal gains generated by the House Functioning tasks.

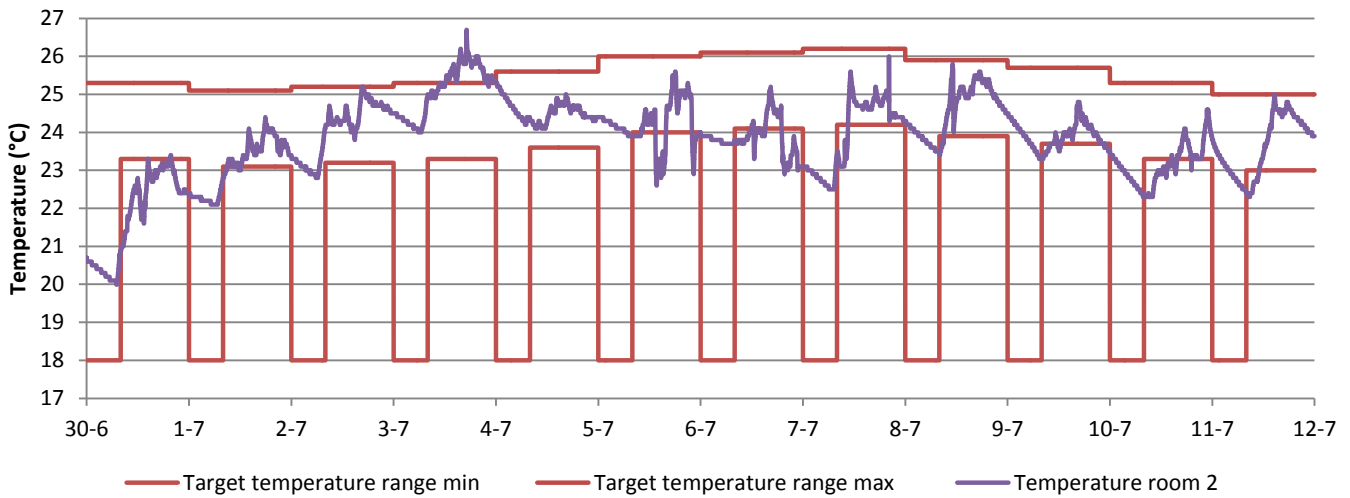


Figure 74 – Example of the measured temperature in room 2, compared to the expected range

2.1.2. Humidity, CO₂ and VOC

10 points for relative humidity and 5 for CO₂ were dedicated to the continuous measurements of air quality. 5 points were available for a single measurement of VOCs present in the air.

Humidity was managed through natural and mechanical ventilation especially when cooking and many people were present, like during the dinner parties. The Parisian exterior climate and high desirable indoor temperatures made managing the humidity level in the range 40 % - 55 % an easily reachable goal, even without equipment for humidifying or dehumidifying. DTU received 9,94 out of 10 points in the sub-contest, which was the best score among all the other teams.

CO₂ levels had to stay below 800 ppm to get full points and in the range 800-1200 ppm to get reduced points. 4,46 points out of 5 were received by Team DTU. All teams received 5 out of 5 points in the VOC test sub-contest, which indicates either all teams were in full control of these pollutants thanks to a high threshold for full points (30 µg formaldehyde per m³) or trouble in getting comparable measurements from the Organization.

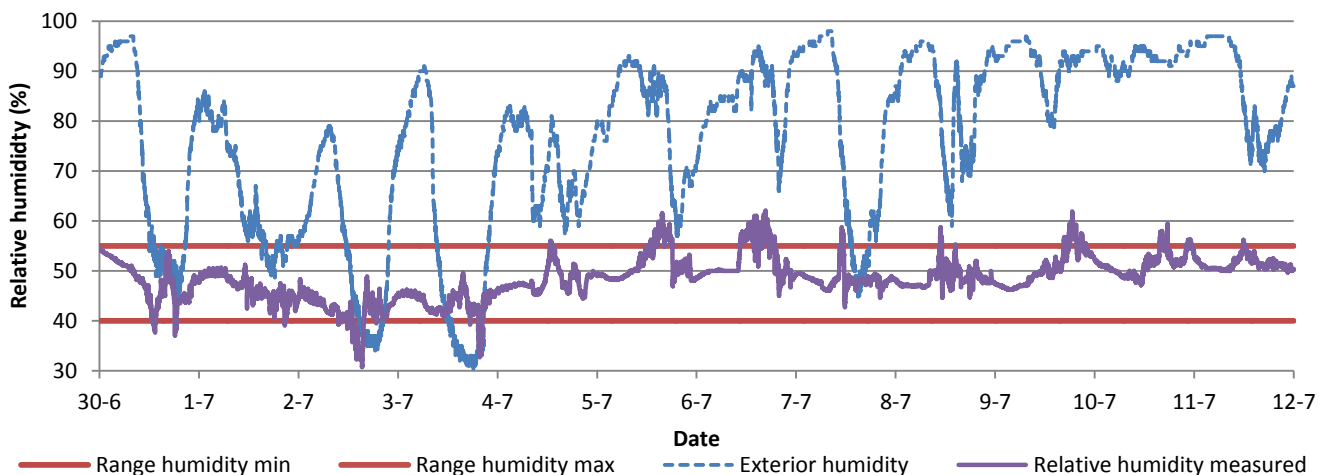


Figure 75 – Relative humidity recorded during the competition

2.2. Electricity production and HVAC consumption

During the competition time in July in Versailles, the HVAC systems were estimated to consume energy mainly for space cooling and heating of DHW, plus the additional consumption of circulation pumps and ventilation fans. The cooling was to be produced partly by nighttime radiative cooling by the unglazed solar collectors, partly by the Daikin Altherma heat pump. The majority of the hot water for draw-off and appliances were expected to be produced by the solar collectors.

As described in section VI.2.1. Indoor climate in the prototype, the weather was unusually cold in the second competition week, which meant low cooling demand and very low solar heating production. The solar collectors also had leakage problems, which means this source was completely unavailable for part of the competition period. Instead, the high temperature set-point, imposed by the SDE2014 Organization, meant heating demand. The team members decided not to switch the heat pump in heating mode, which would have required a considerable amount of energy to warm up the storage tank, and rather rely on a change of weather. Thus heating could only be covered by supplied air from the Nilan ventilation unit. As well, the hot water demand had to be covered by the same unit. It was not possible to both heat air and hot water at the same time, so manually switching in operation modes was necessary and large amounts of energy were required to this single unit. It is possible to see the operation modes of the Nilan Compact P in Annex 9: Nilan Compact P functions. Because of its multiple functions, this is the unit that has the largest energy consumption, as can be seen in the pie charts of Figure 77.

As said, the team decided to set the system for cooling, which means the storage tank was filled with cold water. During the second week, the outside temperature was exceptionally low, which means the cooling demand was inexistent. The radiant floor did not need to be used, and neither did the Daikin heat pump, so they were simply switched off.

The official monitoring of SDE organization only splits the consumption between the home electronics and the appliances (see Figure 76). The home electronics (TV, computer, DVD player) consumed a very small amount of energy thanks to the very efficient devices which were chosen. The space cooling demand was low, and when the house needed to be heated, the strategy was to emphasize passive heating such as using the internal gains due to cooking. The appliances however consumed the major part of the electricity: because of the imposed schedule of the in-house tasks, the team had to run regularly all appliances in order to earn points. Despite the energy-efficient labelled products chosen, the appliances have been the most energy consuming devices of the house during the competition. It has also been noticed that the consumption of the IBI¹ (Intelligent Building Instrumentation) system, used to control the home automation, was unexpectedly high. This technology is still beneficial when the energy saved is higher.

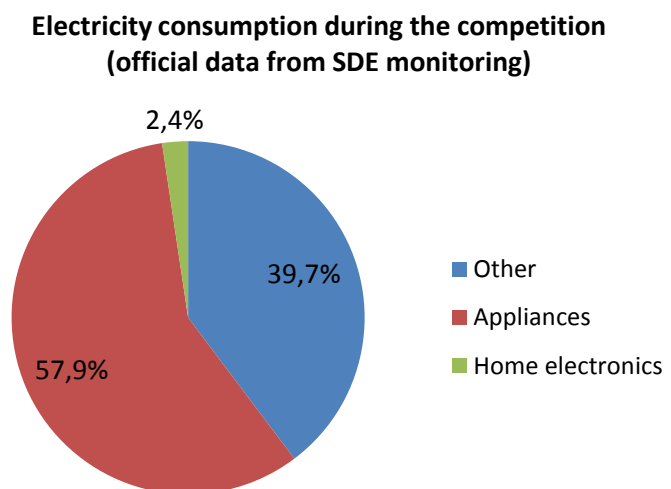
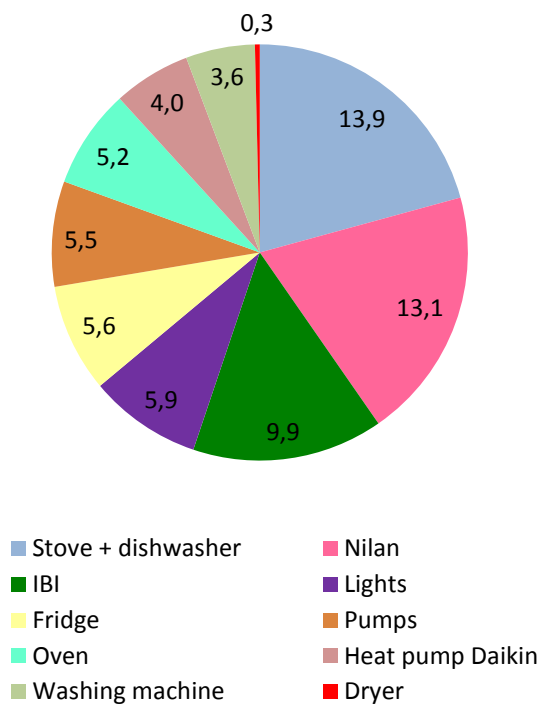


Figure 76 – Repartition of the electricity consumption

¹ The IBI includes PLC (Proportional Linear Control) and IHC (Intelligent Home Control).

Repartition of the overall electricity consumption during the competition (kWh)



Repartition of the HVAC electricity consumption during the competition (kWh)

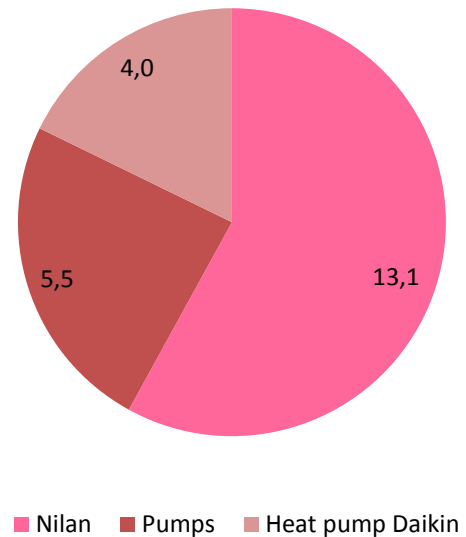


Figure 77 – Subdivision of the electricity consumption during the competition (from Team DTU's own data)

During the competition, the EMBRACE team members observed that the Daikin heat pump connected to the storage tank, sometimes was turning on without any cooling demand at the radiant floor level. In fact the heat pump was activated by temperature set-point in the storage tank and not by room thermostat. Thus, also if the Uponor system was off, the cooling set-point in the storage tank could have been reached, especially in the late afternoon when the sun was facing west and direct radiation was hitting the technical room façade, where the tank was located. The activation of the heat pump when the radiant floor is off would not be a problem if there is cooling demand in a subsequent period. In fact the cooled water would be stored and used afterward. It produces a waste of energy just if cooling is not needed for prolonged periods. Such an issue was already pointed out in the design stage, as described in the chapter IV.1.1. As stated there, the realized configuration of the system was not the optimal one identified. But a combination of issues concerning time, budget, availability of product on the market and practical inexperience of the students has imposed some changes in the realized systems. Anyhow this did not have a strong impact on the consumption, since the Daikin heat pump was most of the time switched off because of the limited need of cooling.

The electricity is produced in EMBRACE through two different types of PV cells, summing up to 5 kW_p, installed on the roof (maximum allowed by the competition). The first part is made of monocrystalline PV square tiles, installed on the glass of the weather shield and arranged in a pattern optimized in order to provide enough daylight and shadow in the sheltered garden below. The other part is made of fully opaque PV panels installed on top of the thermal envelope, where no transparency is needed. 2/3 of the electricity is produced by the opaque panels, and the remaining 1/3 by the tiles above the sheltered garden.

The large roof surface available and the south orientation enabled an optimized production of electricity: this achieved result is visible in Figure 78, where the curve of the production matches with the available solar radiation. Despite the poor weather conditions (cloudy during most of the second week), EMBRACE produced in total 235 kWh, to be compared to its total consumption of 107 kWh during the same period. The house proved to be an actual plus-energy building, producing more than twice its consumption during the competition. The energy production and consumption per day can be seen in Figure 79. Only on July 10th the production was higher than the consumption, given the low available solar radiation (see Figure 78), and therefore the low electricity production.

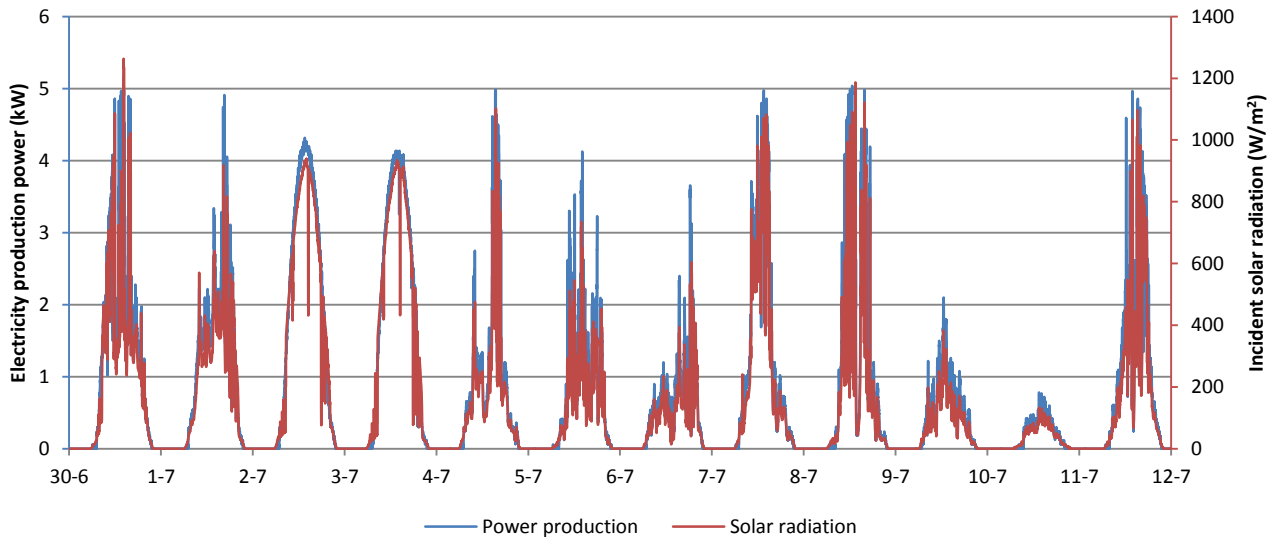


Figure 78 – Electricity production and solar radiation during the competition

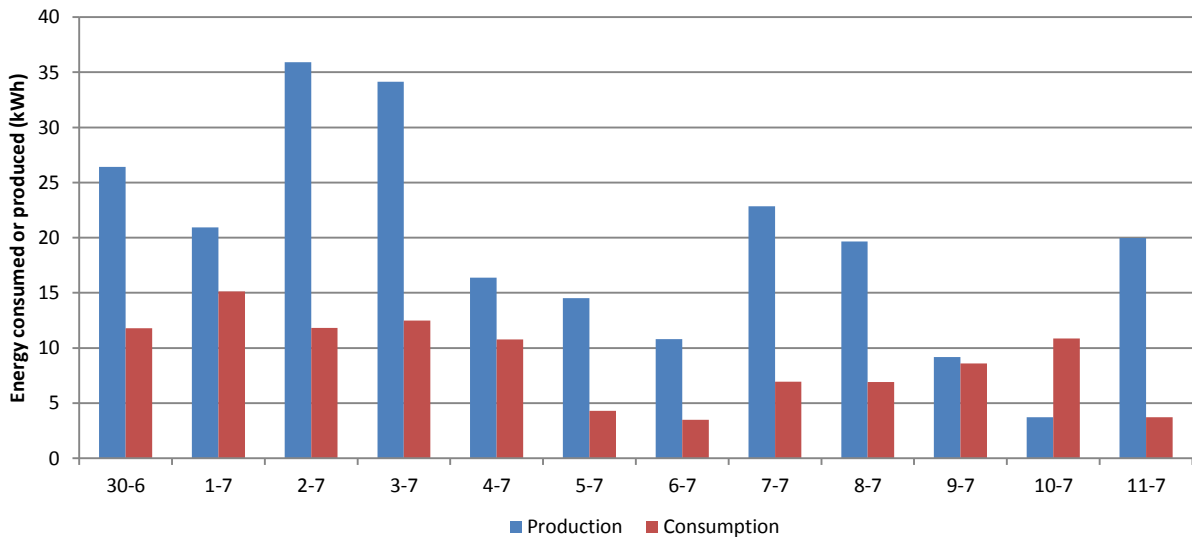


Figure 79 – Energy production and consumption per day during the competition

2.3. Nighttime radiative cooling in Paris

The cooling potential by nighttime radiative cooling has been analysed in Versailles, during the competition. After the competition, the students have performed a further experiment at the Internal Centre for Indoor Environment and Energy (ICIEE), Department of Civil Engineering of the Technical University of Denmark (DTU), described in detail in chapter VII. Nighttime radiative cooling.

2.3.1. Method

The air temperature, air velocity, humidity and clouds cover have been used to determinate the sky temperature and Nusselt number as described in the theory of VII. Nighttime radiative cooling. The cloud base height Z_c is assumed to be 2 km (low, medium clouds) and the cloud emissivity ε_c fixed to 1. The average surface temperature of the collectors has been assumed as the mean between the supply and return water temperature, given by two Vortex Flow Sensors (VFS) from Grundfos.

Thanks to those values the radiative q_{rad} and convective q_{conv} cooling potential has been estimated.

The VFS measure also the water flow rate \dot{q} (m³/s). Using the ΔT , temperature difference between inlet and outlet, the VFS outputs have been applied to the equation $q_1 = c_w \cdot \rho \cdot \Delta T \cdot \dot{q} / A_{collectors}$ (W/m²) obtaining the effective cooling gained q_1 . Where c_w and ρ are the water heat capacity (4200 J/kg·K) and density of water. The supply and return water temperatures have been compared with two PT1000 temperature sensors, located in the bottom and top of the storage tank as shown in Figure 57. The drop of temperature in the tank over the night has been used to determinate the effective cooling gained q_2 . All the 750 litres of the tank are assumed to be at the same temperature, obtained as a mean between bottom and top temperature.

The unglazed solar collectors circulation pump was time controlled. When activated, it runs from 10 PM to 6 AM¹ with a flow rate of 7,3 l/min except for the last day when the flow has been changed to 2 l/min. The area of the unglazed solar collectors installed in Versailles was 7,2 m² and the infrared emissivity of the panel is set to 0,9.

2.3.2. Aim

The aim is that to analyze and compare the cooling obtained applying the weather data to the theoretical physical model, with the effective cooling gained q_1 and q_2 . The values obtained are anyhow not as precise as those derived from the experiment in Copenhagen. In fact they have been considered only for evaluation purpose. The main reason is that the weather data comes from a weather station in Versailles² located not in the same place than EMBRACE and this introduces an unknown degree of uncertainty. Furthermore, the data from Team DTU's own sensors (VFS and PT1000 in storage tank) were received every minute. Those data have been averaged, to meet with the time slot of the weather station data, which were received approximately every 37 minutes.

2.3.3. Results

The results presented in the further data represent only the six nights when nighttime cooling has been activated. Sky temperature, during the considered days (night and day), has been calculated to be in the range between -5 to 22 °C. This range fits with the fact that sky temperature is in general close to ambient temperature at overcast sky and approximately -20°C below ambient temperature at clear sky conditions (Perers B., 2014). The ambient temperature during the same period was in the range between 29 and 11 °C (see Figure 84).

¹ Range of time selected based on TRNSYS simulations

² <http://openweathermap.org/>

The following table shows the accuracy of the different sensors used by the team members.

Table 39 – Range of absolute errors for the different sensor used

Sensor	Accuracy (absolute error)
Storage tank water temperature (PT 1000 ohm, AKS 21W from Danfoss)	$\pm(0,3 + 0,005 T) \cong \pm 0,4$
VFS (water supply and return temperature)	25 to 80 °C, ± 1 °C; 0 to 100 °C, ± 2 °C
VFS flow	0 to 100 °C, 1,5 % / 5 % of the flow (typical 3 %)

The inaccuracy in the temperature range measured by the VFS sensors is the one that can lead to the most considerable errors. In fact if the temperature recorded is lower than 25 °C the absolute error is ± 2 °C. When two measures are summed or subtracted, the total error corresponds to the sum of the absolute errors. So when ΔT between supply T_{sup} and return water temperature T_{ret} is calculated, the error, in the worst scenario, becomes ± 4 K. Such an error can lead to an unacceptable potential inaccuracy of ± 280 W/m² when calculating the cooling power with the equation $\dot{Q} = c_w \cdot \rho \cdot \Delta T \cdot \dot{q}$ (W) and a flow rate of 1 l/min·m².

Concerning the theoretical physical model, it has not been possible to estimate the measurement error or the uncertainty because it is based on data not directly measured by the team members, instead derived from an external weather station. When the measured data are anyhow averaged, to meet the time slot of the weather station, an uncertainty $\pm \delta x$ is introduced. If \bar{x} is the time averaged mean value, the uncertainty can be calculated as $\delta x = \sqrt{\frac{\sum_{i=1}^N (\bar{x} - x_i)^2}{N \cdot (N-1)}}$ where N is the number of averaged values.

Table 40 – Uncertainty introduced when recorded data are time averaged

Time averaged value	Maximum calculated uncertainty $\pm \delta x$ (standard deviation)
Unglazed solar collectors surface temperature (°C)	$\ll 0,1$
ΔT between supply and return water temperature (°C)	$\ll 0,1$
Cooling power measured with VFS (W/m ²)	2

If $t_2 - t_1$ is the time needed for a finite volume of water to flow from the supply VFS to the return VFS, the corresponding temperatures T_{sup} at time t_1 and T_{ret} at time t_2 , should be considered when calculating the effective cooling power (see Figure 81). The estimated time between the two VFS is less than 1,5 and 5 minutes at 1 l/min·m² and 0,3 l/min·m² respectively. During those periods of time, the return temperature can be considered constant and the same can be applied to the supply temperature. For this reason, the cooling power as exposed in Figure 83 and Table 42 has been calculated considering T_{sup} and T_{ret} at the same time. Applying those considerations, the recorded ΔT between T_{sup} and T_{ret} provided a variable cooling power q_1 between 17 and 60 W/m², depending by boundary atmospheric conditions and water flow rate. If the drop of temperature in the tank is applied to all the 750 l of water and divided by the collectors area, cooling power q_2 between 20 and 70 W/m² is obtained. With the available data, the cooling obtained with the theoretical model results to be always considerably higher than the real power gained, see Table 42. The temperature drop in the tank as presented in Table 41 fits with the range obtained with TRNSYS simulations.

Table 41 – Average temperature drop in the tank over the night, weather data and relative radiative and convective cooling power, calculated with physical model

Night number and date	ΔT in the tank (K)	Average of the fractional cloud amount, $0 < n < 1$	Average night air temperature ($^{\circ}\text{C}$)	Average wind speed (m/s)	q_{rad} (W/m^2)	q_{conv} (W/m^2)
1)	4,6	0,18	17,9	2,4	73	22
2)	1,3	0,58	21,5	2,1	41	19
3)	2,7	0,45	19	4,7	50	39
4)	2,8	0,87	19	6,1	28	55
5)	4,4	0,91	14	2	44	71
6)	3,9	0,69	13	3,3	49	35

Table 42 – Comparison of the theoretical and measured average cooling power per night

Average values per night				
Night number	Theoretical (W/m^2) ($q_{rad} + q_{conv}$)	q_1 (W/m^2) From VFS	q_2 (W/m^2) From tank T drop	Flow rate ($\text{l}/\text{min}\cdot\text{m}^2$)
1)	95	57 (40% smaller)	70 (26% smaller)	1
2)	60	60	20 (67% smaller)	1
3)	89	37 (58% smaller)	41 (54% smaller)	1
4)	83	46 (45% smaller)	42 (49% smaller)	1
5)	115	48 (58% smaller)	67 (42% smaller)	1
6)	84	17 (73% smaller)	59 (6% smaller)	0,28

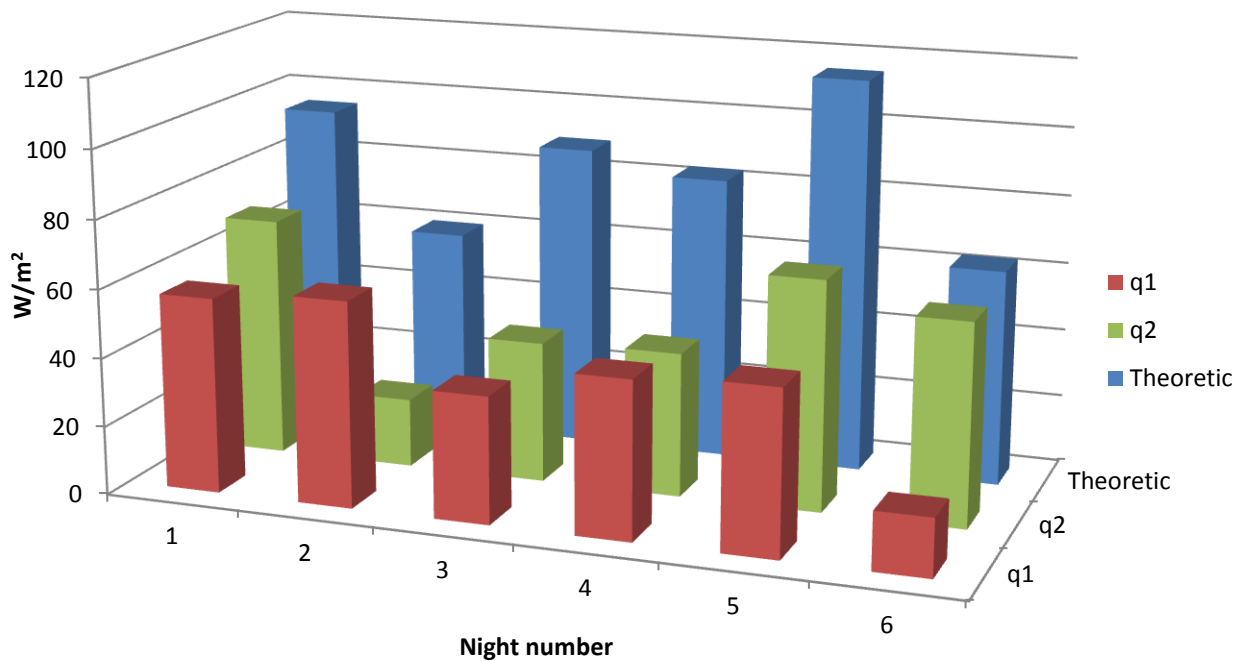


Figure 80 – Graphic visualization of the average cooling power per night obtained with the theoretical model and measured

As previously explained, it has not been possible to elaborate further considerations because of the high degree of uncertainty of the data obtained. The experiment at the ICIEE department of DTU, in Kgs. Lyngby (Copenhagen) has been used to get more accurate and comparable results.

As shown in Figure 81, the return water temperature T_{ret} at time t_2 , before entering in the buffer tank heat exchanger, should be lower than the temperature of the water in the tank, T_{tank} , at the same time t_2 , in order to provide cooling. The recorded values, as shown in Figure 83, show an opposite behaviour. But the temperature in the tank decreases in time with the same trend as the return water temperature. This suggests that the fact that the recorded $T_{tank} < T_{ret}$ at the same time, is probably due to inaccuracy. The reasons could be different; it could be imputable to improper installation of the VFS sensors which could have altered their calibration.

It has been also thought that the cooling obtained during the night within the storage tank could depend by heat losses through the tank and not thanks to the unglazed solar collectors. But the high thermal insulation of the tank (85 mm of insulation) within the experienced range of the surrounding air temperature, would lead to around 0,2 °C temperature drop. In fact the only night when the temperatures in the tank have been recorded for few hours without the circulation pump of the unglazed solar collectors being on, there is no temperature drop of the stored water, see Figure 82.

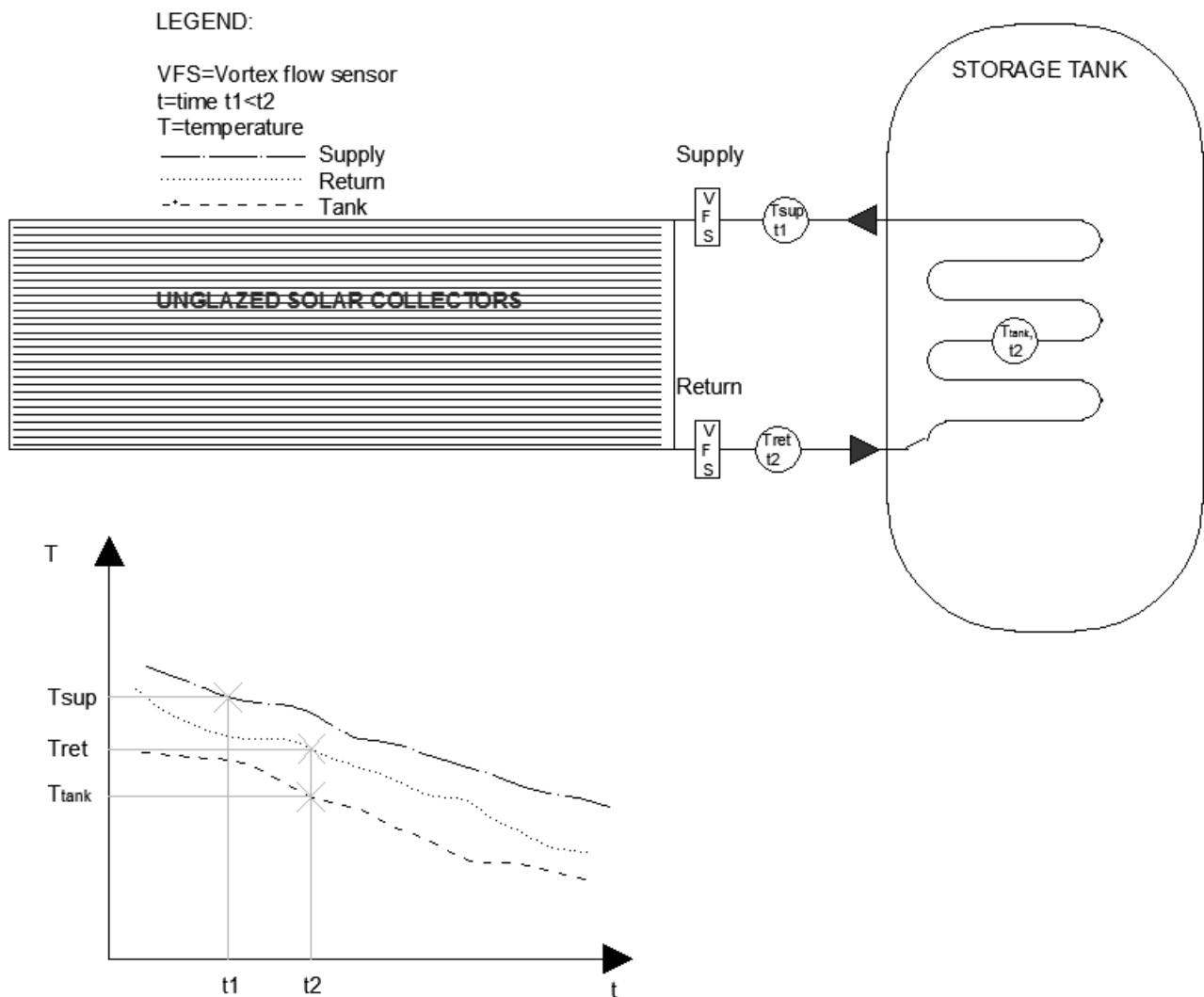


Figure 81 – Scheme and location of the water temperatures recorded and expected trend

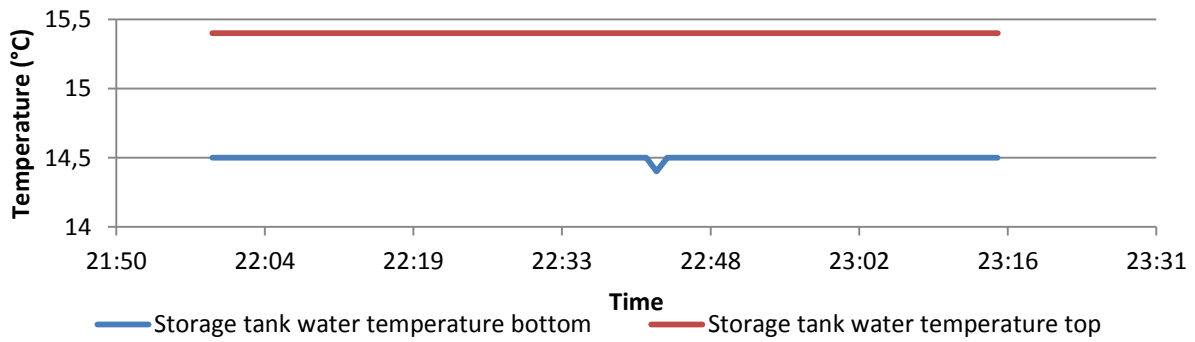
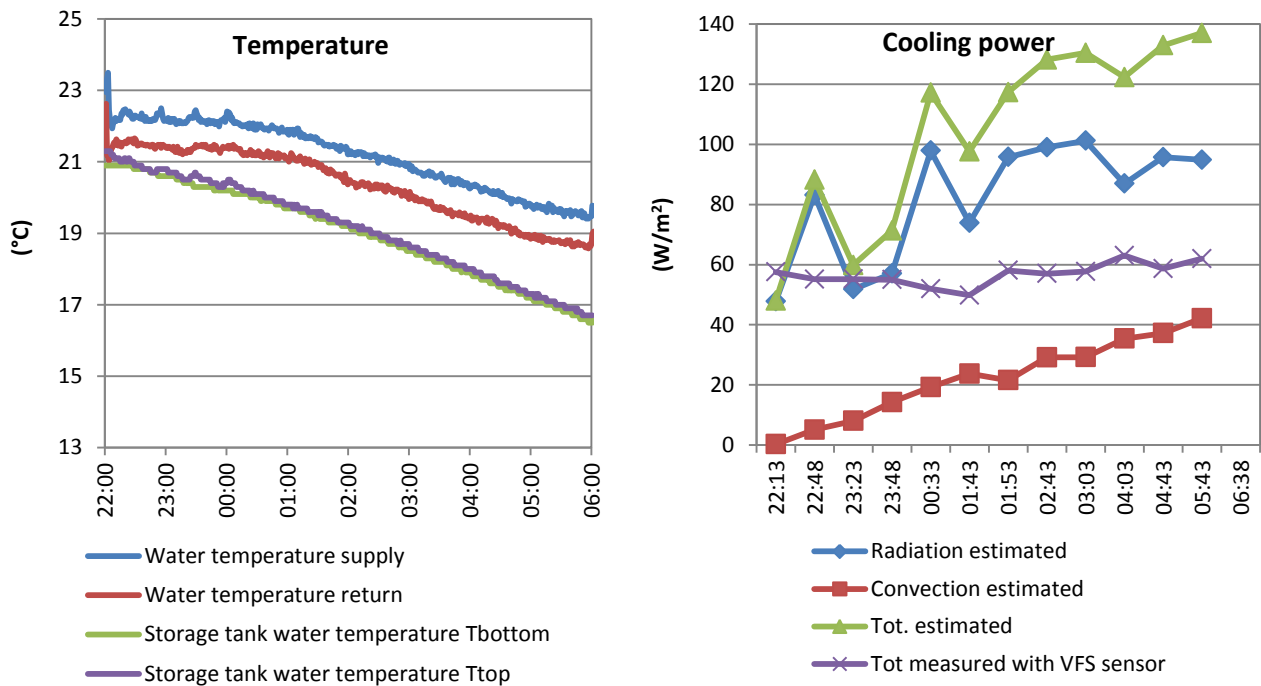
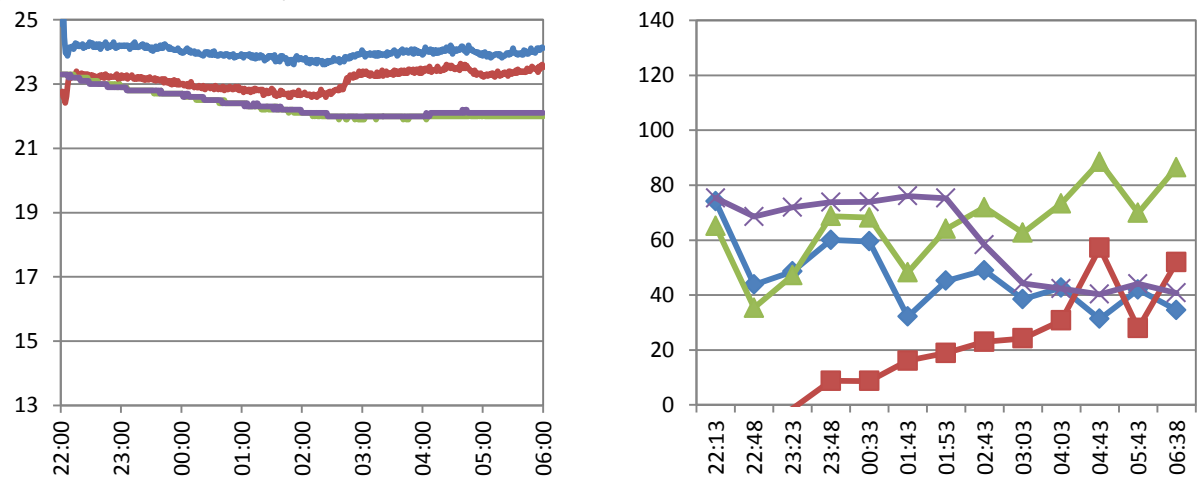


Figure 82 – Water temperature in the storage tank without nighttime radiative cooling. Last monitored night 10/07/2014, available data with no nighttime radiative cooling on, from 22:00 to 23:15

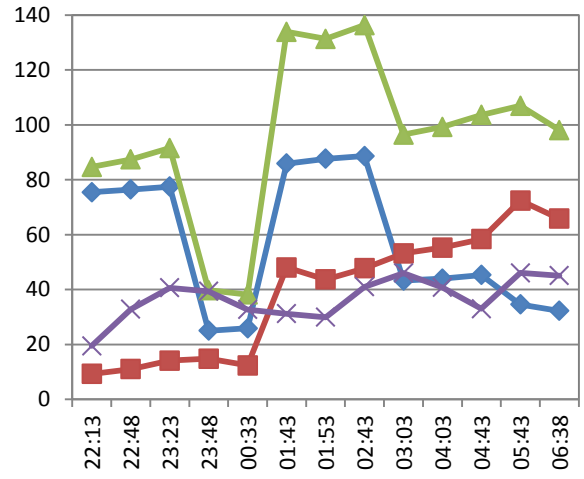
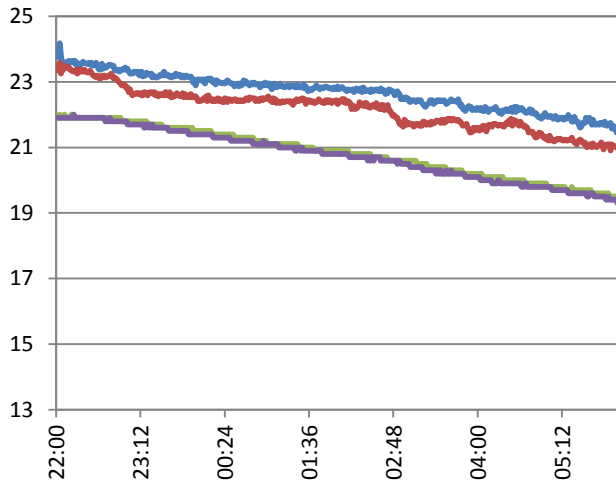
1) Night between 02-07-2014/03-07-2014



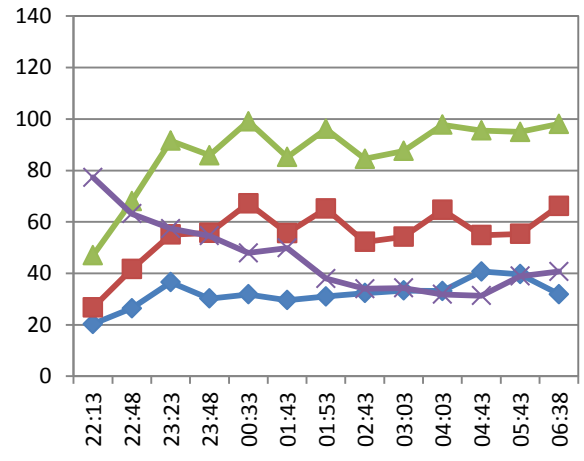
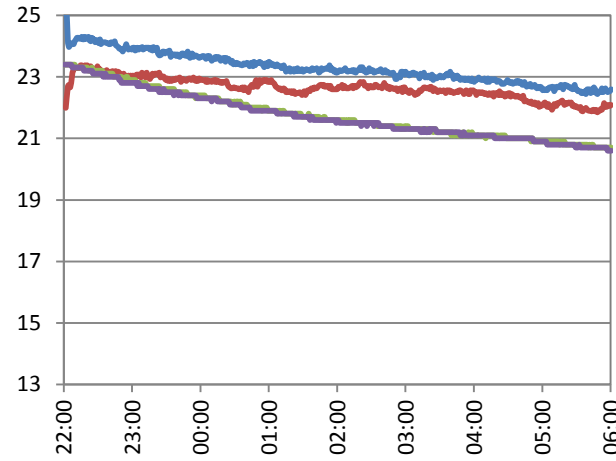
2) Night between 03-07-2014/04-07-2014



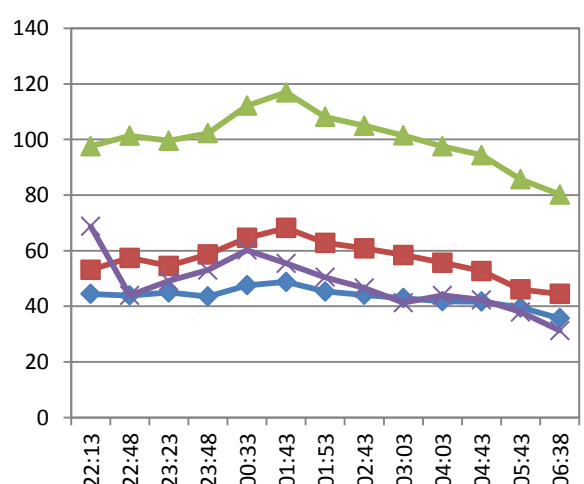
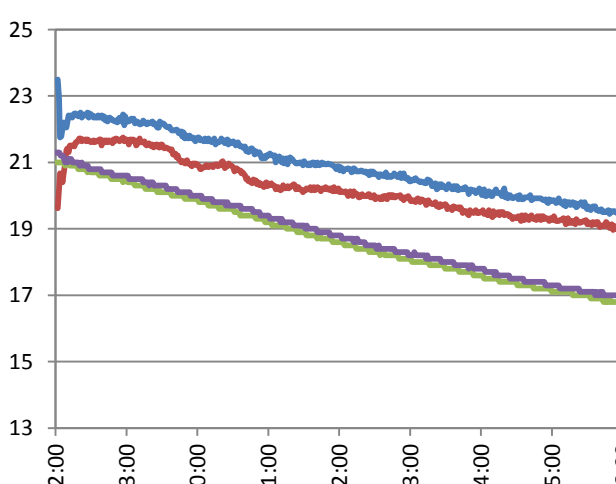
3) Night between 04-07-2014/05-07-2014



4) Night between 05-07-2014/06-07-2014



5) Night between 07-07-2014/08-07-2014



6) Night between 08-07-2014/09-07-2014

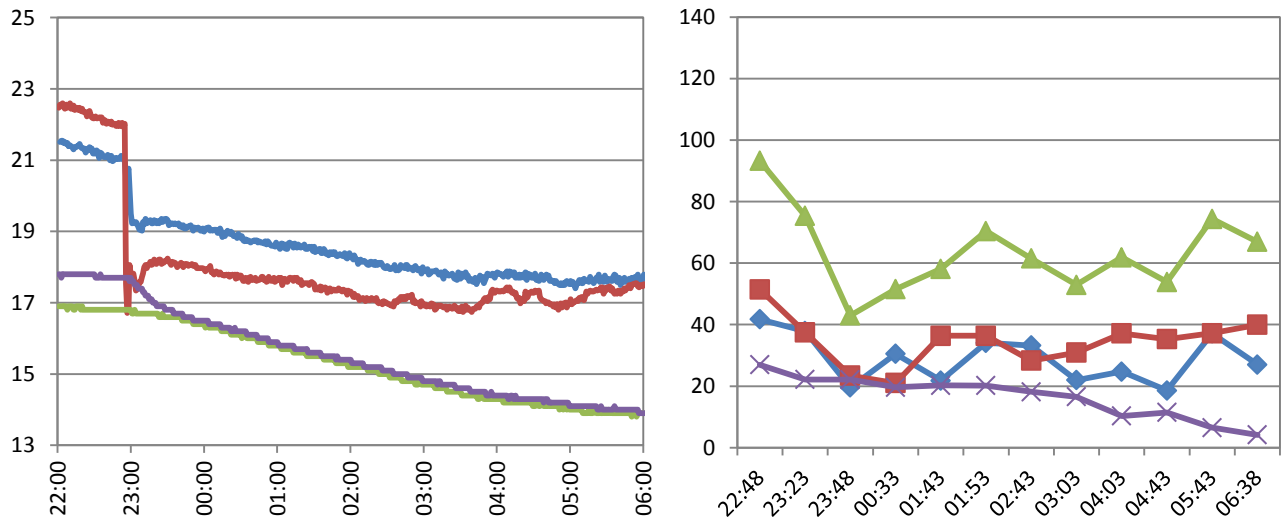


Figure 83 – Water temperatures profiles and corresponding cooling power (measured and modelled) per night

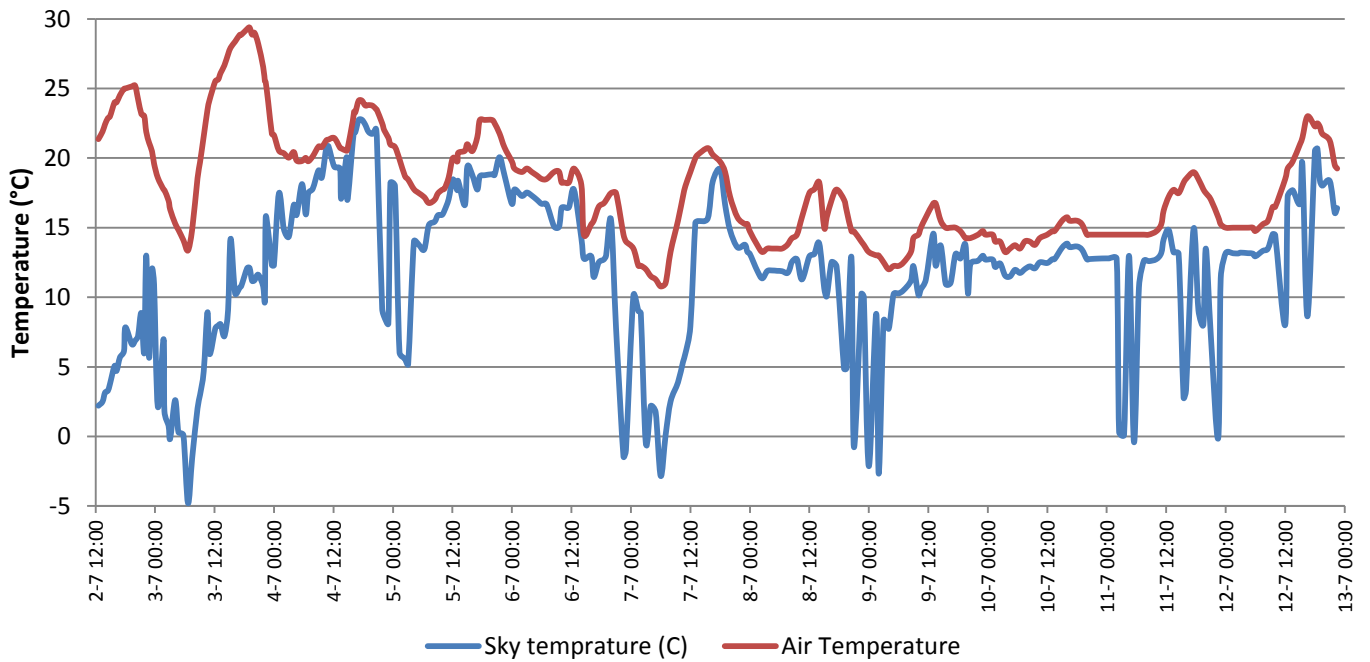


Figure 84 – Measured air temperature and calculated sky temperature during the competition period

3. Conclusion and discussion on the house performance

The calculated total consumption is 32 and 38 kWh/m² of net area per year, in Paris and Copenhagen respectively. This energy is still significant for a plus-energy house, if considered per m² and without taking into account the electricity produced by PVs. This is directly related to the fact that the living area has been reduced to the minimum. In fact the energy needed per person for home electronics, appliances, cooking, DHW, pumps and so forth, is almost unaltered when the living space is reduced. When dividing the electricity used by the small net area of the house, it results in a high consumption value. To avoid being misled by this figure, the new approach of the team is to consider the energy per person and not per area. In this way the strategy of DTU team to encourage people to live in smaller dwellings, where the heated and cooled area is reduced, can be understood better. The simulated energy per person in Copenhagen is 1490 kWh/year while the Copenhagen Commune states in its website¹ that in 2010, more than 5000 kWh/year were consumed in average per inhabitant just for heating.

Both in Paris and Copenhagen, the estimated performances of EMBRACE are not drastically different. High level of insulation and air tightness are indeed desirable in both cities which are located in a similar climate zone. The house has achieved the “Plus-Energy House” requirements both in the computer simulations and during the competition period, producing more than double energy than its total consumption.

During the competition the biggest impact on the energy consumption is imputable to the Nilan Compact P. This finds an explanation when considering that most of the DHW had to be provided by this unit and that the SDE2014 rules impose to tap the same amount of hot water per day to all teams, regardless of the size of the dwelling and the number of people for which it is designed.

The energy frame obtained through the model should be considered as an ideal and not definitive value, since obtained with a simulation program with its own limitations. For instance, during the assembly, human mistakes can occur, leading to unexpected thermal bridges or holes in the vapor barrier, which reduce the performances of the real prototype. Other differences between the simulations and the real prototype are the simplifications introduced in the model; as the definition of the HVAC controls and components, the behavior of the users and so forth.

The weather is another variable parameter. In fact, during the competition period, lower outdoor temperatures have been recorded than the average ones derived from weather climate database for the same dates. This has introduced some heating demand, while the simulation in Paris had shown only cooling demand for both the months of June and July. The heating demand during the competition is also due to high set-points imposed daily by the SDE2014 Organization, while in the model the cooling and heating set-points are fixed values (25°C and 21°C respectively).

Regarding nighttime radiative cooling, the data obtained during the competition period show a high level of inaccuracy and they do not allow detailed analysis. Despite this, the range of calculated sky temperature and recorded temperature drop over the night in the storage tank seem reasonable based on the experiment and TRNSYS results (see section VII.0. and 5.). The cooling power obtained through the VFS and PT1000 sensors also fits with the expected range (between 17 and 70 W/m²). Conversely, the cooling obtained with the theoretical model shows higher values, but this model has been based on few and inaccurate weather data derived from a public weather station, they are so considered unreliable.

¹<http://subsite.kk.dk/sitecore/content/Subsites/CityOfCopenhagen/SubsiteFrontpage/LivingInCopenhagen/ClimateAndEnvironment/CopenhagensGreenAccounts/EnergyAndCO2/Consumption.aspx>

VII. Nighttime radiative cooling

1. Introduction

As recalled in the general introduction, the shortage of energy supply starts becoming an issue, especially in the building sector. Simultaneously the increasing living standards drag along an increase in the energy spent on cooling of buildings. Most of it is traditionally generated by low efficiency air conditioners, which consume important amounts of energy. Given the energy resources depletion, natural sources of cooling need to be investigated and their use spread at a larger scale.

Several natural heat sinks exist for dispersing the heat stored in buildings, like the outside air or the ground. One of them is the sky, which can exchange heat with objects by long-wave radiations. The sky constantly exchanges heat with the earth's surface. During daytime, the incoming solar radiation prevails in this exchange, warming up the objects it hits. At night, the effective temperature of the sky is very low, and then the heat transfer mainly consists of long-wave radiations towards the cold sky, cooling the objects facing the sky. The processes using this physical phenomenon are usually known under the name of 'radiative cooling' applications, and they can cool a heat carrier like water or air several degrees below ambient temperature. This kind of systems stores the heat accumulated by the building during the day, and release it at night by means of a radiator, using the cold sky as a natural heat sink. Part of the heat transfer occurring at the radiator is also due to convection effects, but the effect of radiation should be predominant in order to achieve a correct performance in the cooling process.

Exploiting nighttime radiative cooling has been a research topic for many years. Simple applications included white roofs, insulation removable at night or roof ponds exploiting also evaporative cooling (Cavelius R. et al., 2005) . But radiative cooling systems do not seem to undergo a broad implementation in actual buildings. One solution studied by several researches around the world is to use solar collectors: because there is no solar radiation at night, they are left untapped. By circulating water in them also during the night to exploit radiative cooling, one can make the most of a solar collector installation, using the system on a 24-hours-per-day basis. Among others, some papers studying this sort of applications have been gathered in Table 43, mentioning the cooling power obtained and the type of collector used.

Table 43 – Literature review on nighttime radiative cooling applications

Authors	Type of panels	Cooling power	Location
Erell and Etzion, 1996 (Israel)	Flat plate radiator	80 W/m ²	Desert areas
T.N. Anderson et al., 2013 (New Zealand)	Unglazed solar collectors	50 W/m ²	New Zealand and Australia
Eicker and Dalibard, 2011 (Germany)	PVT	60 to 65 W/m ²	Madrid (Spain) /Shanghai
Hosseinzadeh and Taherian, 2012 (DTU & USA)	Unglazed flat plate collector (copper and iron)	23 to 52 W/m ²	Babol (Iran)
Dobson, 2005 (South Africa)	Radiator panels	60,8 W/m ²	Namibia

In the present study, two types of collectors have been tested: unglazed solar collectors and PVT panels. Unglazed collectors are simple systems made of polypropylene, and they are usually relegated to cheap domestic applications of pool heating. Their simple design and the high emissivity of the material are a source of heat losses, which are undesirable for heating applications, compared to glazed flat-plate collectors for instance. However, what is a weakness for heating becomes a strength for cooling

applications, where high heat losses are sought for. This system has mainly been chosen as a study case for its low cost and simplicity.

PVT stands at the other side of the existing range of solar technologies: they are relatively expensive and at the state-of-the-art of this field. The innovative combination of photovoltaic cells with thermal collectors is relatively recent, therefore few literature is available on the subject. In fact, several standards rule the production of PV cells on the one side, and of thermal collectors on the other side, since those technologies start to be well-trying. But there is no existing standard for PVT, so the panels are often prototypes designed in different ways, without uniformity that could make comparisons easier. PVT panels have been chosen as a subject of study in order to understand better their functioning in different conditions and broaden the knowledge available on the topic.

2. Theoretical analysis

2.1. Cooling power

The main interesting output when discussing nighttime radiative cooling is the total cooling power in Watt. It can be expressed considering the cooling of the water, by calculating the difference in the energy before and after the circulation in the panel, using the following formula:

$$(1) \dot{Q} = c_w \cdot \rho \cdot \Delta T \cdot \dot{q} \quad (W)$$

With:

c_w the heat capacity of water (4200 J/kg.K)

ρ the density of water (1000 kg/m³)

ΔT the water temperature difference between the supply and the return (in K)

\dot{q} the water volume flow rate (in m³/s)

The cooling power obtained in (1) can also be expressed in function of all the heat losses occurring through the panel, which depend on the boundary conditions. A theoretical model is developed in order to calculate the cooling power for different conditions, and compare with the experimental output. The cooling power \dot{Q} can be defined in function of the overall heat transfer coefficient (U):

$$(2) \dot{Q} = U \cdot A_r \cdot (T_r - T_a) \quad (W)$$

In equation (2), T_a is the dry bulb temperature of the air (K), assuming it constant above and below the panel. T_r and A_r are the temperature (K) and surface area (m²), of the radiating panel (used also in equation (5)). The U-value is obtained from the combination of the thermal resistances above R_{top} , below R_{bottom} and on the edges R_{edges} of the collectors' absorber, which are in parallel:

$$(3) U = U_{bottom} + U_{edges} + U_{top} = \frac{1}{R_{total}} = \frac{1}{R_{bottom}} + \frac{1}{R_{edges}} + \frac{1}{R_{top}} \quad (W/m^2 \cdot K)$$

The main contribution to the cooling power comes from the top of the panel, which is exposed to the cold sky and the wind, whilst the bottom of the panel is insulated.

2.2. Bottom and edges' heat losses

R_{bottom} is composed by conductive plus convective and radiative components. Convective and radiative resistances are in parallel with each other, while the conductive resistance of the pipes is in series with the other two. The magnitudes of convection and radiation resistance are such that it is usually possible to assume them equal to zero and assume that all resistance to heat flow is due to the thermal insulation underneath the panel (Duffie J. A. and Beckman W. A., 2013).

Thus, R_{bottom} is approximately:

$$(4) R_{bottom} = \frac{L_{ins}}{\lambda_{ins}} + 0,04 \cong \frac{L_{ins}}{\lambda_{ins}} \quad (m^2 \cdot K/W)$$

Where λ_{ins} and L_{ins} are the insulation thermal conductivity and thickness, respectively.

0,04 is a standard external superficial thermal resistance (UNI EN ISO 6946), due to convection and radiation.

R_{edges} is equal to:

$$(5) R_{edges} = \frac{A_r}{(UA)_{edge}} \quad (m^2 \cdot K/W)$$

with $(UA)_{edge}$ the edge loss coefficient, referenced to the collector area A_r . $(UA)_{edge}$ represents a simple one dimensional heat transfer through the side layer: $(UA)_{edge} = \frac{A_{edge}}{\frac{L_{edge}}{\lambda_{edge}} + 0.04}$, with λ_{edge} , L_{edge} and A_{edge} being respectively the thermal conductivity, the thickness and the area of the edges.

2.3. Top heat losses

The heat losses occurring at the top surface of the panels consist of the combination of three main heat transfer phenomena: convection, radiation and conduction, as shown in Figure 85. The convection comprises the free convection resulting from a temperature difference between the air and the surface, and the forced convection that takes into account the effects of the wind. The forced convection is calculated differently if the wind flow is laminar or turbulent.

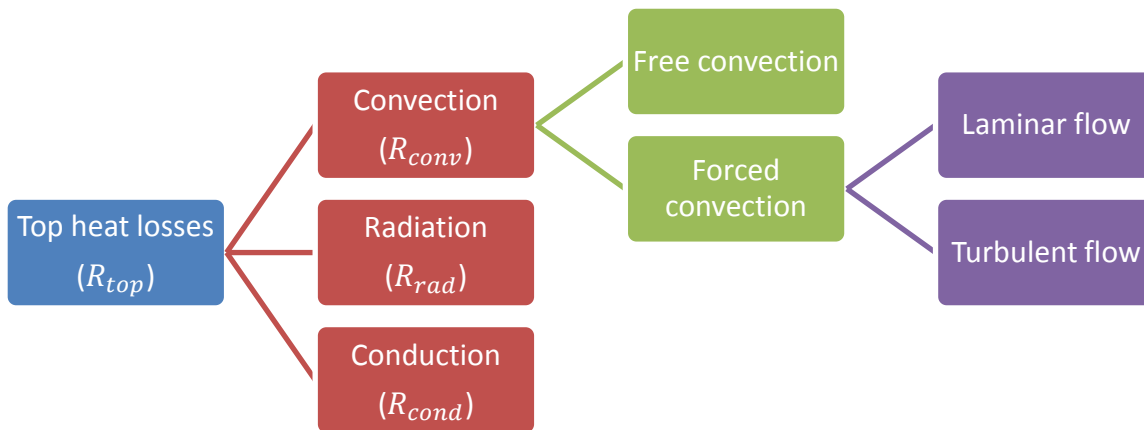


Figure 85 – Scheme of the heat losses through the top surface

As the temperature difference ΔT chosen in equation (2) includes the surface temperature of the panel T_r and not the temperature of the water inside the panel, the conduction effect is already taken into account in the calculation. The resistance R_{top} is therefore only composed by a convective resistance R_{conv} and a radiative resistance R_{rad} in parallel:

$$(6) \frac{1}{R_{top}} = \frac{1}{R_{conv}} + \frac{1}{R_{rad}} = \frac{R_{conv} + R_{rad}}{R_{conv} \cdot R_{rad}} \quad [m^2 \cdot K/W]$$

The convective and radiative resistances are expressed as:

$$(7) R_{conv} = \frac{1}{h_{c,mix}}$$

$$(8) R_{rad} = \frac{1}{h_{rad}}$$

In the following paragraphs the unknown parameters which will be derived are h_{rad} and $h_{c,mix}$ ¹.

¹ The heat transfer coefficients h_{rad} and $h_{c,mix}$ shall be normalized in function of the ΔT between sky and collector surface temperature as in (13), to be used to derive the U value of eq. (2). Otherwise \dot{Q} should be defined as the sum of \dot{Q}_{rad} and \dot{Q}_{conv} , in this way each heat flow could be defined in function of a different ΔT .

An alternative approach is to derive \dot{Q}_{rad} and \dot{Q}_{conv} , to insert them in this equivalent expression of equation (2):

$$(9) \quad \dot{Q} = \frac{1}{\frac{1}{\dot{Q}_{rad(up)} + \dot{Q}_{conv(up)} + \dot{Q}_{cond(down)} + \dot{Q}_{edges}} + \frac{1}{\dot{Q}_{cond(up)}}$$

If the surface temperature of the emitter is used, and not the water temperature, $\dot{Q}_{cond(up)}$ is null; $\dot{Q}_{cond(down)}$ can be express equal to $A_r \cdot (T_r - T_a) \cdot \frac{\lambda_{ins}}{L_{ins}}$, taking into account just the insulation layer beneath the panel and $\dot{Q}_{edges} = \frac{(T_r - T_a) \cdot A_{edge}}{\frac{L_{edge}}{\lambda_{edge}} + 0,04}$.

2.4. Radiative cooling

The upward emitted long wave radiation \dot{Q}_{rad} in W, is a function of the surface temperature (to the fourth power) and the downward long wave radiation (L_{\downarrow}) in W/m^2 , and its amount reflected upward. For non-black bodies, the reflectivity ρ can be expressed with the following equation in function of a given wavelength λ :

$$(10) \quad \rho(\lambda) = 1 - \varepsilon(\lambda)$$

Where $\varepsilon(\lambda)$, $\alpha(\lambda)$ and $\tau(\lambda)$ are respectively the emissivity, absorptivity and transmissivity of the material at the same wavelength. Absorptivity equals emissivity in the long wave band and transmissivity can be considered equal to zero (Baldocchi D., September 10, 2012):

$$\varepsilon(\lambda) = \alpha(\lambda),$$

$$\tau(\lambda) = 0$$

Which, in case of small convex body in a large cavity (Figure 86), taking into consideration the incident, reflected and emitted components, leads to:

$$(11) \quad \dot{Q}_{rad} = A \cdot [\varepsilon_r \cdot (\sigma \cdot T_r^4) + (1 - \varepsilon_r) \cdot L_{\downarrow} - L_{\downarrow}]$$

Where ε_r is the infrared emissivity of the radiating body and σ is the Stefan–Boltzmann constant ($5,67 \times 10^{-8} W/m^2 \cdot K^4$). Equation (11) can be then rearranged in the following way:

$$(12) \quad \dot{Q}_{rad} = A_r \cdot \varepsilon_r \cdot (\sigma \cdot T_r^4 - L_{\downarrow})$$

Where the radiative heat transfer coefficient to be used in (8) is:

$$(13) \quad h_{rad} = \frac{\varepsilon_r \cdot (\sigma \cdot T_r^4 - L_{\downarrow})}{T_r - T_a}$$

Combined with (15), for horizontal panels equation (12) becomes:

$$(14) \quad \dot{Q}_{rad} = A_r \cdot \varepsilon_r \cdot \sigma \cdot (T_r^4 - T_{sky}^4)$$

Where h_{rad} to be used in (8) is equal to $\sigma \cdot \varepsilon_r \cdot \frac{(T_r^4 - T_{sky}^4)}{T_r - T_a}$.

With a tilted angle equal to zero (horizontal panel) the term L_{\downarrow} can be expressed as:

$$(15) \quad L_{\downarrow}(0) = \sigma \cdot T_{sky}^4 = \sigma \cdot \varepsilon_{sky} \cdot T_a^4,$$

Where ε_{sky} is the emissivity of the sky and T_r, T_{sky} and T_a are in Kelvin.

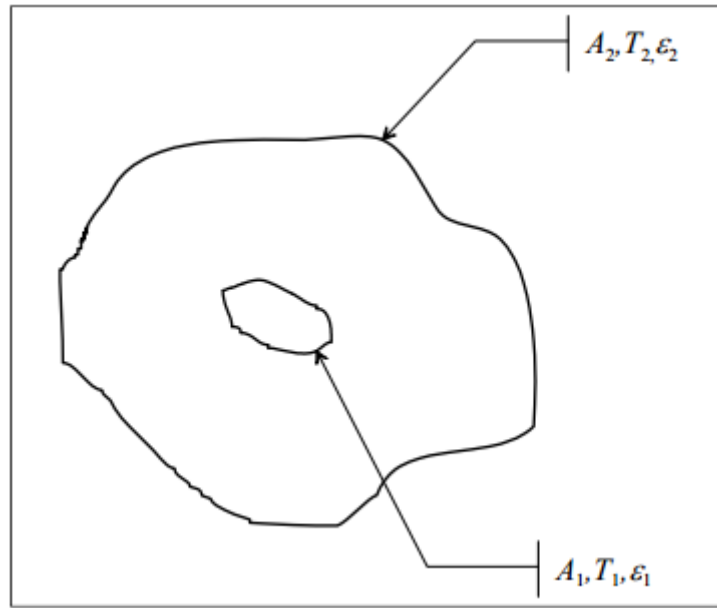


Figure 86 – Small convex body in a large cavity, where $A_2 \gg A_1$.

In the experiment described afterwards, the temperature of the sky facing parallel the radiator is known (see. Chapter VII.4.2.6.) and it is possible to use it directly to calculate the radiative cooling \dot{Q}_{rad} , considering the tilt of the radiator, eq. (21), already included.

Otherwise the emissivity of the sky has to be determined.

Based on previous studies, the model elaborated by Berdahl and Fromberg, (1982), presents a high degree of credibility, modelling with an acceptable accuracy the clear sky emissivity in function of air temperature and relative humidity (Meir M. G. et al., 2003), (Chen B., 1991). The selected equation to model clear sky emissivity would be anyway the corrected formula (17) by Berdahl and Martin (1984). In fact, previous studies based on experimental results showed this model as the most precise (Meir M. G. et al., 2003), (Eicker U. et al., 2011).

2.4.1. Clear sky ($\varepsilon_{sky} = \varepsilon_0$)

$$(16) \quad \varepsilon_0 = 0,71 + 0,0056 \cdot T_{dp} + 0,000073 \cdot T_{dp}^2 + 0,013 \cdot \cos \frac{2 \cdot \pi \cdot t_m}{24} + 0,00012 \cdot (p_{atm} - p_o)$$

$$(17) \quad T_{dp} = C_3 \cdot \frac{\ln(RH) + C_1}{C_2 - [\ln(RH) + C_1]}$$

$$(18) \quad C_1 = \frac{C_2 \cdot T_a}{C_3 + T_a}$$

$$(19) \quad C_2 = 17,08085; C_3 = 234,175 \quad (\text{Berdahl and Martin, 1984})$$

where t_m is the number of hours from midnight in solar time, T_{dp} the dew point temperature in ($^{\circ}\text{C}$), RH the relative humidity, $0 \leq \text{RH} \leq 1$, and T_a is the dry-bulb temperature of air. $(p_{atm} - p_o)$ is the difference between the atmospheric pressure of the ambient and at zero elevation, for Copenhagen can be considered null. The angle of the cosine $\frac{2 \cdot \pi \cdot t_m}{24}$ is expressed in radians, the equivalent in degree would be 15° .

The model by Berdahl and Martin (1984) is based on experimental data which covered for T_{dp} a range of -20 to +30 °C and for $(T_{air} - T_{sky})$ a range of 5 K in a hot, humid sky and 30 K in a cold, dry climate.

Table 44 – Different physical models for cloudless sky

Clear sky models ($\varepsilon_0 = \varepsilon_{sky}$)	
Author (year of publication)	Equation
Swinbank (1963)	$\varepsilon_0 = 0,0552 \cdot T_{amb}$
Bliss (1961)	$\varepsilon_0 = 0,8004 + 0,00396 \cdot T_{dp}$
Elsasser et al. (1942)	$\varepsilon_0 = 0,741 + 0,0062 \cdot T_{dp}$
Berdahl and Fromberg (1982)(night time)	$\varepsilon_0 = 0,727 + 0,0060 \cdot T_{dp}$
Berdahl and Fromberg (1982)(day time)	$\varepsilon_0 = 0,734 + 0,0061 \cdot T_{dp}$
Berdahl and Fromberg (1982)(mean)	$\varepsilon_0 = 0,787 + 0,0028 \cdot T_{dp}$
Clark and Allen (1978)	$\varepsilon_0 = 0,770 + 0,0038 \cdot T_{dp}$
Berger et al. (1984)	$\varepsilon_0 = 0,770 + 0,0038 \cdot T_{dp}$
Berdahl and Martin (1984a)	$\varepsilon_0 = 0,71 + 0,0056 \cdot T_{dp} + 0,000073 \cdot T_{dp}^2$
Berdahl and Martin (1984b)(corrected)	$\varepsilon_0 = 0,71 + 0,0056 \cdot T_{dp} + 0,000073 \cdot T_{dp}^2 + 0,013 \cdot \cos \frac{2 \cdot \pi \cdot t_m}{24} + 0,00012 \cdot (p_{atm} - p_o)$
Chen et al. (2010)	$\varepsilon_0 = 0,736 + 0,00571 \cdot T_{dp} + 0,3318 \cdot 10^{-5} \cdot T_{dp}^2$

2.4.2. Cloudy sky

For cloudy sky Berdahl and Martin (1984) introduce an empirical adjustment to obtain the emissivity of the sky ε_{sky} in function of ε_0 :

$$(20) \quad \varepsilon_{sky} = \varepsilon_0 + (1 - \varepsilon_0) \cdot \varepsilon_c \cdot n \cdot e^{-Z_c/Z_*}; \quad 0 \leq n \leq 1$$

Where Z_* is a reference value fixed to 8,2 km. Z_c is the cloud base height (in km), and has to be obtained from meteorological measurements. The hemispherical cloud emissivity ε_c can be approximated to 1 for low and medium high clouds, while for clouds where $4 < Z_c < 11 \text{ km}$, $\varepsilon_c = 0,74 - 0,084 \cdot (Z_c - 4)$ and for $Z_c > 11 \text{ km}$, $\varepsilon_c = 0,15$. n is the fractional cloud amount of the sky covered by “non-transparent” clouds, with $n = \frac{N}{8}$ and N is a cloud cover factor, which has to be obtained from meteorological measurements ($N = 0$ for clear sky and $N = 8$ for overcast sky).

The presence of clouds in the sky increases the absorbance and hence the sky emissivity and the sky temperature; in this way the ΔT with the radiator is reduced and the cooling power too.

2.4.3. Correction for tilted panels

In case the panel is tilted, the incident downward longwave radiation (L_{\downarrow}) has to be defined in function of the tilt angle α , as the sum of the atmospheric L_A and ground L_G components (Unsworth and Monteith, 1974).

$$(21) \quad L_{\downarrow}(\alpha) = L_A + L_G$$

where:

$$L_A = L_{\downarrow}(0) \cdot \cos^2(\alpha/2) + b \cdot I_7 \cdot \sigma \cdot T_a^4$$

and

$$L_G = \sin^2(\alpha/2) \cdot (\varepsilon_g \cdot \sigma \cdot T_g^4 + \rho_g \cdot L_A)$$

b ranges from 0,07 to 0,14 with a typical value of 0,09. I_7 is a function of the tilt angle α as it can be seen in Figure 87, T_g is the ground surface temperature (K), ε_g the emissivity which can be found in Table 45 and ρ_g the reflectance of the ground which can be considered equal to 0,1 for grass and 0,25 for asphalt or rock (11120 Daylight in Buildings 2012, DTU). If we assume transmission is zero then $\rho_g = 1 - \varepsilon_g$.

Table 45 – Average values of some Infrared Emissivities (Campbell, Norman, 1998)

Surface	Emissivity ε
Plant leaves	0,94-0,99
Glass	0,90-0,95
Aluminum	0,06
Aluminum paint	0,30
Soil	0,93-0,96
Water	0,96

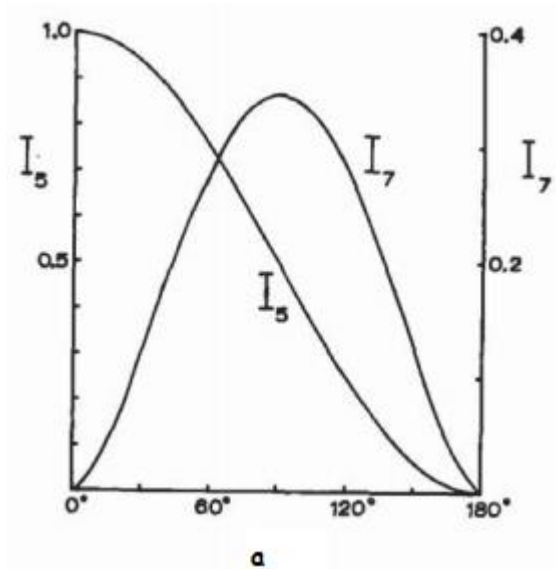


Figure 87 – Dependence of I_7 on α , (Unsworth and Monteith, 1974b)

2.4.4. Surrounding objects

If the shielding effect produced by the surrounding needs to be taken into account, the angle α used in equation (21) needs to be replaced with α' , where:

$$(22) \quad \alpha' = \alpha + \beta$$

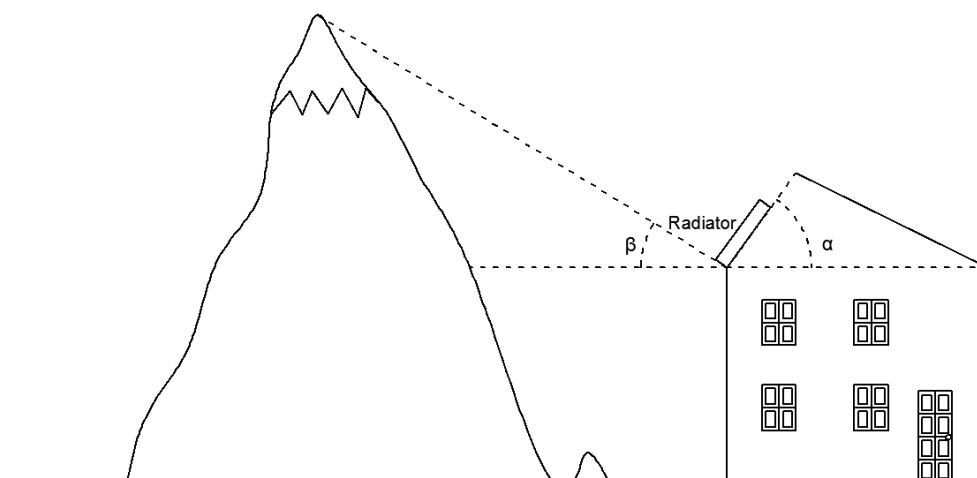


Figure 88 – Angle α of tilted panel and β to consider shielding surrounding.

2.5. Convective cooling

The convective cooling power \dot{Q}_{conv} can be expressed in function of the heat transfer coefficient for mixed convection $h_{c,mix}$:

$$(23) \quad \dot{Q}_{conv} = A_r \cdot h_{c,mix} \cdot (T_r - T_a) \quad (W)$$

$h_{c,mix}$ is defined in function of free $h_{c,free}$ and forced $h_{c,forced}$ convective components:

$$(24) \quad h_{c,mix} = \sqrt[3]{h_{c,forced}^3 + h_{c,free}^3} \quad (W/m^2K)$$

$h_{c,mix}$ may vary from around 6 to 30 W/m²K or more if the wind speed is high.

Two approaches have been investigated and compared:

1) The first is a simplified approach, where for surface is considered without wind screeed. The coefficient for forced convection $h_{c,forced}$ is in the first order a linear function of the wind speed U_w :

$$(25) \quad h_{c,forced} = 2,8 + 3 \cdot U_w \quad (W/m^2K)$$

While the free convection is due to a temperature gradient:

$$(26) \quad h_{c,free} = 1,78 \cdot (T_r - T_a)^{1/3} \quad (W/m^2K)$$

depending on the ambient temperature T_a and the mean collector plate temperature T_r . This approach has been applied also to define the collector efficiency factor F' , used in TRNSYS simulations (Duffie J.A. et al., 2013) (Anderson T.N. et al., 2013).

2) The second approach considers more in detail the air properties and the geometry of the plate, to define the convective capacity:

$$(27) \quad h_{c,forced} = (k_a / L_{c,forced}) \cdot \overline{Nu_{forced}} \quad (W/m^2 \cdot K)$$

$$(28) \quad h_{c,free} = (k_a / L_{c,free}) \cdot \overline{Nu_{free}} \quad (W/m^2 \cdot K)$$

(Zandegiacomo E., 2003)

Where \overline{Nu} in the mean Nusselt number for the entire collector's surface, combined with L_c , the characteristic length of the system and k_a , the conductivity of the air.

2.5.1. Forced convection (calculation of $h_{c,forced}$)

This is the component of convective heat exchange and as previously mentioned, it is mainly due to an external flow (wind) velocity (the velocity is generated by an external force and not by the ΔT between surface of the plate and air).

To determinate $h_{c,forced}$ the method used is the physical model for a flat plate with parallel forced flow:

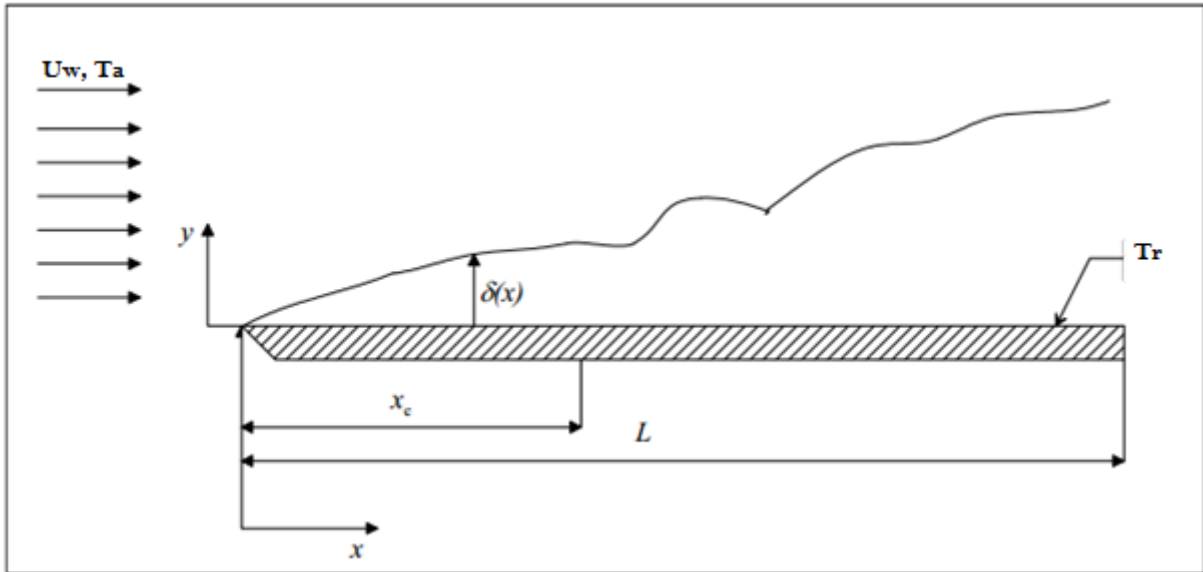


Figure 89 – Flat plate with parallel flow

If the flow is laminar:

$$(29) \quad \overline{Nu}_{forced} = 0,664 \cdot Re^{0.5} \cdot Pr^{1/3}; \quad Re < 5 \cdot 10^5, Pr \geq 0,6$$

If the plate is long enough for the flow to pass from laminar to turbulent, the averaged Nusselt number over the isothermal plate in turbulent region is:

$$(30) \quad \overline{Nu}_{forced} = 0,037 \cdot Re^{0.8} \cdot Pr^{1/3}; \quad 5 \cdot 10^5 \leq Re \leq 10^8, 0,6 \leq Pr \leq 60$$

But if the flow passes from laminar to turbulent, it is needed to consider that until a certain distance x_c , the flow is laminar. So it is needed to do the integrated average between the laminar zone, until and x_c , and the turbulent one, from x_c to L_c , to evaluate \overline{Nu}_{forced} . After performing the integrals and simplifications, one obtains:

$$(31) \quad \overline{Nu}_{forced} = (0,037 \cdot Re^{0.8} - 871) \cdot Pr^{1/3}; \quad 5 \cdot 10^5 \leq Re \leq 10^8, 0,6 \leq Pr \leq 60$$

(Zandegiacomo E., 2003),(Magnani L., 2010),(Bahrami M., 2009).

To determine if the flow is able to pass from laminar to turbulent, one has to check if the length L_c of the panel is superior to the critical distance x_c . The flow is defined turbulent if Re is greater than the critical Reynolds Re_{x_c} which is assumed to be equal to $5 \cdot 10^5$.

x_c can be calculated in the following way:

$$(32) \quad x_c = \frac{v_a}{U_w} \cdot Re_{x_c} \quad (m)$$

If $x_c < L_{c,forced}$ the flow is laminar and eq. (29) can be used to define $h_{c,forced}$

If $x_c > L_{c,forced}$ the flow becomes turbulent and eq. (31) can be used to define $h_{c,forced}$

Now the thermodynamic properties of the air have to be determined, such as the kinematic viscosity $v_a(m^2/s)$, the conductivity of air $k_a(W/m \cdot K)$, the heat capacity of air $c_a(J/kg \cdot K)$ and its density $\rho_a(kg/m^3)$.

From those parameters, the Prandtl number P_r and Reynolds number Re can be derived:

$$(33) \quad P_r = \frac{\rho_a \cdot c_a \cdot v_a}{k_a} \quad (-)$$

$$(34) \quad Re = \frac{L_c \cdot U_w}{\nu_a} \quad (-)$$

where U_w is the wind speed (m/s).

If the plate is infinitely extended in the direction perpendicular to the wind direction ($L1$) and it is limited in the parallel direction ($L2$), then $L_{c,forced} = L2$. If the two directions are comparable to each other then $L_{c,forced} = (L1 + L2)/2$ for forced convection (Magnani L., 2010).

Some properties of air can be found in the table beneath:

Table 46 – Common properties for air at atmospheric pressure¹

Temperature	Density	Specific heat capacity	Thermal conductivity	Kinematic viscosity	Expansion coefficient	Prandtl's number
- T -	- ρ -	- c _p -	- k -	- ν -	- B -	- P _r -
(°C)	(kg/m ³)	(kJ/kg.K)	(W/m.K)	x 10 ⁻⁶ (m ² /s)	x 10 ⁻³ (1/K)	
0	1,293	1,005	0,0243	13,30	3,67	0,715
20	1,205	1,005	0,0257	15,11	3,43	0,713
40	1,127	1,005	0,0271	16,97	3,20	0,711
60	1,067	1,009	0,0285	18,90	3,00	0,709

The authoritative formula for the thermal-conductivity of dry air is from Kadoya, Matsunaga, and Nagashima. A line for the k_a at half air pressure ($P = 50$ kPa) overlays dry air on Figure 90; so air pressure variations do not significantly affect k at the level of a rooftop. For our range of interest k_a can be obtained from:

$$(35) \quad k_a = 0,02241 \frac{W}{m \cdot K} + (T_f - 250 K) \cdot 76,46 \times 10^{-6} \quad (W/m \cdot K)$$

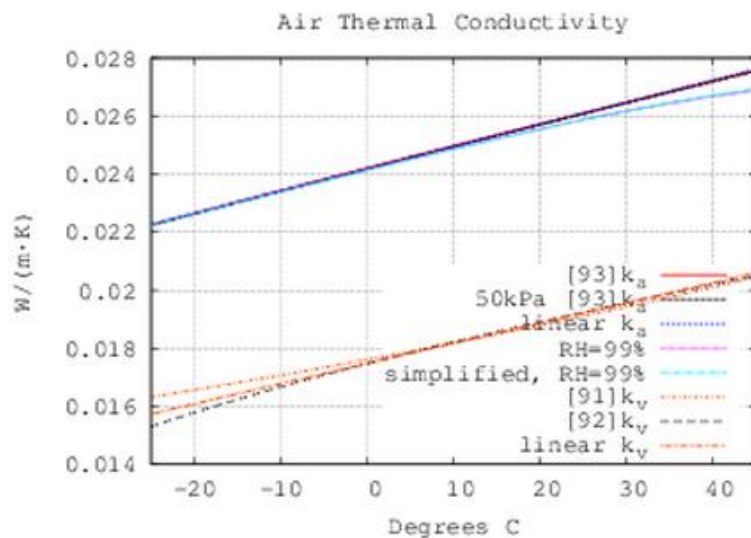


Figure 90 – Thermal conductivity of dry air and water vapor is function of the temperature¹

¹ http://www.engineeringtoolbox.com/air-properties-d_156.html

The thermodynamic properties of the air as in Table 46 should be calculated in function of the film temperature T_f :

$$(36) \quad T_f = \frac{T_a + T_r}{2} \quad (^\circ C)$$

2.5.2. Free convection (calculation of $h_{c,free}$)

This component of convective heat exchange is mainly related to the velocity generated by a difference of density due to a temperature gradient.

Different models to express the Nusselt number in free convection have been investigated and compared (Corcione M., 2007) (Zandegiacomo E., 2003) (Magnani L., 2010). The selected ones showed a high level of accuracy and few discrepancies with the other models, experimental or numerical, conventionally used.

Three models are here described for horizontal panels, in function of the kind of flow and heat direction:

1) flat plate with horizontal upper surface heated isothermally, heat flow upward, laminar flow $10^4 < R_a < 10^7$:

$$(37) \quad \overline{Nu_{free}} = 0,54 \cdot R_a^{0,25}$$

(Similar correlations are the experimental ones, presented by Lewandowski, 1999)

$$\overline{Nu_{free}} = 0,766 \cdot R_a^{\frac{1}{5}}; 10^4 < R_a < 10^9 \text{ and } \overline{Nu_{free}} = 0,173 \cdot R_a^{\frac{1}{5}}; 10^5 < R_a < 10^8$$

2) flat plate with horizontal upper surface cooled isothermally, heat flow downward, laminar flow $10^4 < R_a < 10^7$:

$$(38) \quad \overline{Nu_{free}} = 0,27 \cdot R_a^{0,25} \text{ (correlation of Mc Adams)}$$

3) flat isothermal horizontal plate, turbulent flow $R_a > 10^7$:

$$(39) \quad \overline{Nu_{free}} = 0,14 \cdot R_a^{1/3}$$

Where R_a is the Rayleigh number defined as

$$(40) \quad R_a = G_r \cdot P_r$$

Where P_r is the Prandtl number as defined in eq. (33) and G_r is the Grashof number defined as:

$$(41) \quad G_r = \frac{g \cdot B \cdot L_{c,free}^3 \cdot (T_r - T_a)}{\nu_a^2}$$

Where:

g is the gravitational acceleration $\left(\frac{m}{s^2}\right)$

B is the expansion coefficient. If the dry air is considered as a perfect gas $B = \frac{1}{T_a}$

ν_a is the cinematic viscosity (see Table 46)

In case of free convection on horizontal plate, the characteristic length $L_{c,free}$ is the hydraulic radius, defined as the ratio between area and perimeter of the plate.

(Zandegiacomo E., 2003) (Magnani L., 2010) (Lewandowski, 1999)

If the panel is tilted the function used is:

¹ <http://people.csail.mit.edu/jaffer/SimRoof/Convection/>

$$(42) \quad \overline{Nu_{free}} = 0,14 \cdot [(G_r \cdot Pr)^{1/3} - (G_{r,cr} \cdot Pr)^{1/3}] + 0,56 \cdot (G_{r,cr} \cdot Pr \cdot \cos \alpha)^{1/4}$$

for $10^5 < Gr \cdot Pr \cdot \cos \alpha < 10^{11}$ and $15^\circ < \alpha < 75^\circ$

The critical Grashof number, $G_{r,cr}$, is the value at which the Nusselt number starts deviating from laminar behavior. For α equal to 15° , 30° , 60° and 70° , the $G_{r,cr}$ number is given as 5×10^9 , 2×10^9 , 10^8 , and 10^6 respectively (Churchill S.W., 1976). The $G_{r,cr}$ has been interpolated for 45° based on the previous values, obtaining $1,33 \times 10^9$.

2.6. Discussion

Considering the experiment conditions, the flow is expected to be as in equation (29) or (31). Using the simplified approach (eq.(25)), the results obtained are comparable to those applying eq. (30) with a difference of $h_{c,forced}$ in between 10 and 15% in function of the wind speed. Using eq. (30), the flow is considered turbulent on the entire plate surface. It seems like the simplified method does not consider that the flow can be laminar or that when the flow is turbulent, there is still a laminar component until a distance x_c on the panel surface. In fact in both cases, the convective component of forced heat exchange decreases considerably, leading to an over sizing, in the simplified method, of the order 2-3 times than the value obtained with eq. (31) (laminar flow) and of the order 1,5-2 times when the flow is turbulent, eq.(31).

3. Economical potential of nighttime radiative cooling

3.1. Method

A simplified economic analysis has been performed in order to estimate the economic potential of nighttime radiative cooling. The aim of this investigation is to get an overview of possible payback time, without going into a detailed market analysis.

The price of electricity has been derived from Statistic Denmark and the Danish Energy Association and estimated to be 250 øre/kWh (see Annex 10: Electrical energy price). A discount rate equal to 3% has been used to determine the present value of future cash flows. The cost of the electrical energy for the circulation pump is considered; the pump is assumed to consume an average of 8 W. No maintenance cost is taken into account, while the installation cost is assumed to be 30% of the price of the system.

Three different collectors' prices are here investigated: the PVTs and unglazed solar collector tested during the experiment in Copenhagen (type 1) and the unglazed panel used in Versailles (type 2) for the SDE2014 competition. Based on experimental outputs, the cooling produced with PVTs or unglazed solar collectors is comparable. The production is estimated to be 0,56 kWh/m²/night for all the different types of collectors if the water to be cooled has an initial temperature of 22 °C and is stored in a tank of 750 l. The cooling demand is restricted to three months (June, July and August), based on IDA-ICE simulation.

Table 47 – Price of the three collectors investigated

Price with installation (DKK/m ²)		
Photovoltaic-thermal (PVT)	Unglazed solar collectors type 1	Unglazed solar collectors type 2
1359	1246	468

The payback time takes into account just the cooling potential, without considering the hot water and electricity production.

3.1. Results

Based on the previous assumptions the payback time varies between 4 and 14 years for the cheapest of the unglazed solar collectors and the PVTs respectively.

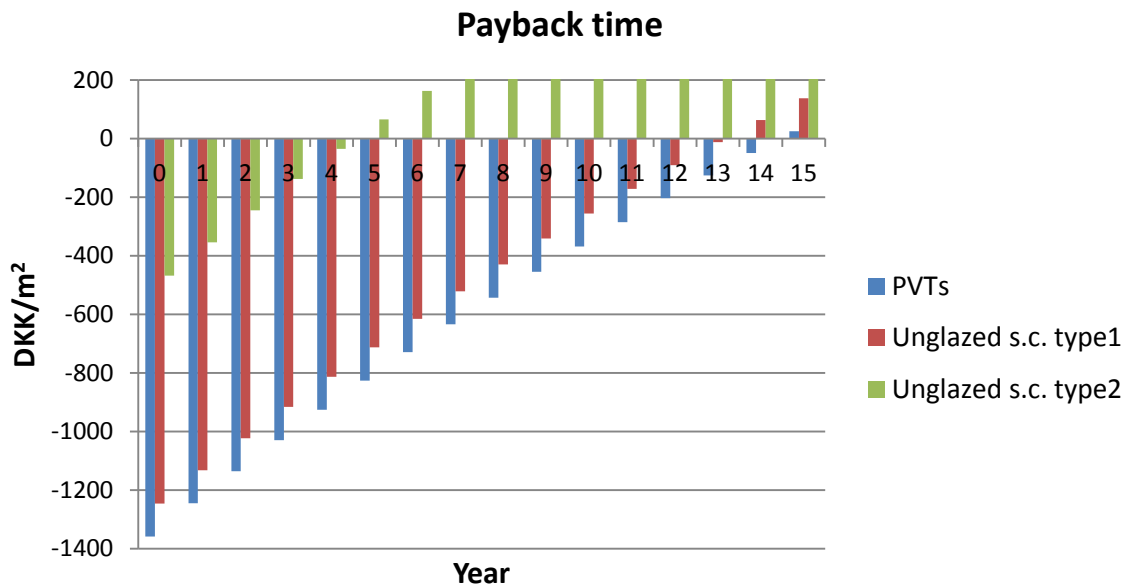


Figure 91 – Payback time in years of the three collectors investigated

3.2. Conclusion

The calculated payback time shows an interesting potential for nighttime radiative cooling also in Denmark, where the need of cooling is limited. In fact all the initial costs investigated are amortized in less than 15 years. For the most expensive technology, the PVTs, a payback time of 14 years is achieved just considering the cooling potential; adding the heating and electricity production it could be drastically reduced. Furthermore the analysed data shows that cheap technologies which allow really short payback time, are available on the market. The choice of the kind of collector to install has to be performed balancing the needs of the specific project: if just cooling is needed the unglazed solar collector type 2 should be preferred, while if also electricity and hot water are needed, the PVT technology could be a good choice. The potential could be even more relevant for public building like offices, where the cooling demand is higher and a bigger installation would reduce the initial cost per m².

3.3. Further considerations

The amount of m² installed needs to be sized in function of the cooling demand. It is also important to investigate the contemporaneity between production and demand, taking into account the monthly distribution of the cooling demand. In this way oversizing can be avoided.

Example:

Looking into the cooling demand of EMBRACE for July, 61% of the days, more than 500 W are needed in Copenhagen (see Figure 92). If the collectors' area is sized based on this power, the cooling demand is 100% covered for 39% of the time, at least 55% of the demand is covered for 71,5% of the time (39%+26%+6,5%) and for the rest of the month, at least 1/3 of the demand is always covered. Assuming an average production of 58 W/m², which corresponds to a cooling of 0,56 kWh/m² per night, the area of collectors can be sized to 8,6 m².

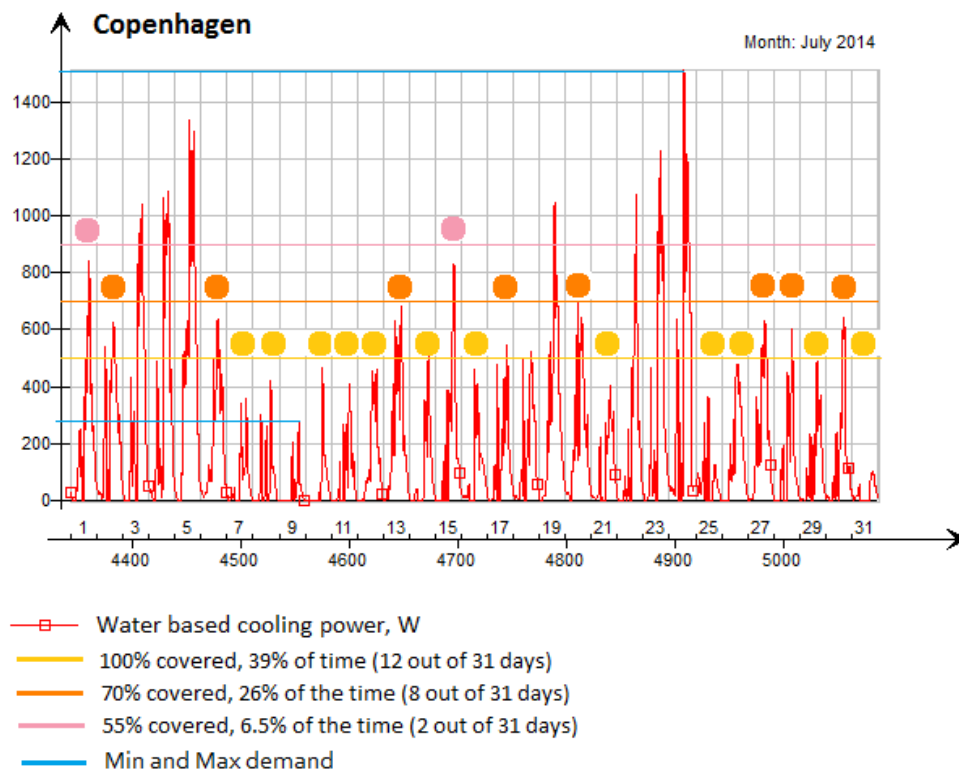


Figure 92 – Daily cooling demand in Copenhagen for the month of June. The demand is here divided in bands to check its distribution in time

4. Experiment

4.1. Description and objectives

The objective of this experiment is to determine the power obtained with nighttime radiative cooling as an output from different types of solar collectors, and compare them. The results can be used to estimate the potential of this system under the Danish climate and set up a physical model. The main aim is to validate a mathematical model able to predict the potential cooling of this technology, in function of input weather data, independent of the location.

Two types of panels are tested:

1. Three PVT panels Solarzentrum¹, Wiosun[®] assembled in series
2. One unglazed solar collector

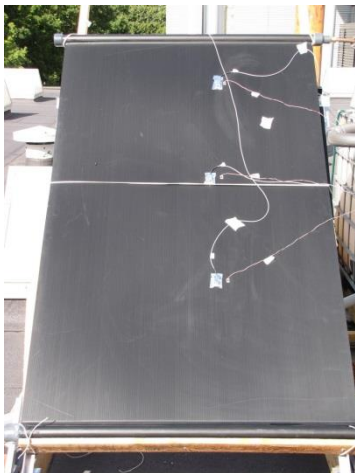
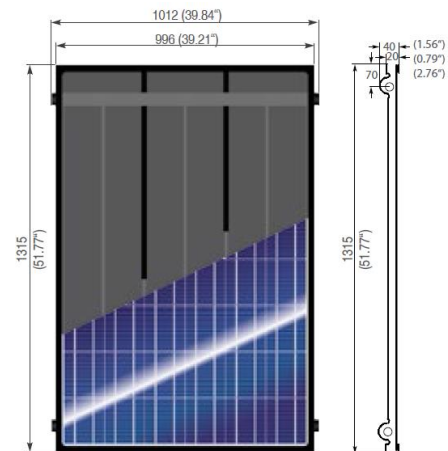


Figure 93 – Unglazed solar collector



Figure 94 – Photovoltaic/thermal panel (PVT)

Those two technologies have been selected because both produce “low temperature hot water”, one is a cheap and simple solution while the other represent a state of the art technology in the solar-thermal field, since able to produce also electricity. In order to have good performance in cooling, the solar collectors to be used should present a certain degree of infrared radiation heat loss. A balance between heating and

¹ <http://www.solarallgaeu.de/en/pv-therm-kombimodul/technische-daten>

cooling production needs to be researched. This is why other technologies with higher performance in heating production have been considered not suitable for cooling.

The two sorts of panels are supplied with water at the same temperature and same flow rate per surface area; the output can therefore be compared between those.

The cooling potential is the main concern of this experiment, but the hot water production has also been monitored. In fact the most likely use of solar collectors for cooling during the night, would integrate the production of hot water during the day. The cooling function could be exploited also in case solar collectors are already used in existing installations, with the conventional purpose of sanitary hot water production. For this reason, a tilted angle equal to 45° towards south has been selected for both the panels, resulting optimal for production of electricity and hot water. In Figure 94 and Table 48 are investigated the optimal tilts in Copenhagen and Rome, cities selected as representative for Northern and Southern Europe, respectively.

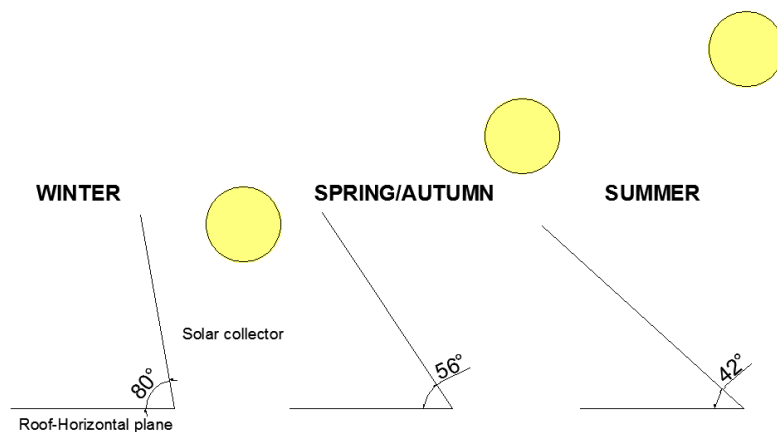


Figure 95 – Optimal tilt in Copenhagen over the year, for the production of electricity and sanitary hot water (Boxwell M., 2012. Solar Electricity Handbook)

Table 48 – Monthly optimal tilt in Copenhagen and Rome, for the production of electricity and sanitary hot water (Boxwell M., 2012. Solar Electricity Handbook)

Copenhagen					
Angle from horizontal plane (°)					
Jan	Feb	Mar	Apr	May	Jun
72	64	56	48	40	32
Jul	Aug	Sep	Oct	Nov	Dec
40	48	56	64	72	80

Rome					
Angle from horizontal plane (°)					
Jan	Feb	Mar	Apr	May	Jun
58	50	42	34	26	18
Jul	Aug	Sep	Oct	Nov	Dec
26	34	42	50	58	66

4.2. Methods

4.2.1. Experiment setup

The experiment has been carried out on the roof of building 412 at the Technical University of Denmark, Kgs. Lyngby (55°47'02.5"N 12°31'19.9"E), during the month of August 2014. The installations mounted for this purpose are presented in the schematic layout of Figure 96.

All the data are recorded every ten seconds and time averaged for five minutes time steps, in order to reduce the fluctuations.

The total water flow is 3,3 l/min, split in two branches: 2 l/min are supplied to the PVT panels and 1,3 l/min are supplied to the unglazed collector. The balancing has been made with the balancing valves, in such a manner that the flow rate per surface area of collector is equal in both branches, with a value of around 0,5 l/min.m² in the present case.

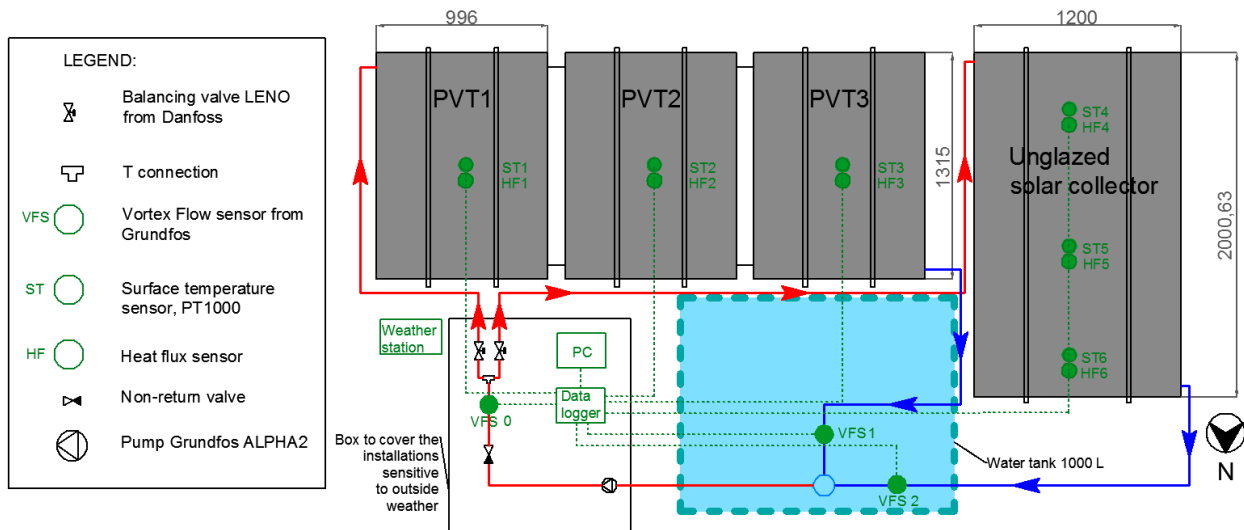


Figure 96 – Schematic layout of the experiment

The cooling capacity of the tested panels is measured with different methods and compared to the values obtained from the theoretical model. In this way, an estimation will be done to evaluate the theoretical approach which fits the most, in particular concerning the ratio between convection and radiation.



Figure 97 – Experiment setup – Back view



Figure 98 – Weather station Vantage Pro2



Figure 99 – Experiment setup – Front view



Figure 100 – Datalogging equipment and pipe work

4.2.2. Materials and sensors used

Solar panels

- Three PVT panels ($3 \times 1,305 \text{ m}^2 = 3,915 \text{ m}^2$)
- One unglazed solar collector ($2,4 \text{ m}^2$)
- Supporting structure for solar panels, fixed frame, tilted 45°

Hydraulic elements

- One storage tank (1000 l), not insulated
- One pump Grundfos ALPHA2 15-40 (5 - 45 W range of operation, 8 W provided for the experiment)
- Two balancing valves from Danfoss, model LENO® MSV-BD (to adjust the pressure drop in the PVTs and unglazed solar collector loops)
- Copper pipes 15x1,5 mm with 15 mm of insulation, $\lambda=0,04 \text{ W/m}\cdot\text{K}$

Measurement equipment and sensors

- Data logger Agilent 34972A with 2 multiplexers 34901A (20 channels each) (Figure 100)
- 3 vortex flow sensors, Grundfos VFS 1-12 QT, 1-12 l/min

Accuracies: $\pm 2^\circ\text{C}$ for the temperature, $\pm 3 \%$ for the flow.

- Weather station Davis Vantage Pro2, software Weather link 6.0.3 (Figure 98)

Accuracies: $\pm 1 \text{ m/s}$ for the wind speed, $\pm 4^\circ$ for the wind direction, $\pm 0,2 \text{ mm}$ for the rain, $\pm 3 \%$ for the RH, $\pm 5 \%$ for the solar radiation, $\pm 0,5^\circ\text{C}$ for the temperature, $\pm 1,7 \text{ hPa}$ for the atmospheric pressure.

- 6 heat flux meters, Rdf Micro-Foil® Heat Flux Sensor (HF)
- 6 temperature sensors, PT1000 Ohm. Hand welded and calibrated. Accuracy $\pm 0,3^\circ\text{C}$.
- Infrared thermo camera, Agema Thermovision®570
- Flat-plane sensor to measure the directional temperature, used to derive the sky temperature (or plane radiant temperature). Hand crafted and calibrated.

Measurements

- Supply temperature, VFS0
- Supply flow rate, VFS0
- Return temperatures of the two panels, VFS1 and VFS2
- Return flow rates of the two panels, VFS1 and VFS2
- Surface temperature of the two panels' types, ST
- Plane radiant temperature (flat plane sensor)
- Heat flux at the surface of the two panels' types, HF
- Wind speed
- RH (Relative humidity)
- $T_{\text{dry air}}$
- Rain precipitation per day
- Solar radiation
- Long wave thermal radiation (from a pyrgeometer situated in DTU building 119, tilted 45°)

4.2.3. Calibration

As the directional sensor was hand-crafted and the PT1000 sensors were hand-welded to the electrical wires, those sensors needed to be calibrated. The calibration has been done in an experiment chamber where it is possible to reach uniform temperature in all the room volume. Conditioned air is in fact spread uniformly from all over the floor area. Temperature steps of 5°C have been used, in the range between 17

and 38 °C. Every time the temperature set point is changed, it is necessary to wait for steady conditions. Once steady state is reached is possible to record the output of every sensor and recalibrate it, thanks to the effective temperature measured with a mercury thermometer. In order to obtain boundary condition as uniform and steady as possible, the sensors were placed inside an insulated calibration box as shown in Figure 101.



Figure 101 – Sensors calibration : outside and inside the insulated box used for the calibration

4.2.4. Infrared thermographic camera

The real emissivity of the two collectors' types has been estimated based on the temperature recorded by an infrared thermographic camera in a point close to where the PT1000 sensors are located. The thermographic camera was set with an emissivity equal to 0.9. The equation used to estimate the emissivity is the following:

$\varepsilon = \frac{(T_{t.camera})^{4 \cdot 0,9}}{T_{PT1000}^4}$, where $T_{t.camera}$ and T_{PT1000} are the temperatures in Kelvin recorded by the thermographic camera and the PT1000 sensor, respectively. The values selected are $\varepsilon = 0,91$ and $\varepsilon = 0,89$ for the unglazed solar collector and PVTs respectively. Another parameter that is fundamental to be considered when using an infrared camera, is that for the camera there is no difference between long wave radiation emitted or reflected. This is why, especially outdoor, overcast conditions are recommended. When the taken pictures are analysed, if spots with particular high temperature are shown, those are probably attributable to reflection; they must not be considered as representative (see Figure 102).

The temperature distribution obtained with the thermographic camera has been used also to evaluate the level of uniformity. This is needed to check the proper distribution of the water in the panels and if the sensors have been located in spots representative of the whole system. In Figure 102 and Figure 103 it is possible to see that during the day, when the water is warmed up in the panels, the flow direction is as expected for both panels' types. The cold water is inlet in the bottom and its temperature increases gradually to the outlet on the top. The unglazed solar collector shows anyhow higher level of temperature uniformity; while in the last of the three PVTs, the one where the water outlet is located, a colder area is shown on the left side. This suggests that the water flow, probably bypasses that part of the panel. Due to the limited amount of this area, this issue has been considered not relevant. Furthermore the sensors seem to be located in areas where the temperature distribution is sufficiently uniform.

Unglazed solar collectors	PT1000	Thermographic camera	Emissivity calculated	Water Tsupply (C°)	Water Treturn (C°)
T _{bottom} (C°)	23,8	25	0,91	25,2	28
T _{middle} (C°)	24,9	26	0,91		
T _{top} (C°)	26,7	26,5	0,90		

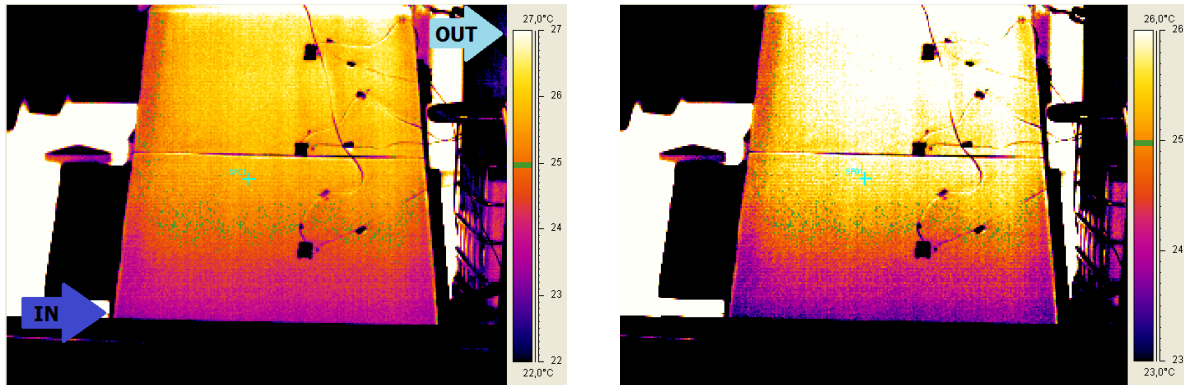


Figure 102 – Infrared pictures of the unglazed solar collector in heating mode. Day 21/08/2014 data recorded and time averaged from 14:40-14 :45, overcast sky, emissivity set in the thermographic camera 0,9. Same picture is shown with two temperature ranges, 22-27 and 23-26 °C respectively.

PVTs	PT1000	Thermographic camera	Emissivity calculated	Water Tsupply (C°)	Water Treturn (C°)
T PVT in (C°)	22,6	21,5	0,89	25,2	25,4
T PVT middle (C°)	22,9	22,5	0,89		
T PVT out (C°)	24,8	23,5	0,88		

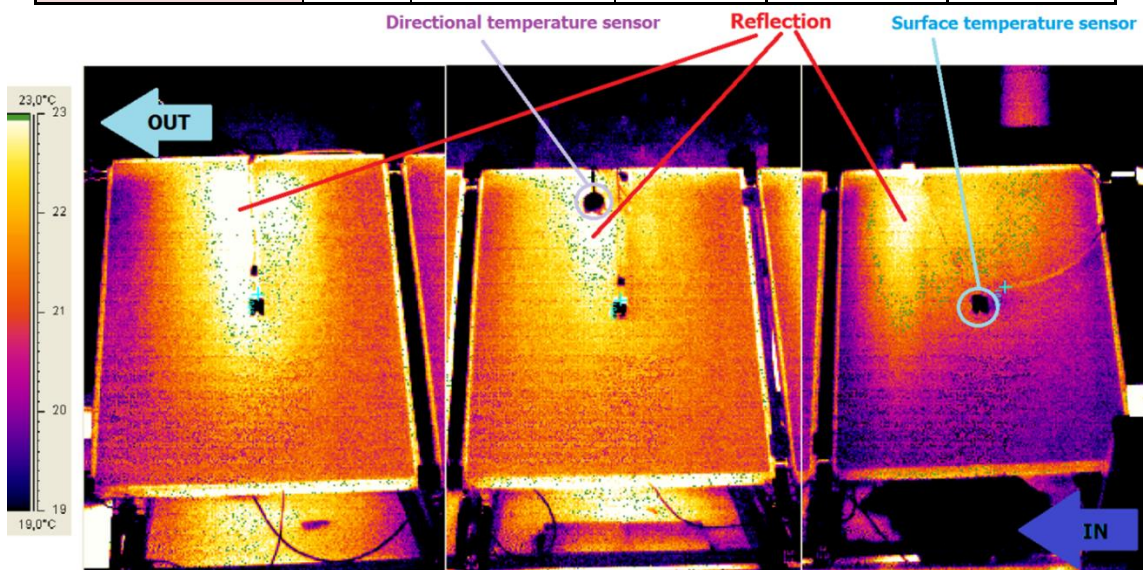


Figure 103 – Infrared pictures of the PVTs in heating mode. Day 21/08/2014 data recorded and time averaged from 14:55-15:00, overcast sky, emissivity set in the thermographic camera 0,9

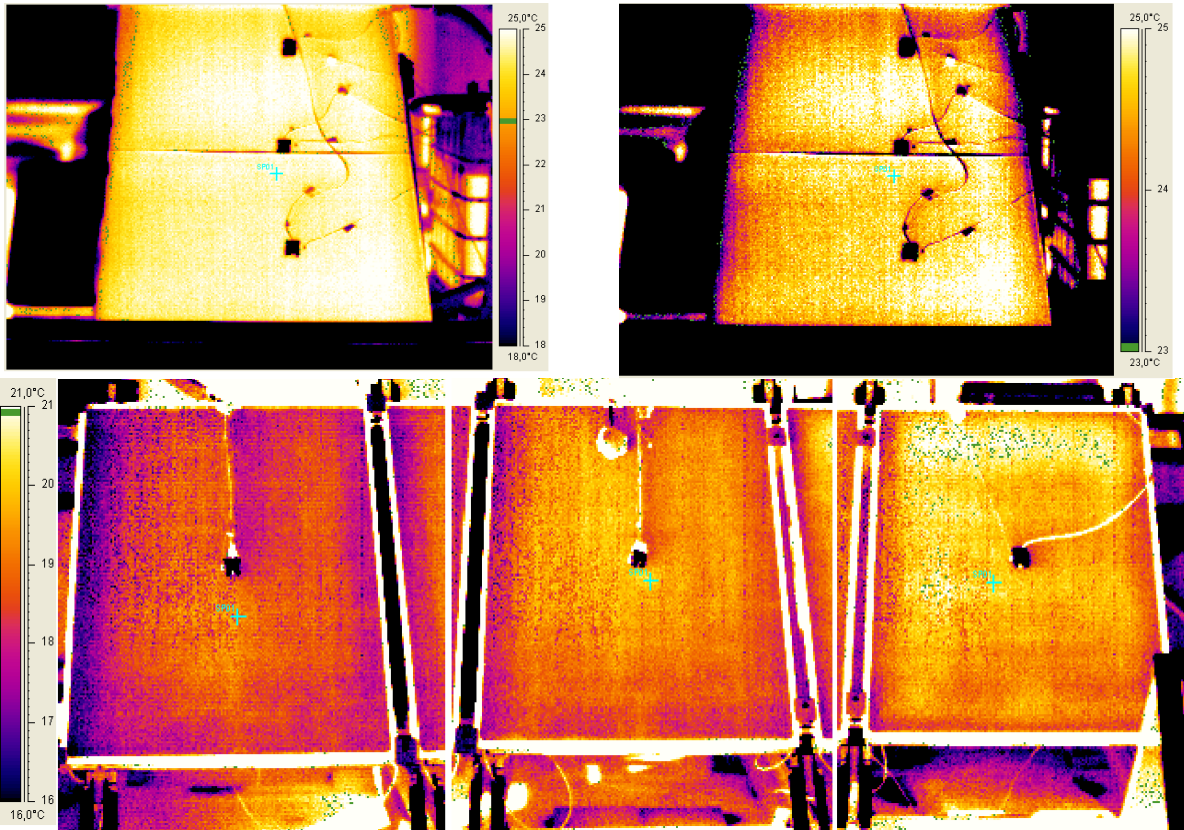


Figure 104 – Infrared pictures of all collectors, in cooling mode. Day 19/08/2014 picture taken at approximately 18:00, overcast sky, emissivity set in the thermographic camera 0,9

4.2.5. Surface temperature sensors

After calibration, the PT1000 sensors have been welded to the surface of the panels with thermal glue, in order to adhere to the surface and to reflect the actual surface temperature. They have been covered with water proof thermal insulation and a low emissivity foil as shown in Figure 105, in order to minimize the influence of the surrounding (radiation, wind, air temperature). This can be seen also in the infrared pictures; where the metallic foil is located (small rectangular shape), lower fictive temperature is recorded (see Figure 103).



Figure 105 – Surface temperature sensor, with and without protection

For the PVT panels, one temperature sensor flux is placed in the centre of each panel, and the three obtained values are averaged to form the output surface temperature for the PVT. For the unglazed collector, the three temperature sensors are placed on a vertical line, and the three obtained values are averaged to form the output surface temperature for the unglazed collector (T_r), see Figure 96.

4.2.6. *Effective sky temperature and plane radiant temperature*

As exposed in the section dedicated to the theory of nighttime radiative cooling (VII.2.), the effective sky temperature is one of the most difficult parameter to estimate. It is defined as the temperature of the equivalent black body that would emit the same amount of long wave radiation (see equation (15) and further). As it is not a real physical parameter, it cannot be measured directly.

The panels installed are not facing the sky horizontally, they are tilted by an angle of 45°. Therefore, in order to calculate the long wave radiation exchange, the sky temperature should be adapted considering the tilt angle and the shading objects in the surroundings. Another approach is to consider directly the plane radiant temperature faced by the panels. This approach has been chosen for the experiment, using two different methods: first with a handcrafted sensor, then the results have been corroborated with measurements from a pyrgeometer. The data from the pyrgeometer are available just for two nights.

Using the plane directional temperature

A handcrafted sensor has been designed for this experiment. It measures the plane directional temperature faced by the panel. This measured temperature is affected by convection and radiation. By applying the theory described in the standard EN 7726 Annex B, the plane radiant temperature $\overline{T_{rad}}$ can be isolated from the measurement, with the following equation:

$$\overline{T_{rad}} = 4 \sqrt{T_g^4 + \frac{h_{cg}}{\varepsilon_g \sigma} (T_g - T_a)}$$

With:

T_g the plane directional temperature, measured by the handcrafted sensor (K)

ε_g is the emissivity of the sensor's surface (-)

h_{cg} is the convective heat transfer coefficient of the sensor (W/m²K). The standard EN 7726 defines this value for the case of the standard black globe, but in the case of the present experiment, the sensor has a flat and circular shape, therefore the method described in paragraph VII.2.5. related to the theory has been used to calculate dynamically this convective heat transfer coefficient, depending on the wind velocity and air temperature.

T_a is the outside dry-bulb air temperature (K), measured by the weather station installed on the experiment site.

The plane radiant temperature $\overline{T_{rad}}$ obtained through this method represents the mean radiant temperature of the half space above the panels. It can then be used to calculate the thermal long wave radiation exchange.

The plane directional temperature sensor has been constructed assembling two PT1000 sensors to aluminum heat diffusion plates and a layer of 5 cm insulation in the middle, which is sufficient to prevent

influence of one side by the other. The sensors are fixed to the plate with thermal glue. One sensor is in direct contact with the surface of one of the PVTs, while the other is facing the sky with the same tilt as the collectors. The heat diffusion plate has been covered with low emissivity paint and the junctions have been made water proof with silicone. The sensor facing the sky records the directional temperature, while the other is used to check any anomaly, since it records the surface temperature which is already known.

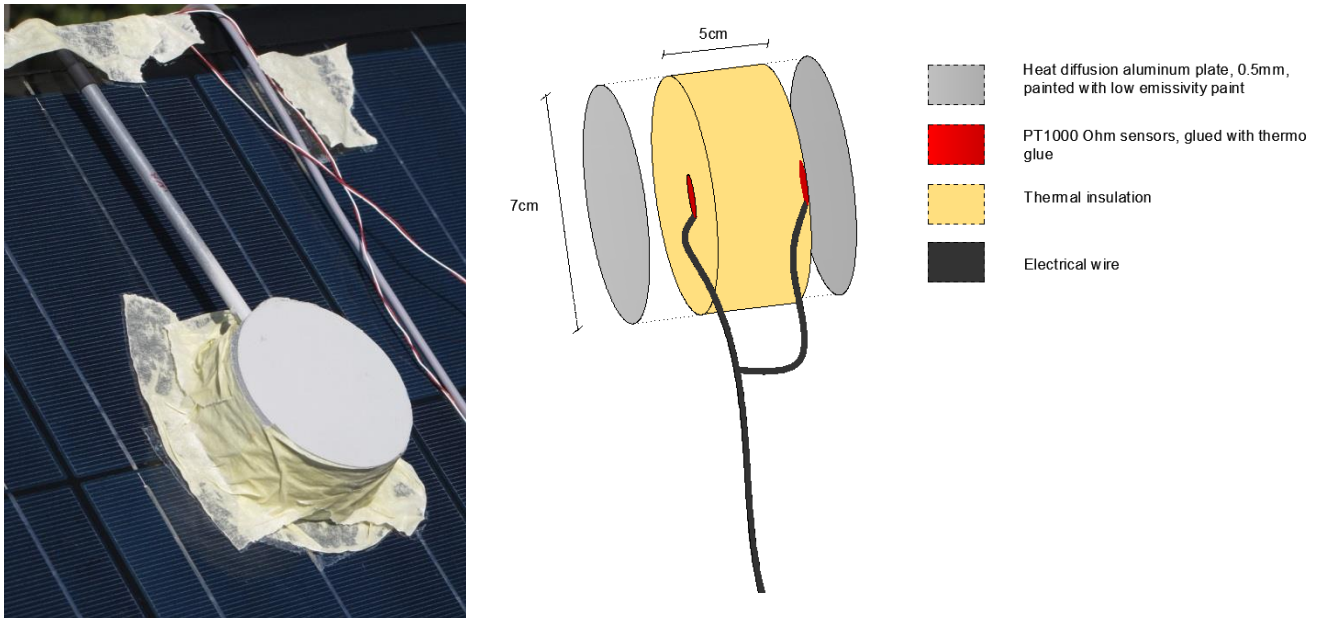


Figure 106 – Hand crafted, plane directional temperature sensor

Using the measurement of thermal longwave radiation with a pyrgeometer

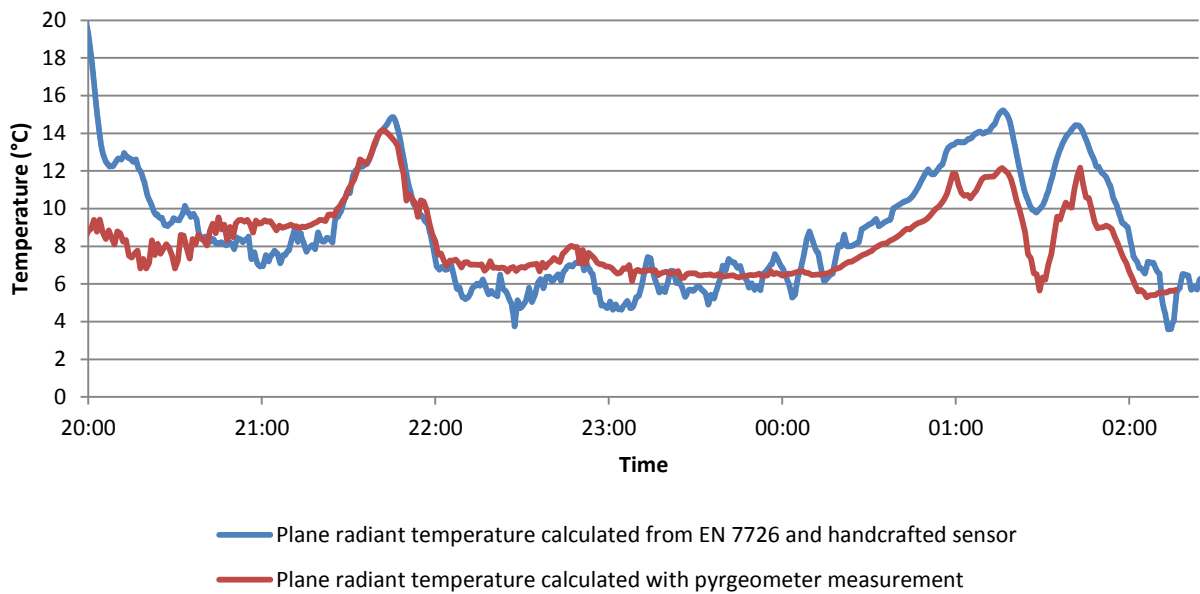
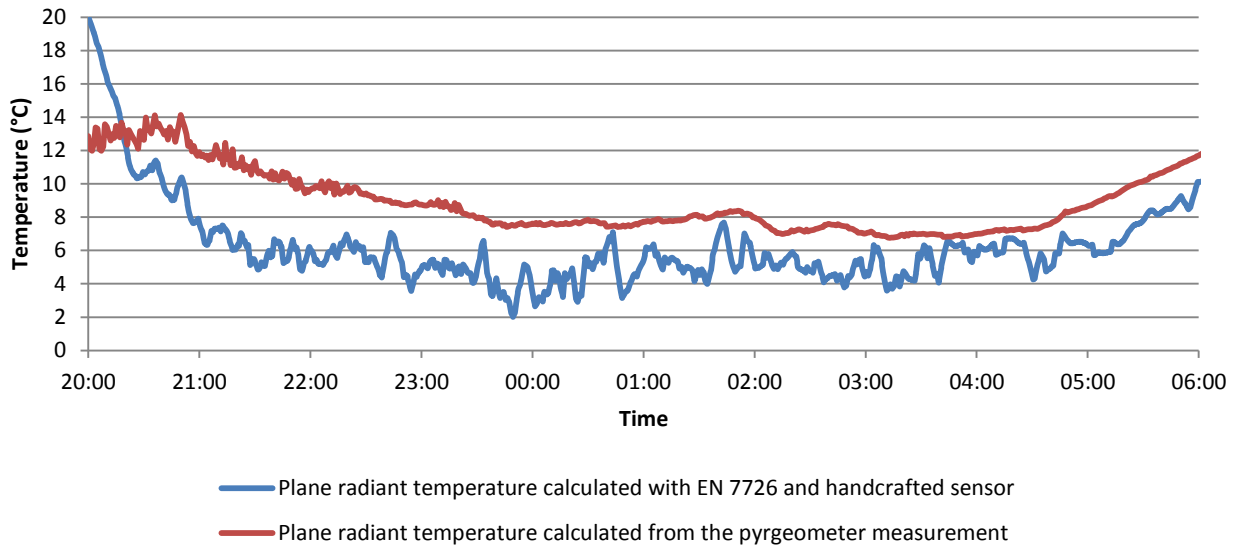
During two nights of the experiment period, the thermal long wave radiation has been recorded by a pyrgeometer and used to calculate the effective sky temperature to confirm the reliability of the approach based on EN 7726. The pyrgeometer is tilted at 45° like the panels and the handcrafted sensor. It measures the thermal long wave radiation \dot{q}_{rad} in W/m^2 and it is already compensating for emissivity, so the following formula applies:

$$\dot{q}_{rad} = \sigma \left(\overline{T_{rad}}^4 - T_{pyr}^4 \right)$$

T_{pyr} is the body temperature of the pyrgeometer. This parameter was not accessible, so it was approximated with the outside air temperature, since the sensor was placed outside. The obtained $\overline{T_{rad}}$ is compared with the one calculated previously, for the two nights where both measurements were available.

In both cases, the two curves show a similar evolution along the night. The average difference between the two calculations is 2,4°C for the night of August 9th and 0,9°C for the night of August 11th.

The reliability of these results could be discussed, since a deviation of 2,4°C cannot be ignored. The two sensors were not situated at the same location, therefore part of the deviation could be explained by the different environmental conditions. The handcrafted sensor is also probably more sensitive to outdoor conditions, contrary to the pyrgeometer that is designed for this purpose. However, the theoretical model based on the handcrafted sensor measurements showed good consistency with other experimental methods, therefore the measurement is considered reliable enough for the purpose of this study.



Figures 107 – Plane radiant temperatures calculated with both methods the nights of the 9th and the 11th of August

4.2.7. Cooling power with theory

The theory developed in part 2. of this chapter VII. is applied to the case of this experiment. The convective cooling power is calculated with both the detailed method and the simplified one, which give different values for the convective heat transfer coefficient $h_{c,mix}$. The cooling in W/m^2 is expressed as follows with equation (23) $\dot{q}_{conv} = h_{c,mix} \cdot (T_r - T_a)$.

The radiative effect is calculated with the plane radiant temperature $\overline{T_{rad}}$ calculated according to the method described in the previous paragraph 4.2.6, using the handcrafted sensor and the calculations from the standard EN 7726. The radiative cooling power is given in W/m^2 by equation (14) $\dot{q}_{rad} = \varepsilon_r \cdot \sigma \cdot (T_r^4 - \overline{T_{rad}}^4)$. The mean surface temperature T_r of the radiator is taken as an average of the temperatures measured by the surface temperature sensors (see paragraph 4.2.5).

4.2.8. Cooling power with VFS

The total cooling power of the water can be calculated with the outputs from the Vortex Flow Sensors (VFS). Equation (1) $\dot{Q} = c_w \cdot \rho \cdot \Delta T \cdot \dot{q}$ (W) can be applied here, knowing the flow rate and the temperatures of the supply and return, all being measured by the VFS. In order to compare with the other methods, the losses through the bottom and the edges of the panels are removed, as well as the losses through the distribution copper pipes. In this way, only the cooling through the top surface of the panel is estimated.



Figure 108 – VFS in the supply (left) and the two returns (right)

The inaccuracy of the VFS for temperature measurement is relatively high, stated as $\pm 2^\circ\text{C}$ in the documentation from Grundfos in the range of temperature concerned by the present experiment. Because the cooling power is calculated via a temperature difference, the uncertainty increases to $\pm 4^\circ\text{C}$, which is important with regards to the actual range of the temperature difference measured. In order to ensure a relevant output from the VFS calculation, the supply temperature has been cross-checked with a digital thermometer placed inside the water tank, close to the pipe pumping the supply water. The correlation between the two temperature measurements are shown on Figure 109: it can be seen that they are relatively close, an average difference of $0,2^\circ\text{C}$. Therefore it is decided to rely on the VFS measurement values to analyse the data, considering that the absolute error is closer to $\pm 0,2^\circ\text{C}$ than to $\pm 2^\circ\text{C}$.

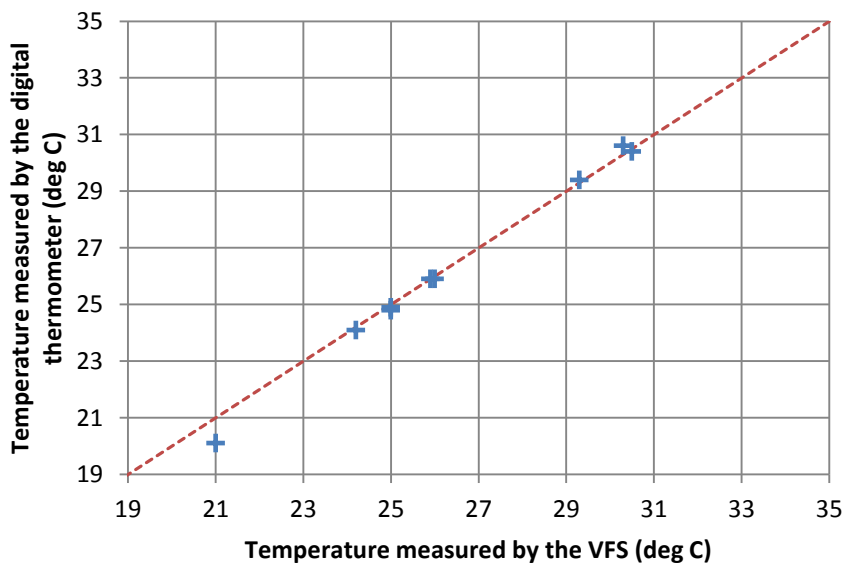


Figure 109 – Correlation between two temperature measurements

4.2.9. Cooling power with heat flux sensors

The heat flux sensors are attached to the surface of the panels with thermal paste, and they measure directly the heat flux between the panel and the environment. Their placement has been studied with the thermographic camera (see paragraph 4.2.4). For the PVT panels, one heat flux is placed in the centre of each panel, and the three obtained values are averaged to form the output heat flux for the PVT. For the unglazed collector, the three heat fluxes are placed on a vertical line, and the three obtained values are averaged to form the output heat flux for the unglazed collector. Those positions have been selected so that to follow the natural distribution of the water flow, in order to picture the change of temperature along its path, from the supply to the return.

The data is averaged for each five minutes. The heat flux sensor measures the heat flux between the top surface of the panel and the environment, therefore there is no need to remove the additional losses (bottom, edges, pipes) to compare its results with the other methods.

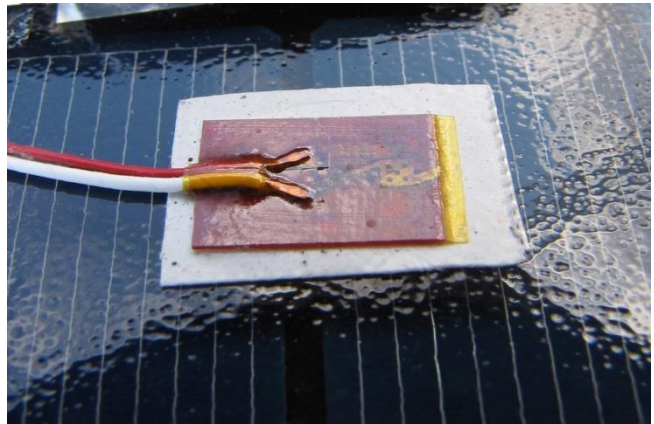


Figure 110 – Heat flux sensor placed on the PVT panel

4.3. Results

4.3.1. Example of a representative night

The results are shown hereafter for one representative night, between August 20th and August 21st, where the sky was clear. The sun set at 20:33 and rose at 05:54. This night is chosen as an example, but the same methods have been applied for all available data during the experiment period which can be found in Annex 13: Power graphs from the experiment (August 12th-25th). During the selected test night, the water is supplied at 23°C at the beginning of the night, cooling down the tank until the supply temperature reaches 12°C at 7:00 AM¹. The temperature outputs are shown in Figure 111, with the outside air temperature and the calculated radiant temperature above the panels plotted as references.

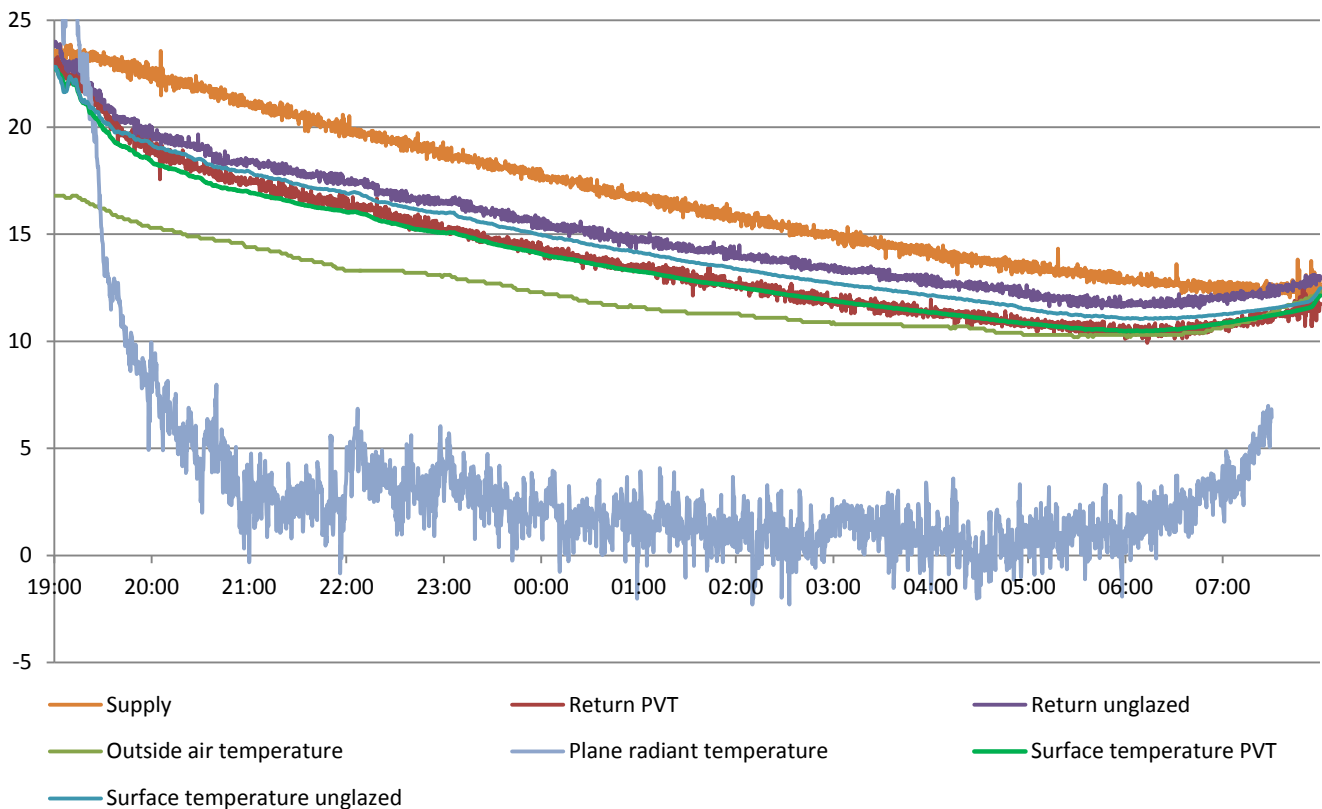


Figure 111 – Temperature outputs of the experiment during the night between August 20th and 21st

It can be seen that the plane radiant temperature calculated according to the method described in 4.2.6 shows plausible results. The radiant temperature is approximately 10°C below the ambient temperature and varies between 0 and 5°C: this represents an acceptable set of values, considering the sky was clear.

The surface temperatures presented here are an average of the three sensors placed on each kind of panel. The curves of the surface temperatures along with the calculated plane radiant temperature have then been used to calculate the cooling power of the panels with the theoretical approaches described in 4.2.7. The flows and temperature measured with the VFS have been used to calculate the cooling power on the side of the water, and the heat flux sensors gave directly a measurement of this cooling power recorded at the upper surface of the panels.

¹ The temperature drop in the tank is also due to the losses in the tank, since it was not insulated. However, all the analysis consider only the cooling power occurring at the panels' side, since the VFS are placed at the supply and return pipes.

4.3.2. Cooling production of the PVT panels

The power curves obtained with the four different methods are plotted for the same night (August 20th – 21st) and presented in Figure 112. The first observation shows a similar evolution of all the cooling powers over the night, with a constant decrease of around 4 W/m² every hour. The results of the theory and the heat flux sensors match remarkably well. Despite having the same trend, the results obtained with the VFS are relatively higher than the three others, with a constant gap of around 50 W/m², a difference that cannot be ignored with regards to the absolute value of the cooling power. The difference can probably be explained by the inaccuracies of the additional losses: the VFS take into account all the cooling effects, including the bottom and edges losses, and the losses in the distribution pipes until the sensors. The pipes and the bottom of the panels have been insulated in order to minimize the difference. The remaining losses have been estimated and removed from the VFS calculation, in order to obtain a value comparable to the ones derived from the heat flux sensors or the theory (which do not take into account those additional losses). The complex geometry of the three PVT panels assembled in series makes it more difficult to evaluate the heat losses through the bottom or the edges, and this is probably why the cooling power is larger. For the unglazed collector (see paragraph 4.3.3), the geometry and the calculation of the additional losses are simpler; therefore the value calculated from the VFS matches well with the three other methods.

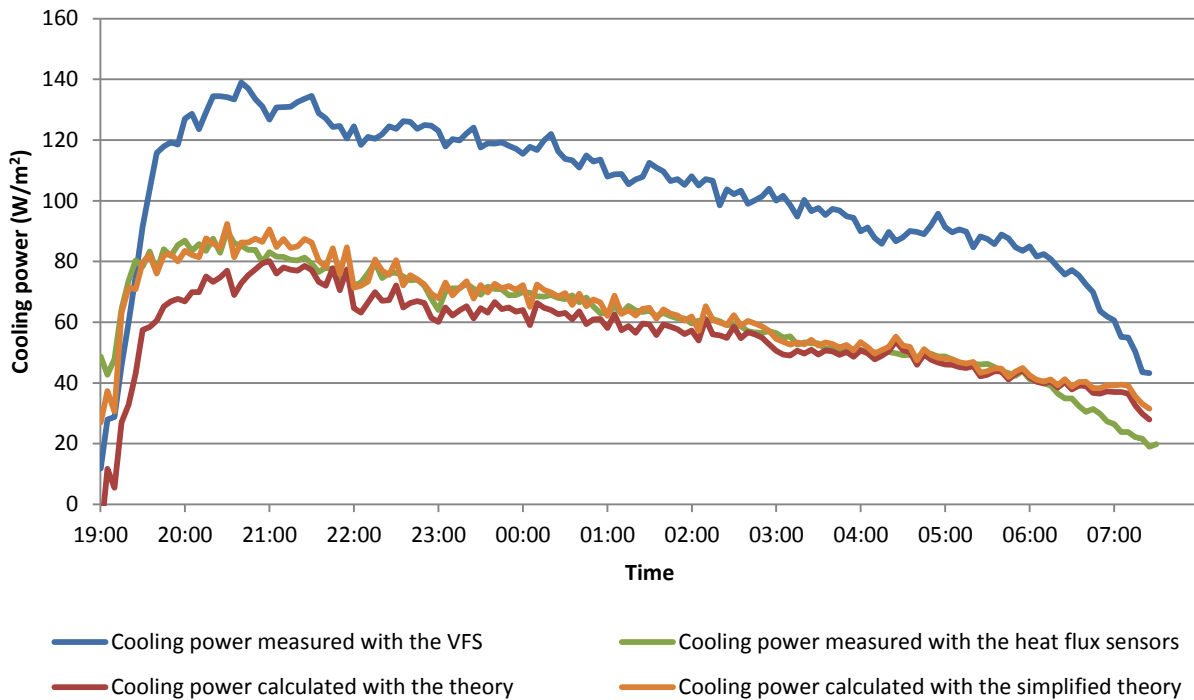


Figure 112 – Cooling power curves for PVT panels (August 20th – 21st)¹

The average cooling power for the three methods is presented in Table 49. Because of the notable difference in the cooling power obtained with the VFS and the values obtained with the other methods, the first value has been discarded. The cooling power selected for further analysis is the average between the other two values. The energy produced over the night is obtained by integration of the power curves from 19:00 to 07:00 (12 hours of operation). In order to quantify the efficiency of the system, the notion of coefficient of performance (COP) is introduced. The COP² is the ratio of the cooling energy produced by the

¹ The edge and bottom losses have been already removed in the VFS curve.

² The COP takes into account the consumption of the pump, which was in fact used to circulate water in both types of panels. It is therefore a low estimation of the COP.

energy consumed by the pump. The circulation pump had an average power of 8 W, which consumes $12 \cdot 8 = 96$ Wh during a night of 12 hours.

Table 49 – Summarized data for the PVT in the experiment period

Date ¹	Average cooling power measured by the heat flux sensors	Average cooling power calculated theoretically	Average cooling power measured by the VFS	Selected average cooling power	Energy produced (12 hours of operation)	COP
	W/m ²	W/m ²	W/m ²	W/m ²	kWh	-
12/08/2014	77,4	71,6	111,8	74,5	3,6	37,2
13/08/2014	68,9	64,6	93,1	66,8	3,4	35,1
14/08/2014	77,0	61,1	100,8	69,1	3,5	36,2
16/08/2014	42,2	30,2	78,8	36,2	1,9	20,0
17/08/2014	32,4	23,3	52,8	27,8	1,3	13,4
18/08/2014	52,0	42,5	76,5	47,3	2,3	23,6
19/08/2014	65,7	55,4	104,6	60,6	3,1	32,2
20/08/2014	62,4	57,4	104,5	59,9	3,0	31,5
21/08/2014	65,2	48,2	106,5	56,7	2,9	30,0
22/08/2014	47,5	28,3	79,3	37,9	1,9	19,7
23/08/2014	68,0	56,7	88,2	62,4	3,1	32,8
24/08/2014	55,5	49,7	89,0	52,6	2,6	26,9
25/08/2014	56,4	48,2	79,1	52,3	2,6	27,2

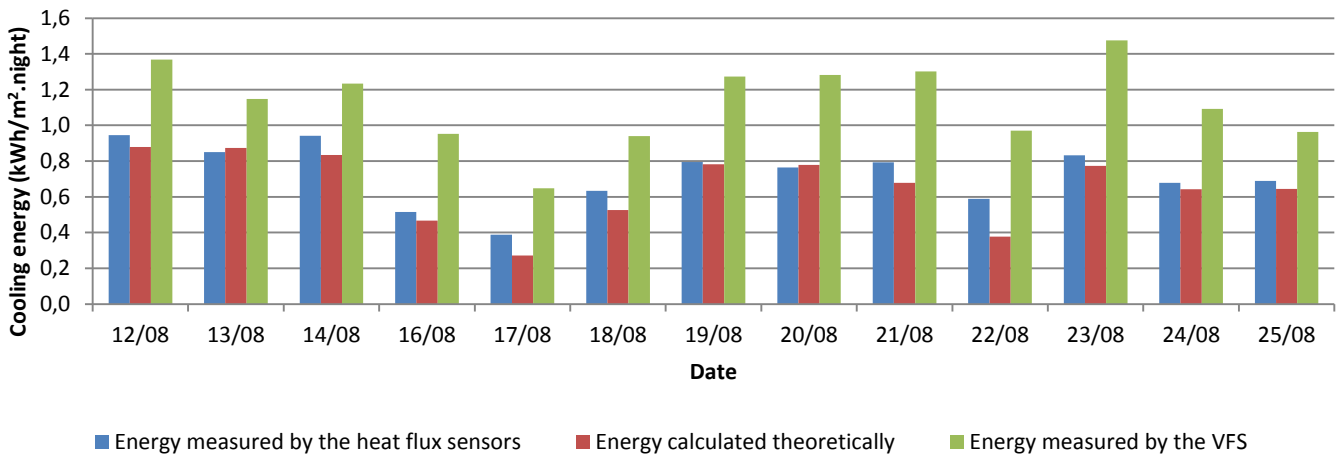


Figure 113 – Cooling energy produced over the night (from 19:00 to 07:00) for the PVT

The obtained cooling power ranges from around 30 W/m² during an overcast night until 60 W/m² during a clear sky night. Those values correspond to the expected values found in the literature for similar setups. The COP shows very high values, ranging from 13 to 33 depending on the outside conditions. This justifies the denomination of “free cooling” sometimes given to radiative cooling applications: it produces between 13 and 33 times the amount of energy consumed, making it an even more efficient cooling process than a traditional heat pump (COP usually not higher than 5).

¹ The date indicated is the date at the starting of the night (i.e. 16/08/2014 stands for the night between August 16th and 17th).

4.3.3. Cooling production of the unglazed collector

The same analysis has been made for the unglazed collector. The power curves obtained with the four different methods are plotted for the night between August 20th – 21st and presented on Figure 114. Contrary to the results concerning the PVT panels, in the case of the unglazed collector the results of the four different methods match remarkably well. As previously mentioned, the calculation of the additional heat losses is simpler in the case of the unglazed collector, this explains why the VFS curve matches here with the others. Therefore the selected cooling power is this time the average between all different methods.

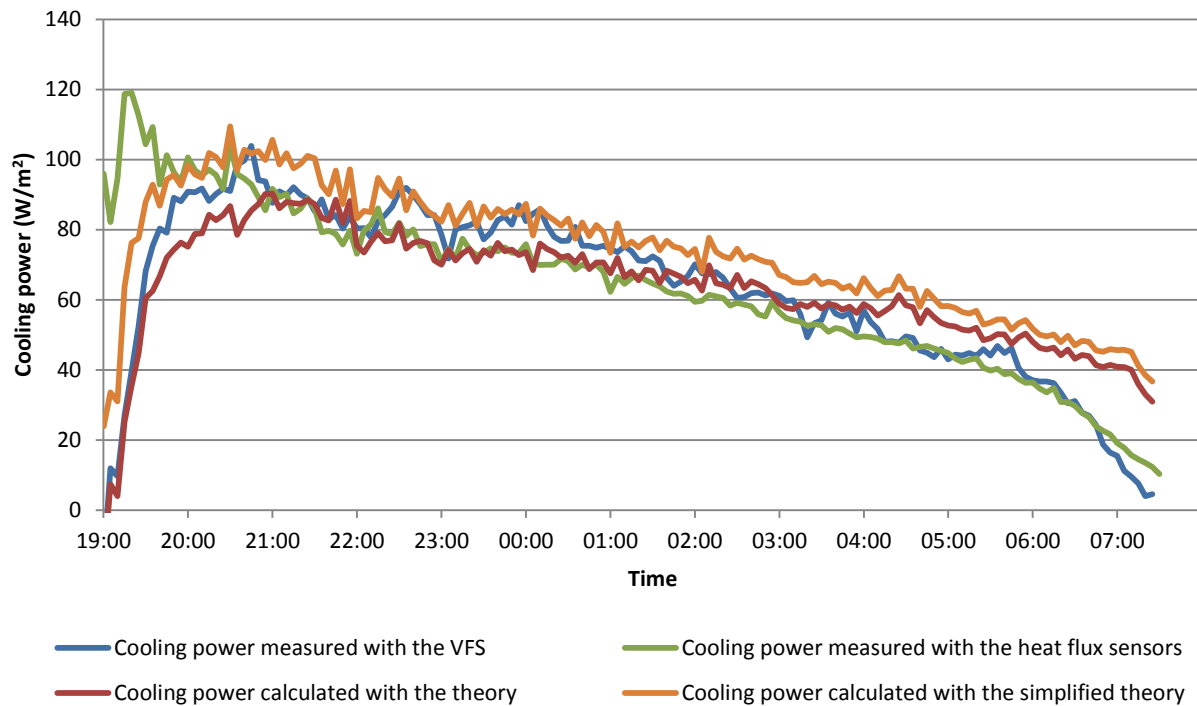


Figure 114 – Cooling power curves for unglazed collector (August 20th – 21st)

Table 50 – Summarized data for the unglazed collector in the experiment period

Date	Average cooling power measured by the heat flux sensors	Average cooling power calculated theoretically	Average cooling power measured by the VFS	Selected average cooling power	Energy produced (12 hours of operation)	COP
	W/m ²	W/m ²	W/m ²	W/m ²	kWh	-
12/08/2014	73,9	73,7	68,1	71,9	2,1	21,6
13/08/2014	67,3	69,7	68,1	68,4	2,1	21,4
14/08/2014	74,8	65,9	75,8	72,2	2,2	22,6
16/08/2014	43,9	32,2	38,9	38,3	1,2	12,4
17/08/2014	22,6	24,6	11,6	19,6	0,5	5,6
18/08/2014	49,6	42,0	38,8	43,4	1,3	13,5
19/08/2014	67,2	61,8	72,3	67,1	2,0	21,0
20/08/2014	66,1	65,5	67,3	66,3	2,0	21,0
21/08/2014	69,6	55,0	63,9	62,8	1,9	19,7
22/08/2014	45,2	33,0	35,9	38,0	1,1	11,8
23/08/2014	75,3	69,1	70,7	71,7	2,2	22,7
24/08/2014	60,0	56,7	56,7	57,8	1,7	18,2
25/08/2014	63,3	58,9	54,0	58,7	1,8	18,3

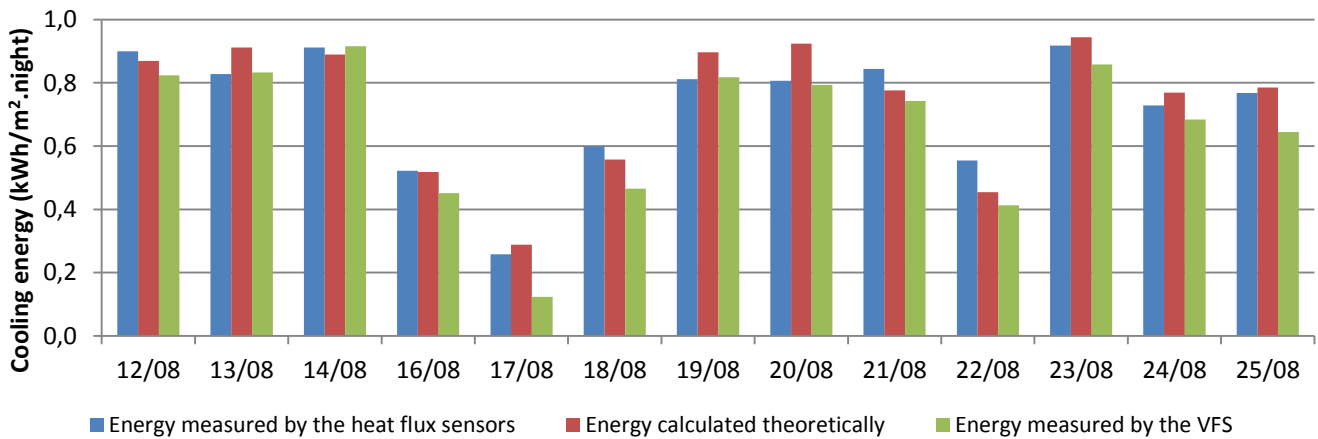


Figure 115 - Cooling energy produced over the nights (from 19:00 to 07:00) for the unglazed collector

4.3.4. Radiative and convective parts

It has been shown in the previous sections that the theoretical model is validated by the experimental values. For the calculation of the theoretical cooling power, the convective and radiative components have been computed separately, and they are plotted on Figure 116 for the test night between August 20th and 21st. The convection here shown is derived based on the more elaborated theory.

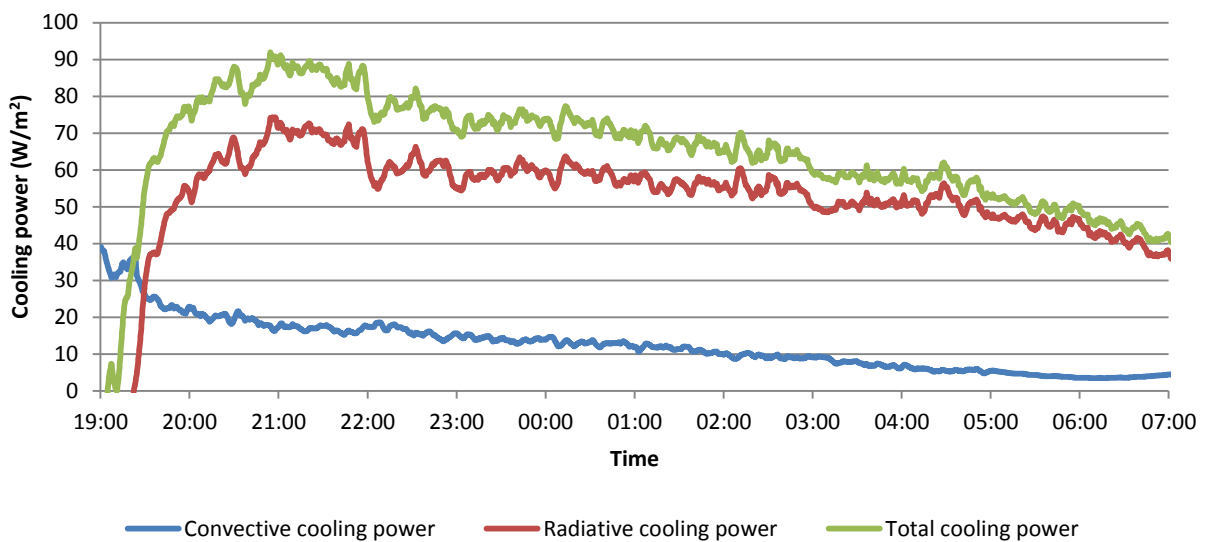


Figure 116 – Convective and radiative components of the cooling power (unglazed collector)

It can be seen that the radiative part is prominent over the convective part, which justifies the denomination of “radiative” cooling. For this night, the radiative part accounts in average for 83 % of the cooling and the convective part for the remaining 17 %.

Table 51 – Radiative and convective components during the night of August 20th-21st

	Unglazed		PVT	
	Theory	Theory simplified	Theory	Theory simplified
Convective part	17 %	28 %	13 %	22 %
Radiative part	83 %	72 %	87 %	78 %

4.3.5. Comparison between the theory and the simplified theory

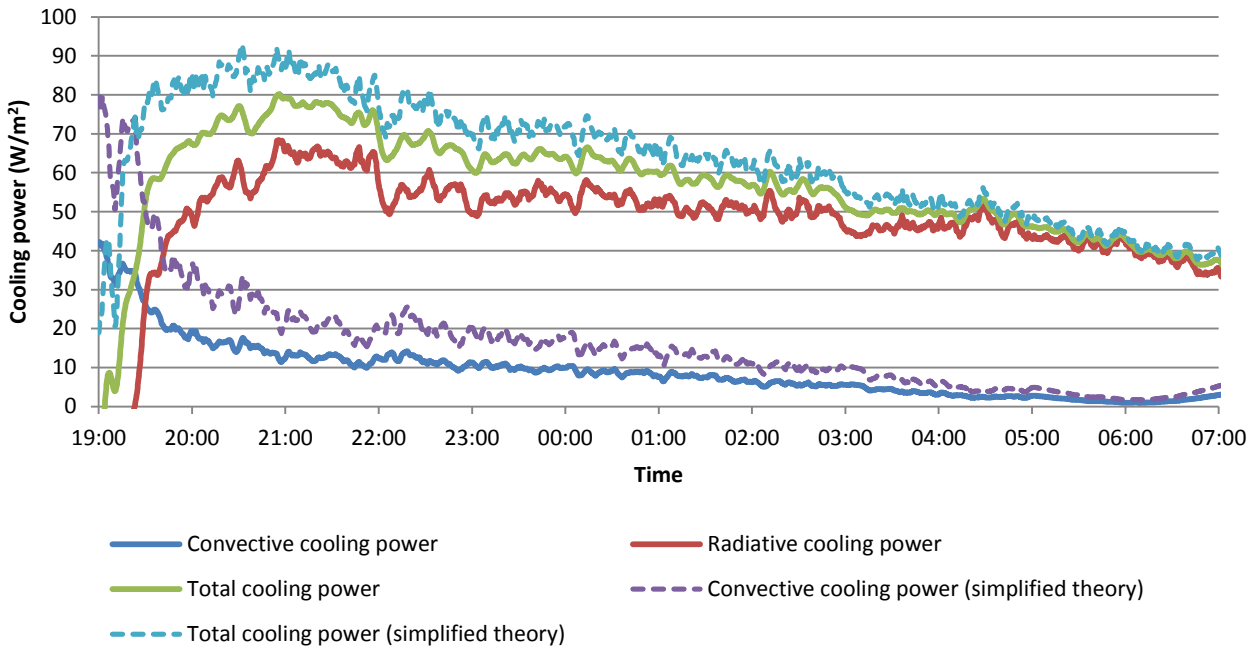


Figure 117 – Convective and radiative components of the cooling power for PVTs, August 20th-21st. The convective component is calculated and plotted with both the simplified and more elaborated theoretical approaches

As previously pointed out in section VII.2.6. of the theory, the convective cooling power obtained with the simplified method (equations (25) and (26)) is higher. Nevertheless as it is possible to see in Figure 112 and Figure 114 the difference does not seem to be so relevant when the total cooling power is analysed. In fact the cooling provided by convection is just a fifth of the total; deviations in the method used to obtain convective power are less evident when it is merged with the radiative component. If just the convective component is considered, it is possible to see that the simplified method produced results up to 50% higher than the complex one (Figure 117). Such a difference is noteworthy but both methods can be used depending by the needs of the designer and the degree of simplification which he/she is willing to achieve.

4.3.6. Heating production

The heating production has not been the focus of this study; however the heating output needs to be considered, since the present research tries to make more profitable an installation of solar collectors by using them both at day and night. The representative day chosen for the study of the water heating is August 28th, which is the only day of the experiment period where the sky was continuously clear and sunny. In fact, the weather conditions were unfortunately not optimal during the month of August for the production of hot water, as can be seen on Figure 118, with overcast skies in general, and temperatures lower than 20°C.

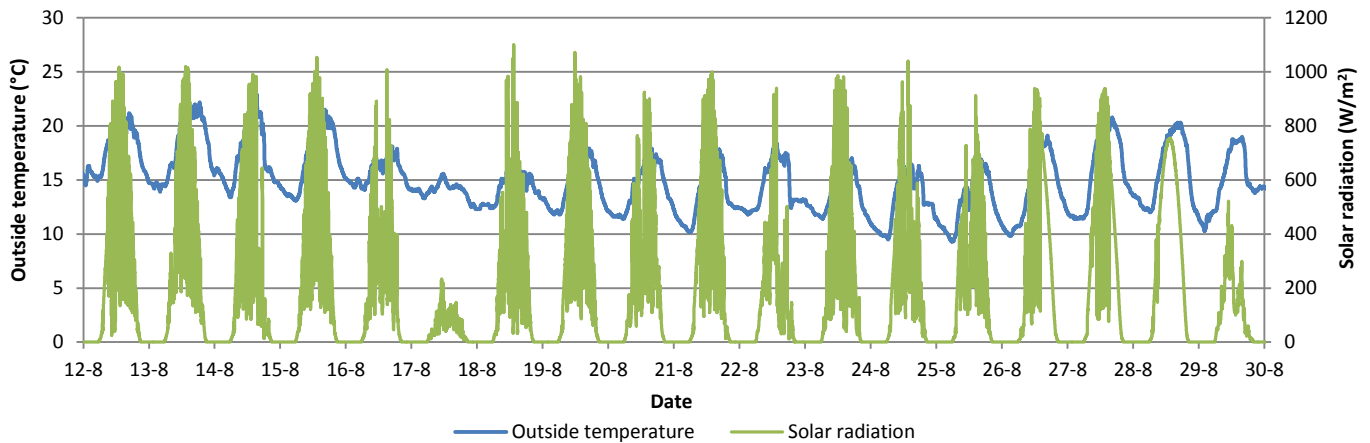


Figure 118 – Weather data in August 2014

The results measured by the heat flux sensors are significantly lower than the ones measured with the VFS, and they reach negative values. The HF curves are plotted as example on Figure 119, but it was decided not to take them into consideration, and to only rely on the VFS measurement, for the main following reasons:

- The HF sensors are meant for indoor use, and they are probably disturbed by solar radiation during a daytime outdoor utilization. The MicroFoil® sensors used are produced by RdF for R&D, measurement and control applications such as structural heat transfer monitoring, proving of HVAC design or aerodynamic wind tunnel studies. No outdoor use of the sensors has been related with direct exposition to the solar radiation, the sensors are probably not suited for such utilization, that is a possible explanation for the odd results. During the night, solar radiation is not an issue therefore the results are still reliable.
- The VFS sensors have a high uncertainty concerning the temperature measurements, and that is crucial for nighttime radiative cooling applications where the ΔT belongs to the same range as the inaccuracy (around 2°C). For water heating applications, the ΔT reaches 10°C, therefore the inaccuracy becomes less important in proportion.

The heating energy has been calculated by integrating the power curves obtained by VFS measurement, from 8:00 to 18:00 (10 hours). The PVT have produced 9,25 kWh that day, and the unglazed collector 5,74 kWh, which represents 2,4 kWh/m² for both types. The average heating power is close in both cases, being respectively 247 W/m² for the PVT and 241 W/m² for the unglazed collector.

The water was supplied at 16°C at the beginning of the day, warming up the tank progressively along the day. The return flow of the unglazed collector reached a temperature of 42°C, while the return flow of the PVT panels reached 41,5°C. The two collectors warmed the whole tank (approximately 750 litres) of around 20°C, reaching a temperature at the end of the day, in the bottom of the tank of 35°C (value recorded from the VFS located at the supply pipe; the water of the supply is inlet from the bottom of the tank).

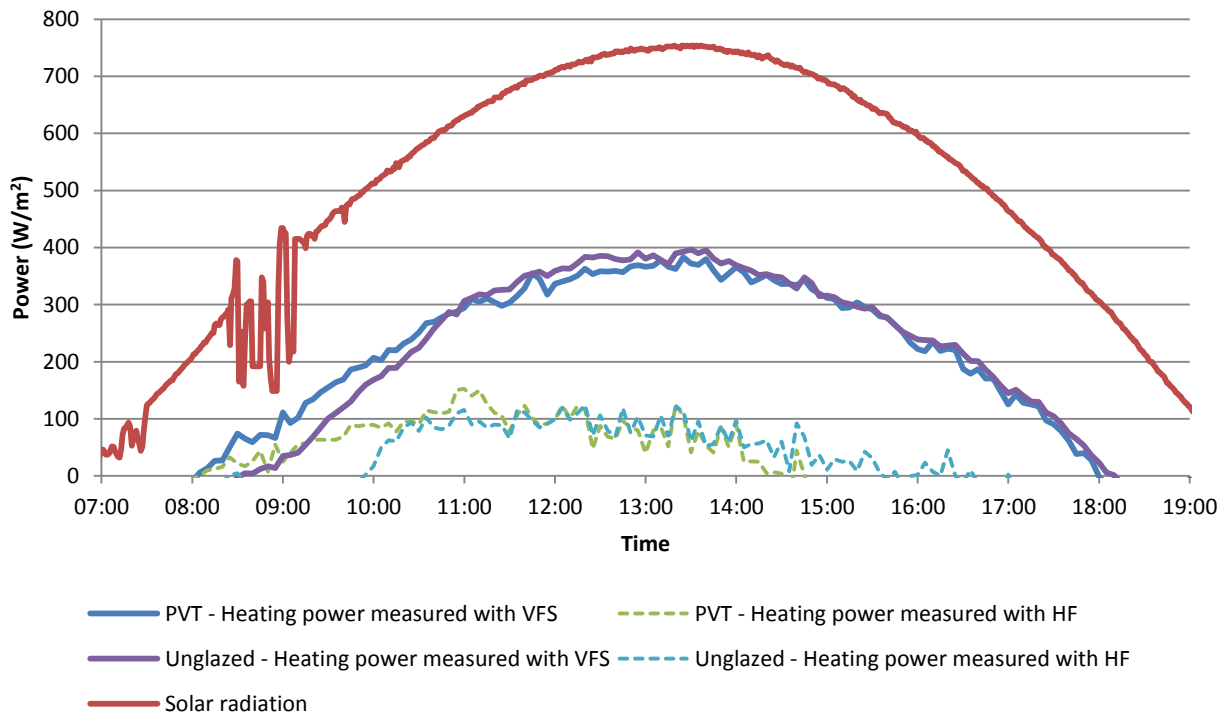


Figure 119 – Heating powers and solar radiation – 28th August

4.3.7. Comparison between PVT and unglazed collector

The cooling power and the cooling energy produced by both types of panels are represented on Figure 120 and Figure 121. It can be seen that the difference of production between PVT and unglazed collector is negligible. It was expected that the PVT panels would produce less cooling than the unglazed collector, because of the lower emissivity and the glazing that hinders the heat transfer, shielding the infrared radiation (so called “green house” effect). It can be verified most of the nights, but the difference between the two is always less than 0,1 kWh/m².night.

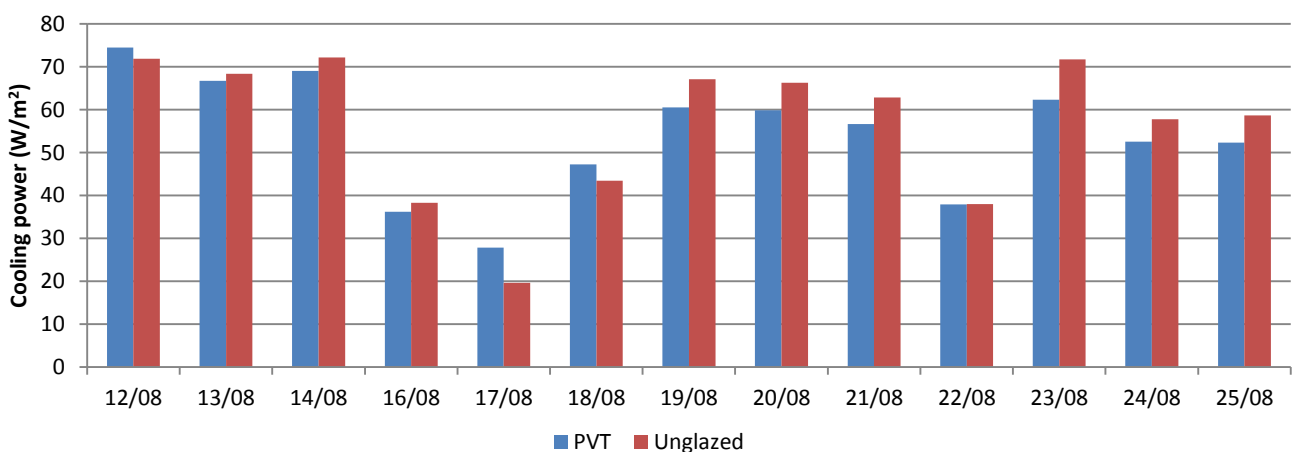


Figure 120 – Comparison in the average cooling power of the PVT and unglazed collector per night

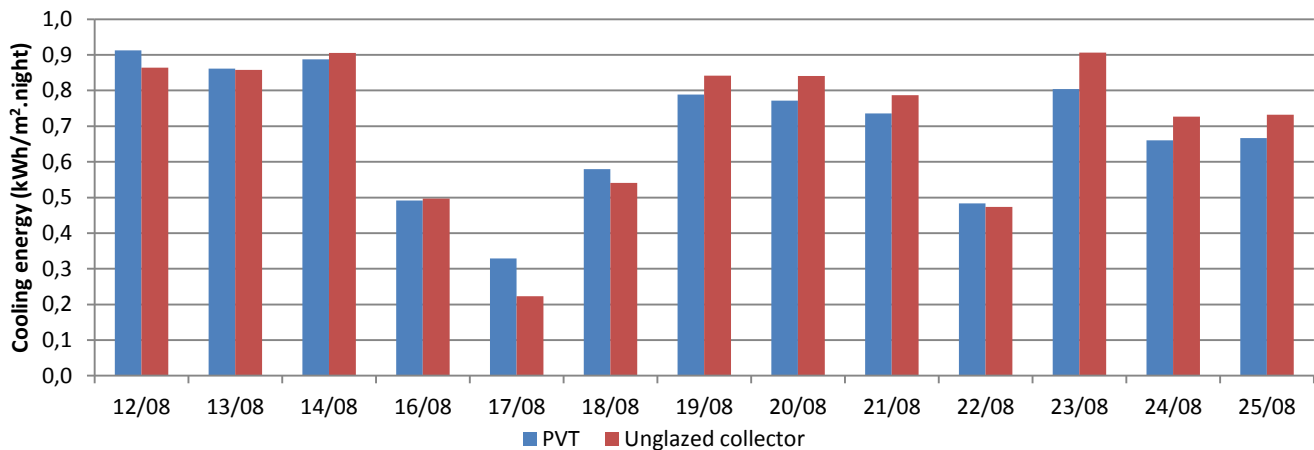


Figure 121 – Comparison of the cooling energy produced by the PVT and the unglazed collector per night

4.4. Discussion and conclusion on the experiment

Any experimental work is subject to discussions concerning the setup of instruments and choice of sensors. The present experiment is no exception, and there are several parameters that could influence the results. For example, the surrounding of the panels can affect their cooling power. Skylights are installed on the roof of building 412, where the experiment has been performed, and they slightly shaded the unglazed collector (see Figure 97 and Figure 99). This shading has not been taken into account in the theoretical model, the skylights being relatively low. The results taken from the pyrgeometer are also measured at a tilt angle of 45°, but in another building of DTU, so there might be some differences in the surrounding environment.

The accuracies of the sensors used for the experiment have been an issue. In particular, the VFS present a high inaccuracy, therefore some precautions have been made in order to make the results reliable enough for further analysis. Other sensors presented a better accuracy, but the recorded data could have been influenced by the outdoor weather conditions. For example, the heat flux sensors have shown high sensitivity to rain: after a rain precipitation, the panels, and therefore the HF sensors were wet. Evaporative cooling then occurred on the side of the HF sensors, explaining the deviation with the cooling obtained with the other methods. This can be seen in the nights of the 17th, 18th and 22nd in Annex 13: Power graphs from the experiment (August 12th-25th). The theory does not take into account possible evaporative cooling, which is why the theoretical cooling power is lower than the one measured by the heat flux. This difference disappears once the panel has dried out. The HF sensors also recorded higher frequency in the variation of the cooling power: they are subject to any change of the conditions in the small portion of panel in which they are located, while the other methods consider the panel as a whole, which gives steadier results. Even after averaging the data every 5 minutes, the HF power curve shows higher peaks than the other methods (see for example the night of August 16th in the Annex 13: Power graphs from the experiment (August 12th-25th)).

The handcrafted plane radiant temperature sensor also presents some inaccuracies, precisely because of its handcrafted characteristic. Even though the results obtained by this sensor have been corroborated with the ones obtained through the pyrgeometer, there is no complete evidence that the plane radiant temperature has been measured within an acceptable range of precision, and the value of the deviation is not known either. As the results match with the other methods used, it can be assumed that the accuracy is sufficient. It should be noted that the surface temperature recorded by the sensor often reached several

degrees below ambient temperature, therefore condensation was then occurring and it could have distorted the results. A pyrgeometer entirely dedicated to the experiment would have been the optimal tool to measure the plane radiant temperature faced by the panels, but this type of sensor is expensive and could not be afforded within the frame of the present master thesis.

Regarding the testing of PVT panels, it can be criticized that the power was not plugged and that the panels could not produce electricity during the day. Since the panels are mainly tested for cooling purpose, it did not represent a major issue, but it could affect the heating production. Other testing experiments of PVT panels for thermal use at DTU have reported that according to the manufacturers, the thermal output is not affected of more than 5 % by the presence or not of the electricity connection, because the efficiency of PVT is relatively low compared to standard thermal collectors.

5. Modeling: evaluation of nighttime radiative cooling potential (TRNSYS)

5.1. Description of TRNSYS

In order to evaluate the potential of nighttime radiative cooling with unglazed solar collectors, the software TRNSYS was used. TRNSYS is a “TRAnSient SYStems Simulation Program”, with a modular structure, which has become reference software for researchers and engineers around the world for many applications including solar systems, low energy buildings and HVAC systems, renewable energy systems. It is adapted to a detailed analysis of any system whose behaviour is dependent on the passage of time (Klein, S.A. et al, 2010). Nighttime radiative cooling systems and solar systems in general belongs to this category of applications, since the outside weather conditions evolve rapidly and do not allow to reach steady-state.

In the Simulation Studio of TRNSYS, the user can create instances of predefined “Types” such as a solar collector or a tank, which are available in specialized libraries. The different objects are then linked together in order to model the real systems, and outside conditions are represented by a standard IWEC weather file (see part III.2. about the Load calculations (IDA-ICE)).

5.2. Model of unglazed solar collectors

In the Solar TESS Library of TRNSYS, there are several different types to model unglazed solar collectors, which require different inputs.

- Type 553: unglazed flat plate collector (efficiency coefficient method). This model should be used when the collector efficiencies are known.
- Type 559: Theoretical unglazed flat plate collector. This model calculates itself the efficiency of the collector based on the geometry of the panel and its absorbance/emissivity.
- Type 1289 and 1290: the efficiency is calculated with the test results from EN 12975.

Unglazed solar collectors are a very low-tech device, which are mostly used by private individuals to warm up the water of a swimming pool. Therefore the producers are not required to provide testing data of their panels, describing the efficiency under standard conditions. The products bought from a company did not have any technical datasheet with more information than necessary for the installation and the good functioning of the solar collectors. The data needed for modelling the panels needs to be found from other sources, either from similar products with more detailed documentation, either looking for each parameter individually, knowing the geometry, the materials and so forth.

Since few detailed data were available, the simplest model of the TRNSYS library was chosen, because it requires fewer inputs. In this way, the model is kept as simple as possible to avoid complications which could distort the results. The results obtained are more generic, but still within a satisfactory range of accuracy, since the physical model is simplified but based on correct inputs. In fact, using a more detailed model, aiming to a high accuracy, could produce the opposite result, when based on wrong or unpredictable values or functions. That is why Type553 is finally used to model the unglazed solar collectors.

With this model, the main parameters influencing the results are the properties of the material. The unglazed solar collectors used for this experiment and for the EMBRACE house are both made of black polypropylene. The absorbance of polypropylene was found in the literature to be between 0,94 and 0,95 (Kurböck M. et al., 2012), and it does not depend on the pigment type included in the material, so 0,95 was chosen. The emissivity of polypropylene was found to be 0,96 (Antar Z. et al., 2012). The emissivity calculated during the experiment with the thermographic camera (0,91) has not been used because TRNSYS has been approached before.

The main input in this model is the collector efficiency factor F' , whose calculation is detailed in (Duffie and Beckman, 2013) and reported below:

$$F' = \frac{1/U_L}{W \cdot \left[\frac{1}{U_L \cdot [D + (W - D) \cdot F]} + \frac{1}{\pi \cdot D_i \cdot h_{fi}} \right]}$$

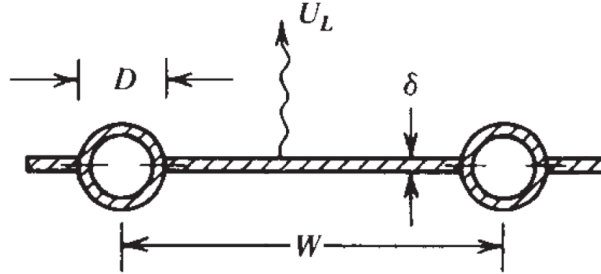


Figure 122 – Section of the unglazed collector

With:

W is the distance between two tubes (m).

D and D_i are respectively the external and internal diameters of one tube (m).

h_{fi} is the heat transfer coefficient inside the tube (between the fluid and the pipe surface)(W/m²K). h_{fi} can range from 100 to 1000 W/m²K from laminar to turbulent flow (Duffie and Beckmann, 2013).

$F = \frac{\tanh(m(W-D)/2)}{m(W-D)/2}$ is the fin efficiency, calculated with $m = \sqrt{\frac{U_L}{k\delta}}$, k and δ being respectively the thermal conductivity [W/mK] and the thickness [m] of the plate between the tubes.

$U_L = U_{bottom} + U_{top} + U_{edges}$ is the sum of the heat transfer coefficient of the bottom, top and edges of the collector.

$U_{bottom} = \frac{\lambda_{ins}}{L_{ins}}$ with λ_{ins} and L_{ins} the thermal conductivity and the thickness of the insulation placed in the bottom of the collector. The convection and radiation below the insulation can be neglected, given the high resistance of the insulation (Duffie and Beckmann, 2013).

$U_{edges} = \frac{(UA)_{edge}}{A_r}$ with $(UA)_{edge}$ the edge loss coefficient, referenced to the collector area A_r . For a well-designed system, the edge losses should be small and do not need accurate calculations (Duffie and Beckmann, 2013), therefore $(UA)_{edge}$ represents a simple one dimensional heat transfer through the side layer: $(UA)_{edge} = \frac{k_{edge}}{L_{edge}} \cdot A_{edge}$, with k_{edge} , L_{edge} and A_{edge} being respectively the thermal conductivity, the thickness and the area of the edges.

$U_{top} = h_r + h_c$ is the sum of the radiation and convection heat transfer coefficient on the top surface of the collectors.

$h_r = \sigma \cdot \varepsilon_r \cdot (T_r^2 + T_{sky}^2) \cdot (T_r + T_{sky})$ with T_r the mean collector plate temperature, T_{sky} the sky temperature and ε_r the collector emissivity (Anderson T.N., et al.,2013).

h_r is normalized in function of the ΔT between sky and collector temperatures. So this is the ΔT to be multiplied by, if calculating the heat flow \dot{Q} [W] with the h_r defined. In fact in this way

$$\dot{Q}_{rad} = h_r \cdot A_r \cdot \Delta T = A_r \cdot \sigma \cdot \varepsilon_r \cdot (T_r^2 + T_{sky}^2) \cdot (T_r + T_{sky}) \cdot (T_r - T_{sky}) = A_r \cdot \varepsilon_r \cdot \sigma \cdot (T_r^4 - T_{sky}^4)$$

The same as in equation (14) of chapter VII.2.4. Radiative cooling.

$$h_c = \sqrt[3]{h_w^3 + h_{nat}^3} \quad \text{combines the effects of natural and forced convection}$$

with $h_w = 2,8 + 3 \cdot v$ depending on the wind velocity v , and $h_{nat} = 1,78(T_{pm} - T_a)^{1/3}$ depending on the ambient temperature T_a and the mean collector plate temperature T_{pm} .

As can be seen in the above equations, the heat loss coefficients depend on the outside conditions (wind v , ambient temperature T_a , sky temperature T_s) and the current conditions (mean collector plate temperature T_{pm}) so they are changing at each moment. The equations have been implemented in the TRNSYS model in order to calculate iteratively the heat loss coefficients and the collector efficiency factor at each time step, taking into account the current conditions. The schematic diagram below helps understanding the TRNSYS model and the interactions between the different types.

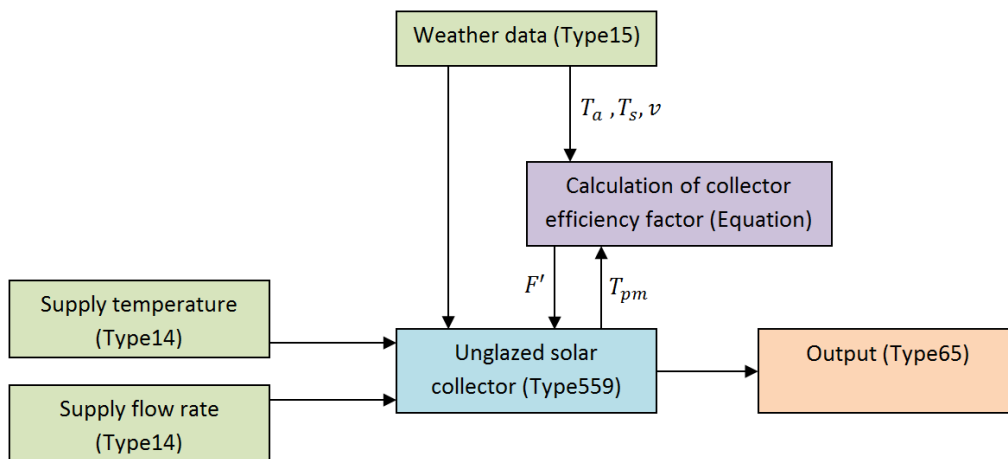


Figure 123 – Schematic diagram of the TRNSYS model

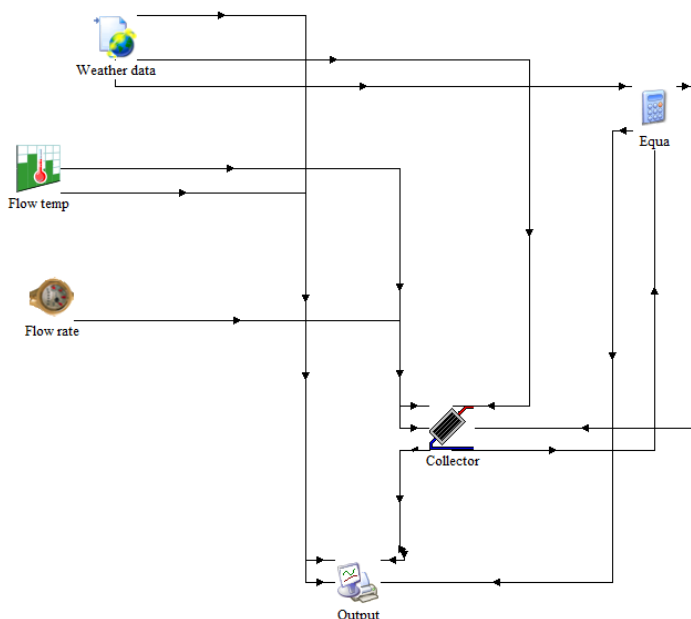


Figure 124 – TRNSYS model

It has been chosen to model with TRNSYS the unglazed solar collector used for the experiment (see next section), so that the results can be compared. The main physical parameters of the collector can be found in Table 52.

Table 52 – Unglazed collector main physical parameters

Parameter	Value	Unit
Thermal conductivity of underneath insulation	0,045	W/mK
Thickness of underneath insulation	0,07	m
Thermal conductivity of the collector material (polypropylene)	0,24	W/mK
Collector Length x Width	2 x 1,2	m
Collector area	2,4	m ²
Collector total thickness	0,006	m
Thickness of the collector wall	0,001	m
Tube pitch	0,006	m
Tube diameter	0,005	m

5.3. Simulations

Different simulations were carried out with the model described above, with different flow rates or supply temperatures as input. All results described below derive from simulations made with the weather data of Paris, France, where the cooling demand is the highest compared to Copenhagen, during the months of July and August.

To exploit and compare the data, the temperature profile of every day of July and August has been averaged over the simulation period. This means that for every time step of the day (every 7,5 minutes), the average outlet temperature of the two summer months has been calculated, resulting in an averaged profile for a summer night. On Figure 125 can be seen the results for the simulation made with a supply temperature of 22°C and a flow rate of 30 kg/h¹. The calculated average curve is plotted, as well as the two worst nights (when the cooling is not effective) and the two best nights (when the cooling is the most effective).

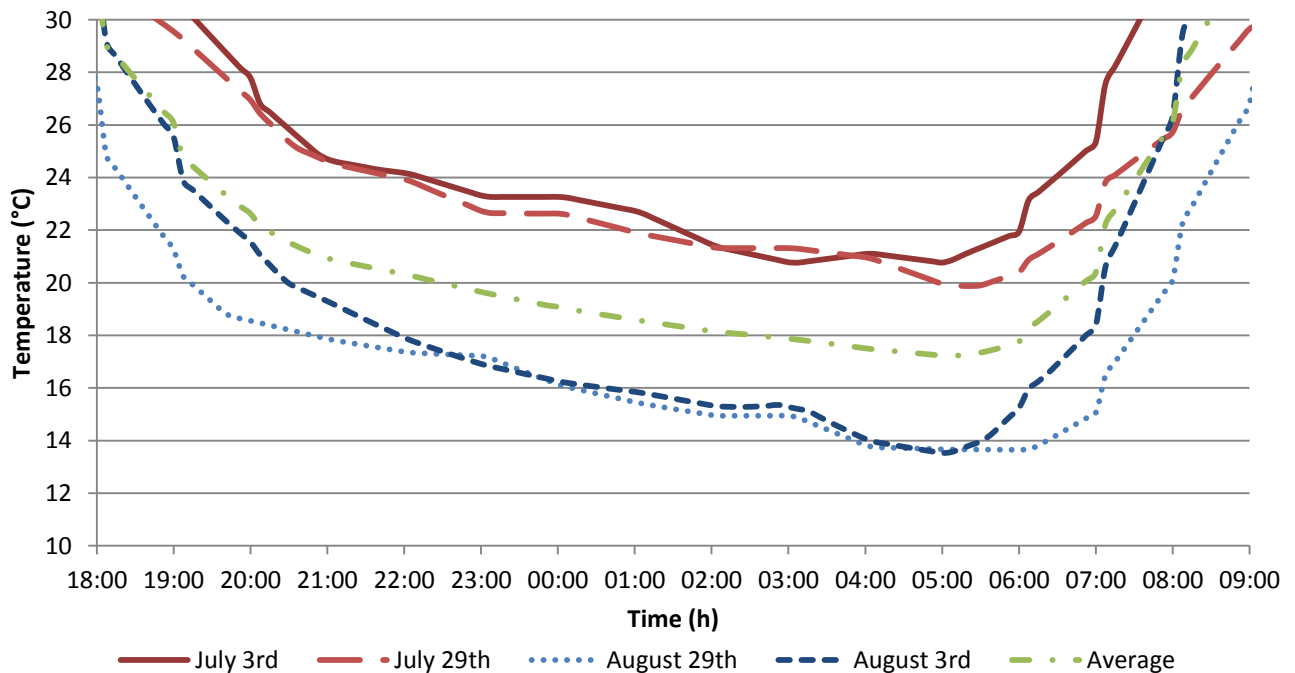


Figure 125 – Outlet temperature for the two best and worst nights, compared to the calculated average summer night

¹ For the first simulations, an arbitrary temperature supply and flow rate of 22°C and 30 kg/h have been chosen. These values belong to the range of operation of the solar collectors, but are just used here to compare the average curves, without considering the absolute values of the output. Detailed studies can be found in the next sections.

On this graph, it can be seen that the calculated mean represents a good average of the situation over the cooling season. Therefore, the average temperature profile is used in all further analysis of the data, and is always referred to as “average summer night”.

5.4. Study on the flow rate

Different flow rates have been investigated, in order to study the impact of this input parameter on the cooling output. The flow rate of the fluid circulated in the collector is given in *liter/(min.m²)*, in order to compare different experiments. In the table below are gathered several flow rates found in the literature for experiments of nighttime radiative cooling.

Table 53 – Flow rates for radiative cooling experiments

Reference	Type of collector	Flow rate
Anderson et al. (2013)	Unglazed collector	0,9 liter/(min.m ²)
Eicker and Dalibard (2011)	PVT	0,3 liter/(min.m ²)
Erell and Etzion (1999)	Flat plate collector	0,72 liter/(min.m ²)
Hosseinzadeh and Taherian (2012)	Unglazed flat-plate collector	0,15 to 0,75 liter/(min.m ²)
Meir et al. (2003)	Unglazed collector	1,0 liter/(min.m ²)

Based on this review, it was decided to take 0,1 liter/(min.m²) as the lowest flow rate for the study. The highest flow rate was decided based on the technical datasheet of the collector, which provides a maximum flow rate that the collector can bear without damage, and which was in this case 240 kg/h (1,7 l/min.m²). The common inlet temperature was chosen to be 22°C for this series of simulations.

Table 54 – Flow rates used for the simulations

Flow rates in l/h	Flow rates in l/min	Flow rates in l/(min.m ²)
14,4	0,24	0,1
43,2	0,72	0,3
86,4	1,44	0,6
240	4,08	1,7

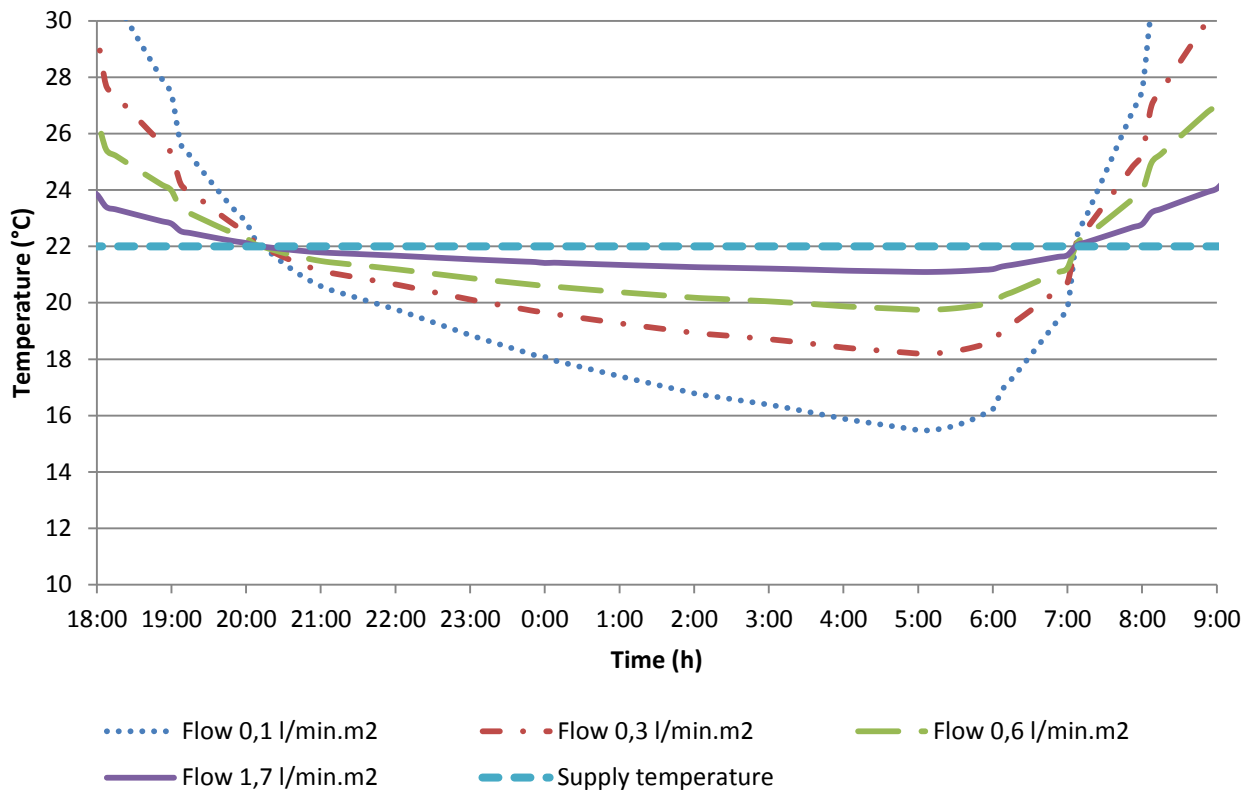


Figure 126 – Outlet temperature during an average summer night for a range of different flows

As can be seen on Figure 126, the cooling hours (i.e. when $T_{outlet} < T_{inlet}$) are almost unaltered by the change of flow rate. The cooling starts at 20:15 and ends at 7:00. It would be inefficient to circulate the water in the panels outside those hours, because it would be heated up instead of cooled down. The choice of the nightly operation schedule of the circulation pump has been based on the following study paragraph, 5.5. Study on the inlet temperature. It was chosen to keep a fixed scheduled control because of its simplicity. A dynamic control algorithm could have been implemented to start the pump when it is beneficial for the system (i.e. when cooling is actually available), but as can be seen in the following studies, the cooling period is relatively stable every night, so a scheduled control seems appropriate and enables to simplify the control system.

It can be noted that for the same inlet temperature, the outlet temperature can vary significantly with the flow rate (difference of up to 6°C). By decreasing the flow rate, the outlet temperature can be lowered down more, but then the amount of cooled water will be decreased too. In order to choose a flow rate, the cooling power must be considered, since it combines the effects of the flow rate and the outlet temperature. The curves of the cooling power are plotted on Figure 127, for the same simulation.

Another relevant parameter for the determination of the appropriate flow rate is the capacity of the storage tank. In the EMBRACE house, the chosen product from Sonnenkraft contains a volume of 750 liters. This amount of water is expected at least be circulated once during the night. Considering a cooling period of 9 hours (from 21:30 to 6:30), this means the flow rate should be at least $750/9 = 83,3 \text{ l/h} = 1,4 \text{ l/min}$, or $0,6 \text{ l/min.m}^2$.

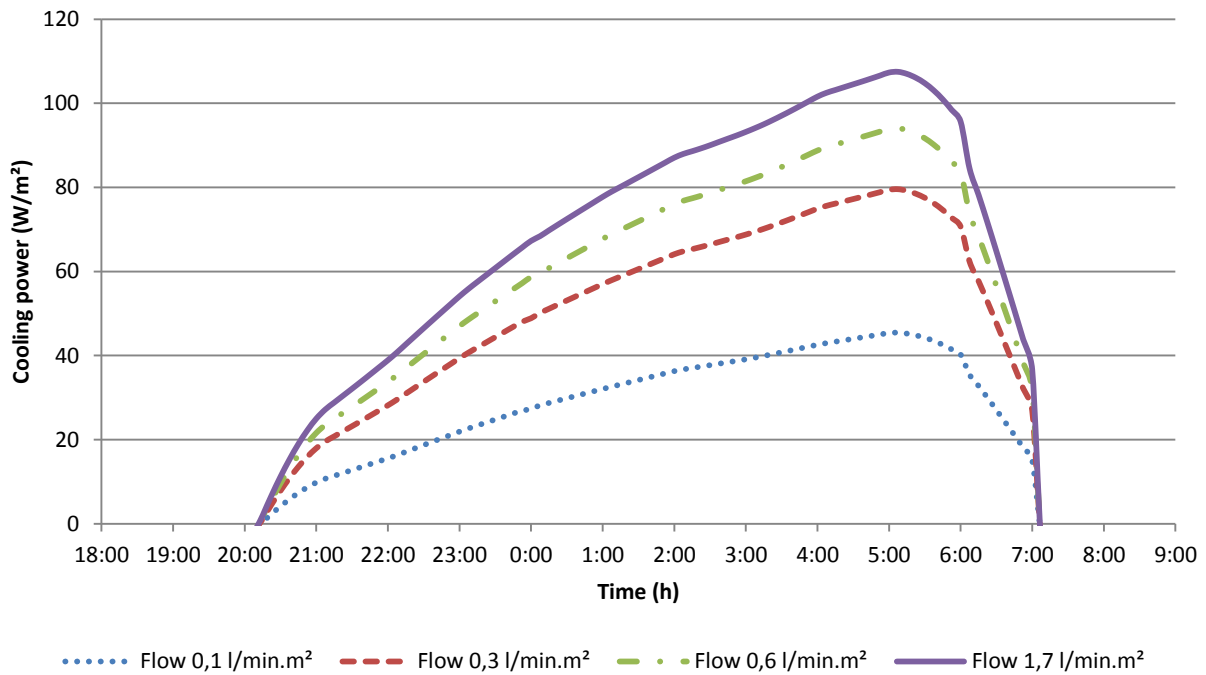


Figure 127 - Cooling power during an average night for a range of different flows

The comparison can be made between the cases presenting the higher cooling powers, which are with flow rates of 0,6 l/min.m² and 1,7 l/min.m² respectively. It can be seen that by increasing the flow rate of almost three times, the peak power is only improved by 12 %, and the temperature drop between supply and return, is halved. It would also increase the pump consumption, hence decreasing the COP. The benefits of such a high flow rate are limited; therefore a flow rate of around 0,6 l/min.m² is preferable.

Table 55 – Average cooling power obtained with inlet water supplied always at 22°C over the night

Inlet temperature fixed at 22°C				
Flow rate, l/min·m ²	0,1	0,3	0,6	1,7
Cooling power per average night, W/m ²	30	53	63	72

5.5. Study on the inlet temperature

When nighttime radiative cooling is activated at the beginning of the night, the circulated water comes from the storage tank warmed up during the previous day. The temperature of the tank at the end of the day is very difficult to evaluate, since it does not depend only on the output of the radiant floor (and therefore on the loads during the day), but it is also influenced by the eventual activation of the heat pump.

For the design case of the cooling season, the supply temperature to the radiant floor has been calculated to be 15,6°C (see Table 16), with a design ΔT of 2°C. That means the water will return from the radiant floor at around 17,5°C. This calculation is valid for the design room, and for the design case of the cooling season.

The return temperature of the radiant floor will generally be higher than this value because the cooling demand during the year is most of the time lower than the design value. The Uponor radiant floor manifold includes a mixing loop between supply and return, in order to control the temperature of the supply based on the demand. It can be assumed that the heat pump will not be activated during the few hours preceding

the activation of the radiative cooling. Therefore, the tank has potentially some time to be warmed up by the house loads before to be cooled down through the collectors. In this way the ΔT between water in the collectors and sky temperature also increases, rising the potential cooling power obtained with nighttime radiative cooling (Nielsen H. M., 2014). As a general conclusion, the temperature in the tank at the beginning of the night is assumed to be always higher than 18°C.

Through the night, the water will be cooled down further by the radiative cooling setup. The average temperature in the tank will decrease gradually; therefore the inlet temperature to the unglazed collectors will also decrease. There is no full mixing in the storage tank; because of the stratification, the water supplied to the unglazed collectors will not immediately decrease, the drop will be limited and delayed.

Based on these considerations, the range 18-24°C for the supply temperature was chosen for this study, with steps of 2°C. Four simulations have therefore been carried out, with a common flow rate of 30 kg/h. This corresponds to the flow rate arbitrarily chosen from the beginning, since the present study focuses on the relative effects of a change in the temperature of the inlet, not directly on the absolute values of the output. The final choice of flow rate is presented in the next paragraph (5.6). The results are presented in the graph below.

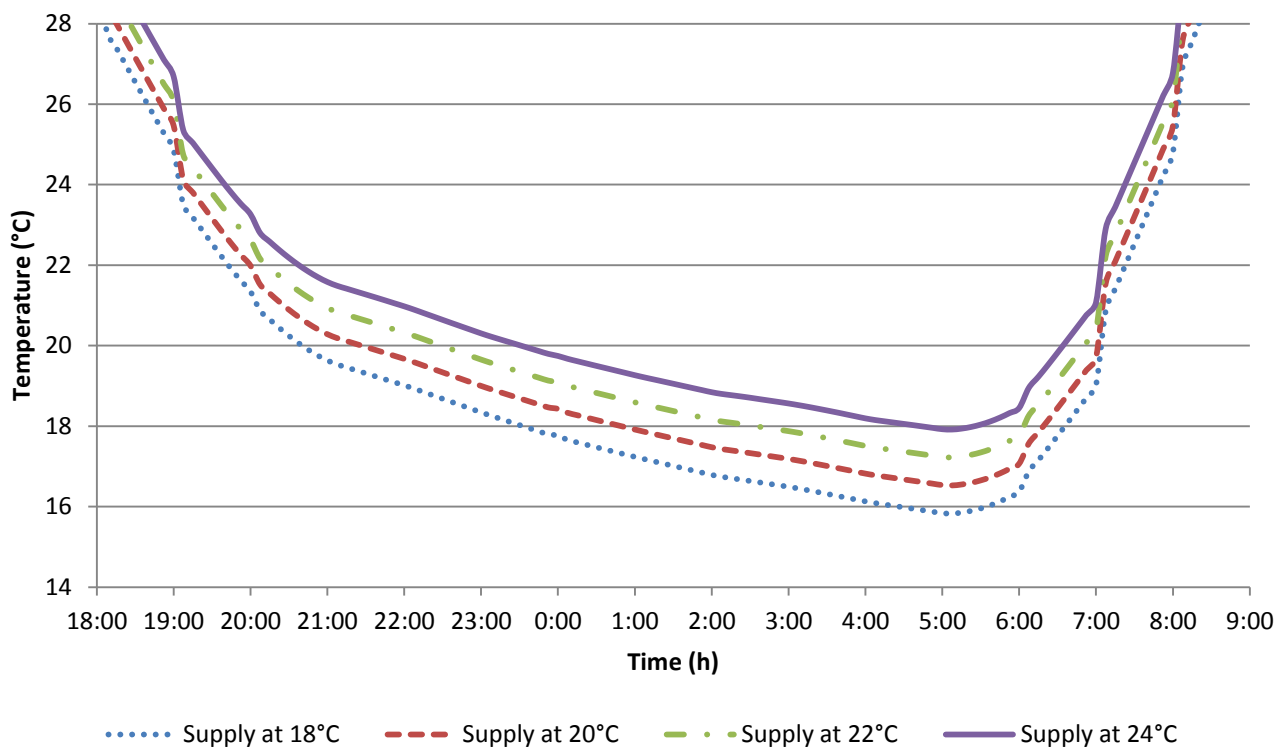


Figure 128 – Outlet temperature during an average summer night for different supply temperatures

In this graph, it can be seen that the four curves have the same profile, only translated according to the supply temperature. The gap between the return temperatures of two curves is fairly constant and calculated to be 0,7°C. This means that the outlet temperature curve of any supply temperature can be obtained for this flow rate deriving an equation. For example, if one wants to calculate the outlet temperature curve $T_{out,23}$ with a supply of 23°C, the following formula shall be used:

$$T_{out,23} = T_{out,18} + \frac{0,7}{2} (23 - 18) \quad (°C)$$

5.6. Final choice of flow rate, size of tank and cooling hours

As seen in the previous studies, the flow rate, the daily cooling period and the size of the tank are closely related and must be considered together for nighttime radiative cooling applications. The flow rate has been chosen in relation with the previous study: the minimum is 86 kg/h (0,6 l/min.m²), so a value of 100 kg/h (0,7 l/min.m²) was finally chosen. Increasing more the flow rate per m² would decrease the temperature drop significantly.

0,7 l/min.m² is obtained considering 2,4 m² of collectors. If a larger area of collectors is installed, the same flow/m² can still be used. In this case the water in the tank is recirculated more than once over the night period, resulting in a bigger temperature drop, as shown in Figure 130.

In order to help the decision-making process, the curves of the cooling power have been plotted. The simulations are done with different supply temperatures and a common mass flow rate. The cooling power is obtained with the following formula, and then divided by the collector area.

$$Q = \dot{m} \cdot c_p \cdot (T_{inlet} - T_{outlet}) \quad (W)$$

With $\dot{m} = 100 \text{ kg/h} = 0,028 \text{ kg/s}$ the mass flow rate (which is the same value as the volume flow rate in l/s, since pure water is assumed).

$c_p = 4180 \text{ J/kgK}$ is the specific heat capacity of water.

T_{inlet} and T_{outlet} are the temperatures of the fluid respectively entering and leaving the collector (K).

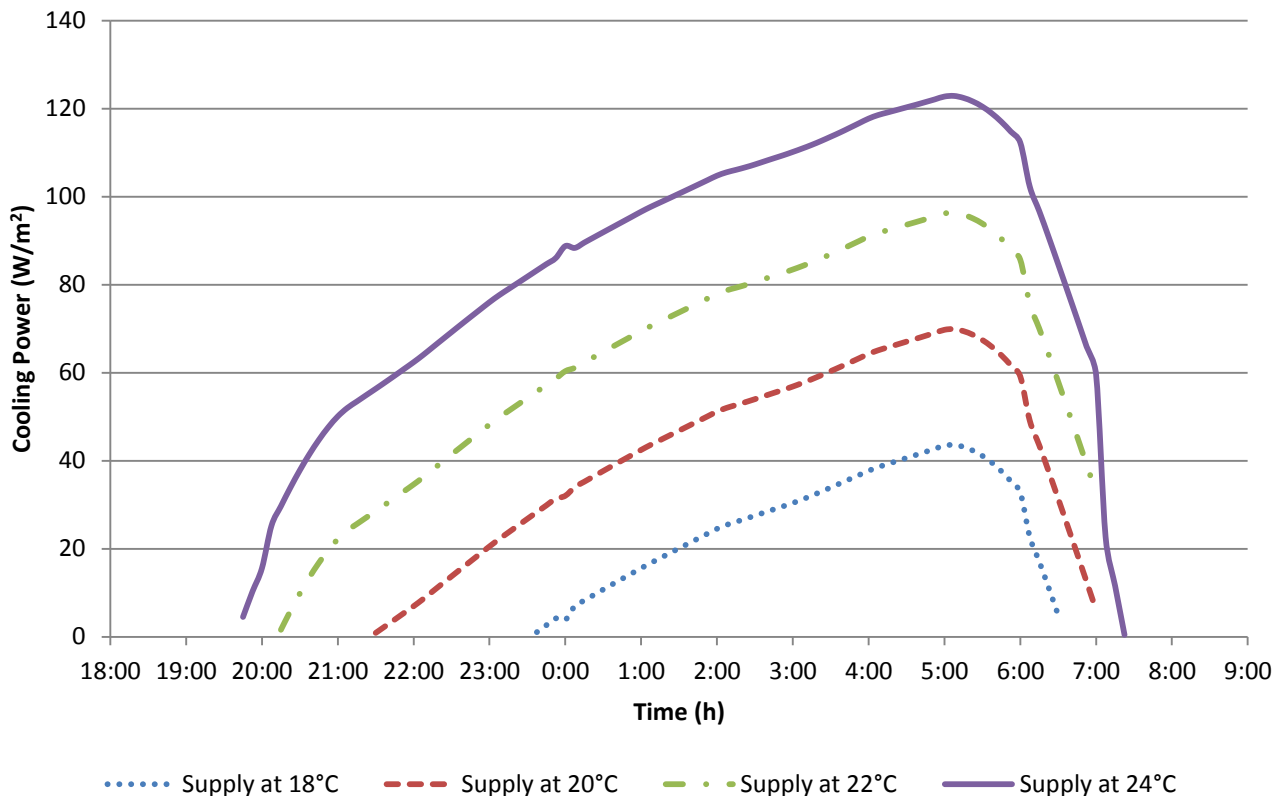


Figure 129 – Cooling power during an average summer night for a range of different supply temperatures

It can be assumed that the temperature of the tank must be the highest possible at the beginning of the night. If the heat pump operation is controllable, then it is possible to stop it few hours before, in order to

let the tank warm up a bit. Considering this, the circulation in the collectors should be started as soon as cooling is available. It is realistic to assume a value of 22°C in the tank at the end of the day, which would make profitable to start the cooling already at 20:15. Nevertheless, this is only an average over the whole summer, so for reasons of safety, because the sun sets at a different hour throughout the summer, it is chosen to start the circulation at 21:30, which also corresponds to the starting time of the cooling if the temperature in the tank is only 20°C.

With these settled parameters, the real cooling power was estimated through an average summer night, for the experimental solar collector of 2,4 m². This means the inlet temperature is no longer constant, it is iterated for each time step, approximated by the average temperature in the tank.¹ The cooling power per square meter of collector is then derived from the inlet/outlet temperatures and the flow rate (see table in Annex 14: Final estimation of cooling power based on TRNSYS simulation).

This cooling power per area is then used to estimate the cooling of the tank in the case of EMBRACE. In that case, there are 7,2 m² of collectors, so the cooling power per square meter is simply multiplied by the new area. Then the energy content of the tank is estimated at each time step, considering an initial temperature of 22°C, and a cooling power profile as calculated previously. The resulting temperature in the tank drops from 22 to 13 °C, 17,5 °C and 20,2 °C if 14 m², 7,2 m² or 2,4 m² of collectors are respectively installed, as shown in the graph below.

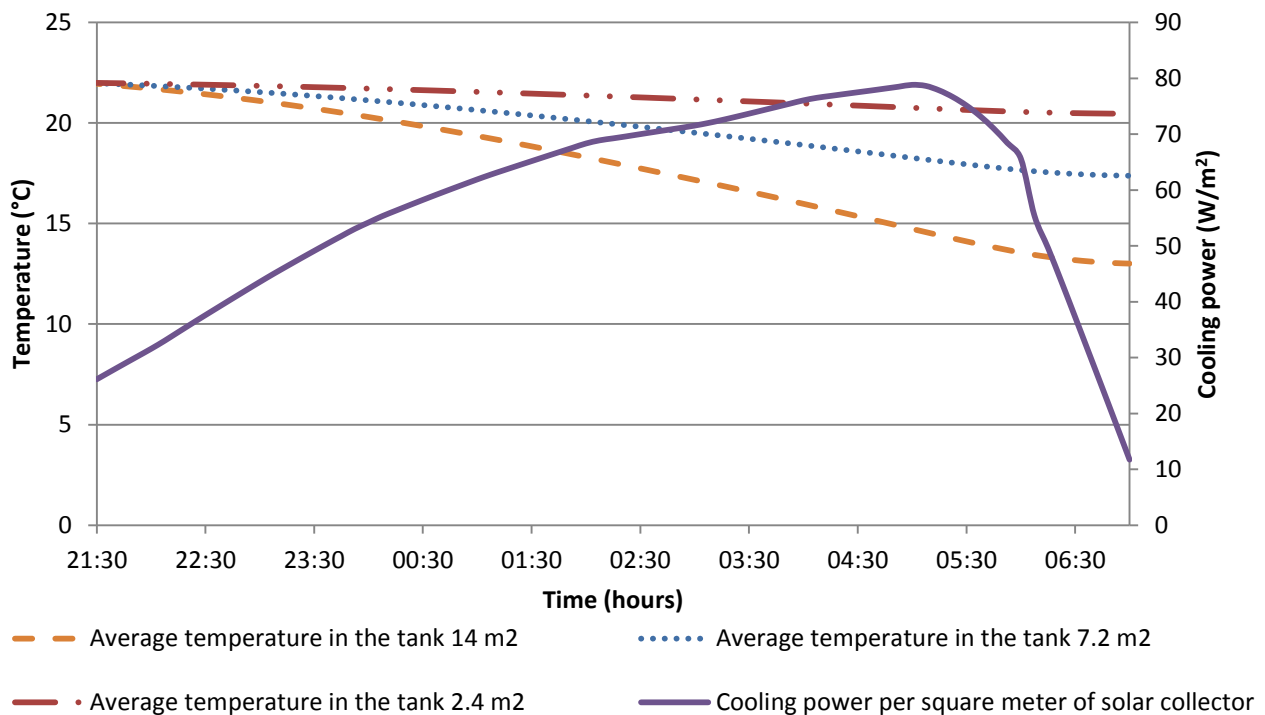


Figure 130 – Average temperature in the tank in function of the area of collectors installed and cooling power

The results based on the TRNSYS simulation show that a peak power of 80 W/m² can be achieved, with an average of 58 W/m². The total cooling energy amounts to 0,56 kWh/m² of collector for one night.

¹ This is an approximation, since there should be some stratification in the tank, so the water leaving to the collectors would be warmer than the average temperature in the tank.

It can be also seen that if the decrease of temperature in the tank over the night is taken into account then the cooling power is lower compared to when the inlet temperature is considered constant, as in Table 55, where the supply is fixed at 22°C. In fact if the temperature in the tank drops, also the supply temperature decreases. In this way the ΔT with the sky temperature is smaller, resulting in a reduction of the obtained cooling power.

6. Comparison between the experimental and simulated results

It is interesting to compare the outputs of a simulation program with actual experimental results. In fact, simulations are sometimes subject to doubts regarding their reliability, since the equations governing their functioning are not always detailed. The opportunity is given here to corroborate the experimental results with the results simulated in TRNSYS. For this purpose, one night has been chosen arbitrarily (August 13th) for testing. The weather data (outdoor air temperature, wind speed) and the supply temperature recorded during that night of the experiment have been averaged for time steps of 12 minutes, and given as inputs to the program. The simulation provided a cooling power which is plotted in Figure 131, along with the other power curves.

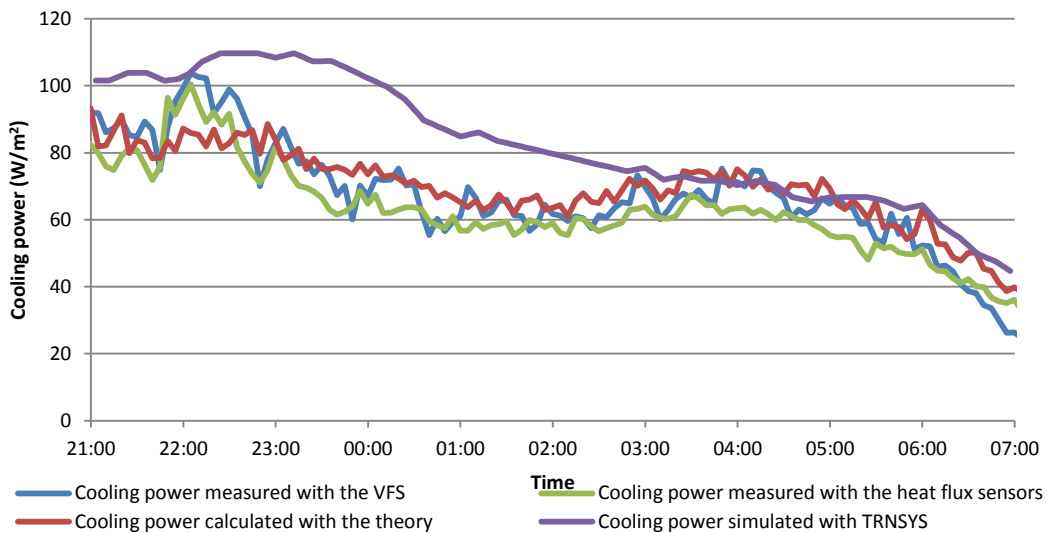


Figure 131 – Comparison of the cooling powers of TRNSYS with the other methods

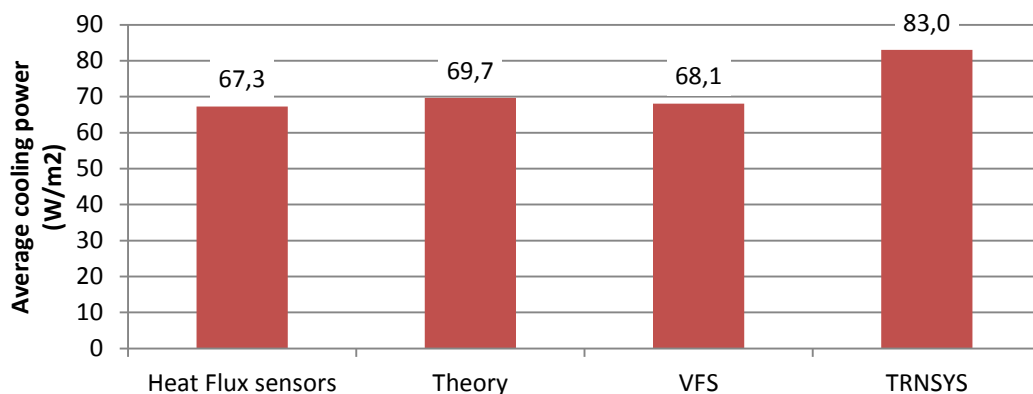


Figure 132 – Average cooling power for four methods

The results from TRNSYS are relatively close to the ones obtained with other methods. The average cooling power shows a slightly higher value in the simulations than in what is observed experimentally.

7. Discussion and conclusion on nighttime radiative cooling

At the theoretical level, the measurement of effective sky temperature and plane radiant temperature has been studied in details. A pyrgeometer would have been the optimal tool to measure it, but the handcrafted sensor designed for the experiment showed enough consistency to be used for the study. In general, the theory matched remarkably well with the experimental results, especially for completely clear sky conditions, showing a predominant contribution of the radiative cooling over the convective cooling.

The three PVT panels (3,915 m²) had an average cooling power ranging from 28 to 75 W/m², producing between 1,3 and 3,6 kWh of cooling energy per night. Because of their high price and their recent development, PVT are not broadly used yet. They can produce three forms of energy: heating, electricity and cooling, as demonstrated in this report. The single efficiencies for the three production modes are relatively low compared to systems that are optimized for only one of these uses. However, when considering the overall efficiency, they still represent a noteworthy investment, because their multiple functions enable to reduce the payback time.

The unglazed collector (2,4 m²) had an average cooling power ranging from 20 to 72 W/m², producing between 0,5 and 2,1 kWh of cooling energy per night. Unglazed collectors are usually restricted to cheap applications of pool heating; using them also for cooling would make such an installation a profitable operation. The payback time was in fact calculated to be 4 years, only considering cooling application, for one of the two models of unglazed collectors purchased. This type of panels can improve the comfort conditions (by warming a pool and cooling down the indoor space of a house) at a low financial and environmental cost, and in a relatively simple way.

The calculated COP during the experiment, ranges from 13 to 37 for PVT and from 6 to 23 for unglazed collector. This calculation of the COP is not completely accurate, because the considered energy consumed was the total one of the circulation pump. However the pump was used to supply both types of panels. In order to calculate more precise COPs, the energy consumption of the pump should be split between the two panels in function of the relative flow rate provided. Another approach is to consider the system as a whole, calculating the overall COP as the ratio between the sum of cooling energies produced by both unglazed and PVT panels, and the total pump consumption. This method shows COP ranging from 19 to 58, which are very high values and emphasize the potential in “free” cooling that solar collectors can provide.

The applications of nighttime radiative cooling can appear limited for residential buildings in Denmark. It has been shown that for EMBRACE, exploiting the passive means is theoretically sufficient to almost take out the cooling needs. However, the potential is larger in southern countries, where nighttime radiative cooling applications could be used at a larger scale, for instance by simply modifying existing solar collectors installations. In Denmark, there still remains a potential for application in office buildings, where the internal gains and cooling needs are higher. One of the main interests in providing those needs with nighttime radiative cooling consists in the synchronization occurring between the cooling needs and the potential of cooling production. Indeed, clear sky conditions can create high solar gains, which will result in high cooling needs during the day, but the cooling production will also be higher during the night, matching the demand.

Discussion

The Solar Decathlon is an international competition, and as such it has its own limitations. The main one probably consists in trying to evaluate and compare houses designed for radically different contexts. One could also reproach the strict constraints of the competition, that make each team build a house in only ten days, resulting in some imperfections that could be improved. Nevertheless, the designs of all the teams showed a high degree of professionalism, recognized by Jury members internationally renowned. Even though the competition might be somehow biased, the event already achieves its goal when universities from all around the world collaborate with professionals to find new environmentally friendly approaches, spreading this knowledge to the general public.

Among the other houses, EMBRACE performed in all contests in an average way, always providing good results but never the best. This tendency is also reflected in the final ranking. One of the future improvements for the team could be to reduce the time and efforts spent in the design stage, and to use them in the construction and testing of the mock up at the University, before the competition. In fact, the limited time assigned for the construction turns it into a critical moment: practical issues can impose hurried changes in the realization, which enables to finish the dwelling on time, but nullifies part of the previous design work. A better management of the tasks and coordination with professionals and sponsors from the earliest steps could help the design process. The difficulty of applying this to the reality is obvious when taking into account the needs of external companies involved and financial issues.

Different simulation programs have been used to support the choices regarding the HVAC. The outputs have been utilized to size and select components, for both the production and emission of heating and cooling. When dealing with simulation tools, their limitations need to be taken into account in order to perform accurate analysis. The level of accuracy of the outputs should not be expected to be perfect or trusted unconditionally. The highest degree of reliability can be obtained when comparing the simulation results with experimental ones, general knowledge or calculations e.g. based on Standards. This approach has been followed in order to state the thermal performances of the radiant floor selected and the HVAC integrated in the designed thermal envelope.

The analyzed control and HVAC layout has overcome a certain degree of simplifications, passing from the design stage to the actual realization. It has been tried to keep the impact of the changes as low as possible. This was done by choosing the modifications that introduced only slight differences in terms of energy production or consumption. A more complex system could have provided improved performance, but the time and efforts needed to reach that level were not available. In particular, it is unfortunate that the heat pump could not be implemented as intended, because it could have validated (or rejected) the conclusions drawn from the design work about its performance in the case of this specific layout.

Nighttime radiative cooling has proved to be an effective strategy to lower the consumption only during the first days of the competition when cooling was demanded. This could point out the unsuitability of this system, especially in a country like Denmark where the cooling demand is limited to a short period. This solution was in fact implemented mainly for Paris. Nighttime radiative cooling has proved to be a quite stable source of cooling regardless of the climate zone because mainly affected by the sky temperature. Thus it can provide a larger benefit in countries where the cooling demand is greater in summer. However it could find a field of application in Denmark for public buildings, which have still a considerable cooling demand. Furthermore, the increase of thermal insulation levels in the new constructions emphasizes the influence of gains, introducing a bigger cooling demand. Thus this technology could be applied to new buildings, coupled with high temperature cooling, like in the present project.

Future research

The facility built for the described experiment at ICIEE department of DTU is planned to be used in the future to study the potential of coupling nighttime radiative cooling with phase change materials (PCM). Solar collectors could be in fact exploited to discharge at night the energy stored by PCM embedded in a building envelope, using radiative cooling.

Another interesting similar approach could be to study the use of solar collectors or PVTs coupled with a heat pump. Haller Y. M. and Frank E., 2011, prolonging the research of Karagiorgas M. et al., 2010, have already analysed the possibility to increase the COP of a water-to-water heat pump, using the water preheated by solar collectors. Auzenet E. et al., 2013, have studied a similar system, preheating air blown in the back of PVT panels.

All those studies have mainly focused on using solar heat for the evaporator of the heat pump. Further steps could include considering cooling applications as well, using solar panels to precool the water circulated then to the heat pump compressor.

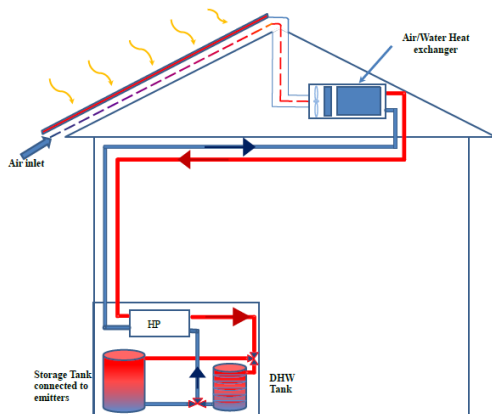


Figure 133 – Preheating of air with PVT
Picture from Auzenet E. et. al., 2013

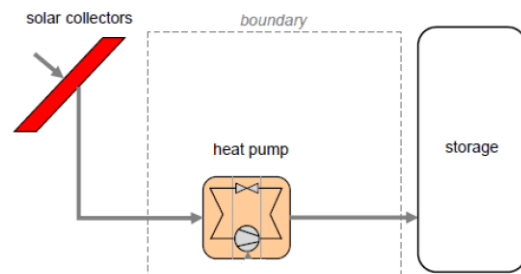


Figure 134 – Coupling of solar collectors and heat pump
Picture from Haller Y. M. et. al., 2011

Conclusion

As a general conclusion, it can be said that the house EMBRACE has performed well during the competition, achieving the overall ranking of 8 out of 20 other teams. Despite the numerous issues encountered all along the design phase, the continuous efforts of the team's students have borne fruit. The measured contests have demonstrated an objective good performance of the house, while the juries have recognized the validity of the strategies and concepts implemented in the project.

The Comfort Conditions have been evaluated as satisfactory, since EMBRACE ranked 8 also in this contest. Team DTU reached the first position in the Humidity measurement, and the seventh position in the Temperature measurement, which was the most important of the contest (65 points available out of 120). In fact, the indoor temperature stayed in the strict range defined by the competition to get the maximum amount of points for more than 70 % of the monitored time. These results show that the choices made by the students during the design phase ended up being appropriate for the conditions, despite the exceptionally cold weather encountered in Paris.

The design strategy has also been appreciated by the Juries, especially the Sheltered Garden used as a buffer zone, and the modularity and flexibility between cold and warm spaces. In their evaluation, the Energy Efficiency Jury¹ mentions "the inventiveness of the materials with ceramic floors that offer a good conductivity as well as a good thermal mass." The floor covering analysis here presented in favour of the ceramic tiles has eventually been fruitful. Innovative technologies have been awarded 15 points out of 15 in the Energy Efficiency contest, which represents a strong recognition of the students' efforts towards integrating all the controls in a single system.

The competition in Versailles represent a particular case of evaluation, since the conditions are rather specific: every day, a large number of visitors enter the house, affecting the internal gains and air tightness of the building, the appliances are utilized in a scheduled and meticulous way, all the mechanical systems are operated manually in order to balance constantly between the energy consumption and the comfort conditions. In order to have a more representative idea of the performance of the house, annual simulations have been carried out in the urban scenario of Copenhagen, which is the designed location for the implementation of EMBRACE. They showed a global electricity consumption of 38 kWh/m² net area per year (equal to 2236 kWh when applying the area), which is less than half the PV production (estimated to 5537 kWh for the whole year). This consumption per m² is still relatively high for a building that aims to be a plus-energy house. The reason can be found in the fact that the consumption of the appliances does not almost depend by the size of a dwelling. That is why the team has proposed to evaluate the consumption per person instead of per surface area. In the concept of small buildings that the team has tried to emphasize, this approach seems more relevant, and it has also been recognized noteworthy by the Energy Efficiency Jury.

The study on nighttime radiative cooling has shown interesting results regarding the output of both PVT panels and unglazed collectors. The average cooling power per surface area did not show substantial differences between both types of panels. In general, the theoretical, simulation and experimental results had a satisfactory correlation. Conclusions can therefore be drawn, stating that unglazed collectors and PVT panels have a large potential for radiative cooling applications, with different targets.

Both types of panels had an average cooling power ranging from 20 to 75 W/m², producing between 0,3 and 0,9 kWh/m² of cooling energy over one night. It corresponds to the values previously found in the

¹ Jury composed by Harrison Fraker, Marija Todorovic, and Thierry Salomon.

literature. With an overall COP¹ observed in the experiment ranging from 19 to 58, the technology shows strong potential in energy savings for cooling. Applications for residential buildings would be more suited to southern countries where the cooling needs are higher and where solar collectors are already used for heating purpose. In Denmark, the potential resides more in professional buildings with higher internal gains, where an installation of solar collectors for DHW heating and nighttime radiative cooling could be beneficial, considering the cost reduction due to large scale equipment.

¹ COP defined as the ratio of the cooling energy produced by both panels divided by the consumption of the common circulation pump.

References

Standards

- [1] ANSI/ASHRAE Standard 55 (2004). *Thermal Environmental Conditions for Human Occupancy*.
- [2] ASHRAE Fundamentals Handbook (SI) (2001). Chapter 28-*Residential Cooling And Heating Load Calculations*.
- [3] DS 418 (2011). Calculation of heat loss from buildings.
- [4] DS/EN 1264-2 (2008). *Water based surface embedded heating and cooling systems – Part 2: Floor heating: Prove methods for the determination of the thermal output using calculation and test methods*.
- [5] DS/EN 1264-3 (2009). *Water based surface embedded heating and cooling systems – Part 3: Dimensioning*.
- [6] DS/EN 1264-5 (2008). *Water based surface embedded heating and cooling systems – Part 5: heating and cooling surfaces embedded in floors, ceilings and walls-Determination of the thermal output*
- [7] DS/EN 15251 (2007). *Indoor environmental input parameters for design and assessment of energy performance of buildings addressing indoor air quality, thermal environment, lighting and acoustics*.
- [8] DS/EN 15377-1 (2008). *Heating systems in buildings – Design of embedded water based surface heating and cooling systems – Part 1: Determination of the design heating and cooling capacity*.
- [9] DS/EN ISO 7726 (2001). *Ergonomics of the thermal environment – Instrument for measuring physical quantities*.
- [10] EN 15316-1 (2007). *Heating systems in buildings - Method for calculation of system energy requirements and system efficiencies - Part 1: General*.
- [11] EN 15316-2-1 (2007). *Heating systems in buildings - Method for calculation of system energy requirements and system efficiencies-Part 2-1: Space heating emission system*.
- [12] EN 15316-3-1 (2007). *Heating systems in buildings - Method for calculation of system energy requirements and system efficiencies - Part 3-1: Domestic hot water systems, characterization of needs (tapping requirements)*.
- [13] EN 15316-3-2 (2007). *Heating systems in buildings - Method for calculation of system energy requirements and system efficiencies - Part 3-2: Domestic hot water systems, distribution*.
- [14] EN ISO 15316-2-3 (2007). *Heating systems in buildings - Method for calculation of system energy requirements and system efficiencies-Part 2-3: Space heating distribution system*.
- [15] UNI EN ISO 13786 (2008). *Thermal performance of building components - Dynamic thermal characteristics – Calculation method*.
- [16] UNI EN ISO 6946 (1999). *Building components and building elements - Thermal resistance and thermal transmittance - Calculation method*.

Articles and Books

- [1] Abushakra B. et al. (2004). "Overview of existing literature on diversity factors and schedules for energy and cooling load calculations". ASHRAE Transactions 2004, Volume 110 Part 1.
- [2] Anderson T.N., Duke M., Carson J.K. (2013). "Performance of an unglazed solar collector for radiant cooling"
- [3] Armstrong S., Hurley W.G. (2010). "A thermal model for photovoltaic panels under varying atmospheric conditions". Applied Thermal Engineering 30, pp.1488-1495
- [4] Auzenet E., Altazin M., Guiavarch A., Hachem Ben Nejma H. B., Lokhat I., Claudon F., (2013). "Demonstration and Modeling of the Coupling of a Heat Pump and Hybrid PV-T Panels Integrated into a Building".
- [5] Berdahl P. and Fromberg R. (1982). "The thermal radiance of clear skies". Solar Energy 29 (4), pp. 299–314.
- [6] Berdahl P. and Martin M. (1984a). "Emissivity of clear skies". Solar Energy 32, pp. 663–664.
- [7] Berdahl P. and Martin M. (1984b). "Characteristics of infrared sky radiation in the United States". Solar Energy 33 (3/4), 321–336.
- [8] Berger X., Buriot D. and Garnier F., 1984. "About the equivalent radiative temperature for clear skies". Solar Energy 32, 725–733.
- [9] Bliss R. (1961). "Atmospheric radiation near the surface of the ground: a summary for engineers". Solar Energy 5, 103–120.
- [10] Boxwell M. (2012). "Solar Electricity Handbook. A simple, practical guide to solar energy - designing and installing photovoltaic solar electric systems".
- [11] Cavelius R. et al. (2005). "Passive cooling technologies". Austrian Energy Agency.
- [12] Brohus H., Heiselberg P., Simonsen A. and Sørensen C. K. (2010). "Influence of Occupants' Behaviour on the Energy Consumption of Domestic Buildings". Clima 2010: 10th Rehva World Congress: Sustainable Energy Use in Buildings, Chapter 8.
- [13] Chen B., Kasher J., Maloney J. and Girgis A. G. and Clark D. (1991). "Determination of the clear sky emissivity for use in cool storage roof and roof pond applications".
- [14] Chen H., Riffat S.B. and Mempo B. (2010). "Numerical Study on the Energy Performance of a Novel Direct Expansion PV/T Heat Pump (DX-PV/THP) System". Proceedings of SET2010 – 9th International Conference on Sustainable Energy Technologies, Shanghai, China (24–27 August).
- [15] Churchill S.W. (1976). "A comprehensive correlating equation for laminar, assisting, forced and free convection". Journal of American Institute of Chemical Engineers 23 (1), pp.0-16.
- [16] Clark G. and Allen C.P. (1978). "The estimation of atmospheric radiation for clear and cloudy skies". Proc. 2nd Nat. Passive Solar Conf. vol. 2, p.676
- [17] Corcione M. (2007). "Heat transfer correlations for free convection from upward-facing horizontal rectangular surfaces".
- [18] Duffie J.A. and Beckman W.A. (2013). "Solar Engineering of Thermal Processes", Fourth edition.
- [19] Eicker U. and Dalibard A. (2011). "Photovoltaic-thermal collectors for night radiative cooling of buildings", Solar Energy, vol. 85, pp. 1322-1335.
- [20] Elsasser W.M. (1942). "Heat Transfer by Infrared Radiation in the Atmosphere". Harvard Univ. Met. Studies N°6, Milton, Massachusetts.
- [21] Erell E. and Etzion Y. (2000). "Radiative cooling of buildings with flat-plate solar collectors"
- [22] Haller Y. M., and Frank E. (2011). "On the potential of using heat from solar thermal collectors for heat pump evaporators". ISES Solar World Congress, 28. August - 2. September 2011, Kassel, Germany.
- [23] Huang Y.J. and Parker D. (1999). "Residential equipment part load curves for use in doe-2".
- [24] Lewandowski W.M., et al., (1999). "Free convection heat transfer and fluid flow above horizontal rectangular plates".
- [25] Meir M. G., Rekstad J. B. and Løvvik O. M. (2003). "A study of a polymer-based radiative cooling system"

- [26] Olesen B.W. (1997). "Thermal comfort requirements for floors occupied by people with bare feet".
- [27] Olesen B.W. (2001). "Cooling and heating of buildings by activating their thermal mass with embedded hydronic pipe systems".
- [28] Olesen B.W. (2007). "Calculation of the yearly energy performance of heating systems based on the European building energy directive and related CEN Standards"
- [29] Swinbank W. (1963). "Long-wave radiation from clear skies". Quarterly Journal of Royal Meteorological Society 89, 339–348.
- [30] Unsworth M. H. and Monteith J. L. (1975a). "Long-wave radiation at the ground—I. Angular distribution of incoming radiation". Quart. J.R. Met. Soc. (1975), 101, pp. 13–24-II.
- [31] Unsworth M. H. and Monteith J. L. (1975b). "Long-wave radiation at the ground—II. Geometry of interception by slopes, solids and obstructed planes". Quart. J.R. Met. Soc. (1975), 101, 25–34.
- [32] Zhao K. et al. (2014). "Dynamic performance of water-based radiant floors during start-up and high-intensity solar radiation", Solar Energy, vol. 101, pp. 232-244.

Other references

- [1] Aggerholm S., Grau K. (2011). SBI-direction 213, 2nd edition: "Energy requirements for buildings , Calculation guide", page 78-79
- [2] Babiak J. (ed.), Olesen B. W., Petráš D. (2007). REHVA Guidebook No 7: "Low temperature heating and high temperature cooling"
- [3] Bahrami M. (2009). "Forced Convection Heat Transfer", course of ENSC 388. Simon Fraser University
- [4] Baldocchi Dennis (September 10, 2012). Lecture 6, Biometeorology. Department of Environmental Science, Policy and Management, University of California, Berkeley.
- [5] Bjerregaard Jensen L. (2008). "B 150 civil engineering futures: The 150th anniversary celebrations of the study of civil engineering in Denmark"
- [6] Blomberg T. (2000). "HEAT2 – A PC-program for heat transfer in two dimensions. Manual with brief theory and examples." Dept. Building Physics, Lund Univ., Lund, Sweden.
- [7] Campbell G.S. and Norman J.M. (1998). "An Introduction to Environmental Biophysics". Springer Verlag, New York.
- [8] Casini M. (2009). "Costruire l'ambiente" Edizioni Ambiente srl, pp 150-153.
- [9] Chinello E. (2013). "Performance evaluation of building thermal mass coupled with photovoltaic/thermal panels", Master Thesis project, Technical University of Denmark.
- [10] Daikin Corporation (2014). "New Daikin Altherma Low Temperature" presentation for internal use.
- [11] EQUA Simulation (2013). Online database.
- [12] Gennari L. and Péan T. (2014). "Subject 3 – Building Services and Energy – Solar Decathlon Team", Technical report for the course 11080 Advanced Building Design, unpublished.
- [13] IDA-ICE version 4.6 Manual (2013).
- [14] Jianhua F. and Olesen B.W. (2013). "Sustainable heating and cooling of buildings, 11127", course lectures. Danmarks Tekniske Universitet.
- [15] Kazanci O. B. and Skrupskelis M. (2012). "Solar Sustainable Heating, Cooling and Ventilation of a Net Zero Energy House", M.Sc. Thesis, Dept. Civil Eng., Technical Univ. of Denmark, Lyngby, Denmark.
- [16] Magnani L. (2010). "Termodinamica applicata", course lectures. University of Pavia.
- [17] Nielsen H. M. (2014), "Holistic Analysis of HVAC System Components for Solar Decathlon Europe 2014", Bachelor Thesis project, Technical University of Denmark.
- [18] Perers B., private communication, July 2014.

- [19] RT2012 Weather data, Centre Scientifique et Technique du Bâtiment, 2011 [Online].
<http://www.rt-batiment.fr/batiments-neufs/reglementation-thermique-2012/donnees-meteorologiques.html>
- [20] Solar Decathlon Europe (2014). "Règlement / Rules / V5.0"
- [21] Team DTU (2014). Solar Decathlon 2014, "Embrace: Delivery 6 Project Manual"
- [22] Uponor (May 2014). "Uponor Radio 24V DEM Training Material"
- [23] Uponor Corporation (2012). "Low-energy guide – Underfloor heating and cooling in low-energy buildings"
- [24] Uponor Corporation (2013). "Free cooling guide-cooling integration in low energy houses"
- [25] Zandegiacomo E. (2003). "Appunti di trasmissione del calore". University of Trieste

Lists of figures

Figure 1 – Main concepts concerning sustainability.....	10
Figure 2 – Final ranking of SDE2014	15
Figure 3 – Outside weather data of Paris in July – Typical year from RT2012	16
Figure 4 – EMBRACE in Versailles (©SDEurope).....	19
Figure 5 – Urban concept: integration of EMBRACE on the rooftop of existing buildings.....	19
Figure 6 – Weather Shield concept.....	20
Figure 7 – Renderings of the Weather Shield and Sheltered Garden (Team DTU, 2014)	20
Figure 8 – Photographs of the constructed Sheltered Garden	20
Figure 9 – Rendering and photo of the ground floor (living room, kitchen and flex room) (Team DTU, 2014).....	21
Figure 10 – EMBRACE main construction elements (Team DTU, 2014)	21
Figure 11 – Two perspectives from the modules assembly	22
Figure 12 – The two different sorts of PV panels in EMBRACE	23
Figure 13 – Example of feedback from the app to the user about his/her energy consumption.....	23
Figure 14 – Specific thermal transmittance, obtained applying the envelope surfaces (W/K)	24
Figure 15 – Heat flux shift obtained with data from IDA-ICE 4.6 program	26
Figure 16 – Passive strategies: main concepts regarding shading, natural ventilation and Weather Shield/buffer zone	28
Figure 17 – Heating and cooling production schemes.....	29
Figure 18 – Coil heat exchangers, of the DHW tank, integrated in Nilan Compact P	29
Figure 19 – Scheme of the heating/cooling/electricity strategies	30
Figure 20 – Photograph of the solar thermal collector module before its mounting on the Weather Shield	31
Figure 21 – Features of the Nilan Compact P unit	31
Figure 22 – COP and heat output for sanitary hot water as a function of the volume flow Data from the Nilan Compact P datasheet	32
Figure 23 – Principle of the Daikin heat pump	33
Figure 24 – Photograph of the Daikin heat pump installed on the wall of the technical room of EMBRACE	33
Figure 25 – Views of the unglazed solar collectors installed for EMBRACE	34
Figure 26 – Heat transfer coefficients of surface heating and cooling (Uponor (2013)- Free cooling guide).....	35
Figure 27 – Chosen system from Uponor	35
Figure 28 – Comparison of the accuracy obtained by opening radiant floor loops’ actuators manually or automatically	36
Figure 29 – Module division and radiant floor loops, ground floor	36
Figure 30 – Construction layers of the designed radiant floor	37
Figure 31 – Heat transfer coefficients of surface heating and cooling (Bjarne W. Olesen, 2012)	41
Figure 32 – Dew point temperature at different air temperatures and relative humidity levels (Uponor, 2013).....	41
Figure 33 – Designed floor sections: two options of floor covering	46
Figure 34 – Type B system as described in EN 1264-2	47
Figure 35 – Characteristic curves of the designed radiant floor as defined in EN 1264-2.	51
Figure 36 – Supply water temperature in heating design load.....	52
Figure 37 – Supply water temperature in cooling design load	52
Figure 38 – HEAT2 model with the materials of the tiles solution, and detail of the mesh	54
Figure 39 – Example of modification pipe (Blomberg, 2000)	55
Figure 40 – Section of the radiant floor (from Uponor documentation)	56
Figure 41 – Photo of the profile of the Uponor aluminum plates used for EMBRACE	57
Figure 42 – Temperature distribution and isotherms in the floor structure, for heating (left) and cooling (right)	59
Figure 43 – Detail of the temperature distribution around the pipe for the cooling case	59
Figure 44 – Detail of the temperature distribution around the pipe for the heating case	60
Figure 45 – Temperature profiles on the floor surface (0 is the center of the pipe)	60
Figure 46 – Control and adaption of an inverter heat pump compared to a non-inverter heat pump	62
Figure 47 – Efficiency of a heat pump related to the load of heating or cooling provided.	62
Figure 48 – Possible operations of a heat pump in relation to the building demand.....	63
Figure 49 – Option 1 simplified representation. The heat pump is located before the storage tank and the radiant floor mixing station controls the supply temperature with recirculation.	65
Figure 50 – Option 2 simplified representation. The heat pump controls the supply temperature so recirculation is not needed.	65
Figure 51 – Option 3 simplified representation. The heat pump can provide water both to the storage tank and radiant floor	66
Figure 52 – Schematic representation of the main components of the heat pump.....	66
Figure 53 – Building demand compared to number of hours of outdoor temperature in heating season for Copenhagen.....	68
Figure 54 – Heating capacity of the heat pump and dwelling demand in Copenhagen	68
Figure 55 – Building demand compared to number of hours of outdoor temperature in cooling season for Paris.....	69
Figure 56 – Cooling capacity of the heat pump and dwelling demand in Paris	69

Figure 57 – Layout of the Sonnenkraft storage tank DWH750 R2, extract from Sonnenkraft datasheet. The connections explained on the right side are those as assembled for the showcase in Versailles	72
Figure 58 – Uponor Didital Display Thermostat T-75 and U@home application	74
Figure 59 – Schematic representation and operation of the 4-ways rotary valve HRB 4 from Danfoss.....	76
Figure 60 – Technical room visualization with components and flow directions, for both cooling and heating mode.....	77
Figure 61 – Solar collectors’ main components in the technical room.....	77
Figure 62 – Implemented system in EMBRACE (storage tank, heat pump, radiant floor and unglazed collectors)	78
Figure 63 – On the right it is possible to see the radiant floor manifold, where the blue covers are the radio controlled actuators on the supply loops. On the right the console for the C-46 control	78
Figure 64 – Temperature distribution from October to April and corresponding heating power demand for the dimensioning room and the entire dwelling	80
Figure 65 – Temperature drop due to heat losses in the water storage tank, when heat is not provided by heat pump	82
Figure 66 – Representation of the outdoor temperature trend in comparison with the indoor set point, in summer and winter	82
Figure 67 – Cooling demand peaks over the cooling season, in Paris	83
Figure 68 – Temperature and cooling load for the design day.....	83
Figure 69 – Example of operative temperature visual distribution, obtainable with IDA-ICE model. Pictures from Copenhagen scenario in January and June	85
Figure 70 – Monthly system energy provided, divided between mechanical ventilation (AHU) and radiant floor (Zone) for both Paris and Copenhagen.....	86
Figure 71 – Calculation concept and building-system boundaries for heating (EN15316-1).....	87
Figure 72 – Loss diagram over the whole year for Copenhagen and Paris	89
Figure 73 – Monthly PV production for Paris and Copenhagen	89
Figure 74 – Example of the measured temperature in room 2, compared to the expected range	92
Figure 75 – Relative humidity recorded during the competition.....	92
Figure 76 – Repartition of the electricity consumption	93
Figure 77 – Subdivision of the electricity consumption during the competition (from Team DTU’s own data).....	94
Figure 78 – Electricity production and solar radiation during the competition	95
Figure 79 – Energy production and consumption per day during the competition.....	95
Figure 80 – Graphic visualization of the average cooling power per night obtained with the theoretical model and measured	98
Figure 81 – Scheme and location of the water temperatures recorded and expected trend	99
Figure 82 – Water temperature in the storage tank without nighttime radiative cooling. Last monitored night 10/07/2014, available data with no nighttime radiative cooling on, from 22:00 to 23:15.....	100
Figure 83 – Water temperatures profiles and corresponding cooling power (measured and modelled) per night	102
Figure 84 – Measured air temperature and calculated sky temperature during the competition period	102
Figure 85 – Scheme of the heat losses through the top surface	107
Figure 86 – Small convex body in a large cavity, where $A_2 \gg A_1$	109
Figure 87 – Dependence of I_7 on α , (Unsworth and Monteith, 1974b).....	111
Figure 88 – Angle α of tilted panel and β to consider shielding surrounding.	111
Figure 89 – Flat plate with parallel flow	113
Figure 90 – Thermal conductivity of dry air and water vapor is function of the temperature	114
Figure 91 – Payback time in years of the three collectors investigated	117
Figure 92 – Daily cooling demand in Copenhagen for the month of June. The demand is here divided in bands to check its distribution in time.....	118
Figure 93 – Unglazed solar collector.....	119
Figure 94 – Photovoltaic/thermal panel (PVT)	119
Figure 95 – Optimal tilt in Copenhagen over the year, for the production of electricity and sanitary hot water	120
Figure 96 – Schematic layout of the experiment	121
Figure 97 – Experiment setup – Back view	121
Figure 98 – Weather station Vantage Pro2	121
Figure 99 – Experiment setup – Front view	121
Figure 100 – Datalogging equipment and pipe work.....	121
Figure 101 – Sensors calibration : outside and inside the insulated box used for the calibration	123
Figure 102 – Infrared pictures of the unglazed solar collector in heating mode. Day 21/08/2014 data recorded and time averaged from 14:40-14 :45, overcast sky, emissivity set in the thermographic camera 0,9. Same picture is shown with two temperature ranges, 22-27 and 23-26 °C respectively.	124
Figure 103 – Infrared pictures of the PVTs in heating mode. Day 21/08/2014 data recorded and time averaged from 14:55-15:00, overcast sky, emissivity set in the thermographic camera 0,9.....	125
Figure 104 – Infrared pictures of all collectors, in cooling mode. Day 19/08/2014 picture taken at approximately 18:00, overcast sky, emissivity set in the thermographic camera 0,9.....	125
Figure 105 – Surface temperature sensor, with and without protection	125
Figure 106 – Hand crafted, plane directional temperature sensor	127
Figures 107 – Plane radiant temperatures calculated with both methods the nights of the 9 th and the 11 th of August	128
Figure 108 – VFS in the supply (left) and the two returns (right)	129
Figure 109 – Correlation between two temperature measurements	129
Figure 110 – Heat flux sensor placed on the PVT panel	130

Figure 111 – Temperature outputs of the experiment during the night between August 20 th and 21 st	131
Figure 112 – Cooling power curves for PVT panels (August 20 th – 21 st)	132
Figure 113 – Cooling energy produced over the night (from 19:00 to 07:00) for the PVT	133
Figure 114 – Cooling power curves for unglazed collector (August 20 th – 21 st).....	134
Figure 115 - Cooling energy produced over the nights (from 19:00 to 07:00) for the unglazed collector	135
Figure 116 – Convective and radiative components of the cooling power (unglazed collector)	135
Figure 117 – Convective and radiative components of the cooling power for PVTs, August 20 th -21 st . The convective component is calculated and plotted with both the simplified and more elaborated theoretical approaches	136
Figure 118 – Weather data in August 2014	137
Figure 119 – Heating powers and solar radiation – 28 th August.....	138
Figure 120 – Comparison in the average cooling power of the PVT and unglazed collector per night	138
Figure 121 – Comparison of the cooling energy produced by the PVT and the unglazed collector per night	139
Figure 122 – Section of the unglazed collector.....	142
Figure 123 – Schematic diagram of the TRNSYS model	143
Figure 124 – TRNSYS model	143
Figure 125 – Outlet temperature for the two best and worst nights, compared to the calculated average summer night	144
Figure 126 – Outlet temperature during an average summer night for a range of different flows	146
Figure 127 - Cooling power during an average night for a range of different flows.....	147
Figure 128 – Outlet temperature during an average summer night for different supply temperatures.....	148
Figure 129 – Cooling power during an average summer night for a range of different supply temperatures	149
Figure 130 – Average temperature in the tank in function of the area of collectors installed and cooling power	150
Figure 131 – Comparison of the cooling powers of TRNSYS with the other methods	151
Figure 132 – Average cooling power for four methods	151
Figure 133 – Preheating of air with PVT	154
Figure 134 – Coupling of solar collectors and heat pump Picture from Haller Y. M. et. al., 2011	154
Figure 135 – Specifications of the BA22 from Batec.....	171
Figure 136 – Scheme of the solar collectors’ connection with the DHW tank (integrated in the Nilan Compact P).....	172
Figure 137 – Schematic representation of the connections of the dryer Miele T 8881 S. Picture extract from Miele website	182

List of tables

Table 1 – Danish energy classes for residential buildings taking into account energy supply for heating, ventilation, cooling and domestic hot water	10
Table 2 – Points distribution and rankings for Team DTU	14
Table 3 – Desired comfort conditions, based on Solar Decathlon 2014 regulation.....	15
Table 4 – Main floors’ areas of EMBRACE	22
Table 5 – Envelope thermal transmittances	24
Table 6 – Characteristics of the south external wall.....	25
Table 7 – Characteristics of the roof.....	25
Table 8 – Thermal inertia and quality of the building envelope (Italian Ministerial Decree, June 26, 2009) (Casini M., 2009).....	27
Table 9 – Three steps of flow rate, defined for the demand controlled mechanical ventilation	32
Table 10 – Radiant floor loops and control.....	36
Table 11 – Boundary conditions for load calculations	43
Table 12 – Internal gains as assigned in the IDA-ICE simulation model.....	44
Table 13 – Main thermal properties of the envelope as defined in the IDA-ICE model	44
Table 14 – Maximum cooling and heating loads W/m^2 , obtained per surface area of radiant floor in each room.....	45
Table 15 – Cooling and Heating maximum demands, for both Copenhagen and Paris	45
Table 16 – Supply water temperature of the dimensioning room, for the different floor covering and methods considered.....	50
Table 17 – Radiant floor parameters for the design conditions	50
Table 18 – Power provided with a fixed temperature difference between average water and room temperature, both in heating and cooling	52
Table 19 – Material layers for case 1.....	53
Table 20 – Material layers for case 2	53
Table 21 – Boundary conditions for the HEAT2 model.....	54
Table 22 – Comparison of the 3 model cases	56
Table 23 – Heat flux results of the different cases	58
Table 24 – Example of the possible operation modes for an inverter heat pump during heating season	63
Table 25 – Design input in the Daikin simulation tool	67
Table 26 – Information concerning the heat pump selected	67
Table 27 – Performances of the heat pump selected, as an output of the Daikin simulation tool, both in Paris and Copenhagen	67
Table 28 – Hot water production with solar collectors per year and efficiency, estimated for Paris	71
Table 29 – Estimation of the expected storage tank cooling with unglazed solar collectors	72
Table 30 – Main equations controlling the mechanical ventilation demanded flow rate	75
Table 31 – Heating demand in function of the outdoor temperature per percentage of time in the heating season	81
Table 32 – Domestic hot water consumption profiles, based on Danish SBI-direction 213 and EN 15316 3-1.....	86
Table 33 – Efficiency of the considered radiant floor sytem, based on EN 15316-2.1 (emission), EN 15316-2.3 (distribution)	87
Table 34 – Estimated energy consumption per year, in Paris.....	88
Table 35 – Estimated energy consumption per year, in Copenhagen	88
Table 36 – Comparison of the electricity consumed and produced with PVs consumed	90
Table 37 – Competition range of indoor temperature for getting 100% points.....	91
Table 38 – Percentage of time during the competition outside the considered comfort ranges.....	91
Table 39 – Range of absolute errors for the different sensor used	97
Table 40 – Uncertainty introduced when recorded data are time avaraged.....	97
Table 41 – Average temperature drop in the tank over the night, weather data and relative radiative and convective cooling power, calculated with physicalmodel	98
Table 42 – Comparison of the theoretical and measured average cooling power per night.....	98
Table 43 – Literature review on nighttime radiative cooling applications	104
Table 44 – Different physical models for cloudless sky	110
Table 45 – Average values of some Infrared Emissivities (Campbell, Norman, 1998)	111
Table 46 – Common properties for air at atmospheric pressure	114
Table 47 – Price of the three collectors investigated	117
Table 48 – Monthly optimal tilt in Copenhagen and Rome, for the production of electricity and sanitary hot water (Boxwell M., 2012. Solar Electricity Handbook)	120
Table 49 – Summarized data for the PVT in the experiment period	133
Table 50 – Summarized data for the unglazed collector in the experiment period	134
Table 51 – Radiative and convective components during the night of August 20 th -21 st	135
Table 52 – Unglazed collector main physical parameters	144
Table 53 – Flow rates for radiative cooling experiments.....	145
Table 54 – Flow rates used for the simulations	145
Table 55 – Average cooling power obtained with inlet water supplied always at 22°C over the night.....	147

Appendix

Annex 1: House envelope, materials properties

Layers from exterior to interior

External wall:

	Layer	1	2	3	4	5	6
Material		Plywood – wind protector	Glass Wool	Glass Wool	Vapour barrier	Glass Wool	Gypsum
Thermal Conductivity (λ)	W/(mK)	0,14	0,03	0,03	0,2	0,03	0,42
Density(ρ)	kg/m ³	530	30	30	620	30	1200
Specific Heat (C)	J/(kgK)	1800	670	670	1500	670	837
Thickness (L)	m	0,015	0,195	0,12	0,0002	0,045	0,013

External floor:

	Layer	1	2	3	4	5	6
Material		Bottom OSB	Glass Wool	OSB	Vapour barrier	Particle board - Floor heat	Porcelain Tiles
Thermal Conductivity (λ)	W/(mK)	0,13	0,03	0,13	0,2	7,7	1,5
Density(ρ)	kg/m ³	650	30	650	620	640	1950
Specific Heat (C)	J/(kgK)	2100	670	2100	1500	1000	800
Thickness (L)	m	0,004	0,295	0,015	0,0002	0,022	0,013

Roof:

	Layer	1	2	3	4	5	6	7
Material		Glass PV Panels	Wood Beams	OSB	Glass Wool	Vapour barrier	Glass Wool	Acoustic cladding
Thermal Conductivity (λ)	W/(mK)	1,06	0,14	0,13	0,03	0,2	0,03	0,072
Density(ρ)	kg/m ³	2500	450	650	30	620	30	480
Specific Heat (C)	J/(kgK)	840	2500	2100	670	1500	670	900
Thickness (L)	m	0,004	0,2	0,012	0,245	0,0002	0,095	0,025

First two upper layers are no considered in the calculation of the U-value (W/m²K), because ventilated.

Windows:

	Window	1	2	3	4
Localisation		South (Living Room)	South 23° Skylight	Norh (Flex Room)	North 67° Skylight (Bed Room)
Height	m	1,3	0,9	0,6	1,6
Width	m	2,35	1,3	2,3	0,9
Number Of Glazing		3	3	3	3
Frame Thermal Transmittance (Uf)	W/(m ² K)	1,7	1,7	1,7	1,7
Glazing Thermal Transmittance (Ug)	W/(m ² K)	0,62	0,5	0,62	0,5
Overall Thermal Transmittance (Uw)	W/(m ² K)	0,83	0,79	0,83	0,79
Light Transmission (Lt)	%	74	74	74	74
Solar Heat Gain Coefficient (Sw)	%	63	40	63	40
Sill Height	m	0	2,6	0	1,45
Offset Between The Glass And The Outside Wall	m	0,05	0	0,05	0

Doors:

	Glazing door	1	2	3
Localisation		East (Bedroom)	East (Flex room)	East (Kitchen)
Height	m	2,1	2,1	2,1
Width	m	0,9	0,9	1,8
Number Of Glazing		3	3	3
Frame Thermal Transmittance (Uf)	W/(m ² K)	1,7	1,7	1,7
Glazing Thermal Transmittance (Ug)	W/(m ² K)	0,62	0,62	0,62
Overall Thermal Transmittance (Uw)	W/(m ² K)	0,83	0,83	0,83
Light Transmission (Lt)	%	74	74	74
Solar Heat Gain Coefficient (Sw)	%	63	63	63
Sill Height	m	0	0	0
Offset Between The Door And The Outside Wall	m	0,05	0,05	0,05

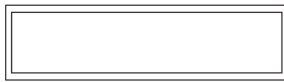
Windows



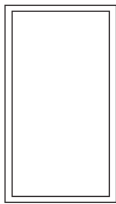
South (Living Room)
Size: 2350x1300mm
Type: Futura+i (Idealcombi)
Thermal Transmittance: $U = 0.83 \text{ W/m}^2\text{K}$



South 23 degree Skylight
Size: 1300x900mm
Type: Vitral A98
Thermal Transmittance: $U = 0.79 \text{ W/m}^2\text{K}$



North (Flex Room)
Size: 2300x600mm
Type: Futura+i (Idealcombi)
Thermal Transmittance: $U = 0.83 \text{ W/m}^2\text{K}$



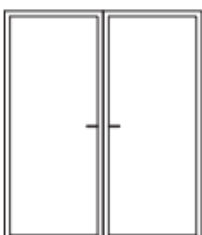
North 67 degree Skylight (Bed Room)
Size: 900x1600mm
Type: Vitral A98
Thermal Transmittance: $U = 0.79 \text{ W/m}^2\text{K}$



External door east - Bed Room
Size: 2100x900mm
Type: Futura+i (Idealcombi)
Thermal Transmittance: $U = 0.83 \text{ W/m}^2\text{K}$



External door east - Flex Room
Size: 2100x900mm
Type: Futura+i (Idealcombi)
Thermal Transmittance: $U = 0.83 \text{ W/m}^2\text{K}$



External door east - Kitchen
Size: 2100x1800mm
Type: Futura+i (Idealcombi)
Thermal Transmittance: $U = 0.83 \text{ W/m}^2\text{K}$

Doors

Annex 2: Tanks size and losses

Tapping program n° 2 from EN 153163-1									
No	Time of the day	Energy E_{tap}	Accumulation of E_{tap}	Flow rate	Volume tapped for each draw-off ($\Delta T = 45^{\circ}C$, tapping at $55^{\circ}C$)	Duration of the draw-off	Duration from 7:00	Δt (duration from 7:00 to the end of the current tapping)	E1 Energy content of the tank
	hh/mm	kWh	kWh	L/min	L	min	min	min	kWh
1	07:00	0,105	0,105	3	2,01	0,67	0,00	0,67	0,097
2	07:15	1,4	1,505	6	26,76	4,46	15,00	19,46	1,267
3	07:30	0,105	1,61	3	2,01	0,67	30,00	30,67	1,234
4	08:01	0,105	1,715	3	2,01	0,67	61,00	61,67	0,960
5	08:15	0,105	1,82	3	2,01	0,67	75,00	75,67	0,893
6	08:30	0,105	1,925	3	2,01	0,67	90,00	90,67	0,814
7	08:45	0,105	2,03	3	2,01	0,67	105,00	105,67	0,736
8	09:00	0,105	2,135	3	2,01	0,67	120,00	120,67	0,657
9	09:30	0,105	2,24	3	2,01	0,67	150,00	150,67	0,394
10	10:30	0,105	2,345	3	2,01	0,67	210,00	210,67	-0,236
11	11:30	0,105	2,45	3	2,01	0,67	270,00	270,67	-0,866
12	11:45	0,105	2,555	3	2,01	0,67	285,00	285,67	-0,945
13	12:45	0,315	2,87	4	6,02	1,51	345,00	346,51	-1,375
14	14:30	0,105	2,975	3	2,01	0,67	450,00	450,67	-2,546
15	15:30	0,105	3,08	3	2,01	0,67	510,00	510,67	-3,176
16	16:30	0,105	3,185	3	2,01	0,67	570,00	570,67	-3,806
17	18:00	0,105	3,29	3	2,01	0,67	660,00	660,67	-4,803
18	18:15	0,105	3,395	3	2,01	0,67	675,00	675,67	-4,882
19	18:30	0,105	3,5	3	2,01	0,67	690,00	690,67	-4,961
20	19:00	0,105	3,605	3	2,01	0,67	720,00	720,67	-5,224
21	20:30	0,735	4,34	4	14,05	3,51	810,00	813,51	-5,626
22	21:15	0,105	4,445	3	2,01	0,67	855,00	855,67	-6,037
23	21:30	1,4	5,845	6	26,76	4,46	870,00	874,46	-4,868

DHW tank losses:

Tank volume	0,18	m ³			
Outer diameter of the tank d_y , without insulation	0,43	m			
Height of the tank H, without insulation	1,22	m			
Insulation thickness	0,05	m	(insulation thickness same for all sides)		
Insulation thermal conductivity	0,04	W/mK			
U-values of the tank			Heat transfer coefficients α		
top	0,14	W/K	top	10	W/m ² K
bottom	0,13	W/K	bottom	5,88	W/m ² K
side	1,35	W/K	side	7,69	W/m ² K
Total U-value	1,61	W/K			

Temperature difference	20	K	(40°C average water T, and 20°C indoor)		
Heat losses from tank	0,032	kW			

Buffer tank, cooling: heat gains

Tank volume	0,75	m ³			
Outer diameter of the tank d_y , without insulation	0,79	m			
Height of the tank H, without insulation	1,66	m			
Insulation thickness	0,085	m	(insulation thickness same for all sides)		
Insulation thermal conductivity	0,04	W/mK			
U-values of the tank			Heat transfer coefficients α		
top	0,27	W/K	top	10	W/m ² K
bottom	0,26	W/K	bottom	5,88	W/m ² K
side	2,03	W/K	side	7,69	W/m ² K
Total U-value	2,56	W/K			

Temperature difference	10	K	(16°C average water T, and 26°C indoor)		
Heat gains from tank	0,026	kW			

Buffer tank, heating: heat loss

Tank volume	0,75	m ³			
Outer diameter of the tank d_y , without insulation	0,79	m			
Height of the tank H, without insulation	1,66	m			
Insulation thickness	0,085	m	(insulation thickness same for all sides)		
Insulation thermal conductivity	0,04	W/mK			
U-values of the tank			Heat transfer coefficients α		
top	0,27	W/K	top	10	W/m ² K
bottom	0,26	W/K	bottom	5,88	W/m ² K
side	2,03	W/K	side	7,69	W/m ² K
Total U-value	2,56	W/K			
Temperature difference	15	K	(30°C average water T, and 20°C indoor)		
Heat losses from tank	0,038	kW			

Annex 3: Solar collectors' data

Batec solar collectors

Datablad for solfanger			
Typebetegnelse:	BA22	Datablad: D 1 03 04	
Fabrikant/levendør:	BATEC Solvarme A/S		
Adresse:	Danmarksvej 8, 4681 Herfølge		
Telefon:	56 27 50 50		
Email:	admin@batec.dk		
Hjemmeside:	www.batec.dk		
Areal af én solfanger:	2,190 m ²	Inddata til Be10 (x antal solf.)	At
Starteffektivitet:	0,767 -	Inddata til Be10	η_0
1. ordens varmetabskoeff.:	3,867 W/(m ² K)	Inddata til Be10	a_1
2. ordens varmetabskoeff.:	0,0100 W/(m ² K ²)	Inddata til Be10	a_2
Vinkelafhængighed	0,95 -	Inddata til Be10	K(50°)
Nominel effekt:	1,406 kW	Ved G = 1000 W/m ² , T _m = 50 °C, T _a = 20 °C	
Nominel årlig besparelse:	1,147 MWh/år	Beregnet med Be10 under referenceforhold	
Nom. årlig CO2-besp.:	0,241 ton/år	Svarende til ovenstående forbrug (naturgas)	
Max. temp. solfanger:	191 °C	Ved G = 1000 W/m ² , T _a = 30 °C	
Basis for godkendelse:	EN prøvning	Prøvningsinstitut/år:	SP - P6 03278_BA
Installationsvejledning:	Installation BATEC	År:	1999
Brugervejledning:	Brugervejledning BATEC	År:	1999
Bemærkninger:	-		
Udstedende instans:	PlanEnergi Sjælland, Aggerupvej 1, 4330 Hvalsø		
Kontaktperson:	Daniel Trier		
Telefon:	25 17 04 00		
E-mail:	godkendelser@planenergi.dk		
<u>Bestemmelse af varmeveksler effektivitetsfaktor til brug i Be10 (Be10 er beskrevet i SBI anvisning 213)</u>			
Effektivitetsfaktoren kan sættes til 0,90 ELLER beregnes af:			
Effektivitetsfaktor =	1,00 -	6,50 * Antal solfanger	/ UAsol
UAsol fås fra	beholderdatablad		

Figure 135 – Specifications of the BA22 from Batec

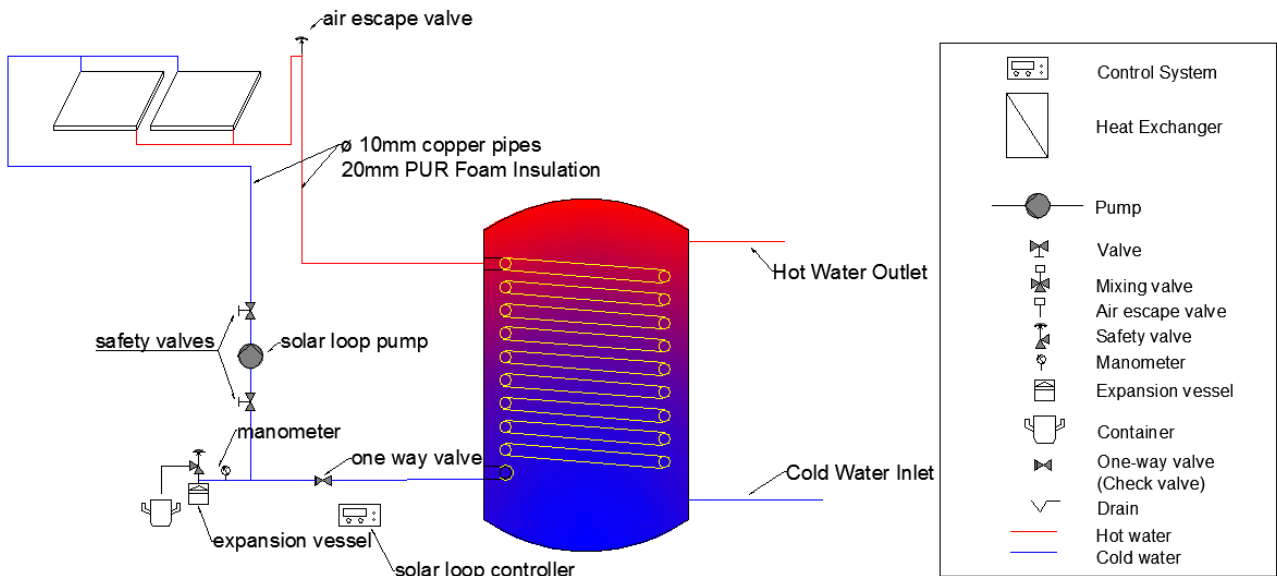


Figure 136 – Scheme of the solar collectors' connection with the DHW tank (integrated in the Nilan Compact P).

Unglazed solar collectors:

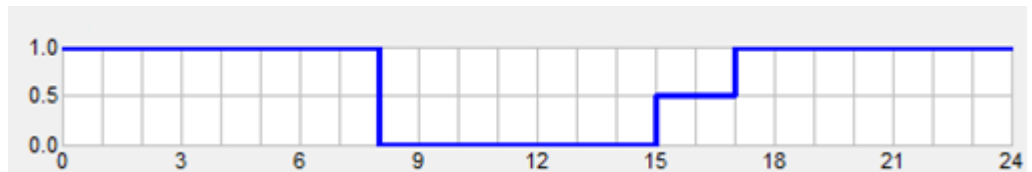
Solar panels. Made in black UV resistant polypropylen (PP).

Size W X L, cm	120 x 200	or	60 x 6000
Connection for hose, external diameter, mm	50		
Thickness, mm	5		
Panel area, m ²	2,4		
Maximum working pressure, Bar	1		
Maximum flow, l/h	240		
Maximum temperature, °C	80		
Pressure drop, Bar	0,01		

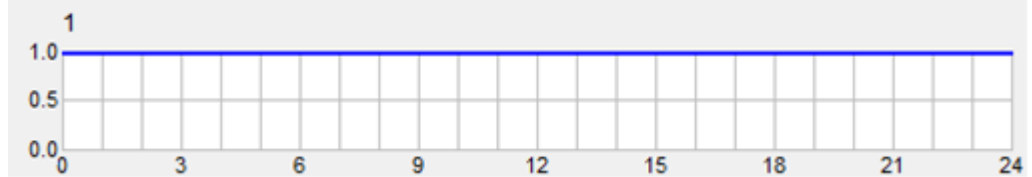
Annex 4: Dynamic simulation schedules

Occupants presence:

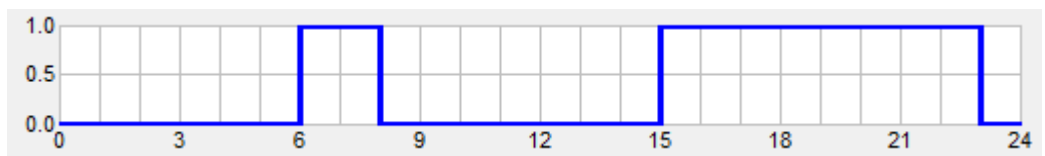
Monday - Friday



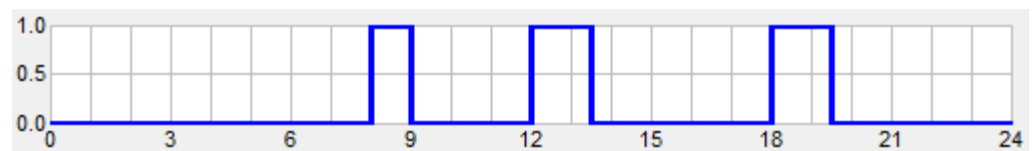
Weekend



Artificial light (all week same schedule):



Kitchen appliances (all week same schedule):



Annex 5: Hydraulic scheme, domestic hot water and space heating/cooling losses

Water pipes

The pipes from the domestic hot water tank to the distribution point are made of PEX 15x2,5 mm. All the hot water pipes will be insulated with at least 15 mm PUR foam with a thermal conductivity of 0,04 W/mK. Thermal resistance of the pipes material has been considered. The thermal conductivity of the PEX is assumed to be 0,4 W/mK. The outer surface heat transfer coefficient of the insulated pipe a_2 is 9 W/m²K.

The waiting time has been calculated just for the kitchen sink. This terminal has been selected because is the furthest one designed for a small tapping of 0,15 l/s. Also the heat flow coefficient [W/mK] and the Φ , heat loss of pipe [W] have been calculated for the kitchen sink flow/routing.

- Waiting time $t = 9$ sec. (domestic hot water loop)

Assumptions:

- Small flow rate of 3 l/min, 0,105 kWh
- Further tapping at a distance of 5,8 m
- Pipe 15x2,5mm, PEX

$$t = \frac{\pi \cdot d_i^2 \cdot L}{4 \cdot q}$$

Where

t is the waiting time (s)

d_i is the internal diameter of the pipe (m)

L is the pipe length (m)

q is the volume flow rate (m³/s)

- Heat loss coefficient U_1 [W/m·K]

<p><u>Domestic hot water loop = 0,188</u></p> <p>Assumptions:</p> <ul style="list-style-type: none"> • Pipe 15x2,5mm, PEX, $\lambda=0,4$ W/m·K • 15 mm insulation, $\lambda=0,04$ W/m·K 	<p><u>Space heating/cooling loop = 0.21</u></p> <p>Assumptions:</p> <ul style="list-style-type: none"> • Pipe 18x2,5mm, PEX, $\lambda=0,4$ W/m·K • 15 mm insulation, $\lambda=0,04$ W/m·K
---	---

$$U_1 = \frac{\pi}{\frac{1}{2 \cdot \lambda_p} \cdot \ln\left(\frac{d_e}{d_i}\right) + \frac{1}{2 \cdot \lambda_{ins}} \cdot \ln\left(\frac{d_{ins}}{d_e}\right) + \frac{1}{h \cdot d_{ins}}}$$

Where

λ_p is thermal conductivity of the pipe (W/m·K)

d_i is the internal diameter of the pipe (m)

d_e is the external diameter of the pipe (m)
 λ_{ins} is thermal conductivity of the insulation (W/m·K)
 d_{ins} is the external diameter with the insulation (m)
 h is the surface transfer coefficient (W/m²·K)

- Heat loss of pipe Φ [W]

<u>Domestic hot water = 35,4</u>	<u>Space heating = 5,3</u>	<u>Space cooling = 6,4</u>
Assumptions: <ul style="list-style-type: none"> • Pipe 15x2,5mm, PEX • 15 mm insulation with $\lambda=0,04$ W/m·K • Length 5,8 m • Average water 52,5 °C, room 20 °C 	Assumptions: <ul style="list-style-type: none"> • Pipe 18x2,5mm, PEX • 15 mm insulation with $\lambda=0,04$ W/m·K • Length 3 m (distance to the upper floor) • Average water 28,4 °C, room 20 °C 	Assumptions: <ul style="list-style-type: none"> • Pipe 15x2,5mm, PEX • 15 mm insulation with $\lambda=0,04$ W/m·K • Length 3 m (distance to the upper floor) • Average water 15,74 °C, room 26 °C

$$\Phi = U_1 \cdot |T - T_e| \cdot L$$

Where

T is the average temperature water in the pipe (°C)

T_e is the ambient temperature (°C)

L is the pipe length (m)

Regarding space heating and cooling, the design demand for the upper floor (bedroom) is considered to calculate the distribution losses. This approach has been selected to be on the safe side, since the bedroom is the furthest room. Based on this demand, according to EN 1264 part 2 and 5, the supply temperatures have been calculated both for heating and cooling. The average water temperature in the distribution pipes is assumed to be the same as the supply temperature, because of the short pipe length, between the generator and the emitter.

The so obtained losses have been divided by the corresponding room demand, in order to obtain the distribution efficiency in percentage.

	Room demand [W]	Heat loss of pipe Φ [W]	Distribution efficiency [%]
Heating	560	5,3	0,99
Cooling	375	6,4	0,98

Radiant floor: heat losses for the heat emission system, method using efficiencies of the emission system.

Emission losses are due to three factors, namely, non-uniform temperature distribution, losses to the outside from embedded heating devices in the structure, and losses due to non-perfect control of the indoor temperature (Olesen B. W.,2007 based on EN15316-2.1).

The additional loss due to the heat emission Q_{em} , in kWh has been calculated with the following equation:

$$Q_{em} = \left(\frac{f_{rad} \cdot f_{int} \cdot f_{hydr}}{\eta_{em}} - 1 \right) \cdot Q_H$$

where

Q_H is the net heating energy of a time period (EN ISO 13790), in kWh;

f_{hydr} is the factor for the hydraulic equilibrium;

f_{int} is the factor for intermittent operation;

f_{rad} is the factor for the radiation effect (only relevant for radiant systems)

η_{em} is the emission efficiency

The total efficiency η_{em} has been obtained as

$$\eta_{em} = \frac{1}{(4 - (\eta_{str} \cdot \eta_{ctr} \cdot \eta_{emb}))}$$

where

η_{str} is the part of the efficiency which takes into account the level of uniformity in the temperature distribution

η_{ctr} is the part of the efficiency which takes into account the kind of temperature control regulation

η_{emb} is the part of the efficiency which considers the position of the emitter (embedded pipes or free surface)

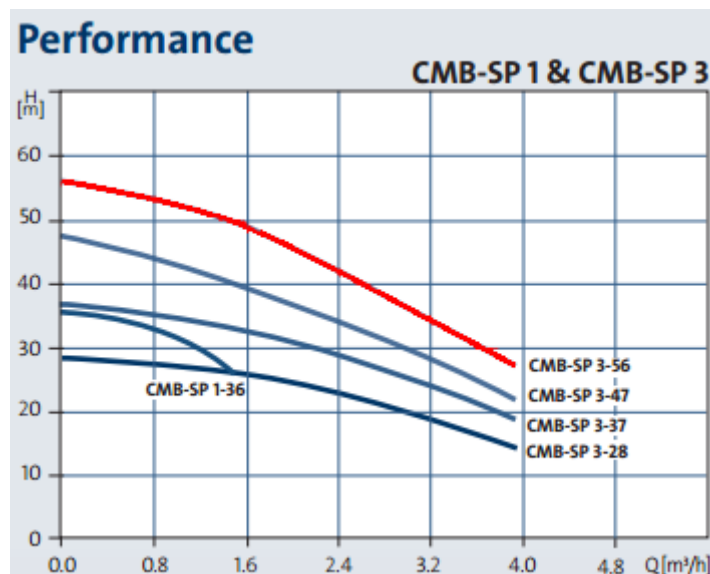
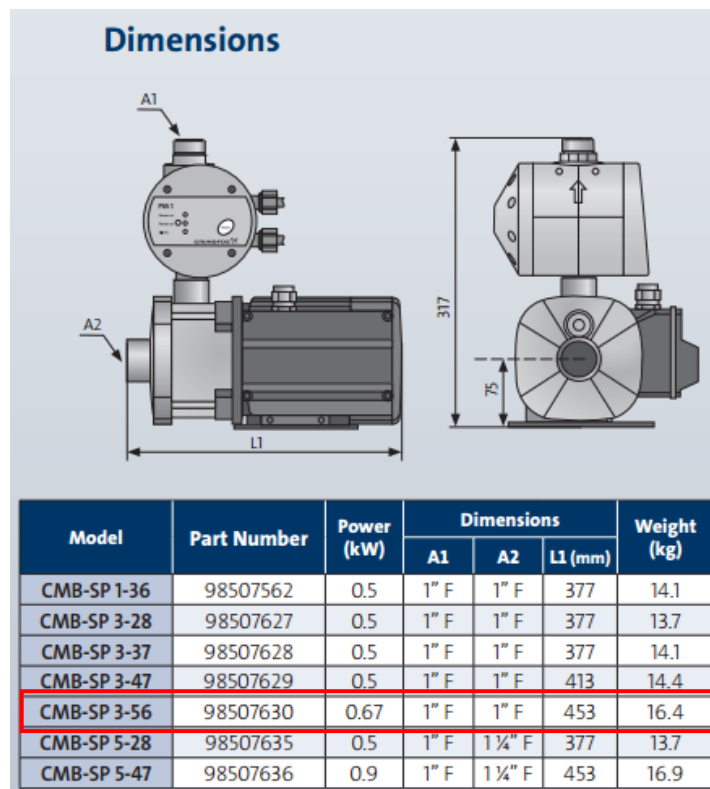
The value selected for the specific parameters is exposed in the further table:

Emitter	f_{rad}	f_{int}	f_{hydr}	η_{str}	η_{ctr}	η_{emb1}	η_{emb}	η_{em}
						η_{emb2}	$\frac{(\eta_{emb1} + \eta_{emb2})}{2}$	
Floor heating	1	0,98	1,03	1	0,95	0,98	0,985	0,94
						0,99		
Additional info			<i>Not balanced</i>	<i>Floor heating</i>	<i>PI-control</i>	<i>Dry system</i> <i>Extra insulation downward</i>		
Floor cooling	1	0,98	1,03	0,93	0,95	0,93	0,96	0,86
						0,99		
Additional info			<i>Not balanced</i>	<i>Ceiling heating</i>	<i>PI-control</i>	<i>Dry-system ceiling heating (similar to floor cooling)</i> <i>Extra insulation downward</i>		

Annex 6: Pumps data and consumption

Pumps data:

Use	Model	Power (W)	Max flow expected (m ³ /h)	Max pressure expected (m)
Water supply	CMB-SP 3-56	670	1,8	25



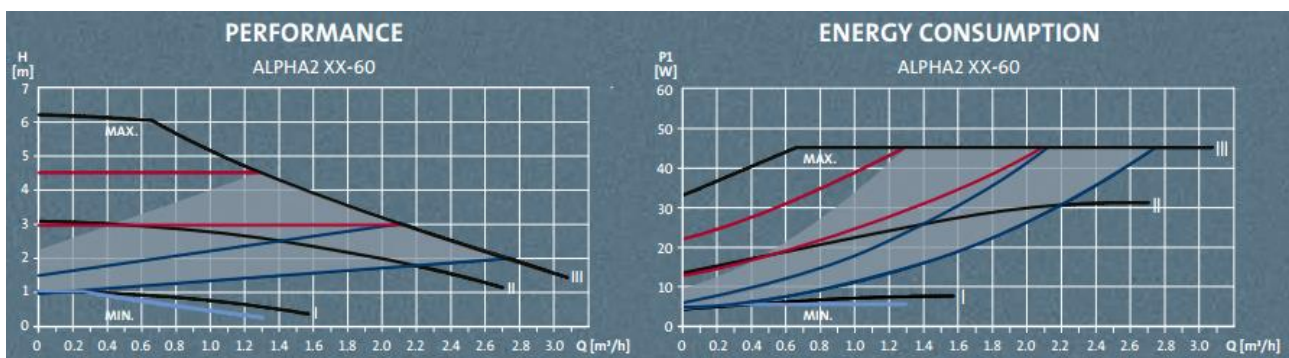
Use	Model	Power (W)
-----	-------	-----------

Drain exhaust	water	SoloLift2 C-3	640
---------------	-------	---------------	-----

Use	Model	Power (W)	Max flow expected	Max pressure drop expected (m)
Glazed Solar Collectors	ALPHA2 15-40 (15 = Φ 15mm) (4=4m)	up to 22, 32 or 45 W. Expected average = 15 (Speed2).	from 0,2 to 0,4 $l/min \cdot m^2$. Tot ~ 4 m^2 . (max 0,1 m3/h)	4

Use	Model	Power (W)	Max flow expected	Max pressure drop expected (m)
Unglazed Solar Collectors	ALPHA2 15-40 (15 = Φ 15mm) (4=4m)	up to 22, 32 or 45 W. Expected average = 6 (Speed1).	around 1 $l/min \cdot m^2$. Tot ~ 14,4 m^2 . (max 0,85 m3/h)	1

Use	Model	Power (W)	Max flow expected (m3/h)	Max pressure drop expected (m)
Radiant floor (integrated in Uponor system)	Alpha2 15-60 (the heat pump has 5,6 m < 6 m, no risk of bypassing the radiant floor)	up to 22, 32 or 45 W. Expected average = 22.	1 (to provide 45 W/m2 in all room for cooling)	1,53 (15,000 Pa)



Energy consumption of the pumps

Hot water Solar collector pump:

Month	Hh	% Solar Irradiance paris	Monthly Hours of operation, according to EN 12976 (2000h TOT)	Pump energy Consumption kWh
Jan	941	0,02	48	0,72
Feb	1600	0,04	90	1,35
Mar	2940	0,08	166	2,49
Apr	4610	0,12	236	3,53
May	5290	0,14	272	4,08
Jun	5820	0,15	266	3,99
Jul	5540	0,14	266	3,99
Aug	4740	0,12	251	3,76
Sep	3630	0,09	182	2,74
Oct	2080	0,05	114	1,71
Nov	1110	0,03	53	0,80
Dec	775	0,02	38	0,57
Year	39076			30

Hh: Irradiation on horizontal plane (Wh/m²/day)

All pumps:

Heating season:

Pump	Model	Max Power (kW)	Average power (kW)	Time of use per day (h)	Additional info	Energy per day kWh
Fresh water circulation	Grundfos CMB-SP 3-56	0,67	0,67	0,44	(Based on EN 15316-1 (program n°2))	0,29
Sewerage	Grundfos Sololift2 C3	0,64	0,64	0,44	-	0,28
Radiant floor	Grundfos Apha 2 (5-45 W)	0,045	0,022	12,0	(Average time based on simulations)	0,26
Solar collectors	Grundfos ALPHA2 15-40 (5 - 45 W)	0,048	0,015	See "Solar collectors loop" previous table		
Unglazed solar collectors	Grundfos ALPHA2 15-40 (5 - 45 W)	0,07	0,006	0	-	0,00
Buffer tank-Heat pump loop	Integrated in the heat pump (5.6 m pressure)	0,05	0,04	1,7	-	0,06

Cooling season:

Pump	Model	Max Power (kW)	Average power (kW)	Time of use per day (h)	Additional info	Energy per day kWh
Fresh water circulation	Grundfos CMB-SP 3-56	0,67	0,67	0,44	(Based on EN 15316-1 (program n°2))	0,29
Sewerage	Grundfos Sololift2 C3	0,64	0,64	0,44	-	0,28
Radiant floor	Grundfos Apha 2 (5-45 W)	0,045	0,022	8,0	(Average time based on simulations)	0,18
Solar collectors	Grundfos ALPHA2 15-40 (5 - 45 W)	0,048	0,015	See "Solar collectors loop" previous table		
Unglazed solar collectors	Grundfos ALPHA2 15-40 (5 - 45 W)	0,07	0,006	8	-	0,05
Buffer tank-Heat pump loop	Integrated in the heat pump	0,05	0,04	0,6	-	0,02

Transition periods (no cooling or heating)

Pump	Model	Max Power (kW)	Average power (kW)	Time of use per day (h)		Energy per day kWh
Fresh water circulation	Grundfos CMB-SP 3-56	0,67	0,67	0,44	(Based on EN 15316-1 (program n°2))	0,29
Sewerage	Grundfos Sololift2 C3	0,64	0,64	0,44		0,28
Radiant floor	Grundfos Apha 2 (5-45 W)	0,045	0,022	0,0	(Average time based on simulations)	0,00
Solar collectors	Grundfos ALPHA2 15-40 (5 - 45 W)	0,048	0,015	See "Solar collectors loop" sheet		
Unglazed solar collectors	Grundfos ALPHA2 15-40 (5 - 45 W)	0,07	0,006	0		0,00
Buffer tank-Heat pump loop	Integrated in the heat pump	0,05	0,04	0,0		0,00

Total yearly energy consumption estimated is 320 kWh, which is around 4 kWh/m² (gross floor area).

Dwellings are conventionally connected to the city network which provides pressurized potable water and sewerage system. Removing the energy required by the potable water supply and waste water pumps, the new energy consumption is 110 kWh/year, which is around 1,4 kWh/m².

Annex 7: House appliances data and energy consumption



Fridge / freezer

Model name		ELECTROLUX EN3613AOW
Energy efficiency class A + + + (most efficient) to G (least efficient)		A + + +
Energy consumption	kWh/year kWh/day	156 0,427
Net capacity, overall refrigerator compartment	L	245
Net capacity, freezer	L	90
Sound level	dB(A)	39

Washing machine

Connected to the hot water circuit (HWC). The heat is mainly provided by solar collectors and transferred to the machine through an heat exchanger.

Model name		SIEMENS WM14Q410DN
Nominal capacity	kg	7,0
Energy efficiency class A + + + (most efficient) to D (lowest efficiency)		A + + +
Annual energy consumption	kWh / year	174
Energy consumption Cottons 60 ° C at full load	kWh	0,81
Energy consumption 60 ° C cotton at partial load	kWh	0,78
Energy consumption cotton 40 ° C at partial load	kWh	0,66
Water Consumption per cycle	L/cycle	from 34 to 66 lt (59 average)
Washing class		A

A + + + (most efficient) to D (lowest efficiency)		
Spinning class A + + + (most efficient) to D (lowest efficiency)		B

Cloth dryer

The company Miele has developed a low energy dryer that uses the heat from solar collector to dry clothes¹. As for domestic hot water, the solar fluid heats the water in a water tank. The hot water then flows to the dryer and heats up the air in the tumble via a heat exchanger. The cooled water returns to the tank to be reheated and reused. In another loop cold water is supplied to the dryer to condensate the water and remove moisture from the dryer. This warmer water is also going back to the tank where it can be reheated. The operation of the solar dryer is shown in the figure below. The product code is T8881S.

This technology enables a saving of up to 80% of the operational cost compared to a condenser dryer. The primary energy efficiency can reach 80%. This results in a consumption of 0,74 kWh per cycle of 116 min (7 kg).

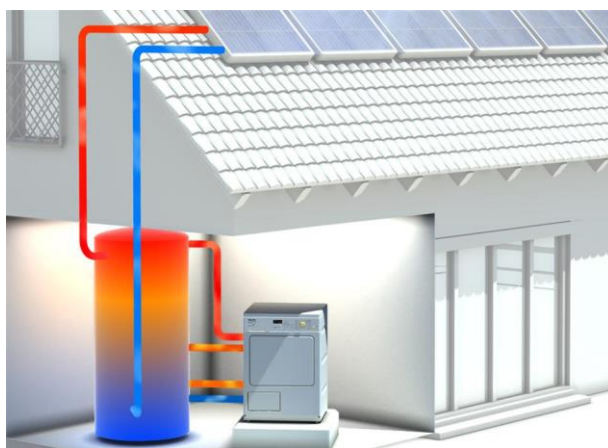


Figure 137 – Schematic representation of the connections of the dryer Miele T 8881 S. Picture extract from Miele website.

Miele		
Model name		T 8881 S
Nominal capacity	kg	7
Energy efficiency class		
A + + + (most efficient) to D (lowest efficiency)		A + + +
Annual energy consumption (AEC 2) 3)	kWh / year	95
Energy consumption of the standard cotton program 2)		
Energy consumption at full load (Edry)	kWh	0,74
Energy consumption at partial	kWh	0,45

¹ http://www.miele-presse.de/de/en/press/article/artikel_123_2011.aspx

load (Edry ½)		
Condensation efficiency class 2)		
Condensation efficiency		
A (most efficient) to G (least efficient)		A
Condensation efficiency at full load (Cdry)	%	92
Condensation efficiency at partial load (Cdry ½)	%	90

Dishwasher

Connected to the hot water circuit (HWC). The heat is mainly provided by solar collectors and transferred to the machine through an heat exchanger.

Model name		Smeg STA4525
Annual water consumption	L/year	2660,00
Energy efficiency class		A++
Efficiency class of washer		A
Energy efficiency class of dryer		A
Energy consumption (for a standard program cycle)	kWh	0,74
Water consumption (for a standard program cycle)	L	9,5
Number of place settings		10

Oven

Model name	Whirlpool Induction Oven - 6th sens Starclean- Ligne Fusion AKZM 89/20/GK		
Product size-cavity	Large		
Height of product (mm)	595		
Width (mm)	595		
Depth (mm)	564		

Energy consumption natural convection (kWh)	0,89	Energy consumption forced air convection (kWh)	0,69
Energy efficiency class	A (without the induction tray)		

Stove

Model name		Whirlpool ACM 804/BA
Number of induction plates		4
Depth	mm	510
Width	mm	580
Number of power levels		9
Booster		yes
Pan detection		yes
Electrical connection rating	W	7200

Television

Philips 3000 series Full HD Slim LED TV with Digital Crystal Clear

Picture/Display <ul style="list-style-type: none">• Display: LED Full HD• Diagonal screen size: 40 inch / 102 cm• Panel resolution: 1920x1080p• Aspect ratio: 16:9• Brightness: 300 cd/m²• Picture enhancement: Digital Crystal Clear, 100 Hz	Power <ul style="list-style-type: none">• Mains power: AC 220 - 240 V 50/60Hz• Ambient temperature: 5 °C to 35 °C• Energy Label Class: A+• Eu Energy Label power: 44 W• Annual energy consumption: 64 kW•h• Standby power consumption: <0,15W• Power Saving Features: Auto switch-off timer, Eco mode, Picture mute (for radio)• Off mode power consumption: < 0,15 W
--	---

Computer screen

LG, LED LCD monitor model 27EA33V

DVD/Blu-ray player

LG, Blu-ray Disc™ Player, model BP125

- Blu-ray Disc™ Playback
- DVD Playback
- Full HD 1080p Upscaling
- Dolby® Digital/TrueHD
- DTS-HD
- Power 12 W
- Stand-by mode 0,5 W

Calculated power and energy consumption

	kWh/year from Standard 4525	kWh/year calculated	Kwh per cycle	N° of time per week	N°of weeks	Min. per cycle	kWp	kW average
Dryer with DHW	95	65	0,74	2	44	116		
Fridge-freezer	156	156	-	-	-	-	-	0,02
Stove	-	370	1,2	7	44	40	7,2	1,8
Oven	-	86	0,65	3	44	60	3,65	0,7
Dishwasher	210	163	0,74	5	44	175		1,3
Clothes washer	174	44	0,5	2	44	60		0,5
Television/Computer	-	53	0,2	6	44	320	-	0,05
TOT	-	1024 ¹						

¹ 272 KWh/year from appliances with hot water connection, 752 KWh/year from appliances connected just to electricity

Annex 8: EN 1264 part 2 and 5 calculations

Input data

Above the pipes:

Tiles covering

	Thermal conductivity (λ)	Thickness (d)	Resistance
	W/(mK)	m	m ² K/W
Indoor surface	-	-	*
Floor tiles (ceramic)	1,500	0,013	0,009
Rubber	0,09	0,0013	0,014
TOT	0,622	0,0143	0,023

Linoleum covering

	Thermal conductivity (λ)	Thickness (d)	Resistance
	W/(m·K)	m	m ² ·K/W
Indoor surface	-	-	*
Linoleum	0,160	0,002	0,0125
Chipboard/wood	0,150	0,015/0,007	0,1/0,047
TOT	0,15	0,017/0,009	0,113/0,059

The thermal output of the linoleum floor covering has been calculated for two chipboard thicknesses.

*	Total exchange coefficient W/m ² K	
	Heating	Cooling
Floor, indoor	10,8	7
Floor, outdoor	25	25

Below the pipes:

MATERIAL	THERMAL CONDUCTIVITY (λ)	THICKNESS (d)	Resistance
	W/(mK)	m	m ² K/W
Aluminum	226	0,001	0,0000043
Particle board - Floor heat	0,15	0,022	0,15
Vapour barrier	0,2	0,0002	0,00
OSB	0,13	0,015	0,12
Glass Wool	0,03	0,295	9,83
Bottom OSB	0,13	0,004	0,03
Outdoor surface	-	-	0,04

Characteristic curve calculation:

Method 1

Heating		Tiles	Wood
B		6,5	
Pipe spacing T	m	0,2	
Thickness of the weight-bearing layer Su	m	0	0,015
Conductivity of the weight-bearing layer λ_E	W/mK	0	0,15
Ratio S_u/λ_E	K/W	0	0,1
Pipe spacing factor aT		1,1	1,075
mT		-1,67	
Covering factor aU		1,49	0,71
Factor bU		0,5	
Characteristic value KWL(L=T)		1,81	1,81
Characteristic value KWL(L=0)		0	0
aWL(KWL=0)		0,37	
aWL(KWL= ∞)		1,06	
aWL(L=T)		1,05	1,05
aWL(L=0)		0,37	
Length of the heat conduction device L	m	0,158	
Heat conduction factor aWL		1,05	1,05
Correction factor for the contact aK		0,92	
f(T)		1,197	
Resistance of floor covering $R_{\lambda B}$		0,023	0,0125
aB		0,82	0,94
Equivalent heat transmission coefficient KH heating		6,50	3,75

Cooling

	Tiles	Wood		Tiles	Wood
Resistance of floor covering $R \cdot \lambda_B$	0,150	0,15		0	0
aB	0,413	0,583		1	1
Equivalent heat transmission coefficient $K \cdot H_{\text{floor}}$	3,27	2,32		7,92	3,98

Equivalent heat transmission coefficient KH cooling	Tiles	Wood
	4,67	3,06

Method 2

Heating		Tiles	Wood
B		6,5	
Pipe spacing T	m	0,2	
Thickness of the weight-bearing layer Su	m	0,0013	0,015
Conductivity of the weight-bearing layer λ_E	W/mK	0,09	0,15
Ratio S_u/λ_E	K/W	0,014	0,1
Pipe spacing factor aT		1,1	1,075
mT		-1,67	
Covering factor aU		1,29	0,71
Factor bU		0,5	
Characteristic value KWL(L=T)		1,81	1,81
Characteristic value KWL(L=0)		0	0
aWL(KWL=0)		0,37	
aWL(KWL= ∞)		1,06	
aWL(L=T)		1,05	1,05
aWL(L=0)		0,37	
Length of the heat conduction device L	m	0,158	
Heat conduction factor aWL		1,05	1,05
Correction factor for the contact aK		0,92	
f(T)		1,197	
Resistance of floor covering $R_{\lambda B}$		0,009	0,0125
aB		0,93	0,94
Equivalent heat transmission coefficient KH heating		6,40	3,75

Cooling

	Tiles	Wood		Tiles	Wood
Resistance of floor covering $R \cdot \lambda_B$	0,150	0,15		0	0
aB	0,413	0,583		1	1
Equivalent heat transmission coefficient $K \cdot H_{\text{floor}}$	3,27	2,32		7,93	3,98

Equivalent heat transmission coefficient KH cooling	Tiles	Wood
	5,08	3,06

Method 3

Heating		Tiles	Wood
B		6,5	
Pipe spacing T	m	0,2	
Thickness of the weight-bearing layer Su	m	0,0143	0,015
Conductivity of the weight-bearing layer λ_E	W/mK	0,619	0,150
Ratio S_u/λ_E	K/W	0,023	0,100
Pipe spacing factor aT		1,103	1,075
mT		-1,67	
Covering factor aU		1,19	0,71
Factor bU		0,5	
Characteristic value $K_{WL}(L=T)$		1,84	1,81
Characteristic value $K_{WL}(L=0)$		0	0
$a_{WL}(K_{WL}=0)$		0,37	
$a_{WL}(K_{WL}=\infty)$		1,06	
$a_{WL}(L=T)$		1,05	1,05
$a_{WL}(L=0)$		0,37	
Length of the heat conduction device L		m	
Heat conduction factor aWL		1,05	1,05
Correction factor for the contact aK		0,92	
f(T)		1,197	
Resistance of floor covering $R_{\lambda B}$		0,000	0,0125
aB		1,00	0,94
Equivalent heat transmission coefficient KH heating		6,35	3,75

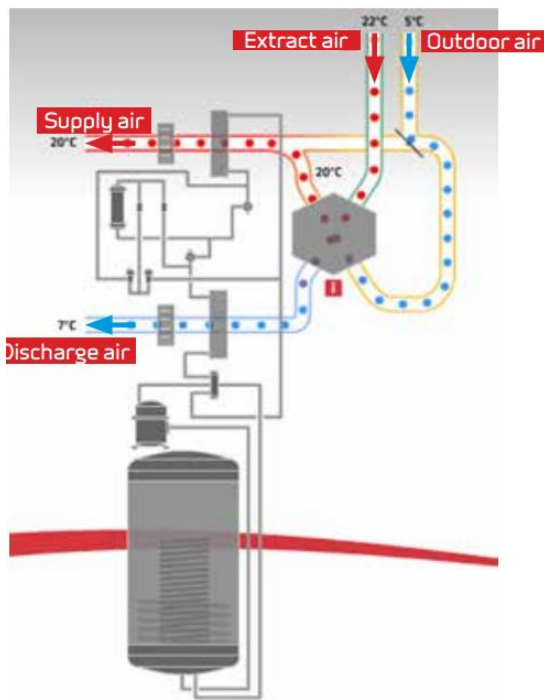
Cooling

	Tiles	Wood		Tiles	Wood
Resistance of floor covering $R \cdot \lambda B$	0,150	0,15		0	0
aB	0,467	0,583		1	1
Equivalent heat transmission coefficient $K \cdot H, \text{floor}$	2,97	2,32		6,35	3,98

Equivalent heat transmission coefficient KH cooling	Tiles	Wood
	4,59	3,06

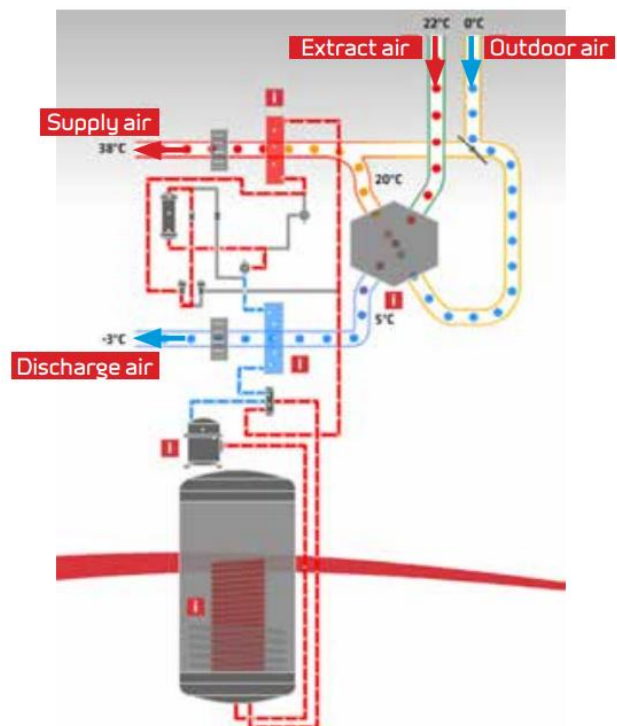
Annex 9: Nilan Compact P functions¹

“[...] Compact P recovers 100% of the heat in the extracted air. Via a counter flow heat exchanger, up to 95 % of the energy in the extracted air is used to heat the supply air. The built- in heat pump uses the remaining energy to further heat the supply air, while also producing hot water. [...] New homes are well insulated and therefore easy to heat. On the other hand, outdoor temperatures do not need to be very high before getting rid of the heat in the home becomes problematic. Compact P has a reversible cooling circuit, to cool the supply air. Due to the low air exchange, it will not function as an air conditioning system [...]”



Passive heat recovery

Passive heat recovery takes place via a counter flow heat exchanger with a high temperature efficiency, whereby the supply air is heated by the extracted air.

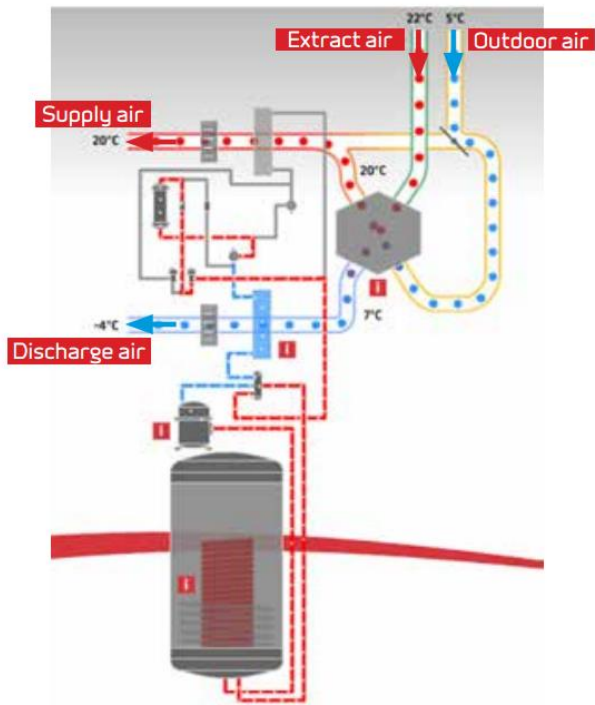


Passive and active heat recovery

Utilizing the residual energy that the counter flow heat exchanger does not use, the heat pump further heats the supply air.

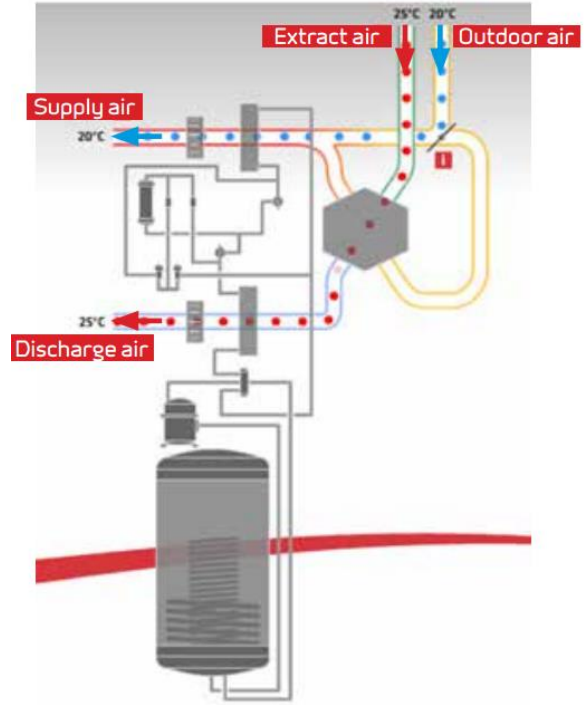
¹Pictures and text extracted from Nilan Compact P data sheet:

<http://www.nilan.dk/en-gb/frontpage/solutions/domestic-solutions/compact-solutions/compact-p.aspx>



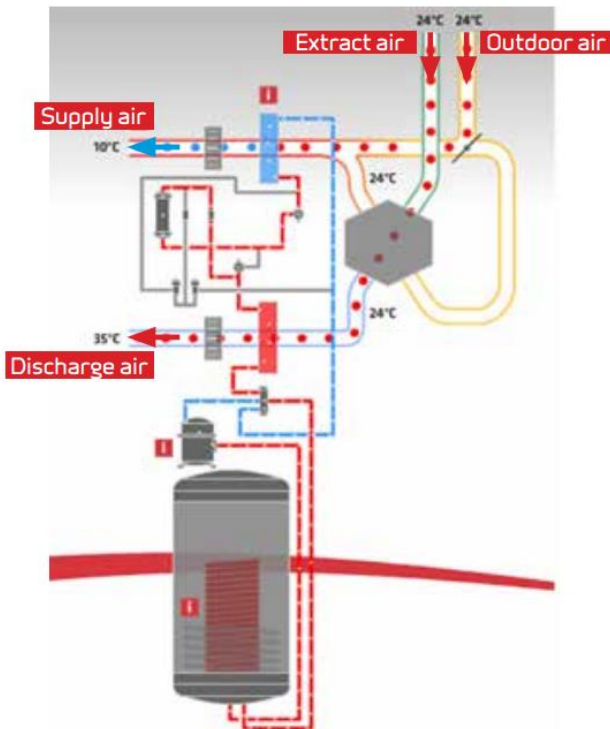
Hot water

Utilizing the residual energy that the counter flow heat exchanger does not use, the heat pump produces hot water.



100% bypass function

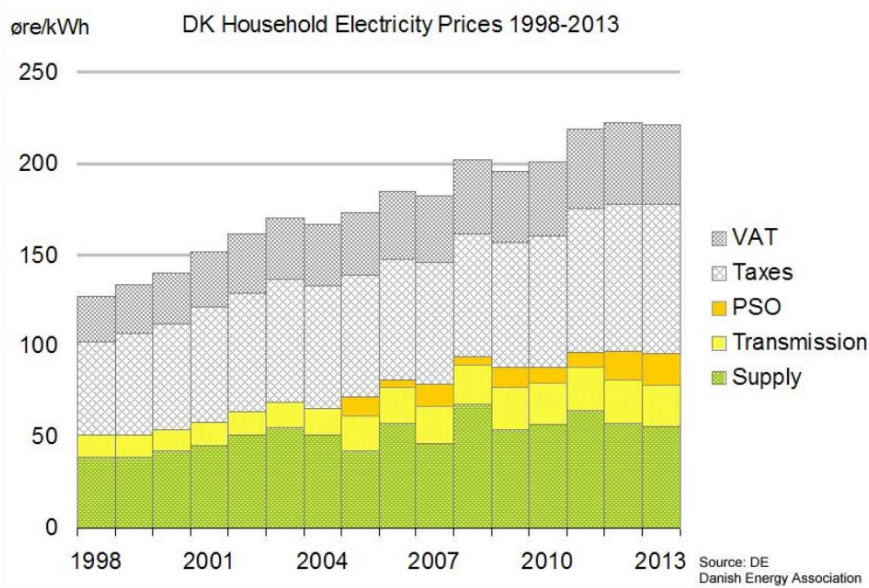
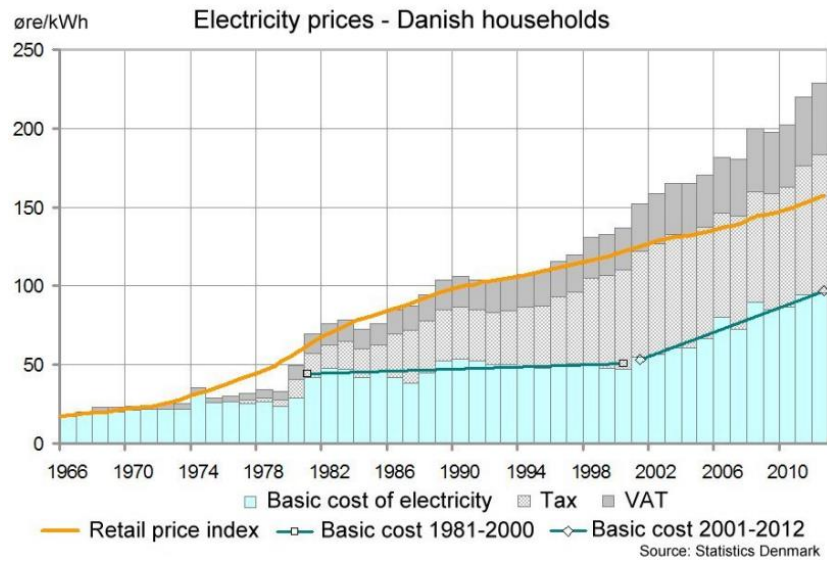
If heat recovery is not required, the bypass damper closes off 100% and leads the outdoor air past the heat exchanger. Hot water can be produced at the same time. Hot water is produced with a high efficiency (COP).



Active cooling

The heat pump has a reversible cooling circuit and can cool the supply air during hot periods. This function does not affect the production of hot water, which takes place with high efficiency (COP).

Annex 10: Electrical energy price



Pictures taken from:

http://www.pfbach.dk/firma_pfb/pfb_skyrocketing_electricity_cost_2014.pdf

Annex 11: Mechanical and instrumentation drawings from PD#6¹, Team DTU

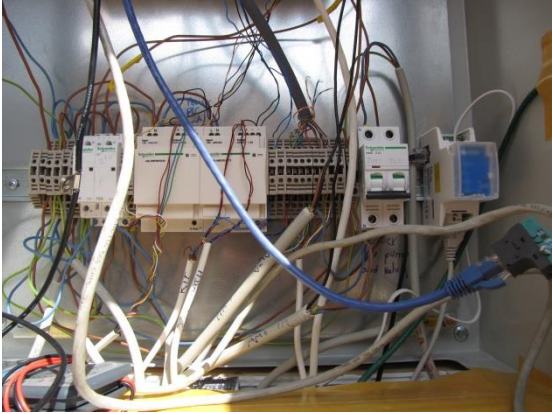
(starting next page)



¹ PD#6 is the Project Drawings of Deliverable n.6, issued June 2nd 2014.

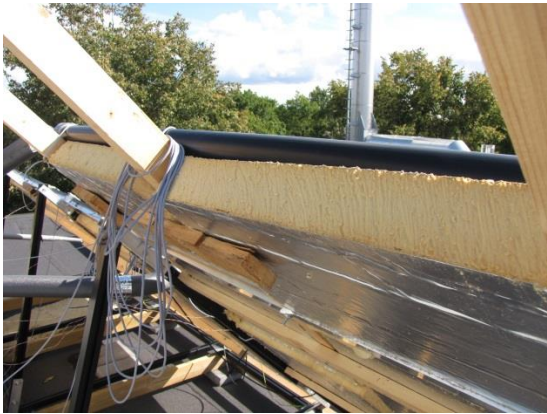
Annex 12: Control drawings from PD#6, Team DTU

(starting next page)



Annex 13: Power graphs from the experiment (August 12th-25th)

(starting next page)



Annex 14: Final estimation of cooling power based on TRNSYS simulation

Time	Outlet temperature curve for a supply temperature of 18°C	Calculated outlet temperature	Average temperature in the tank = Inlet to the solar collectors	Cooling power per square meter of collector	Energy content of the tank	Average temperature in the tank (calculation based on power, for EMBRACE => 14 m2 collectors)
t	T _{out,18}	T _{out}	T _{av,tank} = T _{inlet}	Q	E	T _{av,tank,EMBRACE}
hh:mm:ss	°C	°C	°C	W/m ²	J	°C
21:22:30	18,58		22,00		9,25E+08	22,00
21:30:00	18,55	21,45	21,99	26,12	9,25E+08	2,20E+01
21:37:30	18,52	21,41	21,98	27,50	9,25E+08	21,98152974
21:45:00	18,49	21,37	21,97	28,86	9,25E+08	21,97158708
21:52:30	18,46	21,34	21,96	30,22	9,25E+08	21,96117664
22:00:00	18,43	21,30	21,95	31,58	9,25E+08	21,95029864
22:07:30	18,39	21,26	21,94	33,03	9,25E+08	21,93892095
22:15:00	18,36	21,21	21,93	34,57	9,25E+08	21,92701236
22:22:30	18,32	21,17	21,91	36,10	9,25E+08	21,91457687
22:30:00	18,29	21,12	21,90	37,61	9,25E+08	21,90162027
22:37:30	18,25	21,08	21,89	39,10	9,24E+08	21,88814877
22:45:00	18,22	21,03	21,87	40,59	9,24E+08	21,87416476
22:52:30	18,18	20,99	21,86	42,07	9,24E+08	21,85967105
23:00:00	18,15	20,94	21,84	43,55	9,24E+08	21,84466979
23:07:30	18,11	20,90	21,83	44,98	9,24E+08	21,82917462
23:15:00	18,08	20,85	21,81	46,37	9,24E+08	21,81320073
23:22:30	18,04	20,81	21,79	47,74	9,24E+08	21,7967534
23:30:00	18,01	20,76	21,78	49,10	9,24E+08	21,7798384
23:37:30	17,98	20,72	21,76	50,44	9,24E+08	21,76246276
23:45:00	17,95	20,67	21,74	51,75	9,24E+08	21,74463416
23:52:30	17,91	20,63	21,72	53,05	9,24E+08	21,72635912
00:00:00	17,88	20,58	21,70	54,18	9,24E+08	21,70769293
00:07:30	17,86	20,54	21,68	55,31	9,24E+08	21,68864022
00:15:00	17,83	20,50	21,66	56,29	9,24E+08	21,66924718
00:22:30	17,80	20,46	21,64	57,27	9,24E+08	21,64951847
00:30:00	17,78	20,42	21,62	58,23	9,24E+08	21,62945919
00:37:30	17,75	20,38	21,60	59,17	9,24E+08	21,60907525
00:45:00	17,73	20,34	21,58	60,09	9,24E+08	21,58837393
00:52:30	17,70	20,30	21,56	61,00	9,23E+08	21,56735998
01:00:00	17,68	20,26	21,54	61,90	9,23E+08	21,54603559
01:07:30	17,65	20,22	21,52	62,76	9,23E+08	21,524415
01:15:00	17,63	20,18	21,49	63,57	9,23E+08	21,50251456
01:22:30	17,61	20,14	21,47	64,37	9,23E+08	21,48033784
01:30:00	17,58	20,10	21,45	65,17	9,23E+08	21,45788649
01:37:30	17,56	20,06	21,43	65,97	9,23E+08	21,43516075
01:45:00	17,54	20,02	21,40	66,76	9,23E+08	21,41216278
01:52:30	17,52	19,98	21,38	67,54	9,23E+08	21,38889514
02:00:00	17,49	19,94	21,35	68,32	9,23E+08	21,36535892
02:07:30	17,47	19,91	21,33	68,88	9,23E+08	21,34162879
02:15:00	17,46	19,87	21,31	69,24	9,23E+08	21,31777458
02:22:30	17,45	19,84	21,28	69,61	9,23E+08	21,29379332
02:30:00	17,43	19,81	21,26	70,00	9,23E+08	21,26967963
02:37:30	17,42	19,78	21,23	70,38	9,22E+08	21,24543326
02:45:00	17,40	19,75	21,21	70,76	9,22E+08	21,22105697
02:52:30	17,39	19,71	21,18	71,13	9,22E+08	21,19655241
03:00:00	17,37	19,68	21,16	71,53	9,22E+08	21,17191066
03:07:30	17,36	19,64	21,13	71,99	9,22E+08	21,14710956
03:15:00	17,34	19,61	21,11	72,52	9,22E+08	21,12212652

03:22:30	17,32	19,57	21,08	73,08	9,22E+08	21,09695017
03:30:00	17,30	19,53	21,06	73,66	9,22E+08	21,07157301
03:37:30	17,28	19,49	21,03	74,26	9,22E+08	21,04599215
03:45:00	17,26	19,46	21,00	74,85	9,22E+08	21,02020657
03:52:30	17,24	19,42	20,98	75,45	9,22E+08	20,99421503
04:00:00	17,22	19,38	20,95	76,04	9,22E+08	20,96801939
04:07:30	17,20	19,34	20,92	76,50	9,22E+08	20,94166391
04:15:00	17,19	19,31	20,90	76,84	9,21E+08	20,91519325
04:22:30	17,17	19,27	20,87	77,17	9,21E+08	20,88860912
04:30:00	17,16	19,24	20,84	77,49	9,21E+08	20,86191297
04:37:30	17,15	19,21	20,82	77,82	9,21E+08	20,83510568
04:45:00	17,13	19,17	20,79	78,15	9,21E+08	20,80818462
04:52:30	17,12	19,14	20,76	78,48	9,21E+08	20,78114777
05:00:00	17,10	19,10	20,73	78,82	9,21E+08	20,75399484
05:07:30	17,10	19,08	20,71	78,63	9,21E+08	20,72690602
05:15:00	17,11	19,07	20,68	77,82	9,21E+08	20,70009683
05:22:30	17,13	19,07	20,65	76,64	9,21E+08	20,6736959
05:30:00	17,15	19,07	20,62	75,12	9,21E+08	20,64781842
05:37:30	17,18	19,09	20,60	73,24	9,21E+08	20,62258685
05:45:00	17,22	19,11	20,57	71,01	9,20E+08	20,59812282
05:52:30	17,27	19,14	20,55	68,44	9,20E+08	20,57454589
06:00:00	17,32	19,17	20,53	65,62	9,20E+08	20,55193845
06:07:30	17,53	19,36	20,51	55,42	9,20E+08	20,53284531
06:15:00	17,65	19,46	20,49	49,64	9,20E+08	20,51574519
06:22:30	17,77	19,58	20,48	43,53	9,20E+08	20,50075025
06:30:00	17,90	19,69	20,46	37,24	9,20E+08	20,48792272
06:37:30	18,03	19,81	20,45	30,90	9,20E+08	20,47727673
06:45:00	18,16	19,94	20,44	24,54	9,20E+08	20,46882142
06:52:30	18,29	20,06	20,44	18,16	9,20E+08	20,46256644
07:00:00	18,42	20,19	20,43	11,74	9,20E+08	20,45852121

Annex 15: Operation period and outdoor temperature for Daikin heat pump simulations

Paris:

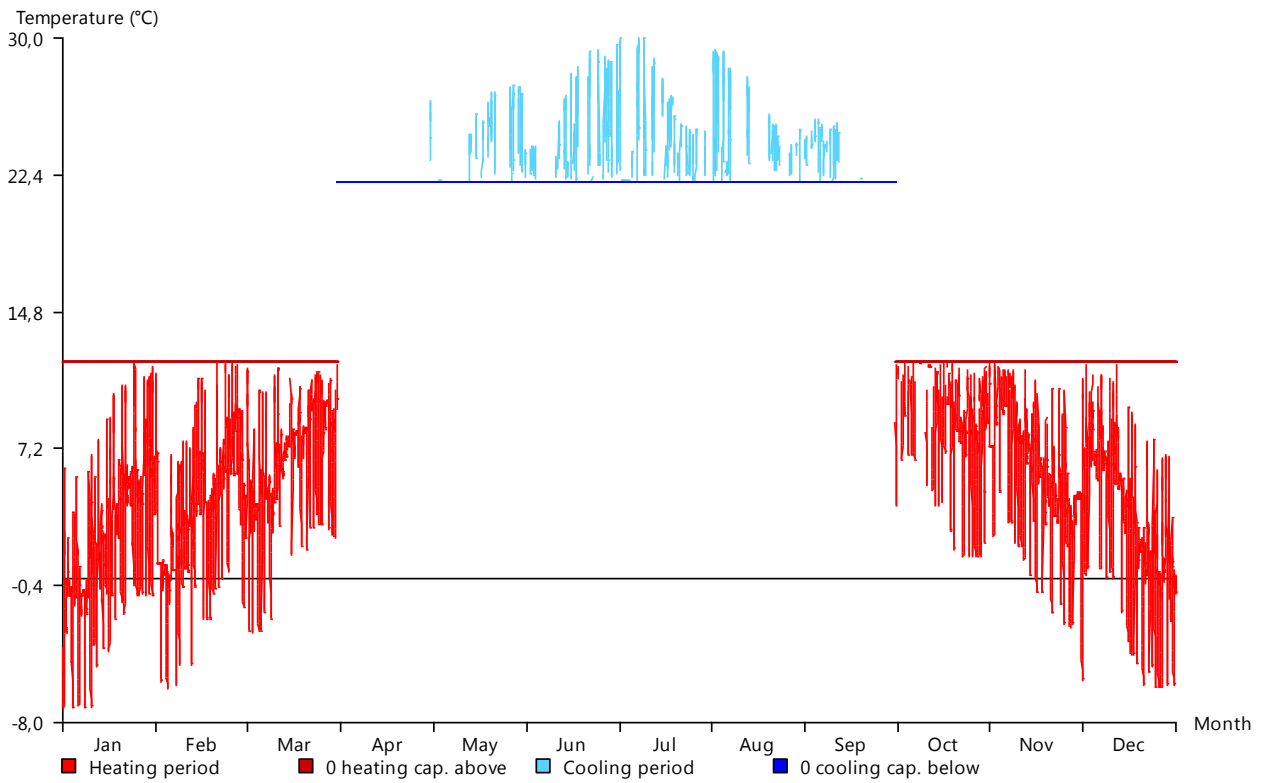


Figure - Outdoor temperature variations within the conditioned months, simulated by the Daikin program (Paris)

Table - Ranges of outdoor temperatures as an input in the Daikin simulation tool for Paris

Country	France
City	Paris
Summer Day	24,6 / 30,0°C ¹
Summer Night	9,6 / 14,1°C
Winter Day	5,5 / 11,9°C
Winter Night	-7,2 / -0,4°C

¹ Temperatures min / max

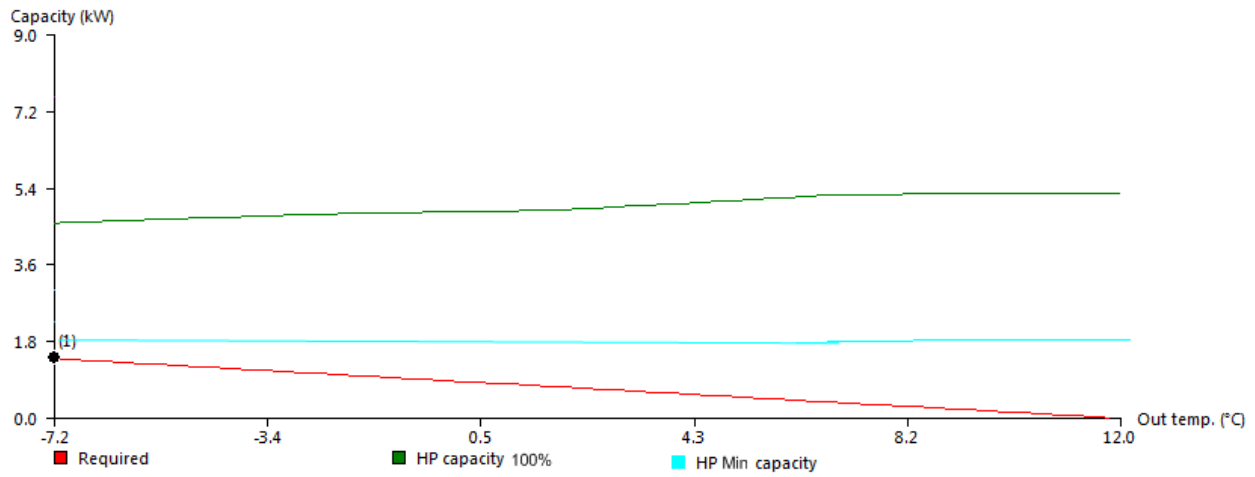


Figure - Heating capacity of the heat pump and dwelling demand in Paris. For Paris cooling is exposed in Chapter IV.2.2

Copenhagen:

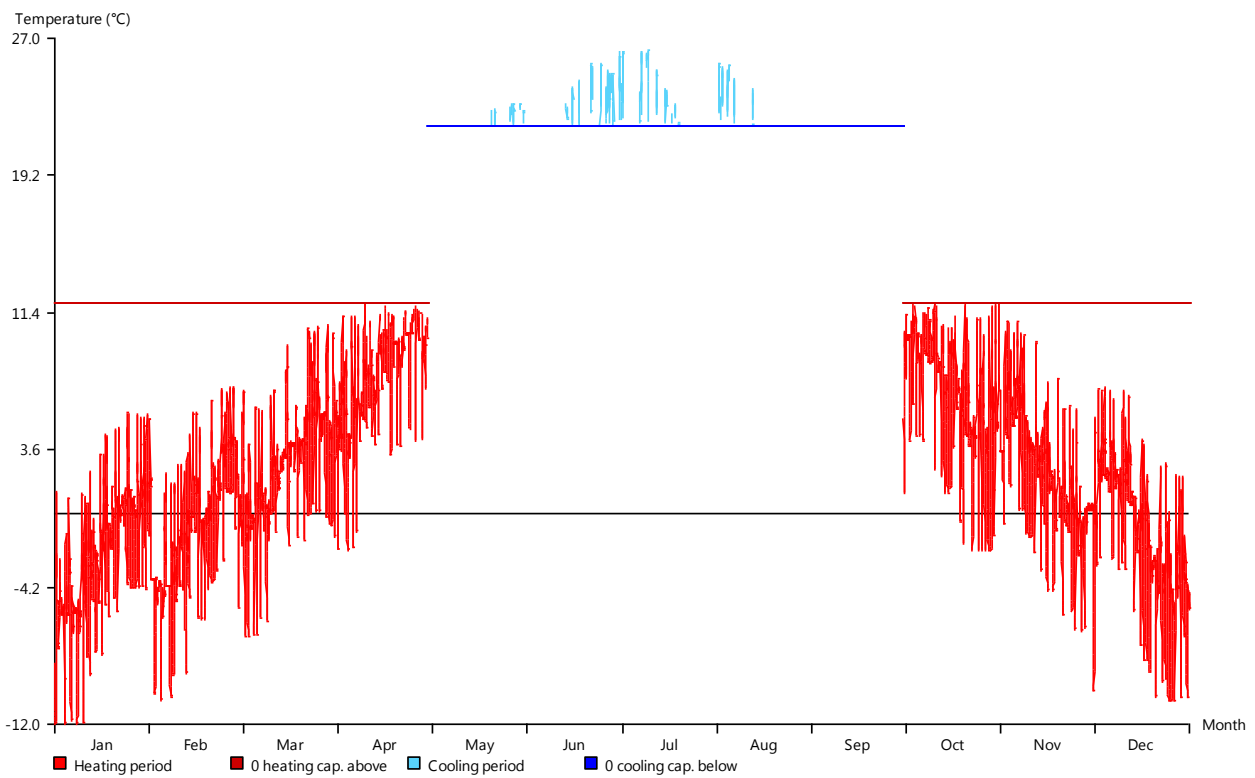


Figure – Outdoor temperature variations within the conditioned months, simulated by the Daikin program (Copenhagen).

Table – Ranges of outdoor temperatures as an input in the Daikin simulation tool for Copenhagen

Country	Denmark
City	Copenhagen
Summer Day	21,1 / 26,3°C ¹
Summer Night	7,7 / 12,4°C
Winter Day	0,8 / 5,8°C
Winter Night	-12,0 / -3,6°C

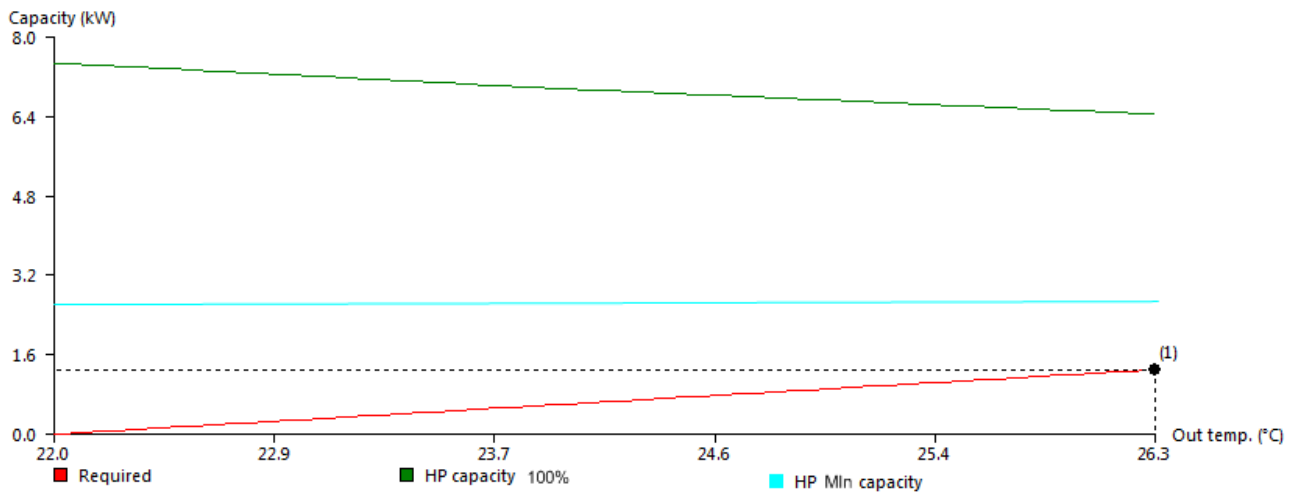


Figure – Cooling capacity of the heat pump and dwelling demand in Copenhagen. For Copenhagen heating is exposed in Chapter IV.2.1.

¹ Temperatures min / max